Aspects of the Stress and Fatigue Performance of Threaded Connectors

James William Hobbs

Thesis submitted for the Degree of
Doctor of Philosophy
December 1998

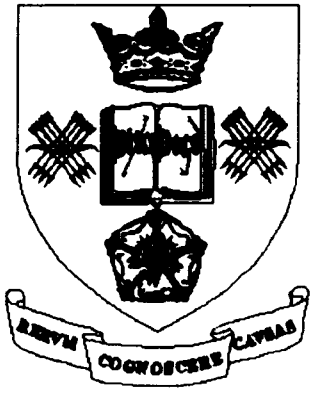

Department of Mechanical Engineering
University of Sheffield

Aspects of the Stress and Fatigue Performance of Threaded Connectors

J. W. Hobbs

Summary

Threaded connectors have been used in a variety of engineering structures for hundreds of years. Although stress analysis of threaded connectors has been performed since the early 1900's, there are still areas that are not fully understood. The way in which eccentricity affects the fatigue performance and stress distribution is one such area, and is the main area of research described in this thesis.

The techniques of photoelasticity and fatigue testing were used to determine the effect of eccentricity on the stresses and fatigue performance of bolts. The results show that eccentric loading has a significant effect on the fatigue performance, but that this effect can be quantified if the local stress amplitude is considered. The photoelastic analysis results show the eccentricity slightly increases the stress intensity factors at the crack tip.

A number of two-dimensional and three-dimensional finite element models were created to determine the salient characteristics of the models. The models were validated against the result from the photoelastic analysis and the results agreed well. Accurate results can be obtained from a two-dimensional model, but the information obtained is limited unless many models are created. However, if a three-dimensional model is created more information can be obtained, but the nut thread run-out must be accurately modelled to obtain the correct stress distribution.

The shape of cracks occurring in cyclically loaded steel bolts and the effect of crack shape on the stress distribution was also investigated. The photoelastic analysis of cracked bolts failed to predict the shapes of cracks occurring in cyclically loaded bolts. It is suggested that the inability of photoelasticity to model plasticity is the cause of this failure and this is supported by results from an elastic-plastic finite element model.

To Sue

Acknowledgements

I would like to thank all those that have given me invaluable help during the research and writing up of this thesis. Firstly, thanks must go to my supervisors, Prof Eann Patterson, Dr Richard Burguete and Philip Heyes. They have provided me with the necessary support and encouragement that has got me through the last few years.

Secondly, I must thank Richard Kay, John Driver, Simon Wiles and Terry Senior for their work manufacturing specimens, grips and for helping in the laboratories and workshop. Also, to Alaster Yoxall, whose help with finite element modelling shortened my PhD by a few years.

Finally, to all the other members of the experimental stress analysis laboratory, especially Elizabeth Olden and Mark Pacey for helping me and being a sounding board to bounce ideas from. Thanks must go also to my wife, Sue, who has supported me in many ways during the course of my work. Her patience in waiting for me to get a 'proper job' is truly appreciated.

This work was funded under the S.H.A.R.P. collaboration between the University of Sheffield and the Health and Safety Laboratory Ltd..

Contents

Nomenclature

μ	Coefficient of friction
δ	Angle between plane of bending and plane of instrumented bolt
ε	Strain
Δ	Range of values
σ	Nominal stress
σ_a	Stress amplitude
σ_m	Mean stress
σ_y	Yield stress
a	Crack length
A_s	Stress area of bolt
c	Crack shape parameter
D	Nominal diameter of bolt
d	Stress diameter of bolt
e	Eccentricity
E	Offset of eccentric load
K	Stress intensity factor
L_A	Applied axial load
L_B	Applied bending load
L_E	Equivalent single load
P	Applied load
r	Pearson correlation coefficient
x	Position around crack front
Y	Geometric calibration function

Chapter 1

Introduction

1.1 Motivation and Aims of Research

1.1.1 The Problems with Nuts and Bolts

Nuts and bolts have been used for hundreds of years in a wide range of industries. Although at first sight, they may appear like very simple components, the analysis of the stresses occurring in them is far from simple. The complex geometry of the threads and the fact that when loaded, the bolt extends and the nut compresses, creating a difference in thread pitch, make analysis by theoretical means almost impractical. The inaccessibility of the areas of real interest, the thread roots, severely limits the possible options for experimental strain measurement. Given these problems, it is not surprising that fatigue testing, photoelastic analysis and the finite element method have been the most popular methods for assessing the problem.

As with most other mechanical structures, failures of bolts can have catastrophic consequences. Even minor failures could cause costly damage or expensive downtime. In the last five years, the Health and Safety Laboratory has investigated at least 20 serious accidents which has resulted from failures of bolts

and/or bolted connections. These include failures of cranes, off-shore lifting equipment, power-presses and fairground rides. Assessment of bolt failures has revealed that in many cases bending loads have been superimposed on the original tensile loads. This loading configuration is not covered by the current design standards, BS 7608:1993[1] "Code of practice for fatigue design and assessment of steel structures". Although the effect of axial loads on bolts has been studied extensively, the effect of eccentric loads is still largely unknown.

1.1.2 Motivation for the Research

This research has been supported by the Health & Safety Laboratory, and has arisen from concerns about the effect of eccentricity on the fatigue behaviour of threaded connections. Often, eccentric loading is suspected as a contributing factor in the failure of bolts, but without sufficient knowledge about the causes or effects of such loading, it is difficult to attribute the cause of failure with any degree of certainty. A better understanding of the effect of eccentricity on the fatigue performance and crack shape in bolts would enable accident investigators to determine the cause of failure more accurately.

Knowing the effect of eccentricity would also be very useful at the design stage. If eccentricity was found to have little effect, designers could save time by not trying to make a component not apply any bending to the bolt. Or, if the effect of eccentricity is significant and known, an appropriate allowance could be made to allow for the reduction in fatigue life.

1.2 Fatigue Tests

Ultimately, it is in fatigue that the majority of bolt failures occur. A failure due to a simple overload is unusual. It is therefore sensible to perform fatigue tests to obtain data on how the threaded connector will perform in actual engineering applications.

It was decided to concentrate on the performance of the nut and bolt in isolation from a bolted joint. The transfer of load between a joint and a bolt are highly complex and still not fully understood, especially under eccentric loads. Eliminating this aspect reduces the number of variables considerably.

Two investigations were carried out in the area of fatigue testing. The first fatigue investigation looked into the effect of changing the number of cycles that fatigue tests are run to. When performing fatigue tests to obtain fatigue limits, a number of cycles must to chosen at which tests are terminated, as tests can not be performed to true infinite life. A cut off point has to be chosen, so that once a component has survived to the predetermined number of cycles, the test is stopped and the bolt is considered to have survived. The number of cycles used by different researchers varies. Notably, the standard in JIS[2] uses 5×10^6 cycles, whereas Burguete and Patterson[3] and BS 7608[1] used the shorter 2×10^6 cycles.

The main fatigue investigation was into the effect of eccentric loading on the fatigue strength of bolts. A number of bolts were subjected to a cyclic load applied with varying degrees of eccentricity. The stress amplitude to cause failure at 2×10^5 cycles was compared to evaluate the effect of eccentricity. From the results from this investigation, the effect of eccentric cyclic loads on the fatigue performance of bolts can be quantified.

The shape of the cracks occurring in the cyclically loaded bolts was noted, to ascertain whether any useful information about the loading history could be extracted from the fracture surfaces. Also, the results from the stress analysis techniques were checked against the crack shapes.

1.3 Photoelastic Analysis

The main aim of the photoelastic analysis was to quantify the effect of eccentric loading on the stresses in cracked bolts. Three-dimensional stress freezing was used to obtain stress intensity factors at the crack tip and the stress distributions at the thread roots for cracked bolts subject to loads of varying eccentricity.

The other aim of the photoelastic analysis was to investigate the effect of crack shape on the stress distribution and the stress intensity factors at the crack tip. The results from the photoelastic analysis were compared to the crack shapes observed during the fatigue testing.

The technique of photoelasticity has been used for a number of years and has been popular for the analysis of threaded connectors. It is practically the only

experimental method that allows the stresses at the inaccessible thread roots to be determined and is therefore very suited to this problem.

1.4 Finite Element Analysis

The finite element method is becoming increasing popular in a wide range of industries as the speed and power of computers is increasing. Once the initial model has been created, changing the loading conditions can be a relatively quick and simple task.

The main aim of performing a finite element analysis was to improve on the models previously created by other authors, most notably Zhoa[4,5], and produce a three-dimensional model that accurately simulated the complex nut thread run-out. This model was then validated against the results from the photoelastic analysis and compared to the crack shapes observed during the fatigue testing.

A large series of models was produced to determine the salient characteristics. The aim of this investigation was to give designers or future finite element analysts guidance on how to create accurate models, and appropriate models, suitable to obtain the desired information.

Chapter 2

Literature Review

2.1 Load and Stress Distribution in the Thread Roots of Threaded Connectors

2.1.1 Introduction

This section covers work on two areas; the stress distribution at the root of threads and the stress intensity factors at crack tips in threads. The special case of a bolt loaded by a nut is considered in greater detail. Experimental and numerical stress analysis techniques are not treated separately but covered together as a number of authors use both methods.

2.1.2 Stress Distribution in the Roots of Threads

An in-depth review of the literature up to 1989 is given by Kenny and Patterson[6]. They describe the development of experimental investigations and theory in the area of load and stress distribution in threads. Therefore, the most relevant aspects covered by these authors will be highlighted briefly and then later work will be discussed in more detail.

Stromeyer[7], in 1918, was one of the first to consider the stresses occurring in threaded connections. He suggested ideas about the effect of differential pitch and the bending of the threads. In 1929 Den Hartog[8] pointed out that since the bolt is in tension and the nut is in compression, the difference in thread pitch causes a non-uniform distribution of the load with the first threads taking most of the load. He derived an expression for the load distribution that had a parabolic form with the first two threads taking 45% of the load. Den Hartog supported this theory with experimental work using celluloid sheet to model threads for photoelastic analysis. Further photoelastic work by Solakian[9] also supported Den Hartog's theory, and obtained a stress concentration factor of 3.95 for the American Standard thread.

Den Hartog's work was later extended by Sopwith[10] and Stoeckly and Macke[11]. Meanwhile, Zhukovskii[12] and Kolenchuk[13] developed their own theories independently.

Other experimental techniques were employed by Moore and Heywood[14], who performed fatigue tests (reported by Thurston[15]), and Goodier[16], who measured the external deformation of the nut.

The first person to report a three-dimensional model was Hetényi[17,18], who produced a Bakelite model and analysed it photoelastically after it had been stress frozen. Stress concentrations were found to be 25% greater than those from Solakian's two-dimensional analysis. He also looked at different designs of nuts and found that using nuts with a tapered lip (the "tension nut") or a tapered thread reduced the stress concentration in the bolt.

The tension nut was investigated further in the 1970s by Seika *et al*[19] using the copper-electroplating technique, theoretically by Motosh[20] using the strength of materials approach and by Doniselli and Mondina[21].

Brown and Hickson[22] used a Fosterite model for their three-dimensional photoelastic analysis, which they claimed was less susceptible to edge stresses than Bakelite. Their stress concentrations were far higher than Hetényi's, probably because of the excessive truncation of the threads and the relatively small external diameter of the nut.

Two new techniques were used by Maruyama[23,24] in the 1970s, finite element modelling and copper-electroplating. For the finite element model the threads were modelled as annular grooves, giving values for the stress concentrations in the thread roots. The results showed that the stress concentrations tend to decrease and to move to the loaded flank as the root radius is increased. Maruyama's finite element results showed fairly good agreement with his copper-electroplating experimental results except for small root radii, where the results differed by up to 24%.

In 1979 Bretl and Cook[25] introduced a novel finite element technique. Instead of modelling individual threads, which required a fine mesh in the area of the threads, they replaced the threaded zone with a layer of elements having orthotropic properties. This gave a reasonable fit to the experimental results of Stoeckly and Macke[11] and were an improvement on the finite element results of Maruyama. These elements have since been used by Grosse and Mitchell[26].

Photoelastic stress freezing was used by Fessler in the 1980s working with Jobson[27] and Wang Jiong-Hua[28]. They looked at the effect of using unsymmetric shapes and loadings on threaded connections. Bolts were screwed in blocks with different cross sections; three rectangular blocks and one circular with a flat. As others had found previously, the maximum stresses in the bolts occurred near the start of contact. They also found that the values depended on the thread configuration at the start of contact rather than on the block cross section.

Tanaka *et al*[29] produced a finite element model of bolt-nut joints including the fastened plates to investigate self-loosening of nuts. Again, the model assumed that the joint was axisymmetric, but the authors claimed that the helix angle was taken into account, although no details of how this was achieved were given. The plates and the nut were assumed to be rigid, which ignores the compression of the nut and difference in thread pitch that this causes.

Later photoelastic analysis was performed by Kenny and Patterson[30] on an axially loaded double ended ISO M30 bolt using a fringe-multiplying polariscope. They showed that the load and stress distributions are not equivalent, as had previously been assumed. The results correlated closely with Sopwith's theoretical load distribution. Sopwith's load distribution was in turn compared to other methods

used to find the load distribution. Deducing the load distribution from the external deformation of the nut was found to be unsatisfactory and the finite element analysis of Bretl and Cook[25] was found to show closer correlation than that of Maruyama[23] or Tanaka *et al*[29].

Kenny and Patterson concluded their paper[6] with a discussion on the techniques available for modelling threaded connections. They stated that three-dimensional photoelastic stress freezing automatically provides natural boundary conditions but can only model elastic behaviour, whereas the thread roots are more likely to have deformed plastically, especially under high preload. The finite element method is commended for being capable of true three-dimensional analysis (although this as yet had not been performed) and for being able to model the elastic-plastic behaviour. For clamped components boundary elements were suggested, but this method is not good for modelling individual threads. They suggested that a combination of finite element and boundary element techniques may be the way forward.

An interesting idea was put forward by Dragoni[31] in 1990 which involved using a nut with a Young's Modulus that varied axially. The aim was to propose a design for a nut that would achieve uniform thread load distribution. A popular equation that described the thread load distribution in a standard nut-bolt connection was extended to incorporate the case of threaded elements with axially variable modulus of elasticity. The composite nut proposed, shown in Figure 2.1, consisted of steel, titanium and magnesium alloy sections to achieve the required Young's Modulus. Dragoni claims that this is a feasible design, although such a composite nut would surely be far more expensive to manufacture than a homogeneous nut. This paper is purely theoretical and no experimental work has been performed in support.

Another method of reducing the stress concentrations in bolts was investigated by Dragoni[32] when he looked at lip-type nuts using photoelasticity. He found that using a nut with a lip covering 60 percent of the total height of the nut resulted in a reduction in the stress concentration in the bolt of almost 40 percent. Thread pitch and lip radial thickness were found to have little effect.

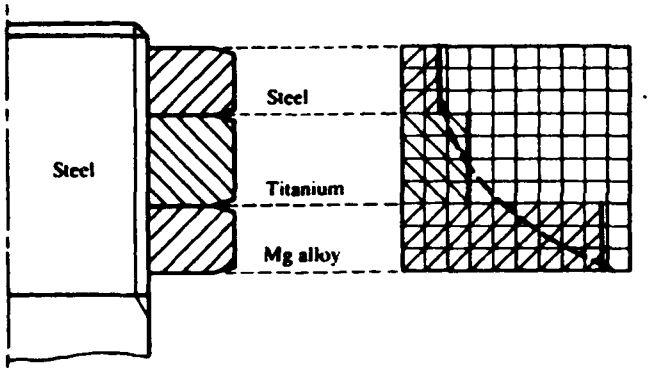

Figure 2.1 Composite nut proposed by Dragoni[31] approximating the theoretical elastic properties required to achieve uniform load distribution

The most recent investigation to use photoelasticity was performed by Burguete and Patterson[33,34]. They used MY750 epoxy resin to model a three-dimensional bolt that was stress frozen and photoelastically analysed. The bolt was loaded in simple bending with an eccentric load superimposed on to an axial load. In each test the total stress was the same but the ratio of bending stress to axial stress (R_σ) was varied. It was found that the shape of the stress versus distance from loaded face curve was similar to that for axially loaded bolts but the peak was lower and flatter. The loading with the lowest peak stress was with equal axial and bending stresses (i.e. R_σ=1).

The use of the finite element method to model threaded connections has increased greatly in recent years with a number of authors producing models. In 1992 Dragoni[35] used finite element models to investigate the effect of friction coefficient and thread pitch on the stress concentration factors in nuts and bolts. Figure 2.2 shows the meshes considered by Dragoni while performing a mesh convergence exercise. All three models were axisymmetric and subjected to identical loading and constraints. After plotting the stress concentration factors at the thread root against the number of elements, the medium density mesh was chosen for the subsequent analysis. The main model was constructed by stacking up a number of these meshes until the required nut height was achieved. Five free threads were included between the loaded face of the nut and the point of application of the bolt load to ensure an even stress before the first engaged thread. Dragoni's results showed very good agreement with the photoelastic

results of Patterson and Kenny[36]. Four different geometries were used to represent the nut in four different positions and this included the change in thread profile due to the run-out of the nut thread. Unfortunately, no details are given of how the run-out was modelled, i.e. whether flat to the loaded face or with a bevel. It was found that for a given nominal diameter and bolt load, the maximum stress increases as the pitch decreases. Also, the maximum stress increases with the coefficient of friction up to a coefficient value of 0.6, beyond which sticking between the nut and bolt occurs and the stress remains constant.

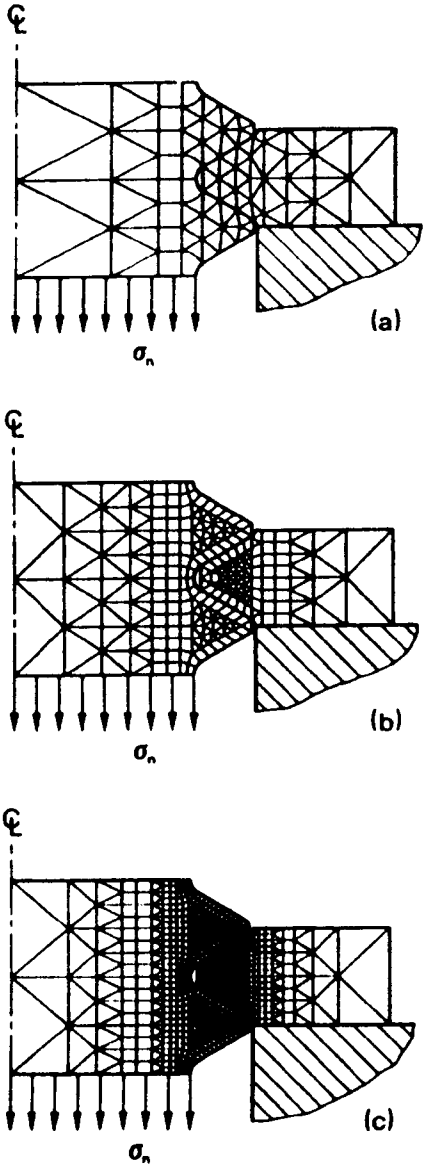

Figure 2.2 Mesh densities considered by Dragoni (from Dragoni[35])

A full three-dimensional model of a nut and bolt including the helix angle was constructed by Zhao[4,5]. The model consists of an ISO M30 bolt with an internal diameter of 0.3 mm in order to model the helix angle and a cornerless nut with outer diameter of 48 mm and length 40 mm. There are nine threads in engagement. It has been found previously that using a hollow bolt with a small internal diameter has little influence on the load distribution (Fukuoka *et al*[37]). The whole model, shown in Figure 2.3, contains just 560 elements, with three elements per thread. This is not fine enough to obtain stress concentration factors at the thread roots so the load distribution was obtained. The results are compared to the analytical solution from Sopwith and the numerical results from Bretl and Cook and found to agree well.

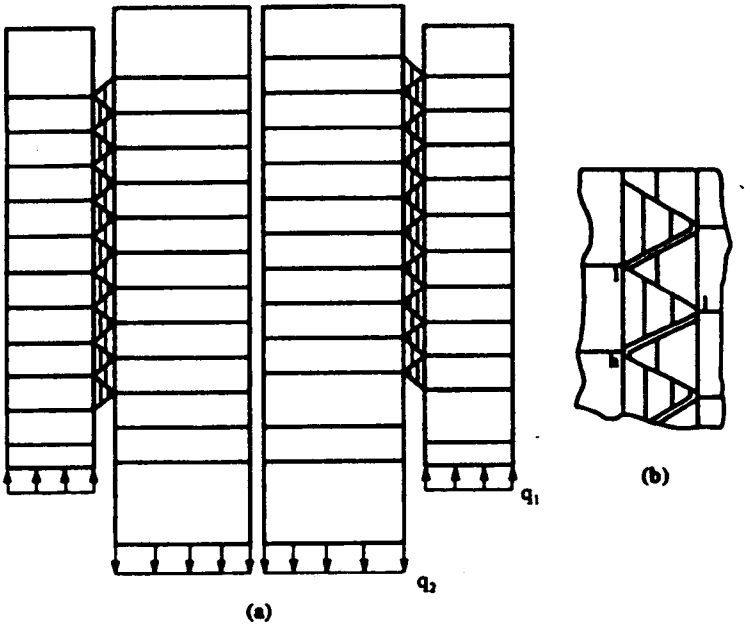

Figure 2.3 Mesh in Zhao's three-dimensional model (from Zhao[4]).

A non-linear finite element model of a joint system, which modelled the elastic/plastic nature of the material, was reported by Joanovics and Varadi in 1995[38]. The joint system was comprised of a nut, bolt, washer and a compressed sheet. The object was to evaluate the load distribution in the threads and the joint load diagram. The model was 2D and axisymmetric with frictionless contact elements between the mating threads, on both sides of the washers and between

the bolt head and the sheet. A number of different analyses were performed, modelling bolts made from different grades of material and both low strength and heat-treated washers. For the lower strength bolts (grade 5.8) it was found that the load shifted up the nut to the second and third threads as the applied load increased to 80% of the ultimate tensile strength. For the medium strength bolts (grade 8.8) this effect was even more marked, with the load distribution peaking at the fourth loaded thread for applied loads of more than 70% UTS. At an applied load of 78% UTS the fourth thread carried over 40% more load than the first thread. These results are not supported by any experimental or theoretical work. The fact that fatigue failures occur in the first loaded thread in the majority of cases seems to suggest that these results are rather inaccurate.

A hybrid modelling approach was used by Bahai *et al*[39] to analyse threaded connections. A substructure model containing three threads of a box and pin pipe joint was modelled, first using a fine mesh, then the stiffnesses obtained were used in the main model. The results were compared to a full three-dimensional model. The box and pin geometry is more complex than the nut and bolt geometry in that the spiral profile has to be taken into account as well as the helix. The full 3D model uses 1400 elements for 7 teeth and, although finer than Zhoa's[4], has a very coarse mesh. The results from the hybrid model and the full 3D model show large discrepancies, with the hybrid model underestimating the peak stress. No experimental work was used to validate the results.

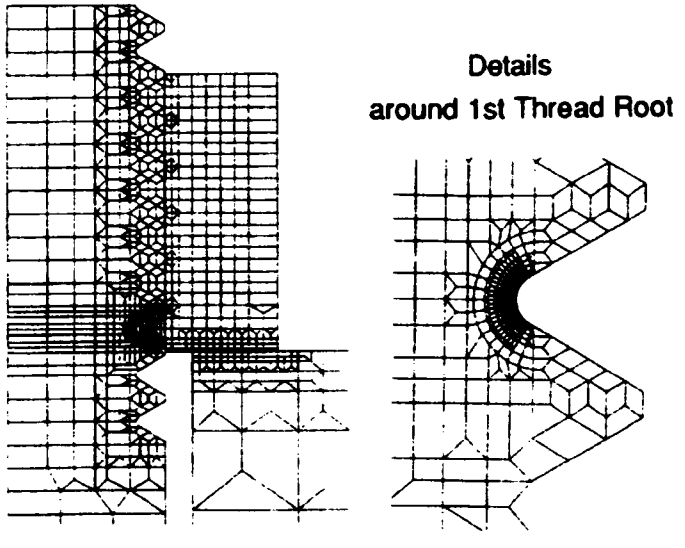

Figure 2.4 Detail of mesh in Fukuoka's model (from Fukuoka[40]).

The most recently reported finite element analyses of threaded connections was Fukuoka's[40] investigation into the reduction of stress concentrations in thread roots by modification to the nut shape. His axisymmetric model, shown in Figure 2.4, consisted of a nut, bolt and a plate in two dimensions. A much finer mesh was used around the first thread root of the bolt as this was where the highest stress concentration was expected. Various shapes of nut were evaluated and it was found that curved and straight bevels on the loaded face of the nut reduced the maximum stress for bolt-nut connections in tension. In addition, the curved bevel was found to reduce the high stress concentration occurring at the loaded surface of the nut. However, as nut failures are almost unknown in practice, this seems insignificant.

To date, a finite element model that models the true three-dimensional nature of the connection with a fine enough mesh to obtain stress concentration factors has not been performed. Zhao[4,5] models the three-dimensional geometry of the threaded connection very well, but the coarseness of the mesh limits the accuracy and usefulness of the model. The meshing used by Fukuoka[40] varies throughout the model, with a finer mesh in the first thread root than in the rest of the model. This is a sensible way to mesh, as it is in the first thread root in which most failures occur and therefore the area of most concern. Only one surface of the thread is actually in contact with the nut thread, assuming that the connection remains in tension, and therefore the mesh could be refined further by having a finer mesh on the contact side of the threads.

The elastic-plastic nature of the material has still not been investigated fully. The high stress concentrations at the thread roots mean that the material is likely to deform plastically and this may alter the load distribution.

The effect of the thread run-out, where the last thread of the nut is not fully formed, has, as yet, been ignored by finite element modellers. It has been found experimentally[33] that the run-out has an effect on the load distribution, with the peak stress occurring half a thread pitch from the loaded face of the nut.

2.1.3 Stress Intensity Factors

There has been a considerable amount of work done to determine the stress intensity factors (SIFs) in cracked round bars but less has been done on screw threads. Examples of work on round bars include Bush[41], who looked at the stress intensity factors in round bars under bending and Blackburn[42], who looked at the stress intensity factors for straight cracks in grooved and ungrooved bars. More recent work on round bars has been performed by Daoud and Cartwright[43], Forman and Shivakumar[44] and Nord and Chung[45] who also looked at threaded bars.

Mackay and Alperin[46] used fatigue crack growth data for bolts to obtain a correction factor for stress intensities that was then applied to semi-circular flaws in bolts.

James and Mills[47] reviewed the existing SIF solutions in 1988 and produced polynomial equations to predict the SIFs in bolts under tension or bending. Polynomial expressions from Daoud and Cartwright[43] and Forman and Shivakumar[44] were reported, as well as their own, for straight-fronted and semi-circular crack shapes in round bars. From this investigation they found that the stress intensity factors were higher at the surface than at the deepest point for semi-circular cracks and that the stress intensity factors for straight cracks were higher than for semi-circular cracks with the same maximum depth.

James and Mills used the SIF values of Cipolla[48], Nord and Chung[45] and Lefort[49] for semi-circular cracks near to thread roots. They found that for small cracks, the stress concentration of the thread had the greatest influence, but as the crack grew the influence of the thread reduced so the bolt could be modelled as an unnotched bar. Therefore, to produce one equation for each loading condition considered (pure tension and bending) for all the values of crack length/bolt diameter (a/D), James and Mills used the SIFs for the bolt up to a/D = 0.1, SIFs for a semi-circular crack for $0.1 < a/D < 0.5$ and the SIFs for a straight crack for $a/D > 0.5$.

The decision to use the SIFs for semi-circular and straight-edged cracks for different crack lengths was based on work by Athanassiadis *et al*[50] and Caspers *et al*[51,52]. They found that cracks in round bars began with a semi-circular shape but straightened out as they grew towards a/D = 0.5. Pacey *et al*[53], looking at crack

shapes in cyclically loaded bolts, found that rather than a semi-circular crack shape, the cracks were crescent shaped (see discussion on crack shape in section 3.2.1). Also, Pacey *et al* used three-dimensional photoelastic stress freezing to obtain stress intensity factors for three different lengths of straight cracks in bolts. The results agreed well with James and Mills' equation for short cracks but were higher than the equation predicted for longer cracks (a/D > 0.1). This is to be expected considering the fact that the equation is based on semi-circular cracks in this region and will naturally give lower values than for the straight cracks used by Pacey *et al.*

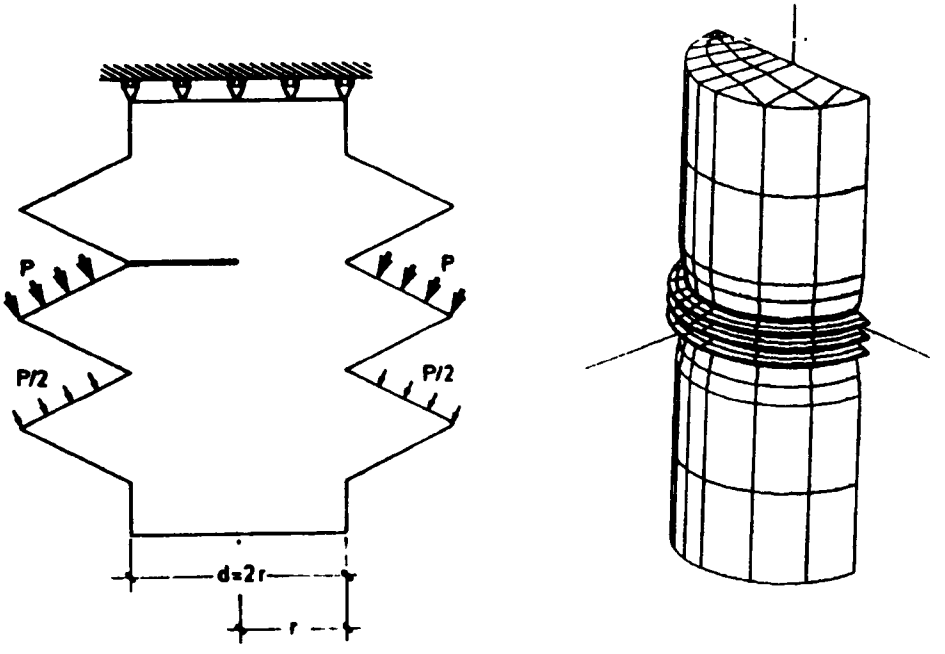

(a) (b)

Figure 2.5 Loading and mesh used by Toribio (from Toribio[54])

In the 1980s, Toribio and his co-workers[54,55] used finite element methods to investigate the stress intensity factors in cracked bolts. An energetic technique was used; namely the stiffness derivative method, which is based on the computation of the energy release rate upon a virtual crack extension. The results were similar to those of James and Mills[47], showing that for shallow cracks, the SIF is higher at the centre of the crack front and for circular cracks it is higher at the end of the crack front where it intercepts the thread surface. The effects of bending and residual stresses were also investigated. The SIFs in the presence of

residual stresses were found to be higher near the crack front but could be neglected for the purposes of predicting crack propagation. The model of the bolt consisted of a shank with three annular threads, neglecting the thread helix angle, as shown in Figure 2.5(b). The nut was not modelled, the load due to the nut was directly applied to the thread flank. The load distribution assumed, shown in Figure 2.5(a), was a value p on the first thread (next to the crack) and half this value (p/2) on the second thread. While this would seem appropriate for an uncracked bolt[48], load shedding caused by the crack (as described by Pacey *et al*[53]) would alter this distribution.

More recently Brennan and Dover[56] have used weight function theory to produce a generic stress intensity factor solution. The reference SIFs used for the solution are a combination of published results representing geometrical features encountered in threaded components.

The weight function theory was also used by Bahai *et al*[57] in conjunction with the finite element method to obtain stress intensity factors for cracks in a threaded pipe joint. The weight function technique was used for the actual calculation of the SIFs, with the finite element analysis providing the stress field through the thickness. The resulting crack growth data was validated using constant amplitude fatigue testing. Although the experimental and weight function results showed similar values, the trends through the thickness were different. It was suggested that this was due to errors in the experimental results from the absence of crack measuring equipment.

It is clear that crack shape has an effect on stress intensity factors, so this is an area that should be researched thoroughly. To date there have been no values obtained for the SIFs for crescent shaped cracks.

2.2 Fatigue Cracks in Bolts

2.2.1 Crack Shape

The shape of cracks under different conditions may be important for two main reasons; (i) knowledge of the crack shape is necessary for use in models to find stresses, (ii) assessing failures may be facilitated if a particular crack shape can be attributed to a certain loading condition.

There has been little research into the shape of cracks in bolts. The majority of investigators assume that the propagation, growth and shape of cracks in bolts can be adequately assumed to be similar to that in notched round bars.

In 1985 Mackay and Alperin[46] performed experiments to find the shape of fatigue cracks in bolts and they found that a machined crack that started with a semi-circular shape straightened out as it grew. The crack was initiated by an electrical discharge machine, and then precracked in a bending mode and was therefore semi-circular to start with. The initial crack can clearly be seen as the dark area shown in Figure 2.6. Later investigations by Pacey *et al*[53], not using an artificially initiated crack, found that the cracks were crescent or sickle-shaped. The crack was found to have a more crescent shape when cyclically loaded under high mean loads, with the crack front almost straight for low mean loads. Stress amplitude and crack depth were found not to affect the crack shape.

Fuchs and Stephens[58] reported the shapes of cracks in smooth bars and bars with mild and sharp notches resulting from a variety of loading conditions. Table 2.1 shows these shapes. A bolt may be best approximated by a sharply notched bar and from Table 2.1 it can be seen that a crescent shaped crack would be expected under tension or unidirectional bending.

Figure 2.6 Fracture face of fatigue crack growth test of a bolt showing markers (taken from Mackay and Alperin[46])

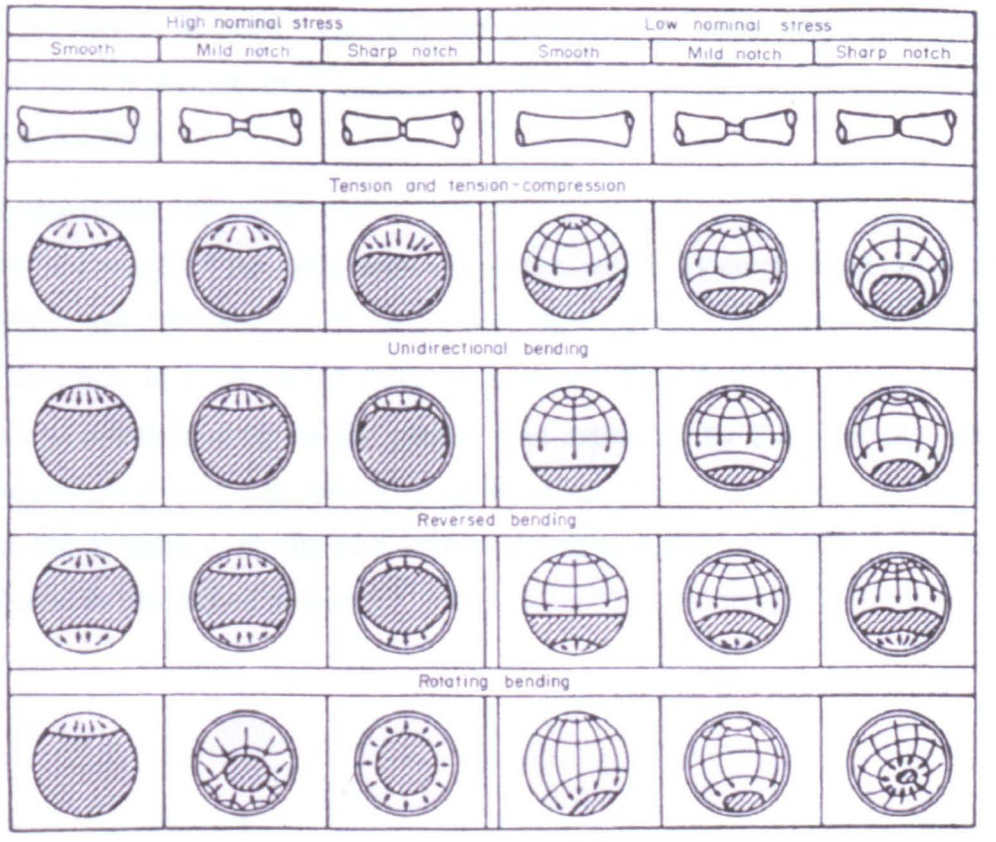

Table 2.1 Crack shapes under various load conditions (taken from Fuchs and Stephens[58])

2.2.2 Secondary Cracking

Secondary cracking here is defined as the occurrence of cracks in a bolt other than the crack that caused the failure. As the main crack usually occurs within the first thread from the load face of the nut, secondary cracking usually occurs in threads further away from the loaded face.

This is an area in which very little work has been done. Hagiwara *et al*[59], Mueller[60] and Burguete and Patterson[34] make passing references to it. Pacey *et al*[53] provide the most thorough investigation of secondary cracking, actively looking for the phenomenon. Bolts previously subjected to fatigue loading (most to failure) were sliced down their length across the diameter so that the failure crack was cut in half; an arbitrary diameter was used for the non-failures. Twenty-four M12 grade 8.8 bolts were examined, and ten were found to contain secondary cracks. The majority occurred in bolts subjected to low mean stresses relative to yield stress. The authors concluded that it was shown qualitatively that the occurrence of secondary cracking was greater at low mean stresses, but that the sample size was too small to be able to draw any quantitative conclusions on relative frequency.

In the experiments by Pacey *et al*[53], the bolts were only sliced in one plane; in the plane of the centre of the main crack. However, secondary cracks need not be in this plane and therefore could be missed, especially if they were short and originated near to ± 90° to the main crack plane. Therefore, the occurrence of secondary cracking could be far greater than estimated by Pacey *et al.* The authors did not present any indication of the effect of secondary cracking on the fatigue life of bolts, or on the load distribution along the threads. This is an area that should be researched further.

2.3 Fatigue of Bolts and Bolted Joints

2.3.1 Introduction

The fatigue behaviour of threaded connections has been of great interest for many years because of the importance of being able to produce safe designs taking fatigue effects into account. In 1943 Arnold[61] reviewed over 150 articles connected to the subject of fatigue in bolts or bolted joints, covering the previous 85 years. He considered many aspects and identified heat treatment, physical dimensions and shape of the thread form as important factors. He suggested that a more rounded thread form improved fatigue performance, and maintaining joint tightness also had a beneficial effect.

Although Thurston[15] took a different approach in his review (considering work on load distribution in threads and its effect of fatigue life) he came to some of the same conclusions as Arnold. He agreed that rolling the thread roots and maintaining sufficient tightness are beneficial, but also that reducing the shank diameter and using a different nut design would help.

More recently, Glinka *et al*[62] used a hybrid approach, combining finite element methods and an electrical analogue to analyse the stresses in the thread roots of tether connections. They also calculated the crack propagation rate using the conventional fracture mechanics methods:

$$\frac{da}{dN} = C(\Delta K)^m$$

It was concluded that the electrical analogue method could be used successfully on different geometries. Generalised equations were derived for the elastic stress field around the tooth, which provides stress concentration factors.

2.3.2 Standardisation of Fatigue Tests

There are various standards for fatigue testing, the main ones will be outlined here.

British Standards BS 3518: "Methods of Fatigue Testing" [63,64,65] describe in detail how fatigue tests must be performed. Part 1[63] gives the general principles and

practice for performing a series of fatigue tests and defines the terms and parameters used in such analysis, such as stress ratio and endurance limit. It is suggested that the minimum number of components tested (a bolt is classed as a component rather than a test piece) is between 12 and 24.

Part 3[64] deals specifically with direct stress fatigue tests for specimens without deliberately introduced stress concentrations. Therefore, this is inappropriate to the testing of bolts, but it is noted that the frequency range at which tests are to be carried out is within the range 5-300 Hz. It is recommended that the number of cycles at which a test is discontinued (representing infinite life) be 10×10^6 for commonly used structural steels and 100×10^6 for other steels and for non-ferrous metals.

Part 5[65] describes the methods by which the test results should be analysed statistically. Details are given as to how *S-N* curves for different probabilities (*P-S-N* curves) should be plotted, and the determination of fatigue limits.

Ohashi *et al*[66] describes the standard 14 *S-N* testing method, using a small sample of 14 bolts to obtain a fatigue limit. Eight bolts are used for the inclined part of the test, successively reducing the stress amplitude until a non-failure occurs. The standard deviation of the points from the best fit line is used as the step size for the second part of the test, the staircase test, which uses the remaining six bolts. The average of the values for the staircase test is taken as the fatigue limit. This is based on the ISO standard[67], the JSME standard[68] and the JIS standard[69]. The Japanese standards are both based on the ISO standard, which is itself based on the British Standards [63,64,65].

2.3.3 Effect of Mean Stress

The effect of mean stress on fatigue limit has been described by the Goodman line[70], the Soderberg line[71] and the Gerber parabola[71], and these have been widely used for un-notched specimens, or with an appropriate stress concentration factor for notched specimens. Although these generally work well for simple geometries, their application to bolts has not been subjected to much experimental verification.

Patterson[72] compared some of these methods for predicting bolt fatigue limits. The approach was to predict fatigue limits from calculated stress concentration factors, using thread load distributions obtained from analytical theories. These results were then compared with results from experimental analysis. The calculated stress concentration factors were compared with results from three-dimensional photoelastic tests, and calculated fatigue limits were compared with fatigue tests.

Burguete and Patterson[3] also looked into the effect of mean stress on the fatigue life of bolts. In addition to the theories predominantly used for un-notched specimens compared by Patterson, models by Gunn[73] and Cook[71] which deal more specifically with notched specimens were compared. It was found that both the models that deal with notched specimens fitted the data far more closely than the general models, with Gunn being slightly more accurate, but Cook being more conservative. A new equation was proposed for high mean stress ($\sigma_m \geq S_y$) which fits the data well.

2.3.4 Fatigue of Bolted Joints

The analysis of bolted joints is even more complex than for bolts themselves as other factors have to be considered, such as stiffnesses of the clamped parts and bolts and preloads. Hagiwara and Yoshimoto[74,75] performed work in this area, and proposed a method for calculating the fatigue life with some factor of safety, and the relationship between bolt load and fatigue limit. However, they admit that the great variability of parameters makes it difficult to evaluate the fatigue strength.

Hagiwara and Yoshimoto also looked at the Haigh diagram for the effect of mean stress. They included lines for $\sigma_m = \sigma_a$ and $\sigma_m + \sigma_a = \sigma_{uts}$, questioning the relevance of bolt fatigue data for $\sigma_m < \sigma_a$. Unlike Cook[71], but like Burguete and Patterson[3], they believe that the fatigue limit does not simply drop to zero when $\sigma_m > \sigma_y$.

The effect of eccentric clamping and loading on fatigue limit has been investigated by Nakagome *et al*[76]. The distance between the clamping position (the bolt) and the loading position, distance a in Figure 2.7, was varied. It was

found that the greater the distance between the two, the lower the fatigue limit. The performance of the bolted connection was predicted from the fatigue limit diagrams for single bolts. The theoretical and experimental results showed close agreement.

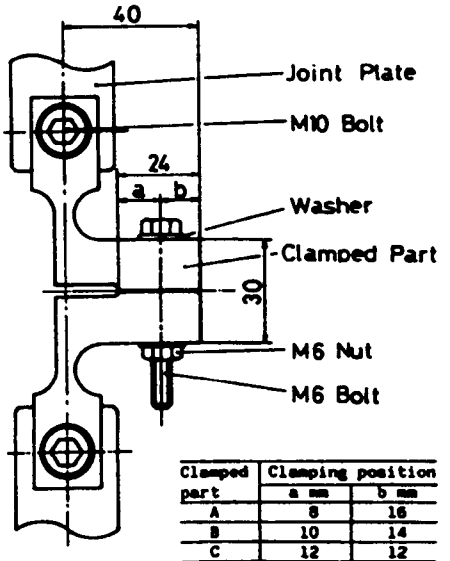

Clamped part	Clamping position a mm	b mm
A	8	16
B	10	14
C	12	12
D	14	10
E	16	8

Figure 2.7 Shape and size of bolted connection used by Nakagome *et al* (taken from Nakagome *et al*[76])

2.4 Bolted Joints

2.4.1 Axially Loaded Joints

Rötscher[77] was the first to describe an analytical method for defining joint stiffness in 1927. He proposed that the joint stiffness could be modelled as a simpler equivalent system, namely the frustum of a cone. This in turn could be modelled as an equivalent cylinder with a diameter equal to the mid point of the frustum line.

Later, the analysis was improved by ten Bosch[78], Bach and Findeisen (referred to in Stuck[79]) by integrating the cone instead of replacing it with a cylinder. This was an improvement on Rötscher's cone that tended to overestimate the joint stiffness, especially if the joint thickness was greater than the bolt hole diameter.

The issue of the point of application of the load was considered by Samonov[80] in 1966. He said that as the effective point of application of the load got nearer to the joint interface, the joint stiffness increased. If the load is applied at the interface the load only acts to reduce the interface pressure and has no effect on the bolt. Conversely, if the force is applied at the bolt head, the bolt 'sees' all the applied load and the joint members have no effect.

In 1976, Motosh[81] reviewed several papers presenting methods of determining joint stiffness and compared them to the experimental results of Fritsche[82] and Stuck[83]. The results of Birger, Vitkup, and Weiss and Wallner (all referred to via Stuck[83]) are the closest to the experimental results. They all use the hypothesis that the joint can be modelled by a semi-infinite plate with loading on an annular area. Motosh proposed a simplified method for calculating the joint stiffness. He used the assumptions made by Fernlund[84] and the photoelastic results of Boenick[85] to propose that there is a spheroidal or conical envelope for the equivalent system. A fourth order polynomial is then defined to describe the joint axial stress as a function of radius and distance from the joint surface. From the resulting expression for compressive stress, the deflection and therefore the stiffness of the joint can be calculated using Hooke's law. These theoretical results show closer relation to the experimental work of Stuck[83] and Fritsche[82] than any of the other reviewed models.

Recently, the non-linear aspects of bolted joints have been studied. Hagiwara[86] was the first to suggest that non-linearity exists in concentric joints, as it does in eccentric joints. He stated that joint separation is gradual and during separation the stiffness is non-linear. Experimental work on two bolted joints confirm this behaviour and show that the non-linear section is larger for joints of larger diameter.

Grosse and Mitchell[87] performed finite element analyses on bolted joints in 1990, and assessed the appropriateness of the current linear theory. A variety of loading conditions were considered, such as shear loading, bending moment loading, combined loading and different friction coefficients at the interfaces. Their main conclusions were that joint stiffness is not linear with applied load, and that there is a beneficial effect due to bending for low to medium loads, which becomes detrimental at higher loads.

2.4.2 Eccentric Loading

The earliest research into the behaviour of eccentrically clamped and/or loaded joints was reported by Beitz and Neuendorf[88] and Junker and Wallace[89], both in 1974. Beitz and Neuendorf studied the load deflection behaviour of eccentrically loaded joints to provide a simple mathematical model that could be used to easily calculate joint behaviour. The simple model used in the Guideline VDI 2230[90] (two springs for joint and bolt) was not applicable to this more complex case but the equations were sufficiently simple to not need computer support. The method can be expanded if the restriction is limited to the section of cantilever beams, where the beams replace the joint members. The model then needs computer support and a program for this was written by Beitz and Neuendorf.

However, Thomala[91] claimed that the methods proposed in the Guideline VDI 2230[90] were still not ideal as it overestimated the joint compliance, thus leading to the use of unnecessarily large bolts. He modified the formulae and got more accurate values for joint load.

Later work by Junker and Wallace[92] is perhaps more useful as it concentrates on the bolt load in an eccentrically loaded bolted joint, and it has been expanded by Boys and Wallace[93] to the design of a bolt tightening system. A new bolted joint diagram has been developed which contains a new line from the origin, offset from the bolt stiffness line. This new line is the lower limit for the applied load as opposed to the x-axis as used in the classical diagram. The new line is calculated empirically, the details of which are described in the Guideline VDI[90].

More recent work in this area was performed by Nakagome *et al*[94]. They developed a simple method for the calculation of joint stiffness and bolt load when eccentrically loaded. Theoretical formulae were developed for four different areas; for the case of joint separation, when one side is at the separation limit, after separation of one side and in the case of full separation. Comparison with their experimental results (using static load and strain gauges) showed good correlation with their theoretical results. They conclude that an increase in eccentricity, or a reduction in initial clamping force leads to a greater bolt load and therefore would be detrimental to the fatigue life.

Burguete[95] provided a comprehensive review on the subject of bolted joints and proposed a classification system for bolted joints. This system looks at the effect of the joint on the bolt, rather than from the point of view of the joint geometry. Three different classes are proposed; axisymmetric joints with concentric loading, axisymmetric joints with eccentric loading and eccentric joint with eccentric loading.

The only work to look in detail at the effect of eccentrically loading bolted joints on the stress with the bolt was performed by Burguete and Patterson[96]. Using three-dimensional photoelastic analysis of eccentrically loaded epoxy resin blocks, clamped by an epoxy resin bolt, the stress concentration factors (SCFs) were found at the thread roots. The results show that the peak SCF is very different to that obtained by simple bending[33]. Also the distribution of SCFs is more spiky for real bending, than for simple bending. The most likely reason for this is that the level of bending achieved in the bolt is much lower than for simple bending.

Although bolted joints are now better understood, the load occurring in the bolts is still largely unknown. Therefore, more research should be performed on the subject of bolt load in bolted joints, especially eccentrically loaded joints.

2.5 Objectives

From the review of the literature, the following areas have been highlighted for research:

- The effect of eccentric loading on the fatigue life of bolts.
- The crack shape in bolts subject to axial and eccentric loading.
- The stress intensity factors for crescent shaped cracks in bolts.
- The development of a three-dimensional finite element model.

Chapter 3

The Determination of Infinite Life

3.1 Introduction

The number of cycles over which it is appropriate to run fatigue tests is an important consideration for the researcher. There is a compromise to be reached between the length, and therefore cost of the tests, and the accuracy. The 14 *S-N* testing method described by Ohashi *et al*[66] uses 5×10^6 cycles to represent infinite life. If a bolt survives to 5×10^6 cycles, the test is terminated, and it is assumed that the bolt would have survived indefinitely. However, Burguete and Patterson[3] shortened this to 2×10^6 cycles for their *S-N* tests. This investigation into the effect of the number of cycles taken to represent infinite life has shown that there is a statistically significant difference between using 2×10^6 cycles and 5×10^6 cycles.

3.2 Method

The method employed was as similar as possible to that used by Burguete and Patterson[3] to ensure a fair comparison of results. The only differences between the tests was that a different batch of nut and bolts were used and the number of

cycles to termination of the tests. In these tests, the bolts were cycled to 5×10^6 cycles before the tests were stopped and the bolts were assumed to survive indefinitely.

Standard high tensile bolts bought "off the shelf" were used to provide realism and reduce cost and time. The bolts used were M12 × 120 Metric coarse thread, high tensile grade 8.8 according to BS 3692 and they were used with corresponding M12, grade 8 nuts. The threads of the bolts were manufactured by rolling, rather than cutting the threads, which is likely to result in residual stresses in the threads. Before being tested, the bolts, nuts and washers were cleaned in an ultrasonic cleaner using 1,1,1-Trichloroethane. The bolts were then brushed with wire wool to remove any remaining dirt and checked for thread damage. Any bolt on which a nut could not freely spin was rejected. The remaining bolts were then oiled using a general-purpose oil before being tested, to prevent corrosion and to provide standard lubrication.

The bolts were tested in a 100kN Amsler vibrophore machine, as shown in Figure 3.1. The grips were designed to load the bolts axially, with not bending induced, but with was not checked. It is likely that some bending was present in the bolts, caused by the nuts, but using the same testing method as Burguete and Patterson[3] was more important than eliminating bending. The tests were run at a frequency of approximately 100 Hz. The washers were not perfectly flat but were slightly 'dished' so care was taken to ensure the orientation of the washers was the same for every test. They were positioned so that the concave face lay against the grip. The nuts were positioned in the middle of the threaded portion of the bolt.

A series of eight *S-N* curves was obtained at various different values of mean stress in the range $\sigma_a < \sigma_m < S_y$, where:

S_y is the yield strength of the material (measured by Burguete and Patterson and found to be 756 MPa)

σ_a is the stress amplitude

σ_m is the mean stress.

Within this range, the fatigue limit is accepted to be constant[3,71]. Each *S-N* curve was obtained in a similar way to that described by Ohashi *et al*[66]. The sloping part of the *S-N* curve is obtained by progressively reducing the stress amplitude

until a non-failure occurs (defined as survival beyond 5×10^6 cycles). A best-fit line is then fitted through the data and the standard deviation is taken as the step size for the staircase section of the test.

The staircase section is produced by testing bolts at stress amplitudes dependant on the outcome of the previous test. If a bolt fails, defined as complete fracture of the bolt, the stress amplitude for the next test is reduced. If a bolt does not fail after 5×10^6 cycles the test is stopped and the bolt is assumed to have survived. It is then discarded and the next new bolt is tested at a stress amplitude one step size higher. The fatigue limit is then taken to be the average of the stress amplitudes used for the staircase test. An example is included in Table 3.1 to illustrate the procedure.

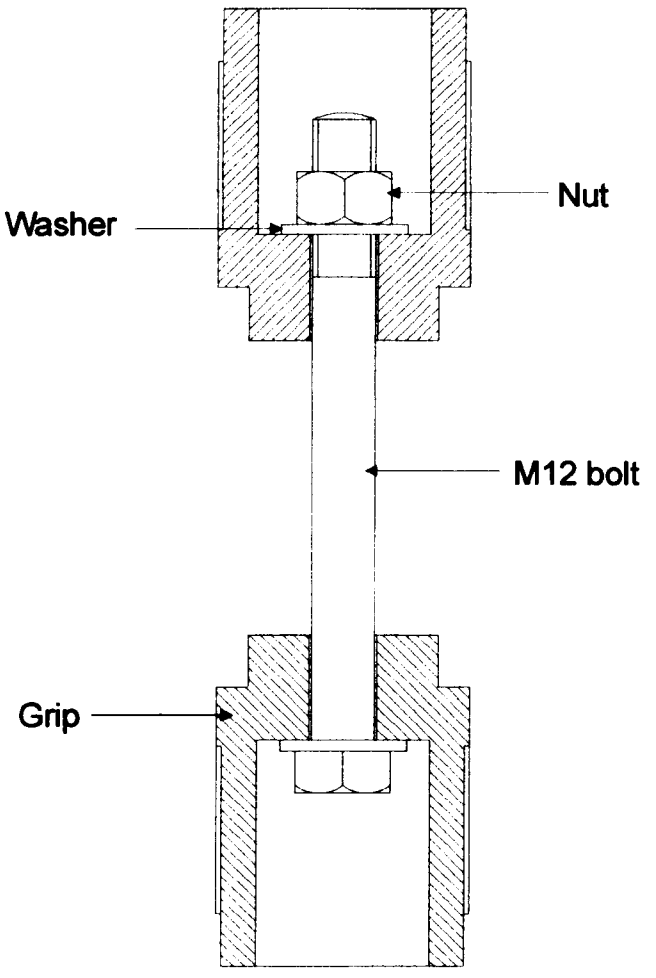

Figure 3.1 Loading arrangement for axially loaded bolts

Load Range (kN)	Cycles	Notes
8.0	$>5x10^6$	Initial non-failure. Value not included in fatigue limit calculation. Load range increased by step size for next test.
9.2	3,612,100*	Failed - Decrease load range for next test
8.0	$>5x10^6$	Survived - Increase load range for next test
9.2	$>5x10^6$	Survived - Increase load range for next test
10.4	1,242,600	Failed - Decrease load range for next test
9.2	3,277,900*	Failed - Decrease load range for next test
8.0	NOT TESTED	Not tested, but value used for fatigue limit calculation

*** Bolts that would have been counted as non-failures using 2×10^6 cycles to represent infinite life**

Table 3.1 Example of procedure for the staircase section of the S-N plots

3.3 Results

The S-N plots for each series of tests are shown in Figure 3.2 to Figure 3.9. The legend for all the plots is shown below. It should be noted that the numbers of cycles to failure on the x-axis do not apply to the staircase parts of the tests. The points in this part are plotted in the order in which they were performed.

The results from this series of tests were compared to those of Burguete and Patterson[3] who performed similar tests but used 2×10^6 cycles to represent infinite life. Using the higher number of cycles resulted in a fatigue limit 9% lower. The confidence level associated with this difference is 99%.

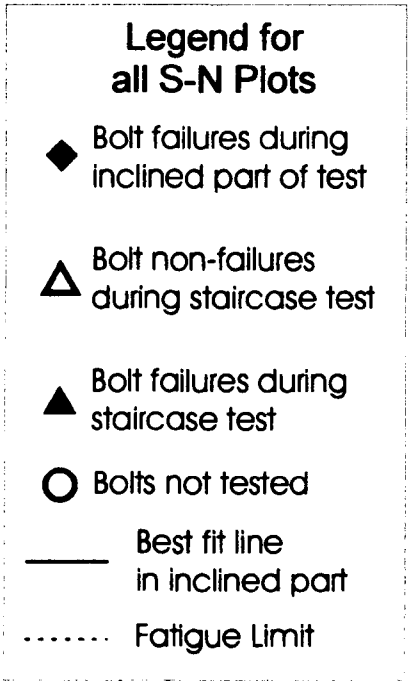

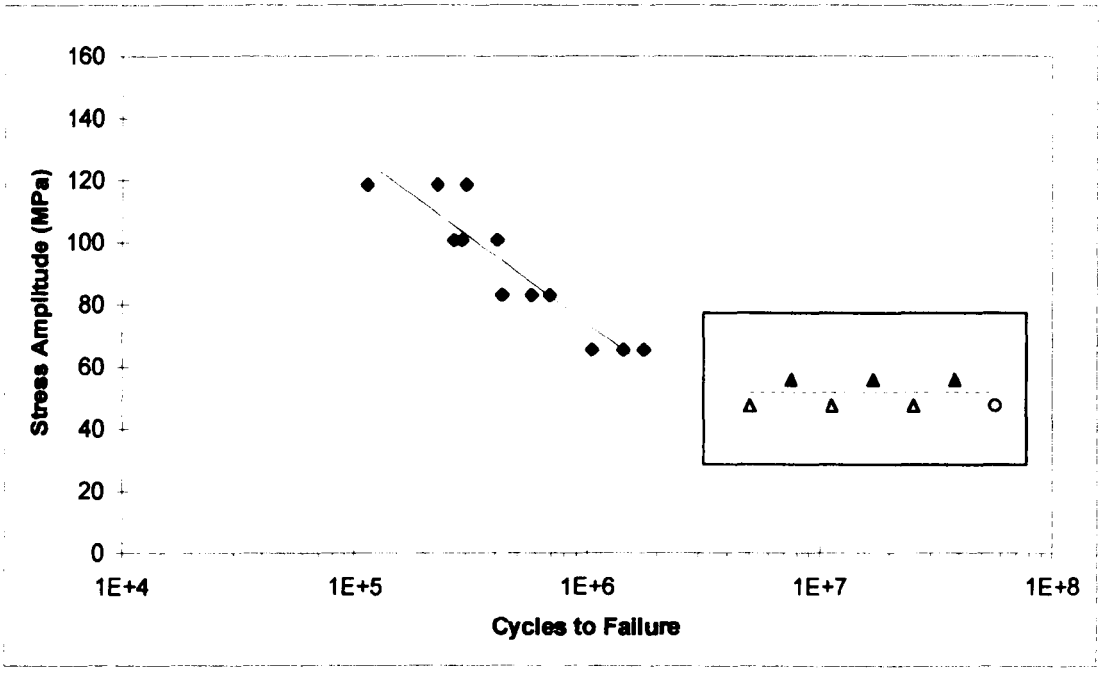

Figure 3.2 S-N Plot for mean stress of 166 MPa

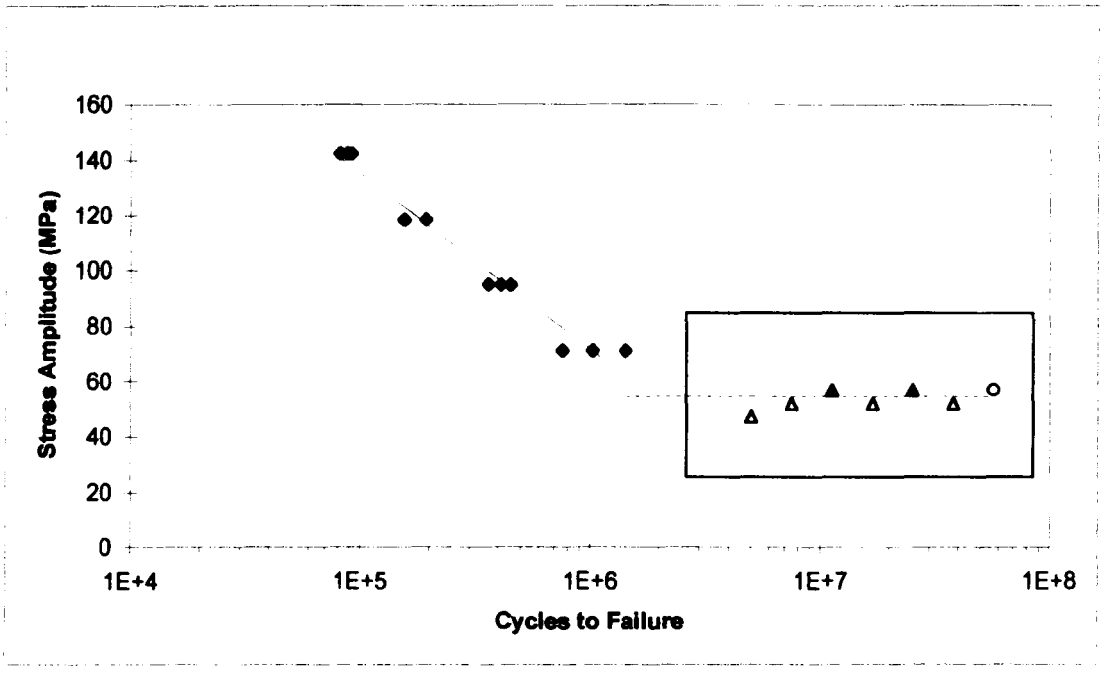

Figure 3.3 S-N Plot for mean stress of 237 MPa

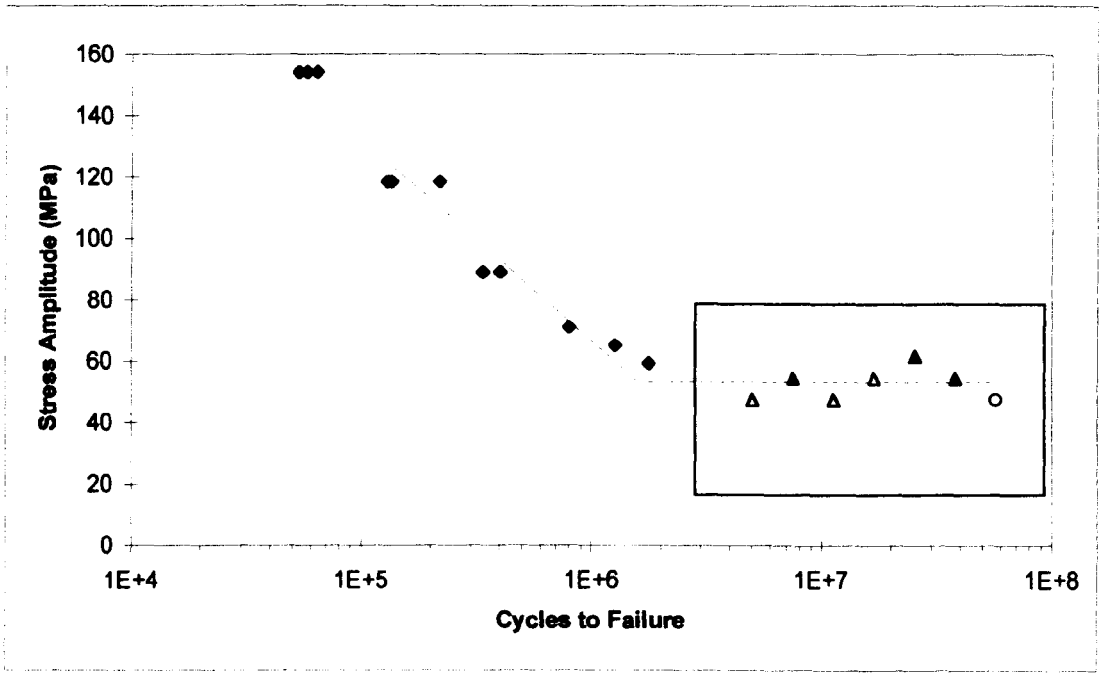

Figure 3.4 S-N Plot for mean stress of 285 MPa

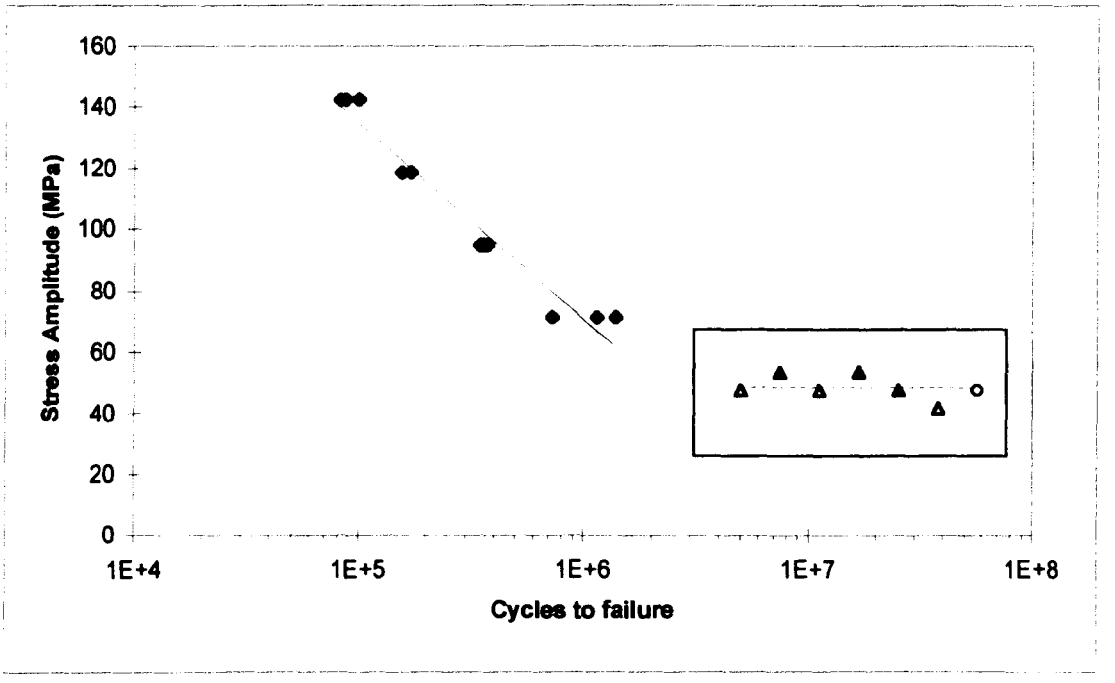

Figure 3.5 S-N Plot for mean stress of 356 MPa

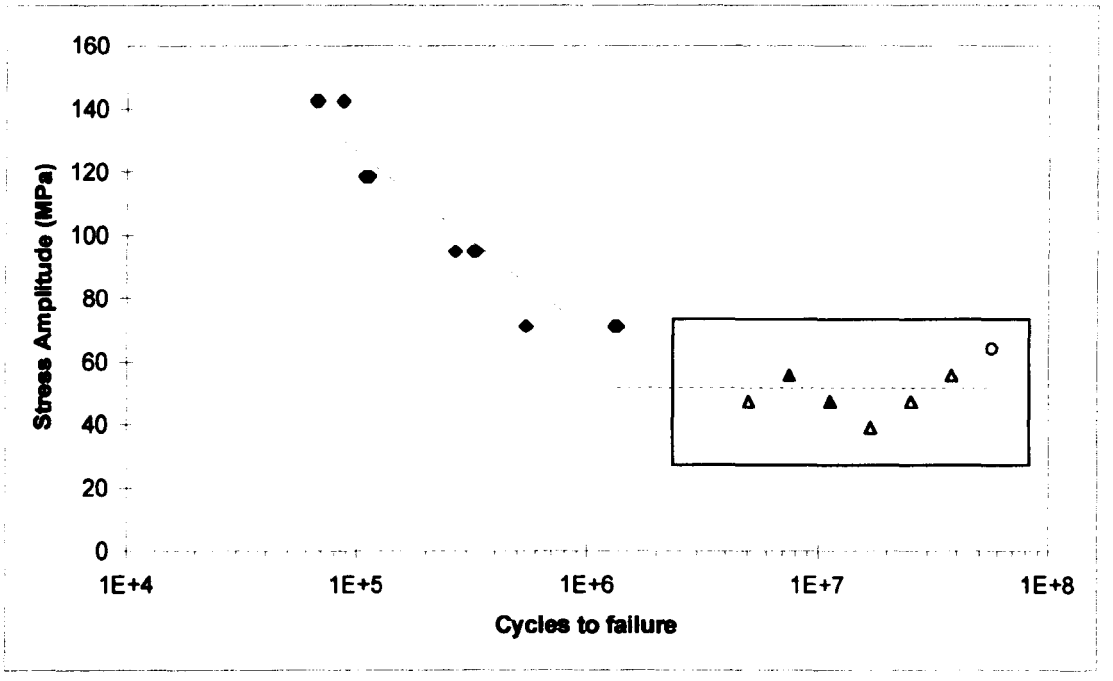

Figure 3.6 S-N Plot for mean stress of 415 MPa

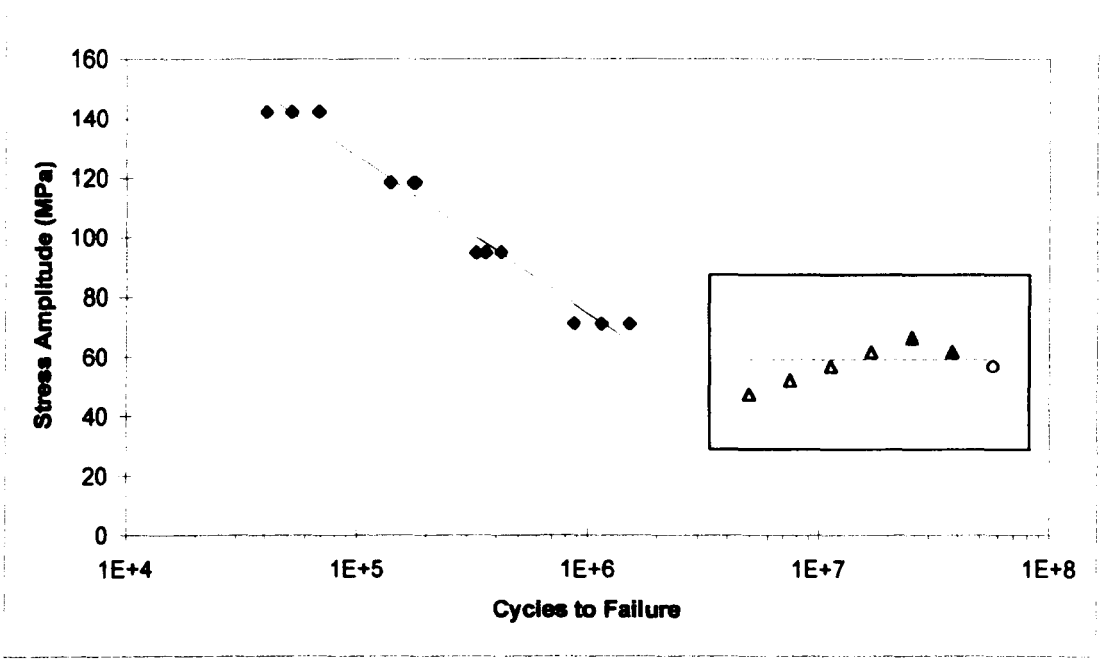

Figure 3.7 S-N Plot for mean stress of 475 MPa

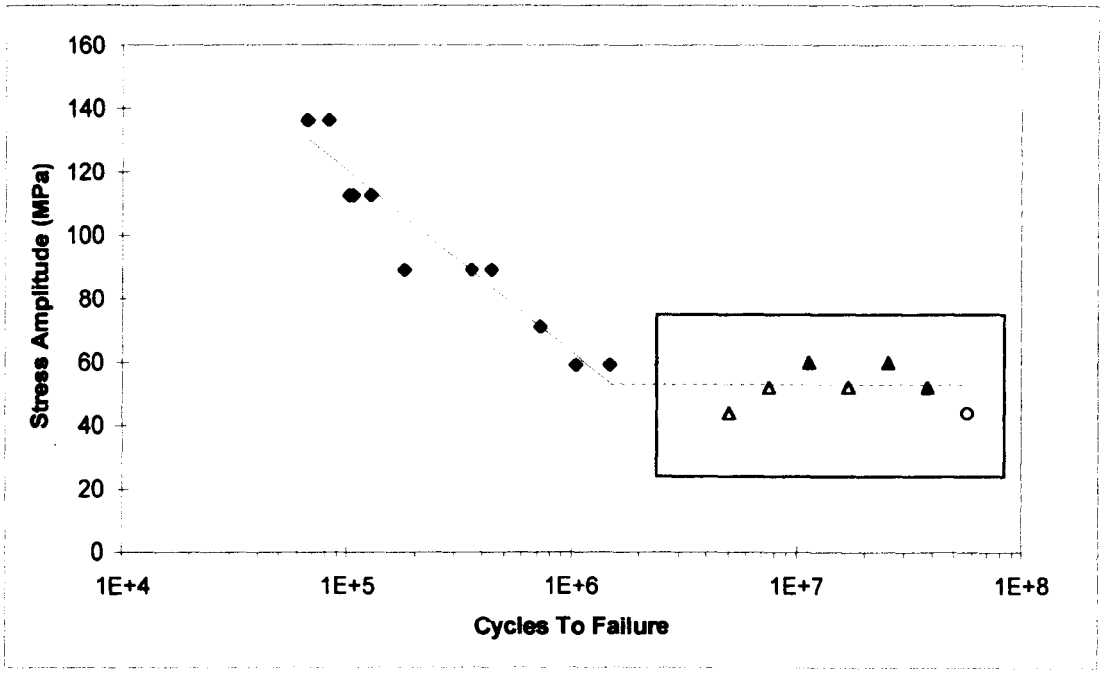

Figure 3.8 S-N Plot for mean stress of 534 MPa

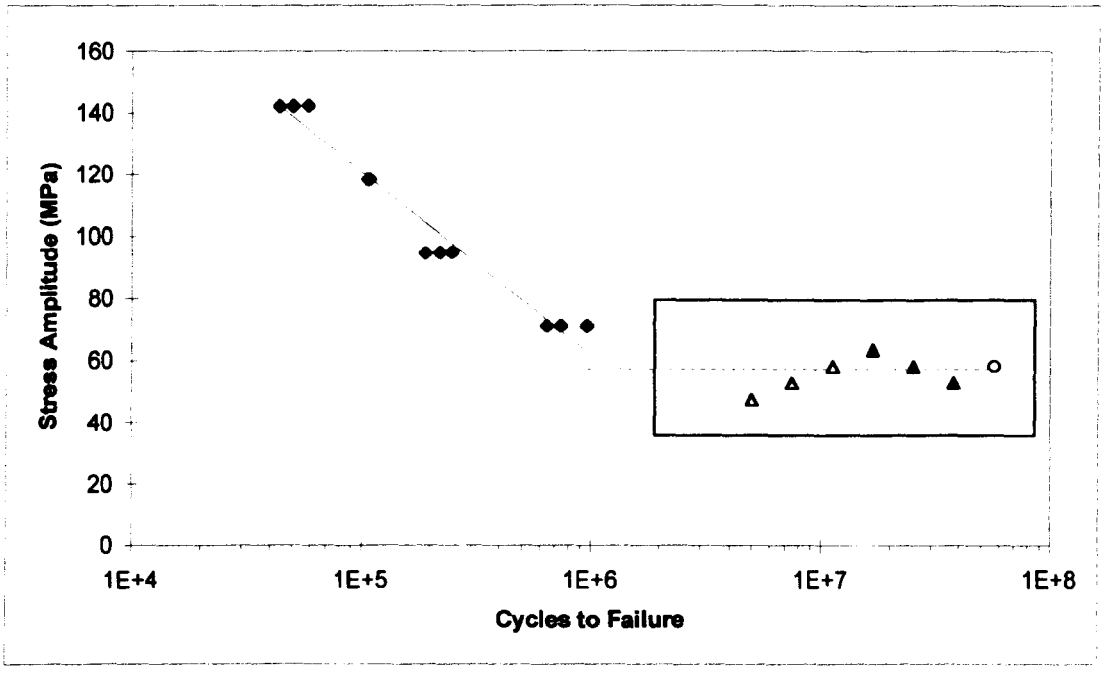

Figure 3.9 S-N Plot for mean stress of 712 MPa

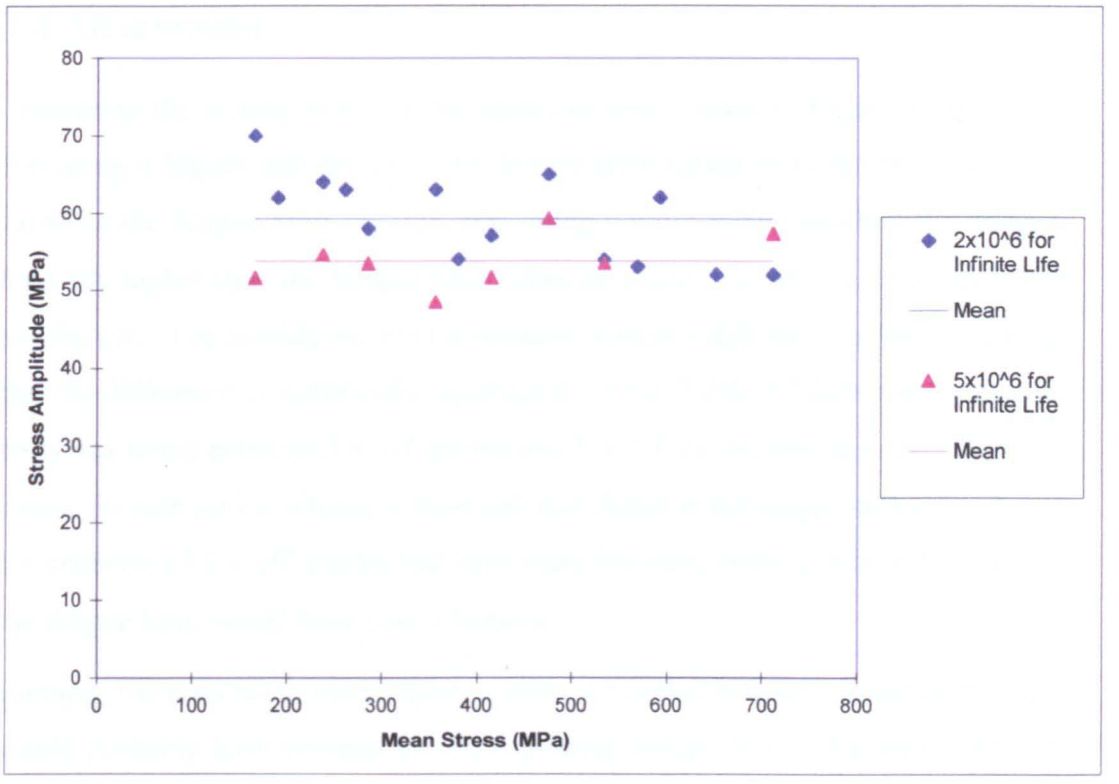

Figure 3.10 Comparison of fatigue limits using 2×10^6 (Burguete and Patterson[3]) and 5×10^6 cycles (present investigation) to represent infinite life

Mean Stress (MPa)	Fatigue Limit (MPa)	Standard Deviation (Staircase step size) (MPa)	No. of bolts failing between 2×10^6 and 5×10^6 cycles
166	51.6	7.12	3
237	54.6	4.74	2
285	53.4	8.30	2
356	48.4	5.93	3
415	51.6	8.30	1
475	59.3	4.74	2
534	53.5	7.71	1
712	57.2	5.34	1

Table 3.2 Main results and number of bolts failing between 2×10^6 and 5×10^6 cycles for each staircase test

3.4 Discussion

Comparing the results from the two series of tests shown in Figure 3.10, shows that using a higher number of cycles before terminating tests results in a lower value for the fatigue limit. In this case, using 2×10^6 cycles resulted in a fatigue limit 9% higher than the fatigue limit obtained using 5×10^6 cycles to represent infinite life. The confidence level associated with this difference is 99%, showing that the difference is statistically significant. Also, Table 3.2 lists the number of bolts that failed between 2×10^6 cycles and 5×10^6 cycles for each level of mean stress. In each series of tests, at least one bolt failed in the range, indicating that if the criterion of 2×10^6 cycles had been used for these tests, a different value for the fatigue limit would have been obtained.

Running the tests to an even higher number of cycles before terminating the test would probably have resulted in an even lower fatigue limit. An absolute value for the fatigue limit can not be obtained because tests can not be performed to true infinite life and this investigation has shown that the length of test does have an effect on the fatigue limit. BS 3518 Part:(1963)[64] recommends using 10×10^6 cycles for fatigue tests of steel components. However, the more recent standard, BS 7608:(1993)[1] recommends using 2×10^6 cycles and reducing the result by two standard deviations. Two standard deviations of the results for 2×10^6 cycles represents a decrease in fatigue limit of approximately 20%, taking the fatigue limit well below that obtained by using 5×10^6 cycles. Therefore, using 2×10^6 cycles to represent infinite life can lead to a safe estimation of the fatigue limit, provide an appropriate allowance is made.

To avoid the problem of choosing a number of cycles to discontinue tests, the eccentric fatigue tests (described in section 4) will be quantified by the difference in stress amplitude at a fatigue life of 2×10^5 cycles. All the fatigue tests will be performed at stress levels that will definitely produce failures removing the need to choose a number of cycles to represent infinite life. Also, the tests will be much shorter, so more tests can be performed in the given time.

Chapter 4

Eccentric Fatigue Tests

4.1 Introduction

The effect of eccentric loading on the fatigue life of bolts is still largely unquantified. The aim of this set of tests was to determine how eccentric loading affects fatigue life. A series of *S-N* curves have been produced for different levels of eccentricity. Twenty bolts were cyclically loaded until failure at different levels of stress amplitude for each *S-N* curve. These curves were then compared to the corresponding curve obtained for axially loaded bolts. The difference between the curves were quantified by the difference in stress amplitude at 2×10^5 cycles. The stress amplitudes at which the bolts are loaded was chosen to give life times close to this value, between 1×10^5 and 4×10^5 cycles. The levels of eccentricity were expressed in terms of the distance of the bolt axis from the loading axis normalised by the nominal diameter of the bolt.

Before the fatigue tests were performed the grips used to apply the eccentric loading were thoroughly tested to deduce the level of bending transferred to the bolt. It was found that poor quality nuts could cause bending in the bolts, and this was also investigated.

4.2 Method

The nuts and bolts used were similar to those used for the investigation into infinite life described in the previous chapter. The only difference being that in this case the bolts were slightly shorter, 80 mm instead of 120 mm. They were prepared in exactly the same way. The nuts were subjected to a far more stringent quality control procedure, which is described in full in section 4.5.

The bolts were tested in a 100kN Amsler vibrophore machine. Special grips were designed to apply the load eccentrically and are shown in Figure 4.1. The eccentricity was varied by using a range of different inserts with the bolt holes at different distances from the centre. The inserts were prevented from rotating in the grips by using a grub screw. The eccentricities applied by the grips are shown and discussed in section 4.4.

For each level of eccentricity, twenty bolts were cyclically loaded to failure at different stress amplitudes to obtain an S-N curve. The levels of stress amplitude were chosen to obtain lifetimes of between approximately 1×10^5 and 4×10^5 cycles.

To determine if any trends in the values were present, the Pearson product moment correlation coefficient, r, was calculated. The value of this coefficient ranges from -1 to 1 and reflects the extent of a linear relationship between two sets of data. Values of -1 and 1 represent a perfect correlation for negative and positive gradients respectively, and a value of 0 reflects no correlation. The equation for r is:

$$r = \frac{n(\Sigma XY) - (\Sigma X)(\Sigma Y)}{\sqrt{\left(n\Sigma X^2 - (\Sigma X)^2\right)\left(n\Sigma Y^2 - (\Sigma Y)^2\right)}} \qquad \textbf{Equation 4-1}$$

where n is the number of data points.

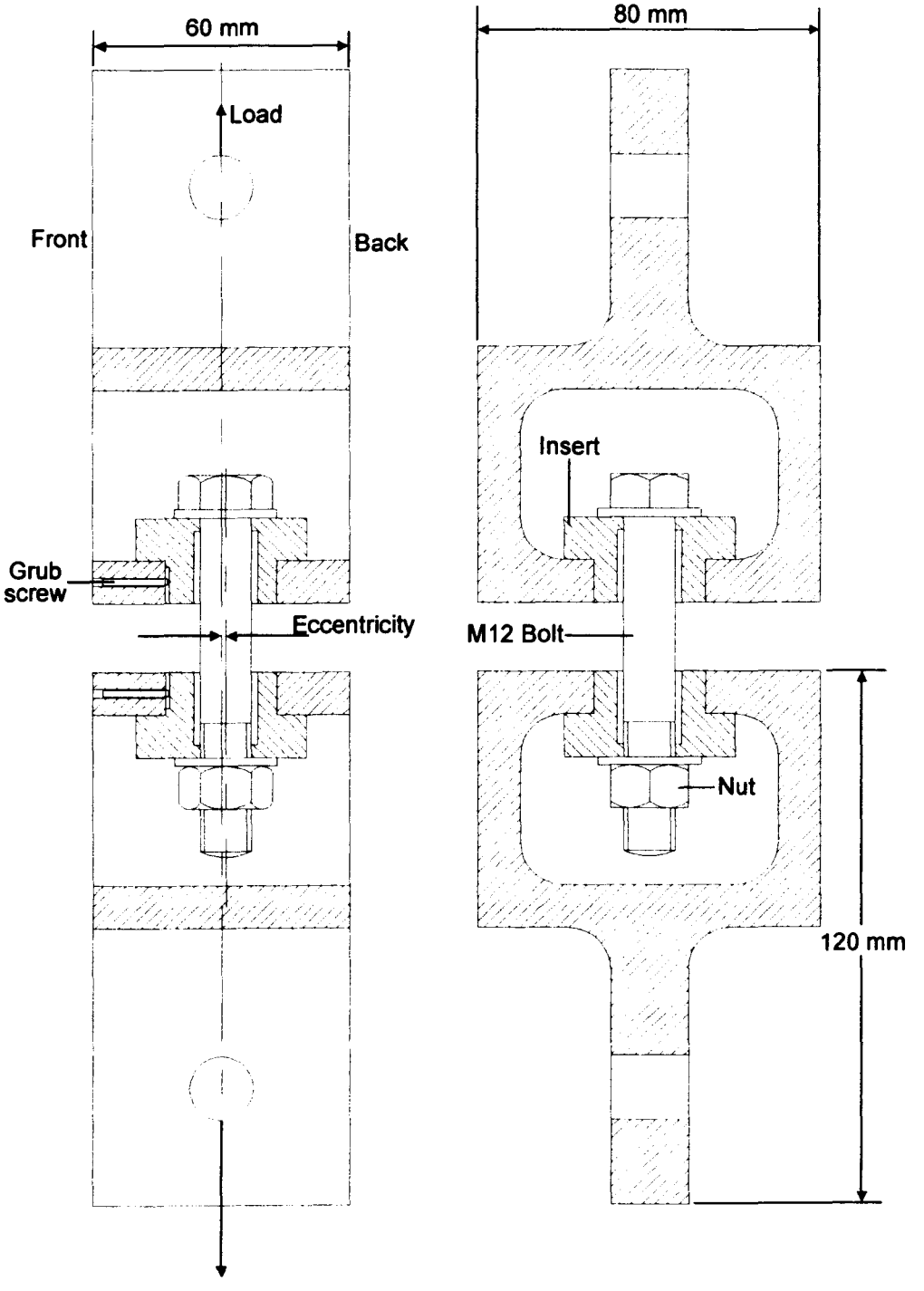

Figure 4.1 Design of grips to apply eccentric load.

4.3 Measuring the Bending in a Bolt

The bending caused by the eccentric grips varies with load. The relationship between bending and load was investigated using an instrumented bolt before fatigue tests were performed. The instrumented bolt had four small flats machined half way down the unthreaded shank of the bolt. Strain gauges were then applied to these flats, aligned with the axis of the bolt. The gauges were labelled north, east, south and west, and the bolt was positioned so that the north gauge faced the front of the grips. The inserts were designed to hold the bolt slightly towards the back of the grips, therefore applying bending in the N-S plane with a greater load being applied to the north face.

4.3.1 Determination of Direction and Magnitude of Bending

Although the north gauge was aligned with the front of the grips, so it would experience the highest load, it could not be assumed that this would lie in the plane of bending or be the highest strain in the bolt. Misalignment of the instrumented bolt, eccentricity caused by the nut or unintentional bending caused by the grips would cause the bending to lie in a different plane. This causes the north and south gauges to experience a lower bending strain as they will no longer lie in the plane of bending. Figure 4.2 shows this graphically, with the angular error, δ. It is the readings from the east and west gauges that indicate that there is a misalignment. If no misalignment were present, these gauges would read the same value, equal to the axial strain. In the example in Figure 4.2, the east gauge, being slightly nearer the front of the grips, would read higher than the west gauge.

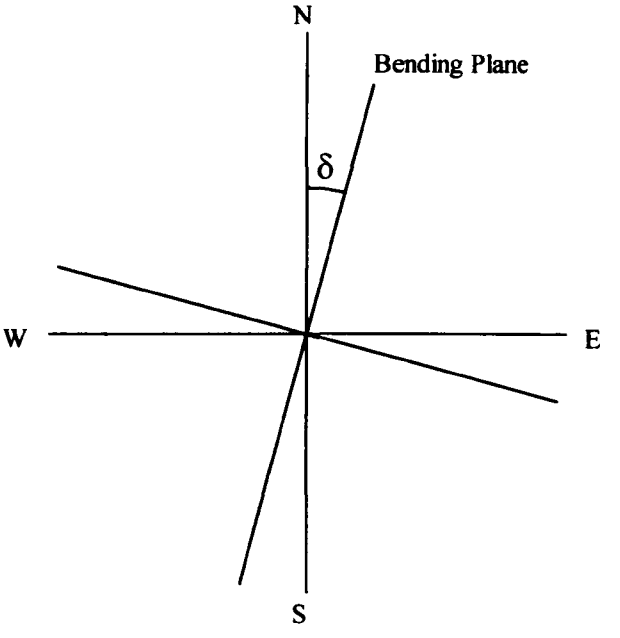

Figure 4.2 Misalignment of instrumented bolt with bending plane

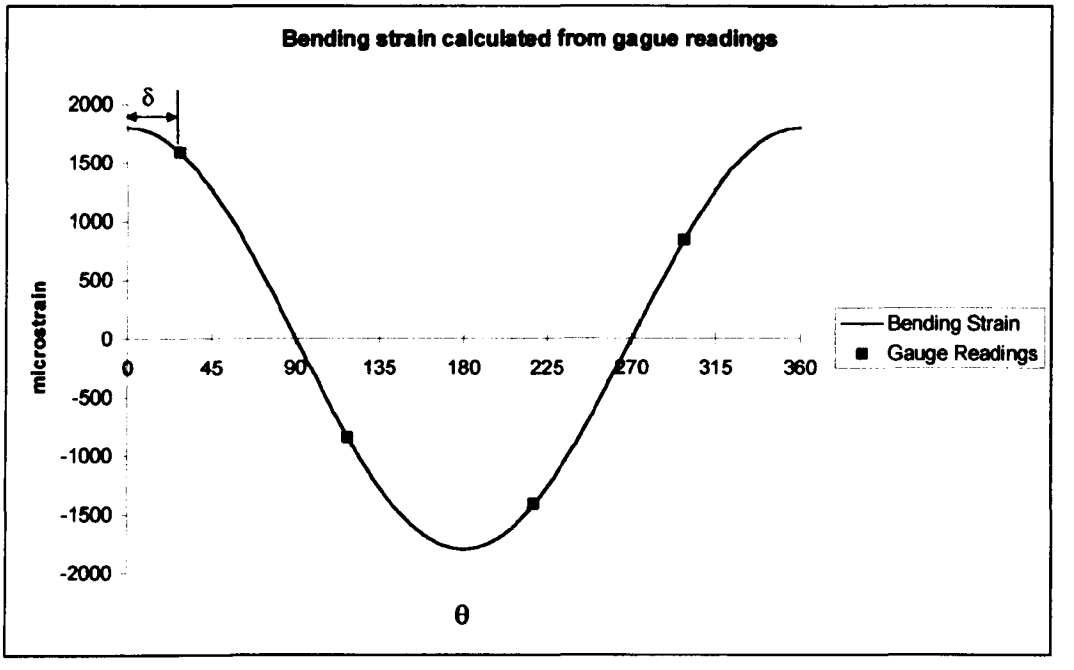

Figure 4.3 Typical bending strains around bolt and gauge readings

This error can be compensated for by calculating the angle of misalignment and then calculating the maximum bending strains. Subtracting the average strain from the measured strain gives the strains due to bending. This strain should vary sinusoidally around the bolt, as shown in Figure 4.3 and the strain, ε, at any point can be calculated as

$$\varepsilon = \varepsilon_{max} \cos(\theta) \qquad \textbf{Equation 4-2}$$

if 0° is defined as the point where maximum bending occurs.

Similarly, from Figure 4.2, it can be seen that, if δ is defined as the angle between the ε_{max} and ε_N, then

$$\varepsilon_N = \varepsilon_{max} \cos(\delta) \qquad \textbf{Equation 4-3}$$

$$\varepsilon_E = \varepsilon_{max} \cos\left(\pi/2 + \delta\right)$$
$$\varepsilon_E = \varepsilon_{max} \sin(-\delta) \qquad \textbf{Equation 4-4}$$

where ε_N and ε_E are the readings from the north and east gauges respectively.

Therefore, to determine δ

$$\frac{\varepsilon_E}{\varepsilon_N} = \frac{\varepsilon_{max} \cos(\delta)}{-\varepsilon_{max} \sin(\delta)}$$
$$\frac{\varepsilon_E}{\varepsilon_N} = -\tan(\delta) \qquad \textbf{Equation 4-5}$$
$$\therefore \delta = \arctan\left(-\frac{\varepsilon_E}{\varepsilon_N}\right)$$

Once δ has been found, calculating ε_{max} is simple, thus:

$$\varepsilon_{max} = \frac{\varepsilon_N}{\cos(\delta)} \qquad \textbf{Equation 4-6}$$

4.4 Grip Characteristics

4.4.1 Bending Caused by the Grips

The strains measured by the four gauges for the 2 mm eccentric inserts are shown in Figure 4.4. The east and west gauges show a linear relationship with load, as they are effectively measuring the axial load and should not experience any bending load. The east and west gauge readings are not identical, indicating that the instrumented bolt is not perfectly aligned with the plane of bending, as discussed in the previous section.

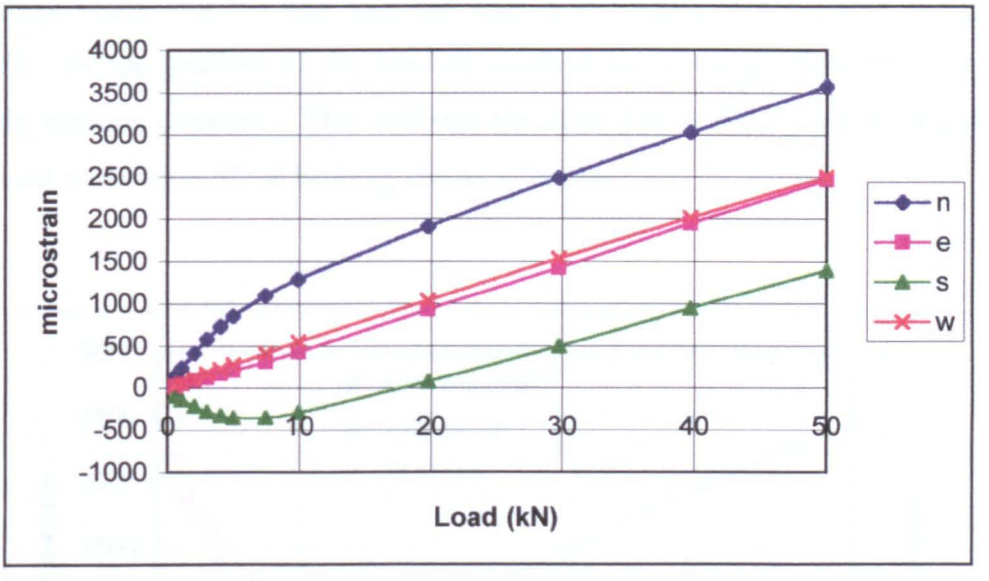

Figure 4.4 Gauge reading for the four strain gauges (2 mm eccentricity).

The north and south gauges show how much bending the bolt is experiencing and the values should be equidistant from the axial strain. Initially, the south gauge experiences compression as the load is applied because the axial strain is very low and the moment caused by the large eccentricity is high. Similarly, the north gauge reading increases very rapidly as the load is first applied. It is the north gauge reading that is likely to be the most significant in terms of the fatigue life of the bolt as the change in stress over the cyclic load range, and therefore, ΔK, the cyclic variation of the stress intensity factor, is normally greater.

Figure 4.5 shows the variation in bending with load expressed in terms of bending strain (difference between the maximum and minimum strains) and in terms of R_σ (ratio of bending strain to axial strain).

The eccentricity of the applied load produces a bending moment, P.e, where P is the applied load, and e is the distance between the load axis and the bolt axis. Assuming that the grip's surfaces, bolt head and nut face are all initially perpendicular to the axis of the bolt, the grips will swing as the load is applied, thereby bending the bolt. As the grips swing, however, the bolt axis moves towards the load axis and the eccentricity decreases. Therefore, the bending moment per unit load reduces as the load increases. This explains the steep gradient of bending strain against load for low loads in Figure 4.5, and how the gradient reduces as the bolt axis and load axis come closer together at higher loads. As the gradient of the bending strain reduces, the gradient of the axial strain remains constant. This explains the variation in the R_σ value, which is defined as the ratio of the bending and axial strains.

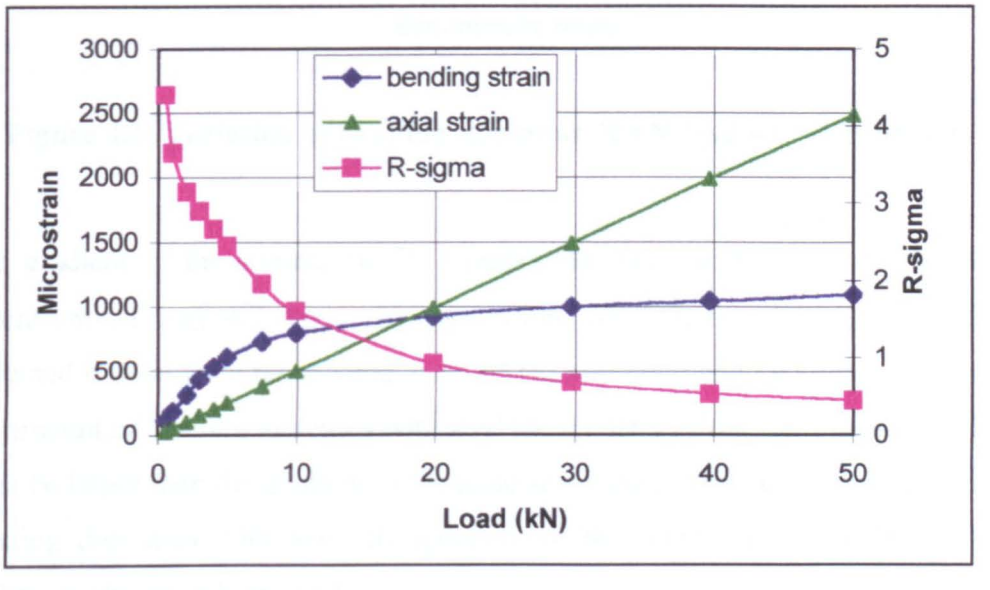

Figure 4.5 Bending and axial strains and R_σ (2 mm eccentricity)

The relationship between the bending strain and initial eccentricity can be seen in Figure 4.6 which shows a plot of the bending strain at 40 kN load against initial eccentricity. Above an eccentricity of 1 mm, the relationship is clearly linear

showing that the bending caused by the grips is proportional to the initial eccentricity. Below 1 mm eccentricity, the bending appears higher than would be expected and this is probably due to eccentricity caused by the nut used for these tests or some unwanted eccentricity caused by the grips.

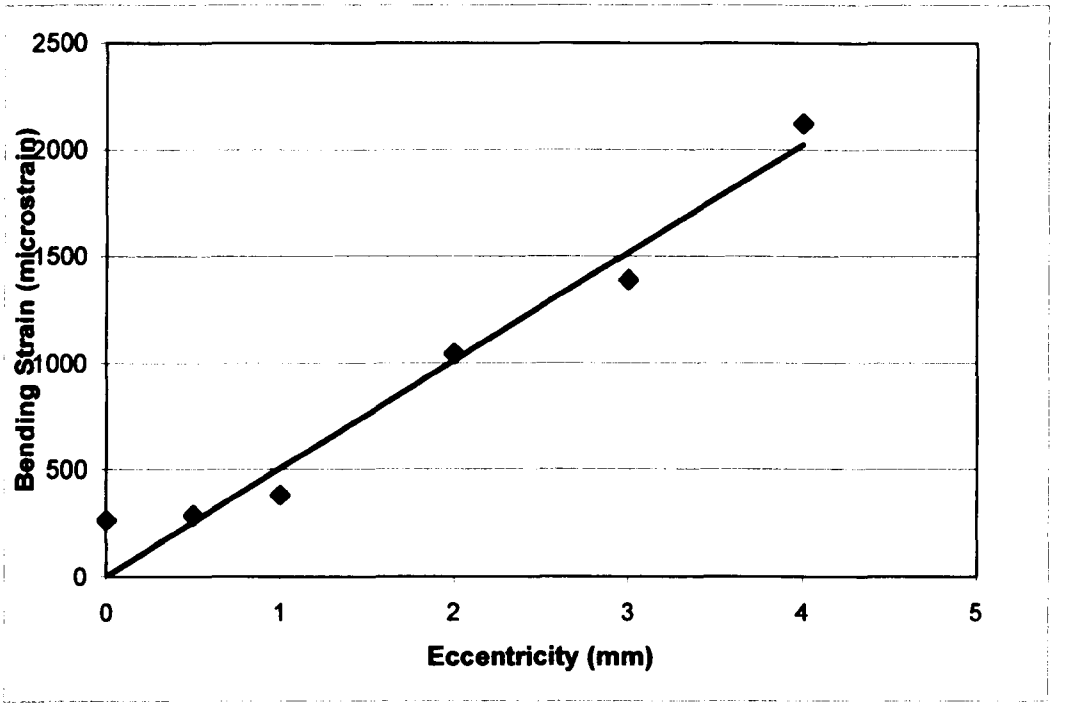

Figure 4.6 Variation of bending strains at 40 kN load with eccentricity

The gradient of the strains, $\partial\varepsilon/\partial P$, is important and varies with the amount of eccentricity. Figure 4.7 shows the axial strain, which is the strain that would be expected if there were no bending and also the minimum and maximum strains. If the amount of bending increases with load the gradient of the maximum strain line must be larger than the gradient of the axial strain line. However, if the amount of bending decreases with load, the gradient of the minimum strain line will be higher, as shown in Figure 4.8.

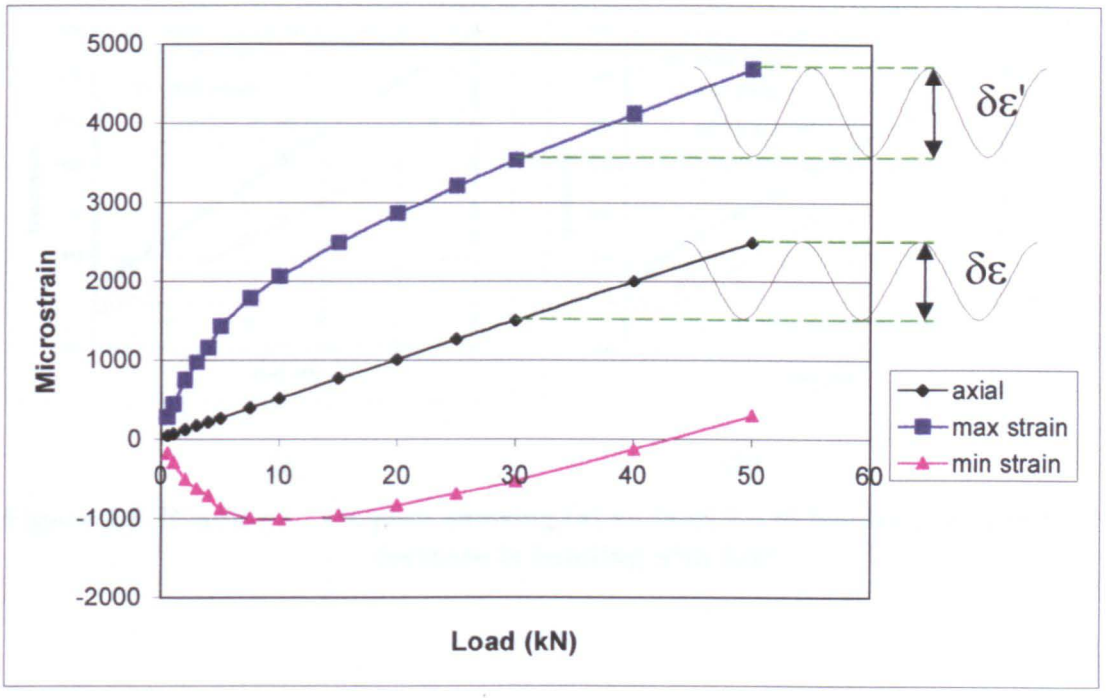

Figure 4.7 Definition of nominal strain, $\partial\varepsilon$, and local strain, $\partial\varepsilon$'

The maximum and minimum strains and the bending strains for all six sets of inserts are shown in Figure 4.9 to Figure 4.14. The largest gradients of the strain lines, $\partial\varepsilon'/\partial P$, between 30 and 50 kN are listed in Table 4.1. As just discussed, the largest gradient, $\partial\varepsilon'/\partial P$, need not occur for the maximum strain, ε_{max}. It is possible that the minimum strain, ε_{min}, could vary more with load over a certain load range. This did occur for the 0 mm eccentricity insert and therefore the gradient quoted is for ε_{min}. For all other levels of eccentricity, the quoted maximum gradient is for ε_{max}.

The different strain gradients indicate different stress amplitudes. The local stress amplitude is defined as the stress amplitude due to the highest strain gradient, $\partial\varepsilon'/\partial P$. The global stress amplitude is defined as the stress amplitude due to the axial strain gradient. These are both nominal stress amplitudes, as they do not take into account the stress concentration effects.

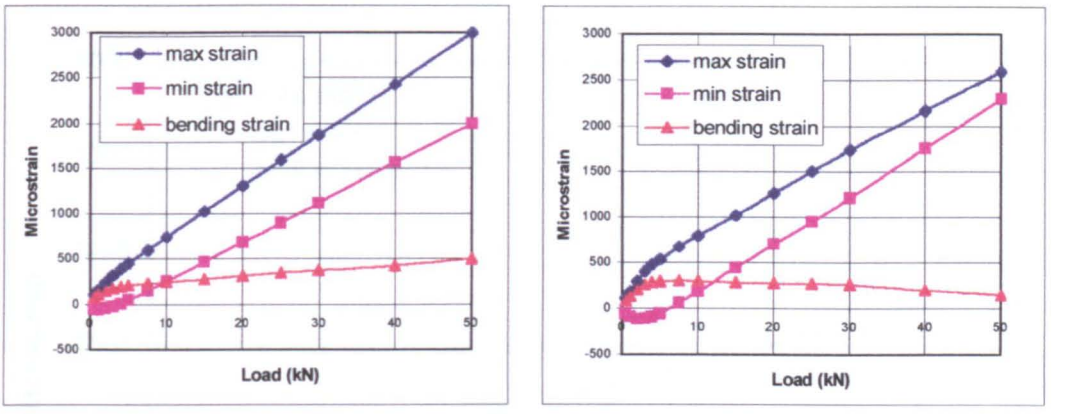

(a) (b)

Figure 4.8 Bending strain plots showing (a) an increase in bending and (b) a decrease in bending with load

Eccentricity (mm)	e/D	Maximum gradient of strain, $\partial\varepsilon'/\partial P$, between 30 kN and 50 kN (microstrain / kN)
0	0	51.5
0.5	0.04	51.6
1	0.08	52.9
2	0.17	54.6
3	0.25	55.9
4	0.33	57.2

Table 4.1 The maximum gradient of strain, $\partial\varepsilon'/\partial P$, for each set of inserts

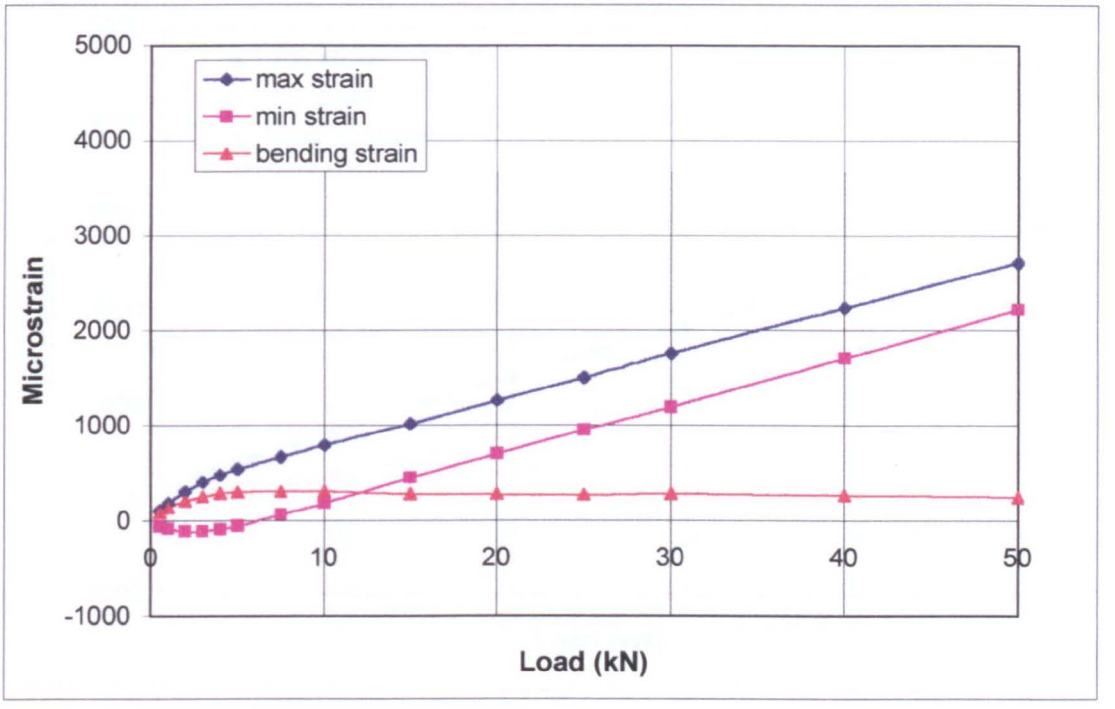

Figure 4.9 Strains caused by 0 mm insert (e/D = 0)

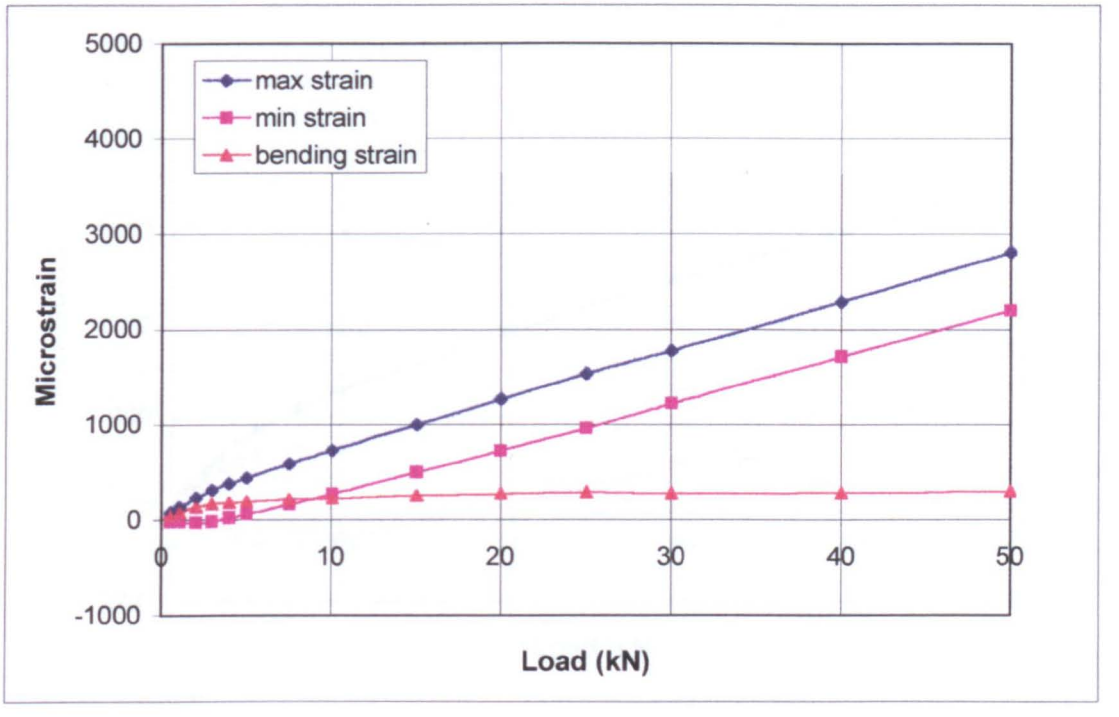

Figure 4.10 Strains caused by 0.5 mm insert (e/D = 0.04)

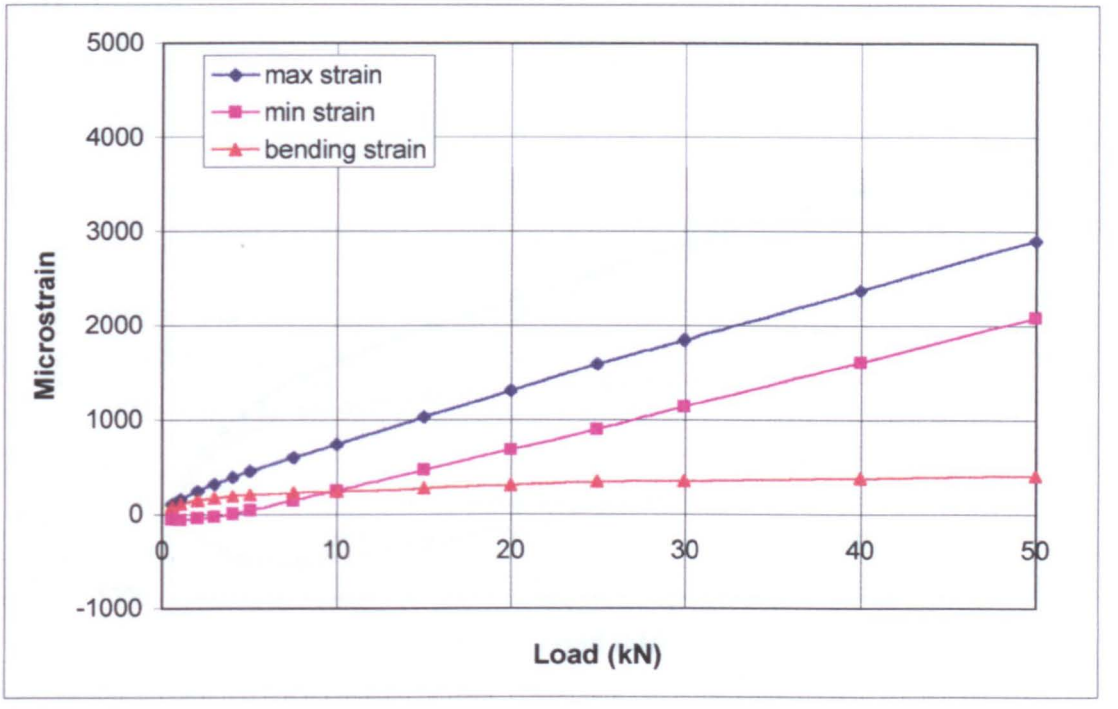

Figure 4.11 Strains caused by 1 mm insert (e/D = 0.08)

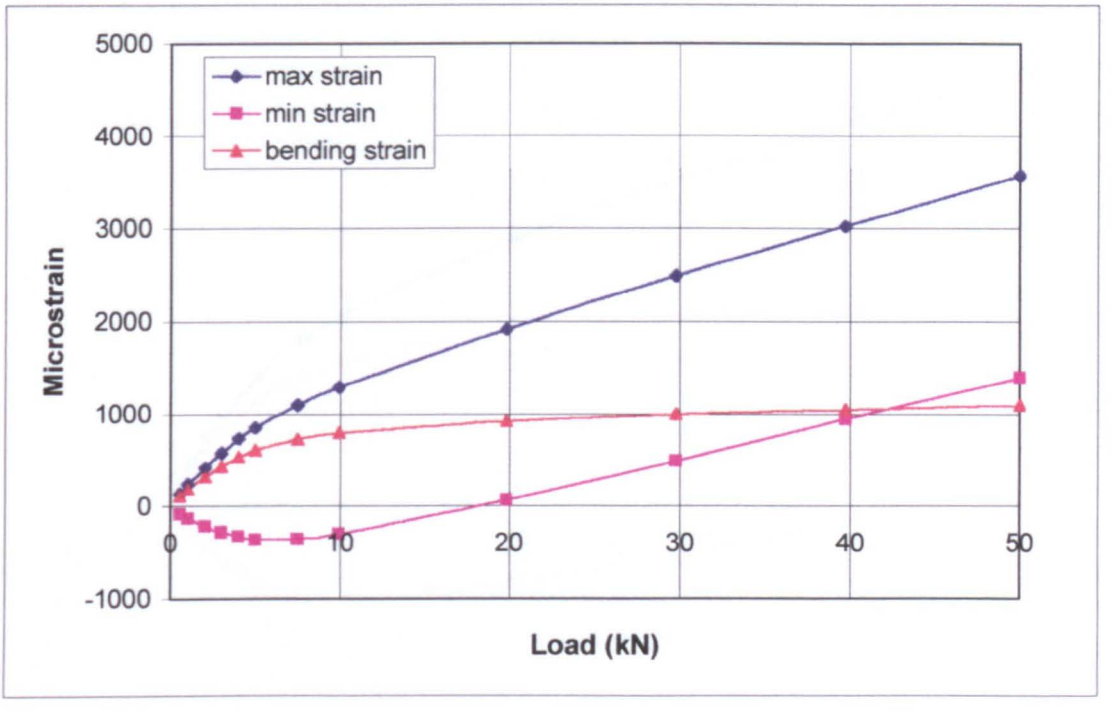

Figure 4.12 Strains caused by 2 mm insert (e/D = 0.17)

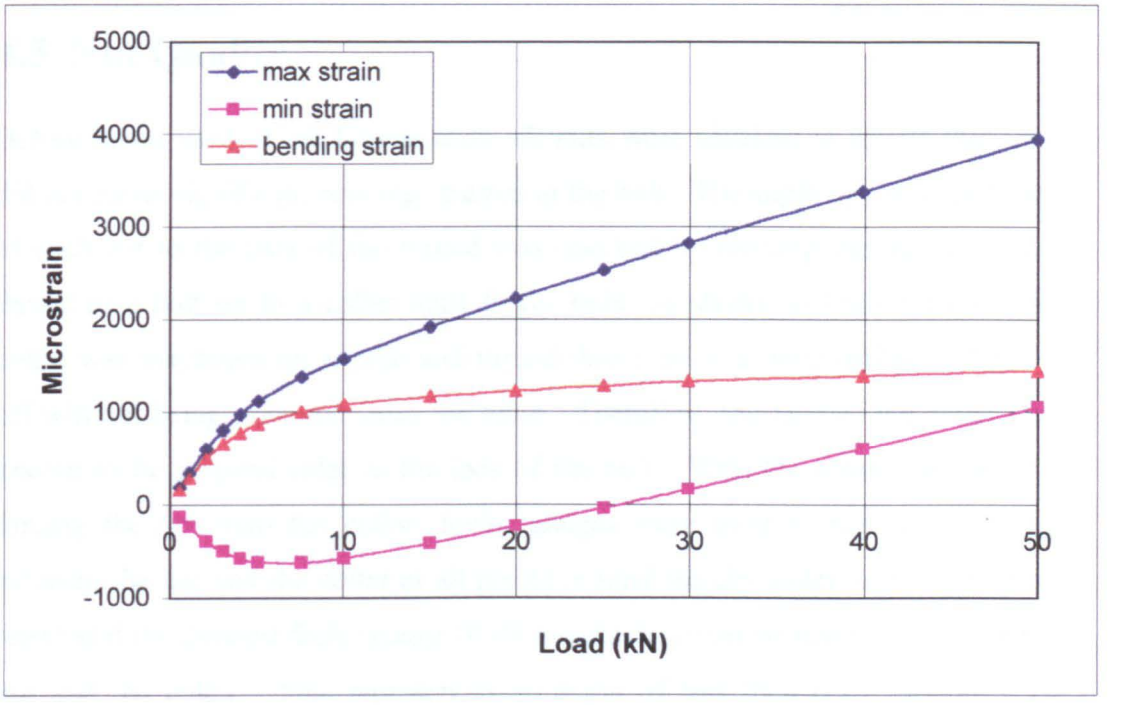

Figure 4.13 Strains caused by 3 mm insert (e/D = 0.25)

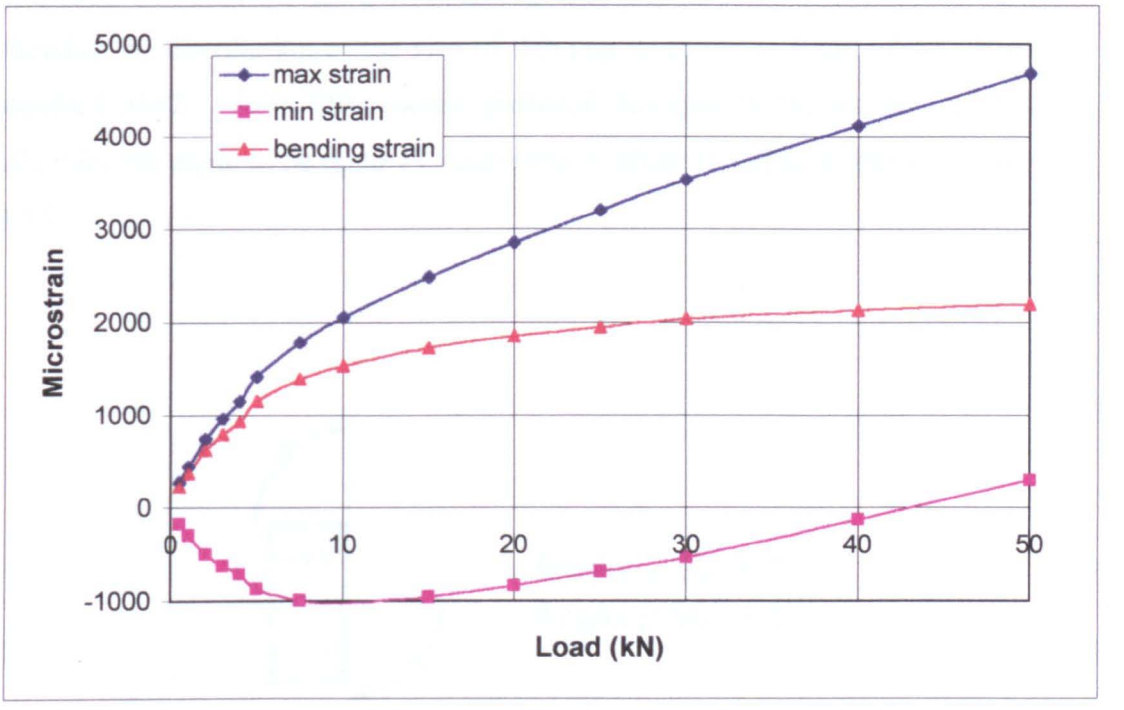

Figure 4.14 Strains caused by 4 mm insert (e/D = 0.33)

4.5 Nut Quality

Before being used in the fatigue tests, all nuts were checked to ensure that they did not cause significant bending stresses in the bolt. The angle of the loaded face of each nut to the axis of the thread was checked by running the nut down the thread of a bolt on to a collar until finger tight, as shown in Figure 4.16. The collar was machined on a lathe and turned down, internal hole drilled and faced off without being removed from the lathe. Therefore, the face of the collar was known to be perpendicular to the axis of the bolt. With the tension in the bolt forcing the nut onto the collar, feeler gauges were used to measure any gap between the nut and the collar at all points around the circumference. Nuts were rejected if the thinnest feeler gauge (0.05 mm thick) could be inserted between the nut and the collar. This represented an angle of less than 0.2°. Figure 4.16 graphically shows a nut that failed this test, with a gap between the nut face and collar of over 0.8 mm. The rejected nuts were sorted according to the maximum thickness of feeler gauge that could be inserted into the gap. A histogram showing the distribution of the size of this gap is shown in Figure 4.17. British standard 3692 (1967) "ISO metric precision hexagon bolts, screws and nuts" allow for the angle to be up to 1°, equivalent to about 0.3 mm, as shown in Figure 4.15.

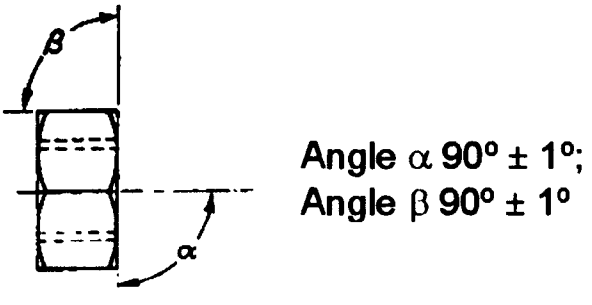

Figure 4.15 Angularity of the nuts as defined by BS 3692 : 1967

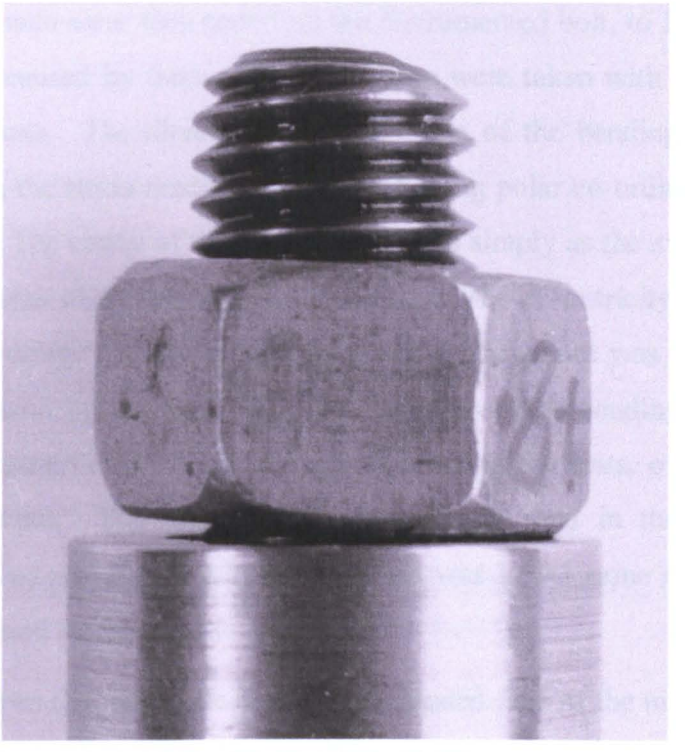

Figure 4.16 Poor quality nut against collar showing difference in angle

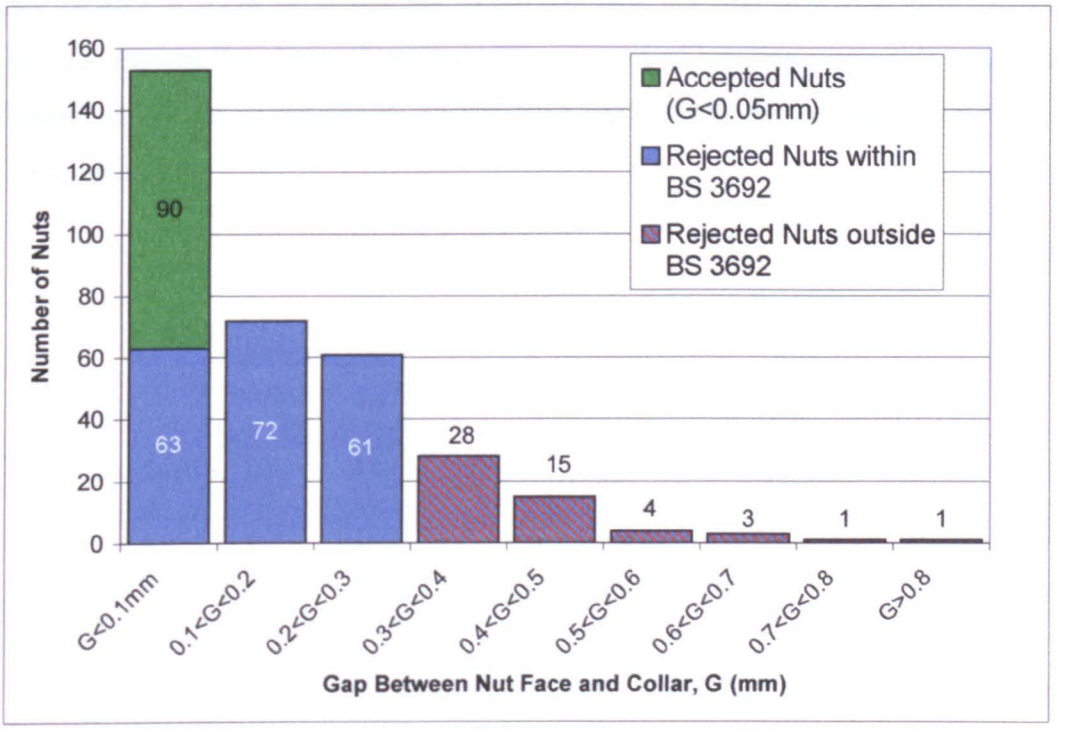

Figure 4.17 Histogram showing the numbers of nuts found with various angularities (338 nuts tested).

The remaining nuts were then tested on the instrumented bolt, to find the amount of eccentricity caused by them. Strain readings were taken with each nut in six different positions. The direction and magnitude of the bending stresses were calculated from the strain readings and plotted using polar co-ordinates, as shown in Figure 4.18. The centre of the points, calculated simply as the average of the x- and y-co-ordinates of the points, was taken to be the eccentricity caused by the grips and the average distance of the points from the centre was taken to be the eccentricity caused by the nuts. Any nut found to cause bending strain greater than 110 microstrain at 25 kN was rejected. During the tests, over 75% of the nuts were rejected. The nuts still remaining were used in the fatigue tests, positioned so that any eccentricity they caused was in the same direction as the eccentricity caused by the grips.

Figure 4.19 shows that the angle between the loaded face of the nut and the plane perpendicular to the thread axis has an effect on the eccentricity caused by the nut at a load of 25 kN. The values for the bending strain were obtained as described above. The angles shown are the deviations from perpendicular to the thread axis. When load is applied, the face of the nut is forced against the clamped part. If the face of the nut is not perpendicular to the bolt axis, the bolt will bend until the nut face lies against the clamped surface. The amount of bending stress this causes is dependant on the deviation of the nut face angle from the perpendicular to the thread axis.

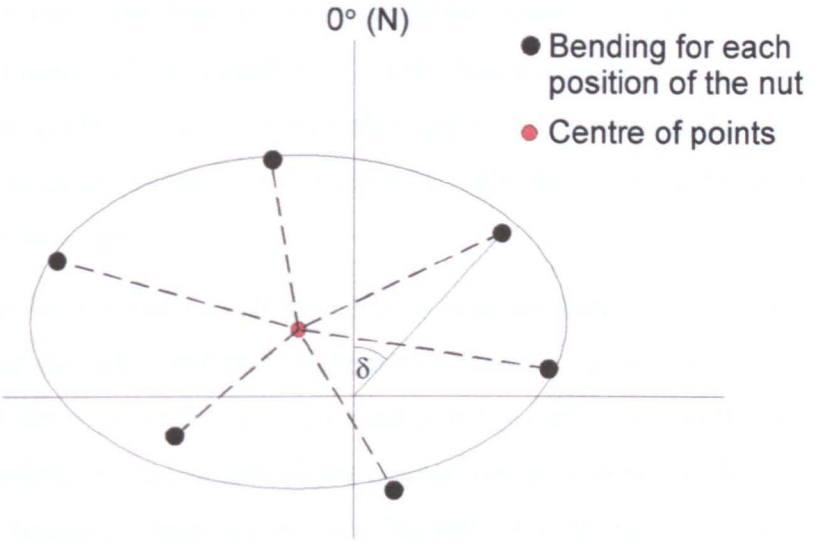

Figure 4.18 Direction and magnitude of maximum bending caused by the nut in different positions

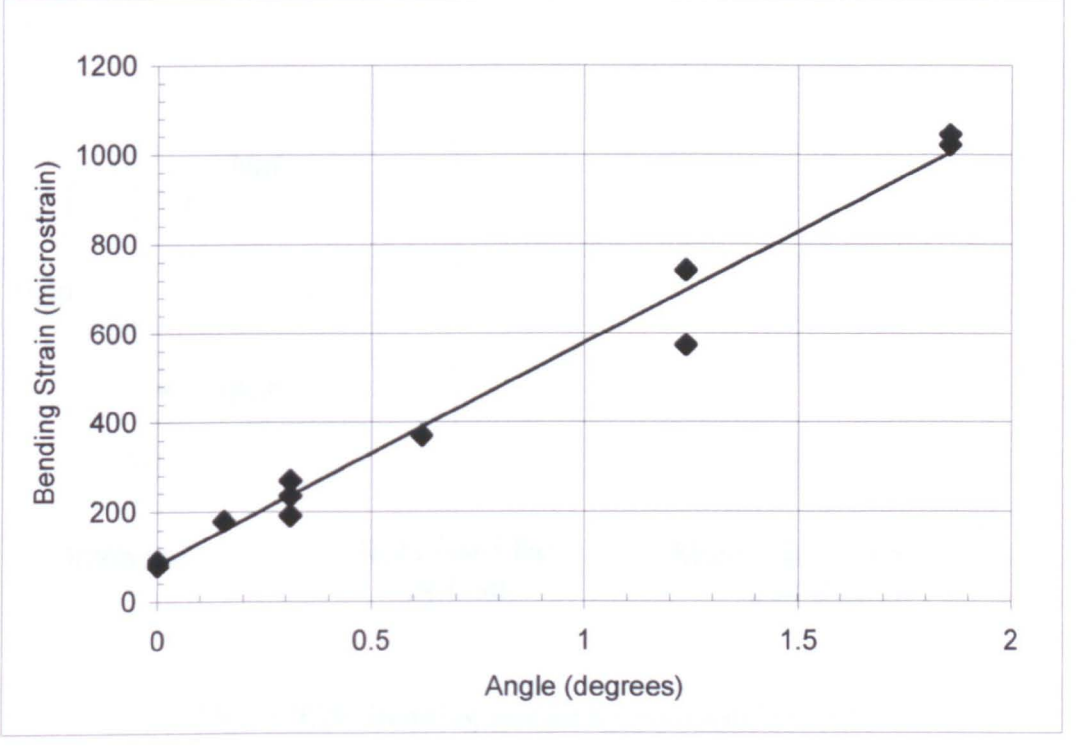

Figure 4.19 The effect of the nut face angle on bending strain at 25 kN load

For three of the nuts, with gaps of 0.1, 0.3 and 0.6 mm, strain-load curves were obtained in that same way as for the different levels of eccentricity. These are shown in Figure 4.21 to Figure 4.23. The maximum gradients of strain, $\partial\varepsilon'/\partial P$, are listed in Table 4.2. For the nut with a gap of 0.1 mm the highest gradient was from the maximum strain line. For the other nuts, the highest gradient is from the minimum strain line.

The reason for the decrease in bending as load increases is illustrated in Figure 4.20. When the bolt is not loaded, the nut does not lies against the face of the grip because of the angle of the face of the nut is not perpendicular to the bolt axis. As load is applied, the nut is forced flat against the grip, bending the bolt. At this point, the bending strains are at their highest. Increasing the load beyond this point has the effect of straightening the bolt slightly, thus reducing the bending strains. In this case, it will be the side of the bolt with the compressive bending strain that experiences the highest variation is strain due to cyclic loading as the strain on this side would equal the change in axial strain plus the effect of the bolt straightening out.

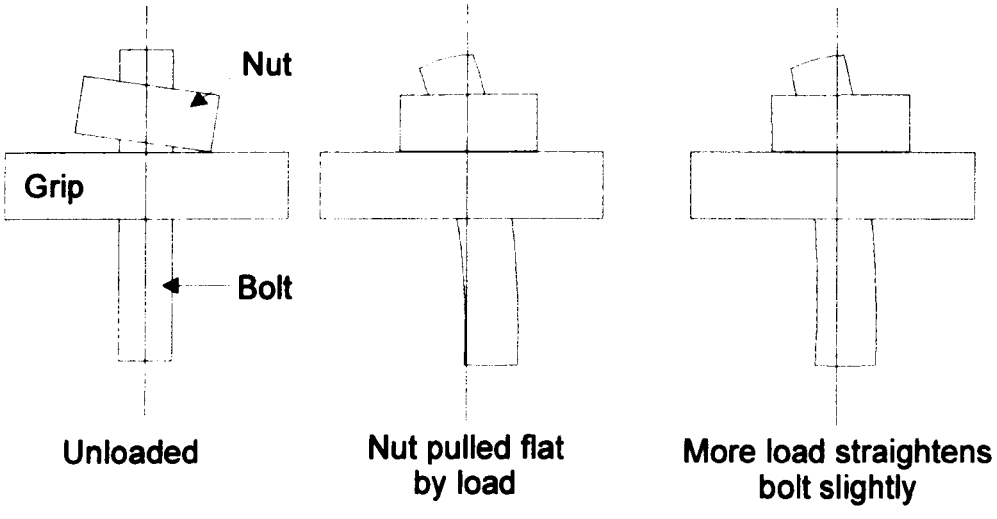

Figure 4.20 Bending caused by poor quality nut

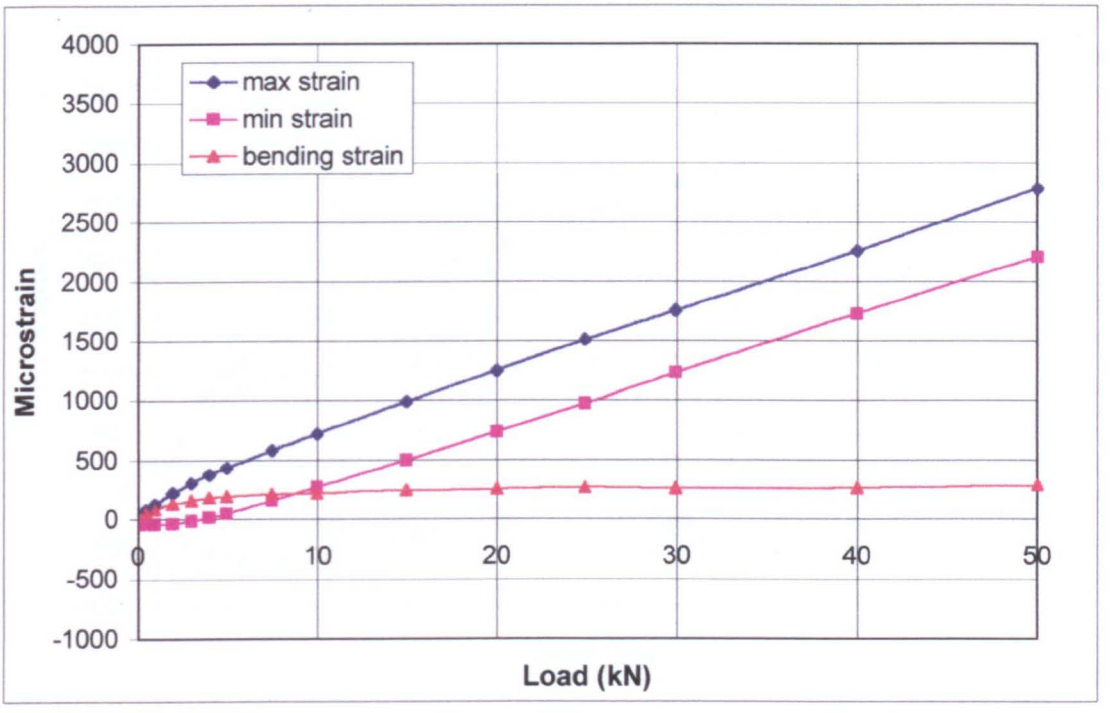

Figure 4.21 Bending strains caused by a nut with 0.1 mm angularity

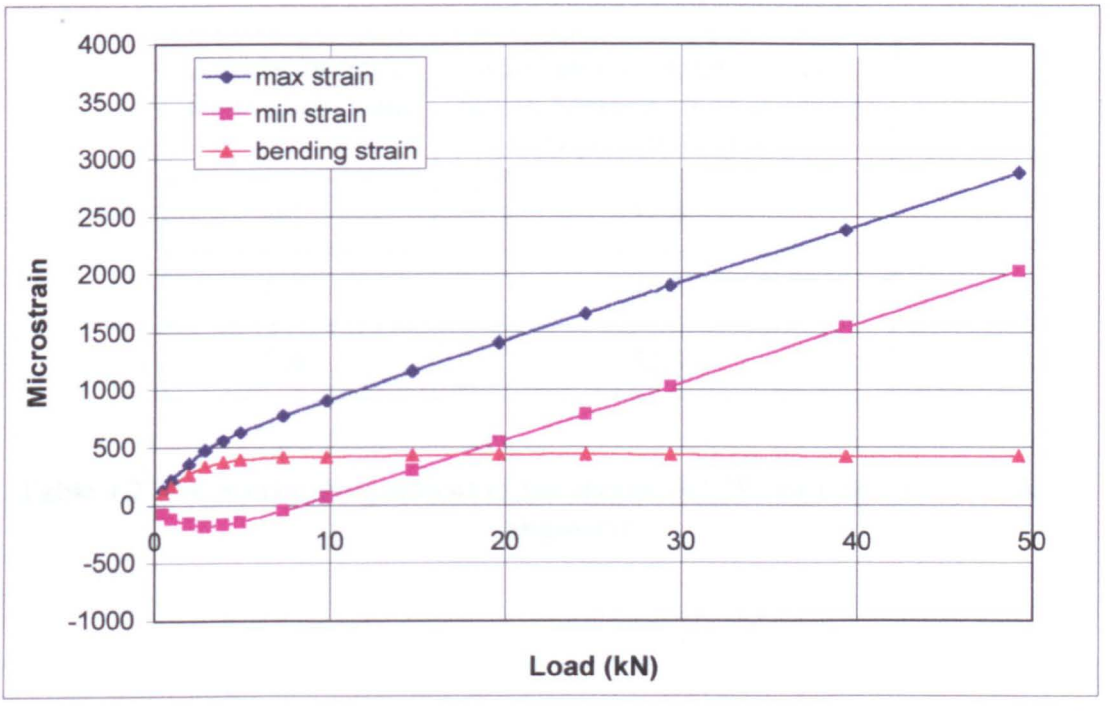

Figure 4.22 Bending strains caused by a nut with 0.3 mm angularity

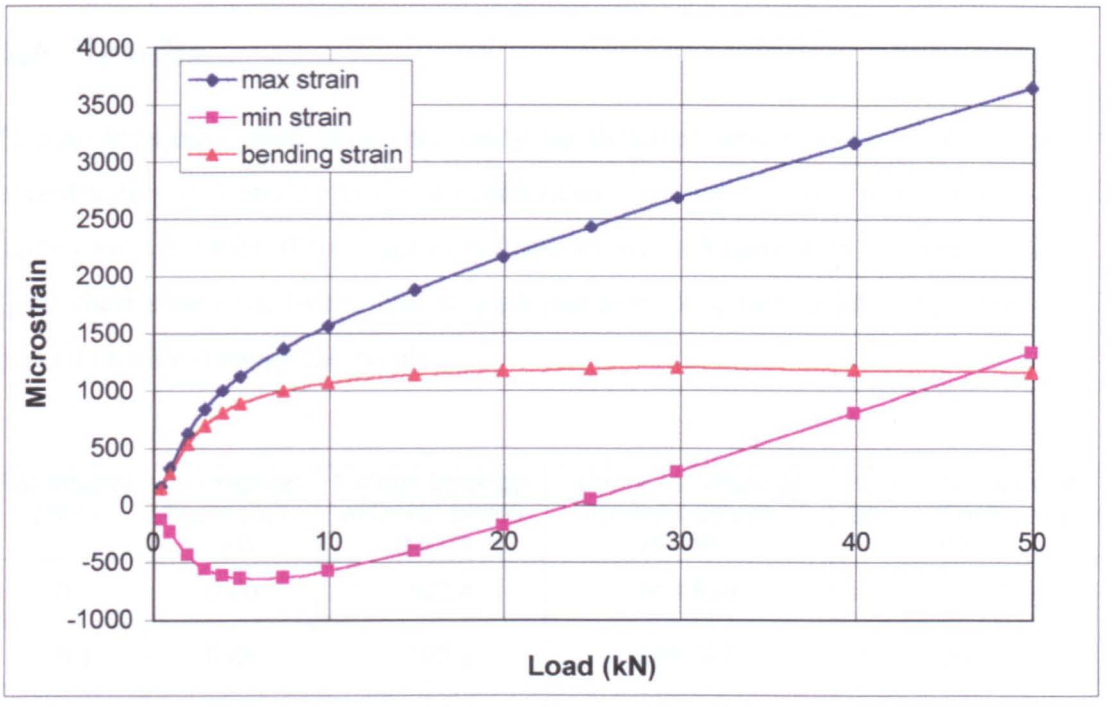

Figure 4.23 Bending strains caused by a nut with 0.6 mm angularity

Angularity (max. feeler gauge mm)	Maximum gradient of strain, $\partial\varepsilon'/\partial P$, between 30kN and 50kN (microstrain / kN)
0.1	51.6
0.3	49.5
0.6	52.4

Table 4.2 The maximum gradient of the strain, $\partial\varepsilon'/\partial P$, for nuts of different angularity

4.6 Results

Fatigue tests have been performed using six different sets of inserts, with actual eccentricities (e_0) and normalised eccentricities shown in Table 4.3. The S-N curves for the series of tests performed are shown in Figure 4.24 to Figure 4.29. Each chart shows the twenty points each representing a bolt failure and a line of best fit passing through the points.

Eccentricity (mm)	Normalised Eccentricity e/D	Fatigue Strength at 2×10^5 cycles (MPa)	Cycles to failure at Stress Amplitude of 80 MPa	Cycles to failure at Stress Amplitude of 100 MPa
0	0.00	103.4	514,550	227,802
0.5	0.04	103.2	535,577	230,430
1	0.08	105.4	535,517	246,483
2	0.17	98.8	393,148	191,732
3	0.25	96.7	359,136	177,899
4	0.33	94.7	320,515	168,975

Table 4.3 Eccentricities used and main results

Figure 4.30 shows the variation in the fatigue strength at 2×10^5 cycles with eccentricity for both nominal and local stress amplitude. Both sets of values were calculated from the equations of the lines of best fit through the fatigue points. The global stress amplitudes were calculated by simply dividing the applied load amplitude by the stress area of the bolt. The local stress amplitudes represent the stress amplitude calculated for the tension side of the bolt, but do not take into account any stress concentration effects. These are calculated from the gradient of the maximum strains, shown in Table 4.1. For example, the gradient, $\partial\varepsilon'/\partial P$, for the 4 mm eccentric insert was 57.2 microstrain/kN. The gradient of the axial strain for all levels of eccentricity was 50.0 microstrain/kN. Therefore, over a given load range, the strain would vary by 14.4% more for a point on the bolt that experienced the highest strain than for a point experiencing the strains caused by axial load. So if the global stress amplitude that caused failure at 2×10^5 cycles was 94.7 MPa, the local stress amplitude would be 14% higher, i.e. 108 MPa.

The effect eccentricity has on the cycles to failure is shown in Figure 4.31. The cycles to failure at two different global stress amplitudes (80MPa and 100MPa) are shown.

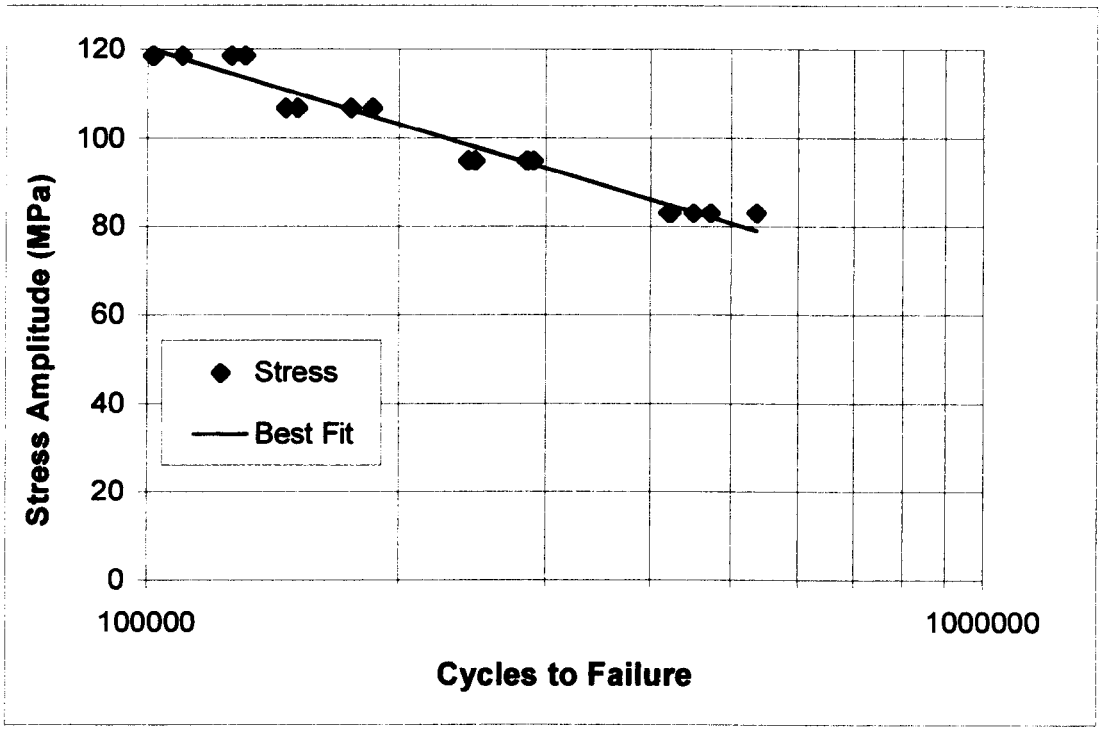

Figure 4.24 S-N curve for fatigue tests using inserts with 0 mm eccentricity (e/D = 0)

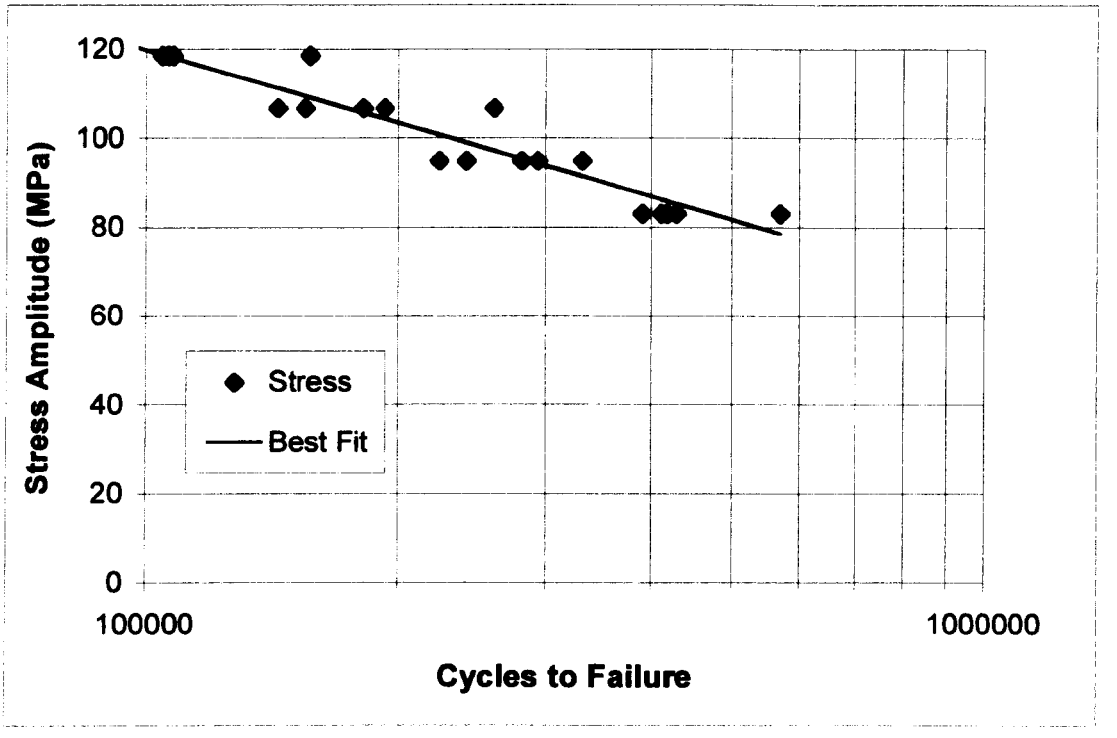

Figure 4.25 S-N curve for fatigue tests using inserts with 0.5 mm eccentricity (e/D=0.04)

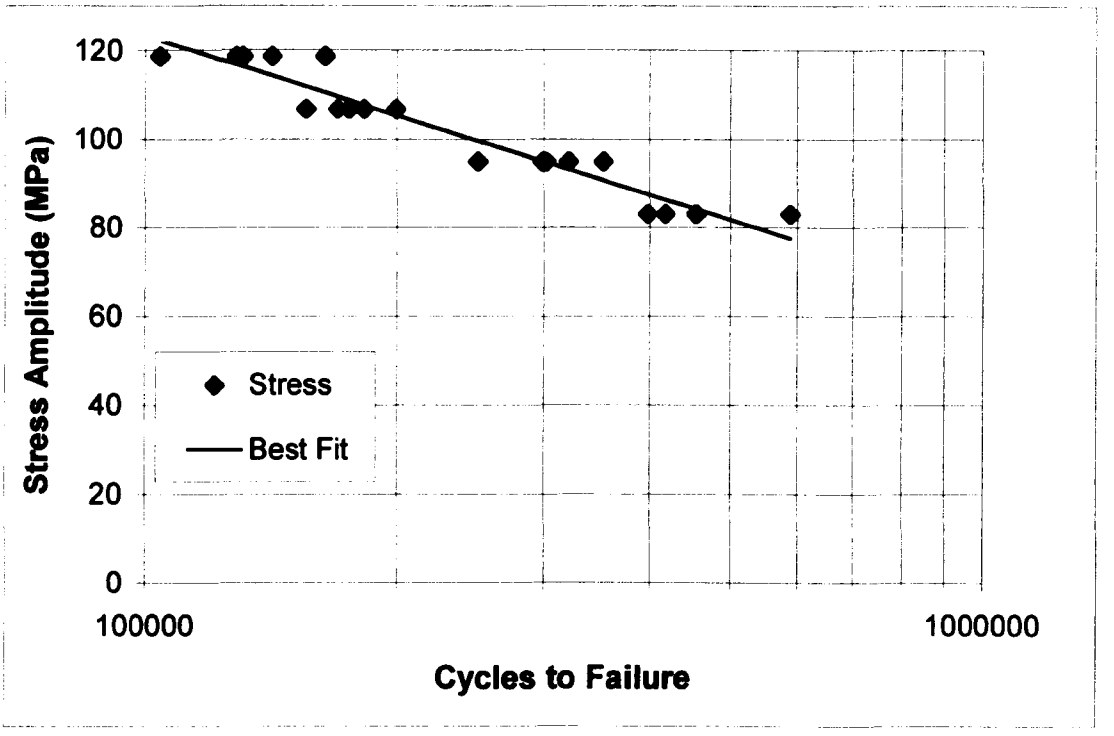

Figure 4.26 S-N curve for fatigue tests using inserts with 1 mm eccentricity (e/D = 0.08)

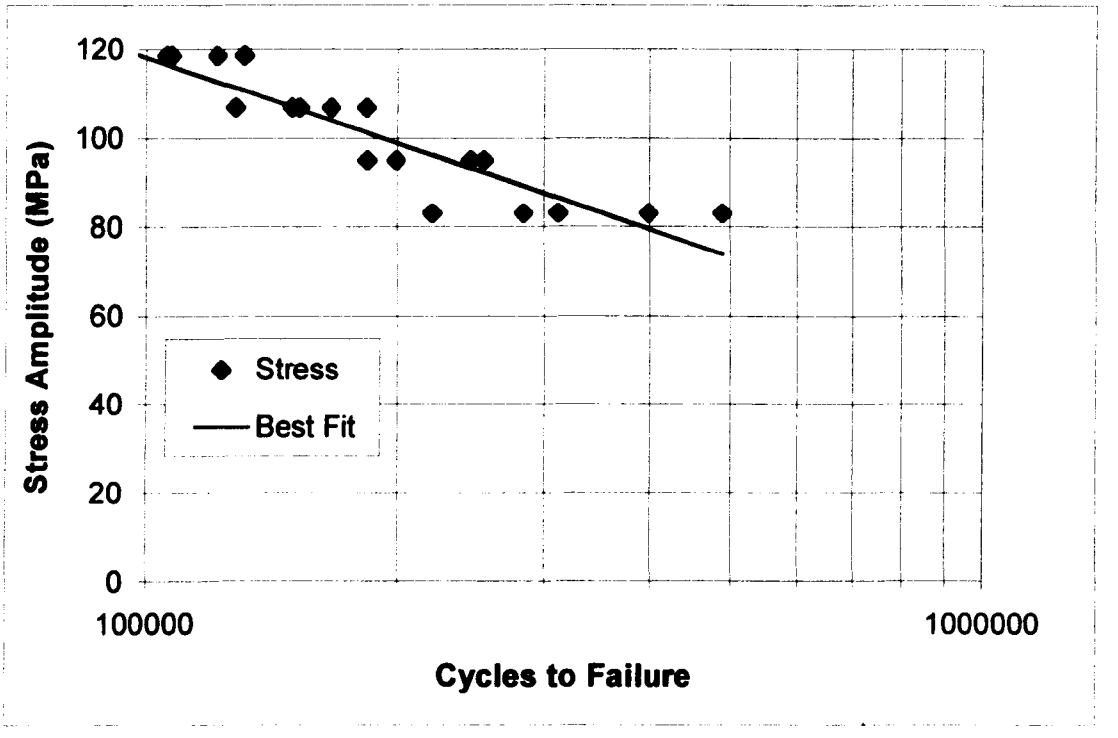

Figure 4.27 S-N curve for fatigue tests using inserts with 2 mm eccentricity (e/D = 0.17)

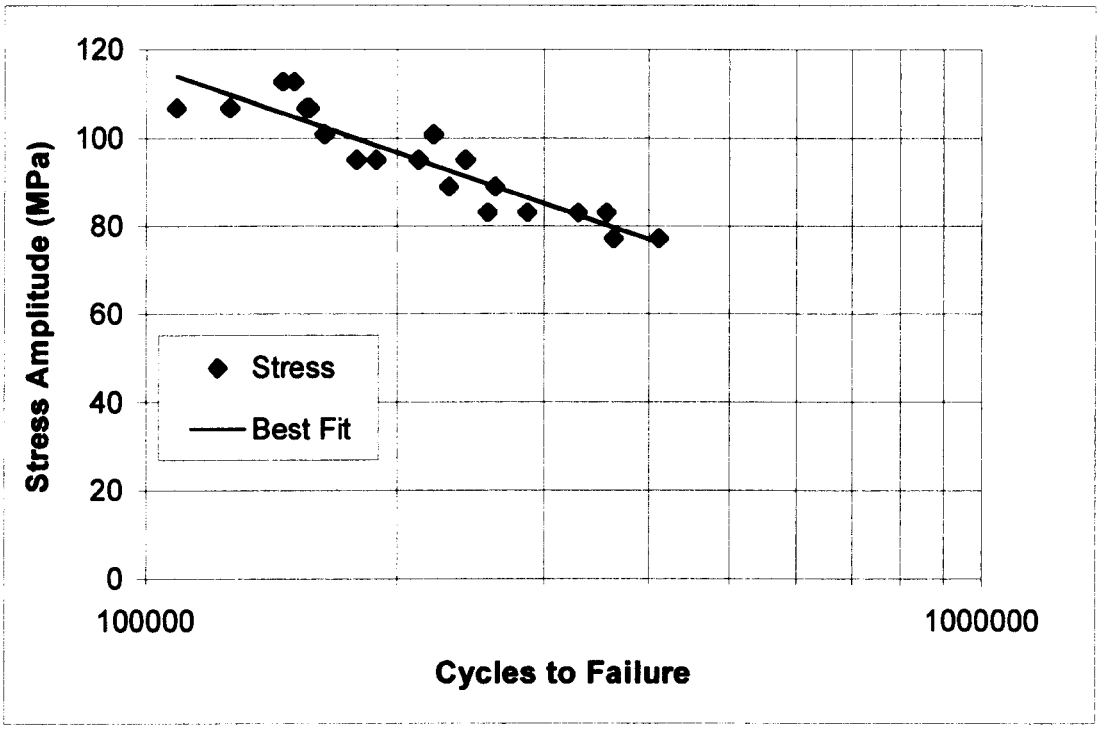

Figure 4.28 S-N curve for fatigue tests using inserts with 3 mm eccentricity (e/D = 0.25)

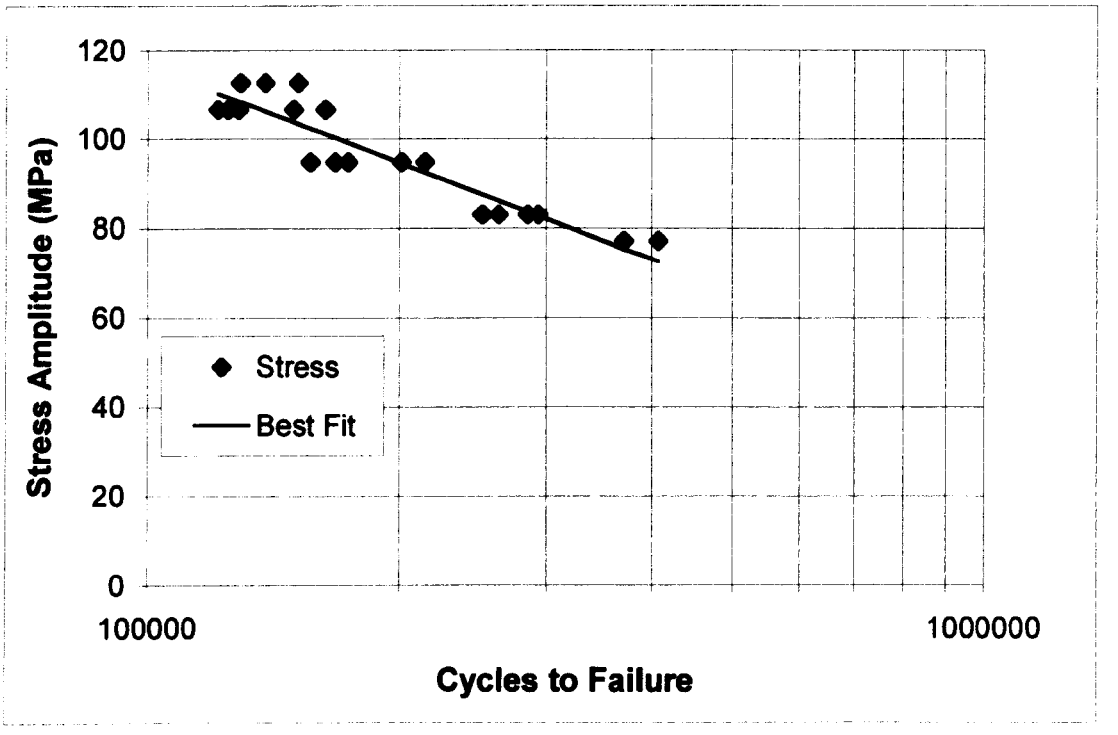

Figure 4.29 S-N curve for fatigue tests using inserts with 4 mm eccentricity (e/D = 0.33)

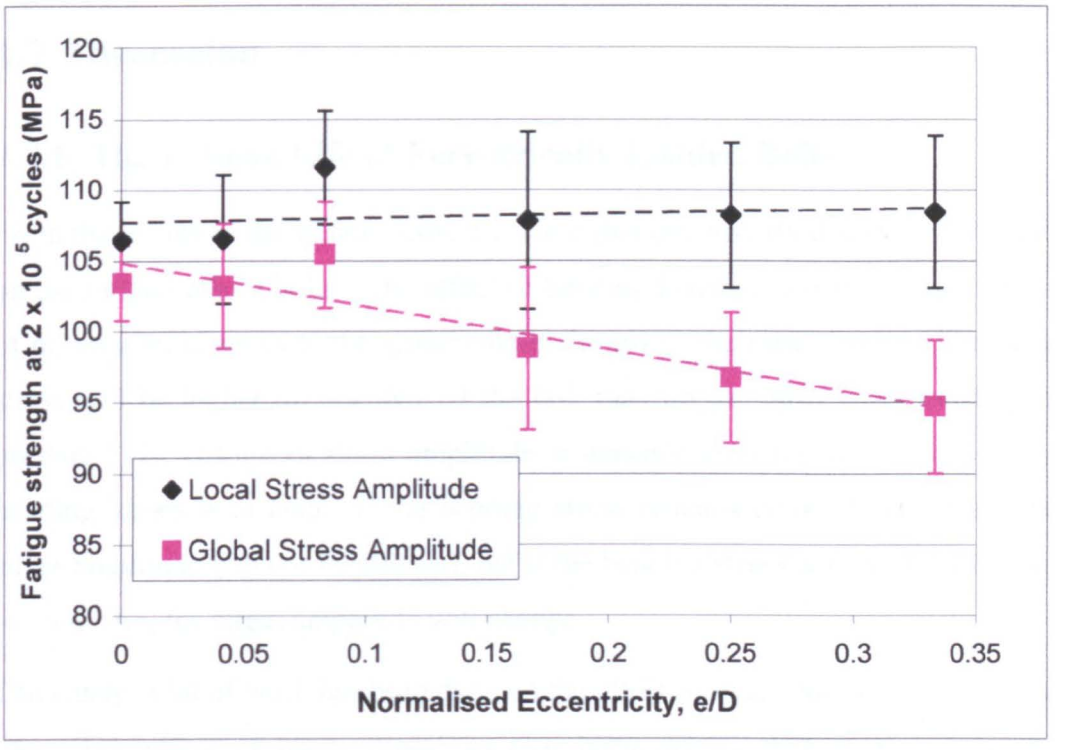

Figure 4.30 Values of local and global stress amplitude at 2×10^5 cycles for various levels of eccentricity with best fit lines and error bars of 1 standard deviation

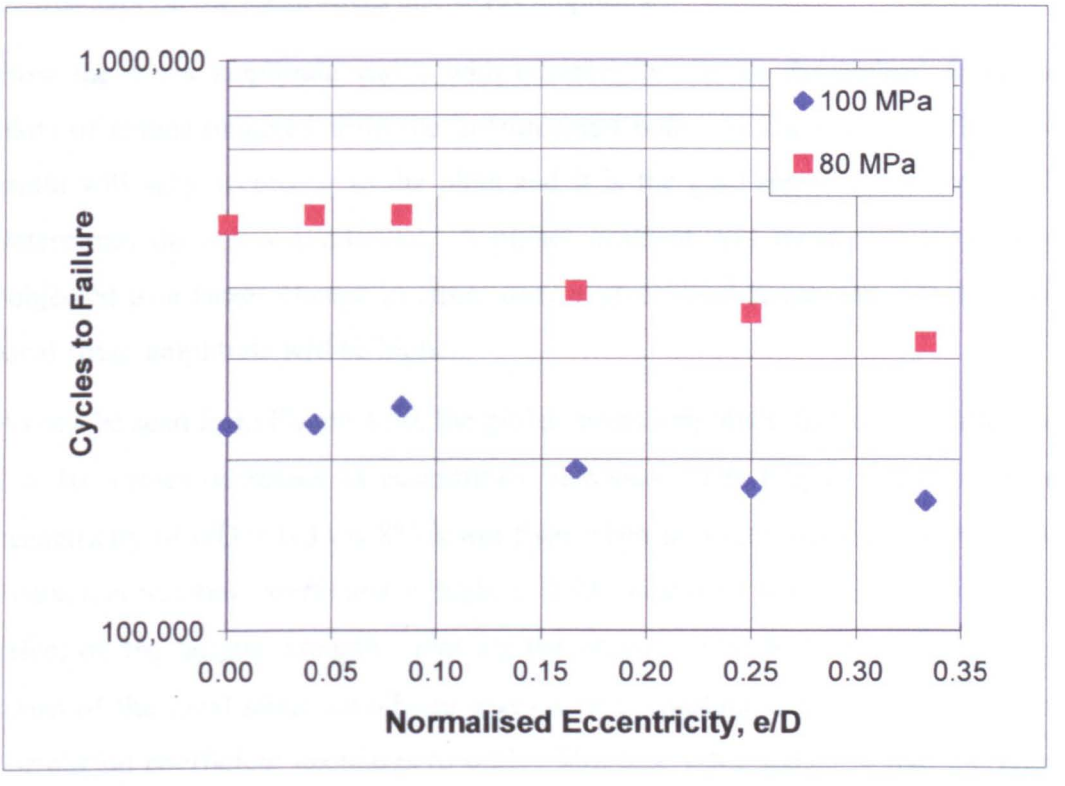

Figure 4.31 Cycles to failure obtained at stress amplitudes of 80 MPa and 100 MPa against eccentricity

4.7 Discussion

4.7.1 The Fatigue Life of Eccentrically Loaded Bolts

From the results of the fatigue tests, it is clear that eccentricity does have an effect on the fatigue life of bolts. The effect of bending loads on a bolt can be thought of in terms of changes to the stress amplitude and to the mean stress. The mean stress will be higher on one side of the bolt than on the other when bending is present. The change in stress amplitude is dependent on the way in which the bending varies with load. If the bending stress remains constant with load, the stress amplitude will not be affected, but if the bending stress does vary with load, as seen here, the stress amplitude will change.

Obviously, a lot of work has been done on the effect of stress amplitude on fatigue life. The effect of mean stress has also been investigated, most notably by Burguete and Patterson[3] who looked at M12 bolts. From this investigation, and using past investigations it should be possible to determine whether the fatigue life of bolts under eccentric loads can be predicted by knowing the effect of the eccentricity on the mean stress and stress amplitude.

How the stress amplitude varies with eccentricity can be determined from the plots of strains obtained from the instrumented bolt. As the load is cycled, the strain will vary according to the plots and it is the gradient of the strain which determines the stress amplitude. A higher gradient will mean that the bolt is subjected to a larger change in stress over a given load range and therefore the local stress amplitude will be higher.

As can be seen from Figure 4.30, the global stress amplitude that causes failure at 2×10^5 cycles decreases as eccentricity increases. The fatigue strength for an eccentricity of e/D = 0.33 is 8% lower than when no eccentricity is present. The Pearson correlation coefficient is high, at 0.93, indicating that eccentricity has an effect on the fatigue strength. Plotting the fatigue strength at 2×10^5 cycles in terms of the local stress amplitude gives a near constant value and the Pearson correlation coefficient decreases to 0.21. This low value indicates that the local stress amplitude to cause failure at 2×10^5 cycles is independent of the eccentricity. This shows that the life of eccentrically loaded bolts is dependent on

the highest local stress amplitude rather than on eccentricity, but obviously, the local stress amplitude is itself dependent on eccentricity. Therefore, if the local stress amplitude can be determined, the effect of bending on fatigue life can also be determined. This means, basically, that the principle of superposition holds true for eccentric loading for the stress amplitude, but the issue is complicated somewhat by the fact that the bending stress is not constant.

As mentioned earlier, eccentricity also has an effect on the mean stress experienced by the bolt. Burguete and Patterson[3] found that mean stress had little effect on the fatigue limit across a wide range but that the fatigue limit dropped quickly for mean stresses beyond the yield strength of the material, as shown in Figure 4.32. The Haigh diagram also shows the points for the eccentric tests, plotted in terms of the local mean stress and local stress amplitude. It should be noted that the stress amplitude for the eccentric tests is much higher because of the different number of cycles used to mark failure. It can be seen that the stress amplitude remains fairly constant over the range of mean stress even beyond yield, where Burguete and Patterson found the stress amplitude to drop sharply.

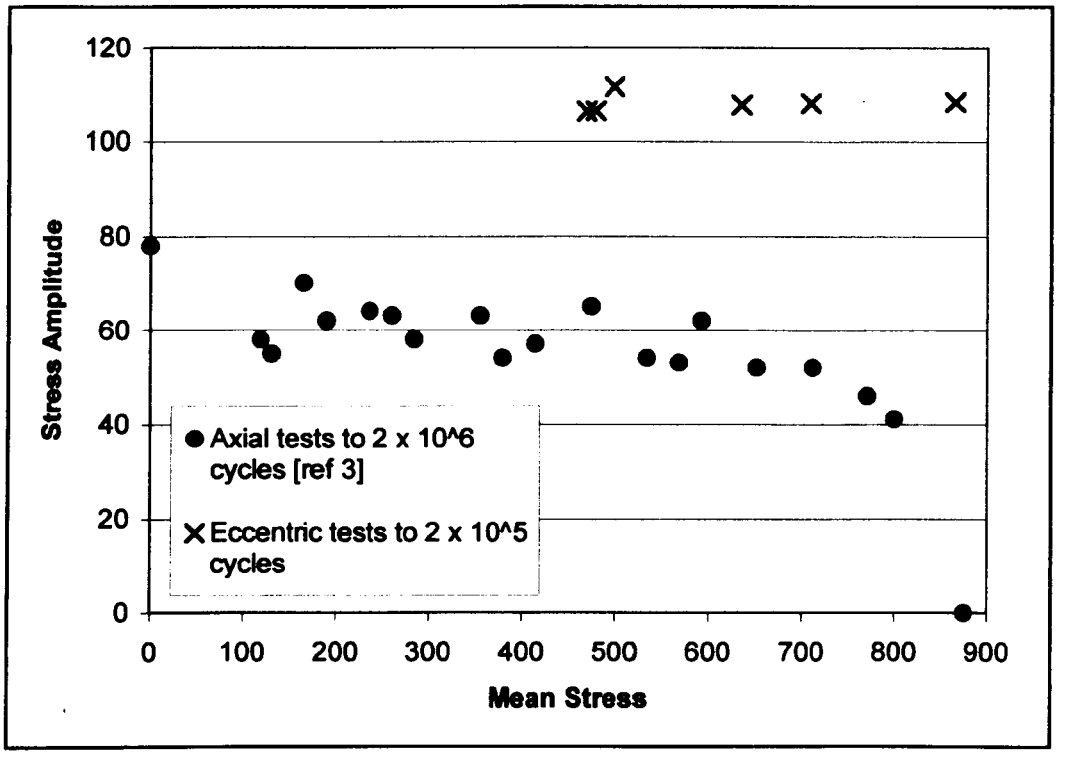

Figure 4.32 Haigh diagram showing axial and eccentric fatigue results

With eccentric loading the high mean stress is localised to one side of the bolt, and therefore plastic deformation causes the load to be redistributed. Under axial loading, more of the bolt is subjected to the very high which leads to general yielding and early failure. Therefore, the principle of superposition does not work when considering the mean stress.

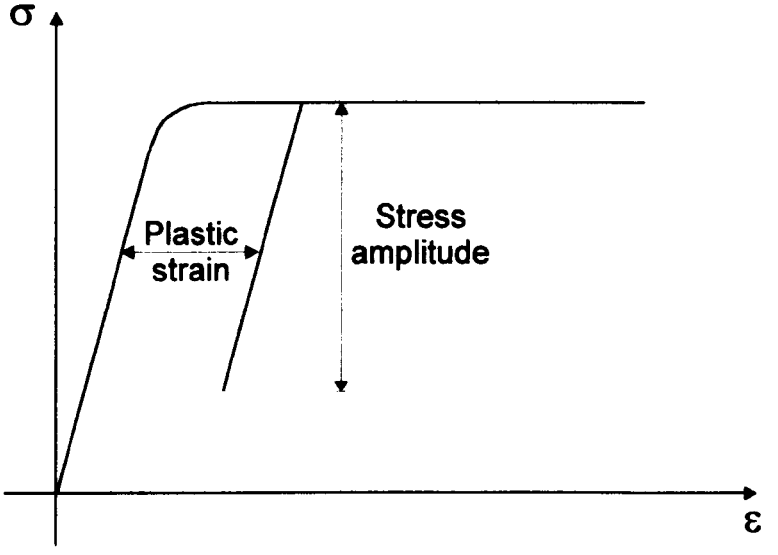

Figure 4.33 Stress-strain curve showing stress amplitude after plastic deformation

Figure 4.33, above, shows a possible stress-strain curve for material that is subjected to a high mean stress and a cyclic stress. Under the high load, the material deforms plastically until the load is taken by another part of the component. The cyclic stress then causes the material to behave in a similar manner to material that has not plastically deformed and therefore the yielding is not detrimental to the fatigue life of the component. This explains why the mean stress has little effect on fatigue life; at a high mean stress more material yields in this way but the stress amplitude is not affected.

4.7.2 Quality of Nuts

The quality of the nuts and the bending strains caused by poor quality nuts at first looks alarming. With a nut with a gap of 0.6 mm between the loaded face and a flat collar causing a similar bending strain to grips with 2 mm eccentricity (e/D = 0.17) and with about 15% of nuts tested found to lie outside the British Standard there is cause for concern. However, would a poor nut contribute to early fatigue failure of a bolt?

As for the eccentrically loaded case, eccentricity caused by nuts will have an effect on the local stress amplitude and mean stress experienced by the bolt. Considering the stress amplitude first, when calculating the highest gradient of the strain, shown in Table 4.2, it is found that the gradient of strain, $\partial\varepsilon'/\partial P$, reaches 52.4 microstrain/kN for a nut under which a 0.6 mm feeler gauge could be inserted. This is approximately equivalent to an eccentricity of 1 mm (e/D = 0.08). This does not seem to significantly affect the fatigue strength, as shown in Figure 4.30.

At lower loads, where the strain gradient is higher, the local stress amplitude may be significantly higher than the global stress amplitude. This would be expected to have the effect of shortening the life of bolts if at a very low mean load. It should be noted that no fatigue tests have been performed to verify this.

One danger of using poor quality nuts is that the bending caused may increase the mean stress in the bolt. However, from the results for the eccentric loading it is thought that the increase in mean stress does not effect the fatigue life. Therefore, the use of poor quality nut with a high angularity should not adversely effect the fatigue life of bolts if the bolt is properly tightened.

The interaction between bending caused by a poor quality nut and eccentric loading is difficult to predict. The mechanisms are different with the highest strain gradient, and therefore, local stress amplitude, occurring in the low stress side of the bolt for bending caused by a nut but on the high stress side of the bolt for bending caused by eccentric loading. It is likely, therefore, that if the nut and the load cause bending in the same direction, the overall effect on the local stress amplitude would be slightly lower then if the nut was of good quality. However, the mean stress could be very high on the high stress side.

4.8 Conclusions

The main conclusions that can be drawn from this work concern the effect of eccentricity on the fatigue life of bolts and the effect of poor quality nuts on the bending in a bolt.

- Eccentric loading does have an effect on the fatigue life of bolts. The global stress amplitude needed to cause failure at 2×10^5 cycles is 8% lower at an eccentricity, e/D = 0.33 than when no eccentricity is present.
- This can be accounted for by the gradient of the strain, $\partial\varepsilon'/\partial P$, from which the local stress amplitude can be calculated. The local stress amplitude to cause failure at 2×10^5 cycles remains fairly constant with eccentricity. The localised high mean stress caused by eccentricity does not have a detrimental affect on the fatigue life.
- An eccentricity, e/D = 0.33, would reduce the fatigue life of a bolt by almost 40% for a global stress amplitude of 80 MPa. The reduction is slightly less at higher stress amplitudes.
- Many nuts were found with large angles between the loaded face and perpendicular to the thread axis, and this was shown to cause bending in the bolts. However, when considering the strain gradient associated with these poor quality not, a nut on the limit of the British Standard was roughly equivalent to an eccentricity of e/D = 0.08. This level of bending would be unlikely to significantly affect the fatigue performance of the bolt.

Chapter 5

Crack Shape

5.1 Introduction

The shape of cracks occurring in cyclically loaded bolts is still unresolved. Work that has been performed on axially loaded bolts has shown different results, with Mackay and Alperin[46] reporting semi-circular cracks and Pacey *et al*[53] reporting crescent shaped cracks. To date, no work has looked at the shape of cracks in eccentrically loaded bolts.

5.2 Axially Loaded Bolts

5.2.1 Method

The crack growth through a bolt subject to an axial cyclic load has been studied. Grade 8.8 M12 x 120 coarse series bolts were used for the tests with grade 8 M12 nuts. The bolts were cleaned in an ultrasonic cleaner and brushed with wire wool. They were then checked for abnormalities by running a nut down the thread then oiled.

Two levels of mean stress were tested; 250 MPa and 534 MPa both at a stress amplitude of 130 MPa. To observe how the cracks grew through the bolt, beach marks were made on the fracture surface by reducing the stress amplitude by

approximately 50 % for 100,000 cycles. The level to which the stress amplitude was reduced to was dependent on the estimated length of the crack in an attempt to achieve the same stress intensity factor at the crack tip. The aim is to have a very small amount of crack growth, enough to leave a visible mark on the surface but small enough to avoid affecting the growth characteristics. Trial and error was used as the length of the crack could not be known at any time. Several attempts were needed to achieve good beach marks.

5.2.2 Results

Photographs of the fracture surfaces of two bolts are shown in Figure 5.1. The bolt on the left of Figure 5.1, was tested at a mean stress of 534 MPa and the bolt on the right of Figure 5.1 was tested at a mean stress of 250 MPa. It is clear that the crack in the bolt tested at a higher mean stress has a more crescent-like shape. It can also be seen from the beach marks that the crack has a crescent shape even when short.

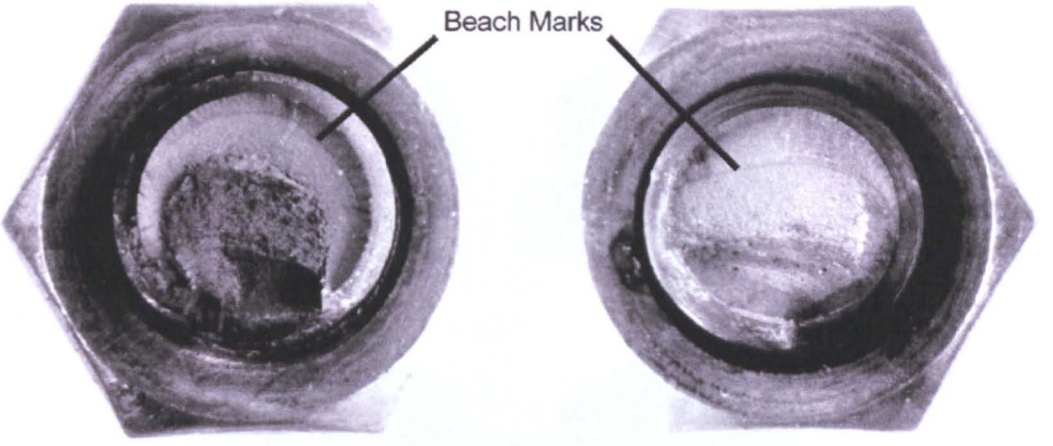

Figure 5.1 Typical fracture surfaces of cyclically loaded bolts showing beach marks

5.3 Eccentrically Loaded Bolts

5.3.1 Crack Shape

No beach marking tests were performed with the bolts loaded eccentrically, but the axially loaded beach marking tests showed that the crack shape changed little as the crack grew. Therefore, only the final crack shape was considered. Figure 5.2 shows crack shapes occurring in cyclically loaded bolts. As can be seen, there is no obvious trend in the crack shape with either eccentricity or with stress amplitude. At high stress amplitude, the fatigue crack is slightly shorter, as the higher peak stress causes failure with a short crack.

Unfortunately, it appears that no useful information about the level of eccentricity experienced by a bolt can be obtained by examining the shape of the fatigue crack. Mean stress has a far greater effect on the crack shape for the ranges of mean stress and stress amplitude selected here.

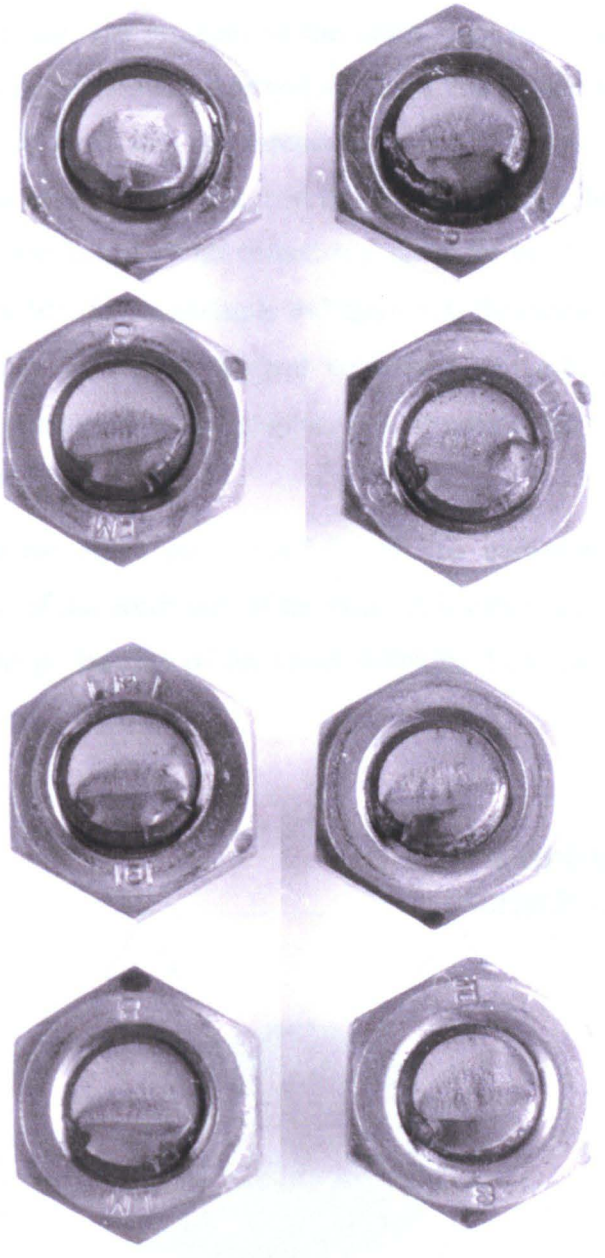

Figure 5.2 Typical crack shapes occurring in bolts subjected to eccentric, cycling loads. High eccentricity on the left (e/D = 0.33), low eccentricity on the right (e/D = 0.08). Stress amplitude decreases from top of bottom.

5.3.2 Position of Crack

Although the shape of the crack does not appear to be affected by the level of eccentricity experience, the position of the crack may be. The fractured bolts were examined to determine the orientation of the crack relative to the plane of bending. Figure 5.3 shows this diagrammatically. The position of the centre of the crack front was estimated by eye, and the face of the nut closest to the centre of the crack front was noted. This effectively gave the position of the centre of the crack front to ± 30°. In the example in Figure 5.3, the centre of the crack front is nearest to the face of the nut aligned with the north side of the bolt. The number of cracks orientated in this position was compared for the different levels of eccentricity tested.

Figure 5.4 shows the effect of eccentricity on the percentage of cracks that initiated within 30° of the north side of the bolt. It is clear that high eccentricities greatly increase the probability of the crack initiating from the north side of the bolt, where the stress is highest.

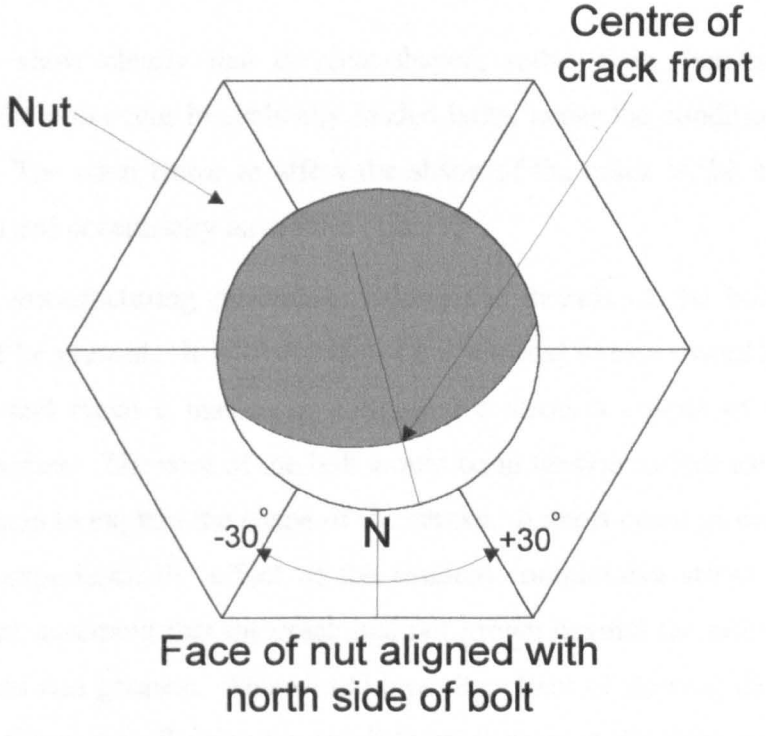

Figure 5.3 Determination of orientation of crack relative to the plane of bending

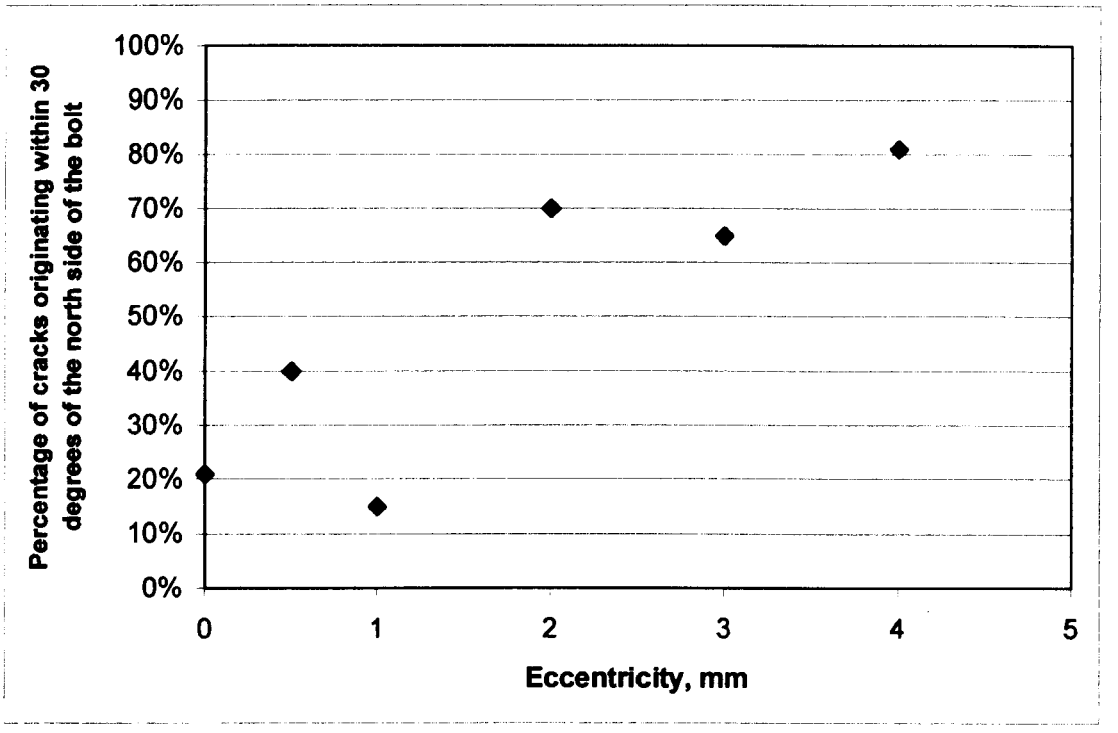

Figure 5.4 Effect of eccentricity on the percentage of cracks originating from the north side of the bolt

5.3.3 Discussion

The results show clearly that crescent-shaped, rather than thumbnail-shaped, cracks are likely to occur in cyclically loaded bolts, under the conditions used for these tests. The main factor to affect the shape of the crack is the mean stress; crack length and eccentricity have little effect.

Due to the manufacturing process of rolling the threads of the bolts, residual stresses will be present. It is likely that these residual stresses would be zero at the surface and reach a maximum compressive stress a couple of millimetres below the surface. The core of the bolt would be in tension to balance the forces. This could help to explain the shape of the cracks. A short crack growing into the bolt would experience the effect of the residual compressive stress most at its deepest point, assuming that the crack had not grown beyond the point where the residual stress was greatest. This would have the effect of slowing the growth of the crack at this point, allowing the crack to grow more at the sides, resulting in a crescent-shaped crack.

However, the cracks shapes shown in Table 2.1[58] show that crescent-shaped cracks occur in notched bars without the effect of compressive residual stresses. Also, the residual stress theory does not explain the different crack shapes resulting from different mean stresses. It is thought, therefore, that it is plasticity at the thread root that causes the crescent shape of the cracks. The high stress concentration due to the thread root will cause localised yielding of the material which will shed load further round the thread helix. The higher the mean stress, the more yielding will take place, and therefore the more crescent shaped the crack will become, as seen. While eccentricity increases the mean stress, which should cause the crack to be more crescent-shaped, it only increases the mean stress on one side of the bolt. On the other side of the bolt, the mean stress is lower, the net result being no change in crack shape.

The results obtained agree with those of Pacey *et al*[53] who performed similar tests on axially loaded bolts. They found that the shape of the crack front was a crescent for bolts tested at a high mean stress, becoming less markedly crescent shaped at low mean stresses.

Chapter 6

Photoelastic Analysis

6.1 Introduction

The series of photoelastic tests is split into two sections; (i) an investigation into the effect of crescent shaped cracks in axially loaded bolts and (ii) the effect of eccentricity on cracked bolts. The stress distribution around the thread helix and the stress intensity factor (SIF) along the crack front have been investigated by a number of authors. However, where cracked bolts have been modelled, the cracks have been either semi-circular or straight fronted. No crescent shaped cracks have been modelled. Since the crack shape affects the SIF along the crack front it is important to obtain values for cracks that actually occur in real life. The results from the investigations into crescent shaped cracks and eccentrically loaded cracked bolts are reported and discussed.

6.2 Crescent Shaped Cracks

6.2.1 Method

The shapes of the eight cracks modelled are shown in Figure 6.1. Two crack lengths, 2 mm and 4 mm were used with a range of crack shapes. The cracks formed an arc of a circle, the centre of which was a distance, c, from the centre of the bolt. For a constant crack length, a, the greater the distance, c, the larger the crack front radius and therefore the straighter the crack front. Small distances, c, produce cracks that follow the thread root round almost a whole turn. The cracks, cut into the thread root about half way down the threaded section of the bolts, were cut at the helix angle and follow the thread root, therefore the shapes shown are projections onto the plane perpendicular to the bolt axis. The red shaded area represents the crack, the black shaded area represents the remaining bolt. The nuts and bolts used are double scale ISO M12, machined from MY750 epoxy resin, prepared according to Kenny[97]. The dimensions of the epoxy nut, bolt and washers are shown in Figure 6.2. The nuts were cornerless, for ease of manufacture. This has been shown by Patterson and Kenny[98] to not affect the stress distribution in the bolt.

A sophisticated 3D method of cutting crescent shaped cracks into photoelastic models was developed. This involved holding the bolt eccentrically in the chuck of a lathe, as shown in Figure 6.3. A saw of diameter 32 mm and thickness 0.2 mm was placed to the side, which cut a crack into the bolt with the radius of curvature equal to the distance of the saw blade from the centre of the lathe axis. The saw was moved along the axis at a rate of 3.5 mm/bolt revolution to keep the saw in the thread root.

The bolts were placed in an oven and loaded as shown in Figure 6.4 with loads listed in Table 6.1. Then the temperature was increased to 144°C at a rate of 10° per hour, soaked at that temperature for 6 hours and then cooled at a rate of 2° per hour. The material was calibrated by subjecting a loaded tensile specimen to the same heating cycle for each set of bolts. Each tensile specimen was taken from the same batch of epoxy resin as the bolts and measured 6 mm × 10 mm cross section. The gauge length was 80 mm and the specimens were loaded with

approximately 30 N. The geometry and loading of the tensile specimen can be seen in Figure 6.5

The nuts were glued onto the bolts after stress freezing using a cold setting epoxy resin, taking care to maintain the relative orientation of the nut and bolt. It is important to know where the nut was positioned in relation to the bolt threads during stress freezing so the nuts were glued in position. If the nuts had not been glued on, the nut sections would detach from the bolt once sliced, making it difficult to determine which thread was the first loaded thread, and making handling of the slices more difficult.

Slices, approximately 1 mm thick, were then taken from the nut and bolt using a diamond slitting wheel. The diamond wheel removed approximately 1 mm of material from each side of the slice as it cut. The slicing arrangements are shown in Figure 6.6. The number of slices that could be removed from one bolt was limited due to the amount of material lost when each slice was taken. The first slice is always taken through the middle of the crack and provided stress intensity factor information at the crack tip and stress concentration factor information at 180° intervals around the thread helix. The other slices were chosen to get a range of SIF values at different points around the crack front.

Once removed, the slices were examined in a polariscope, as shown in Figure 6.7. The location of the highest fringe order in the thread root was found using Mesnager's theorem, with the value of the fringe order at this point being found using Tardy compensation. The stress was then calculated from the fringe order.

To obtain stress intensity factors, photoelastic data was captured with a CCD camera and processed using the phase-stepping methodology described by Patterson and Wang[99]. The map of fringe order around the crack tip is used in a modified version[100] of the Multiple Point Over-Deterministic method proposed by Sanford and Dally[101]. Figure 6.8 shows the fringe pattern around the crack tip, with points showing the position of the data points used. This modified version uses Fourier series to describe the passing stress field, which is allowed to vary spatially. The crack tip stress field is defined using the Muskhelishvili[102] approach. The stress intensity factor is solved using a least-squares surface fitting routine to match the stress field equations to the isochromatic fringe data.

In all cases, the stress intensity factors where normalised against K_o, which was calculated as:

$$K_0 = \sigma\sqrt{\pi a} \qquad \textbf{Equation 6-1}$$

where σ is calculated as the applied load divided by the stress area of the bolt and the crack length is a.

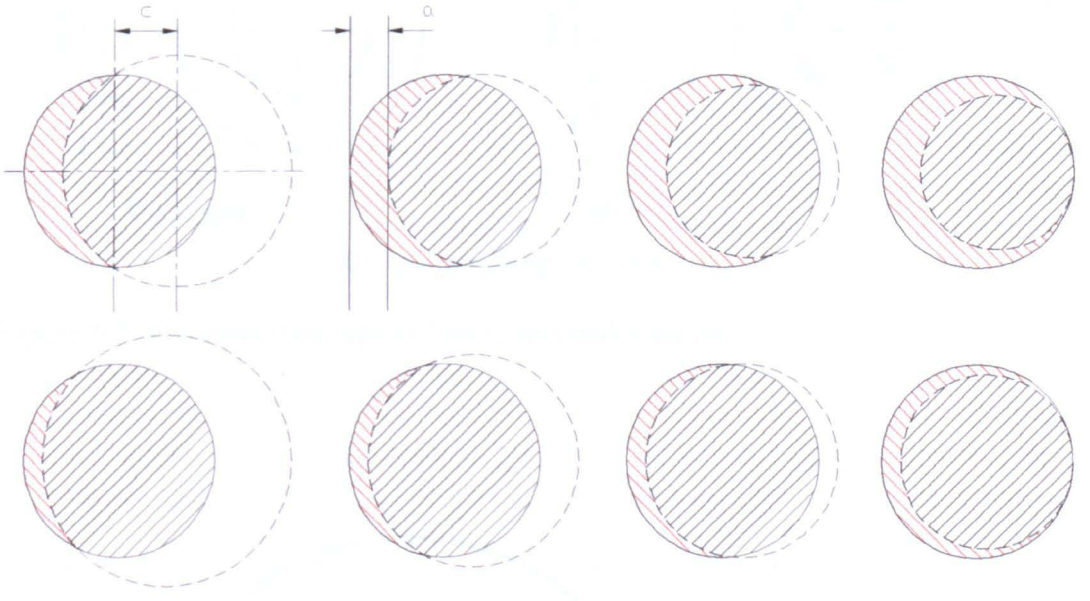

Figure 6.1 Projected shapes of cracks (red) and the remaining bolt (black)

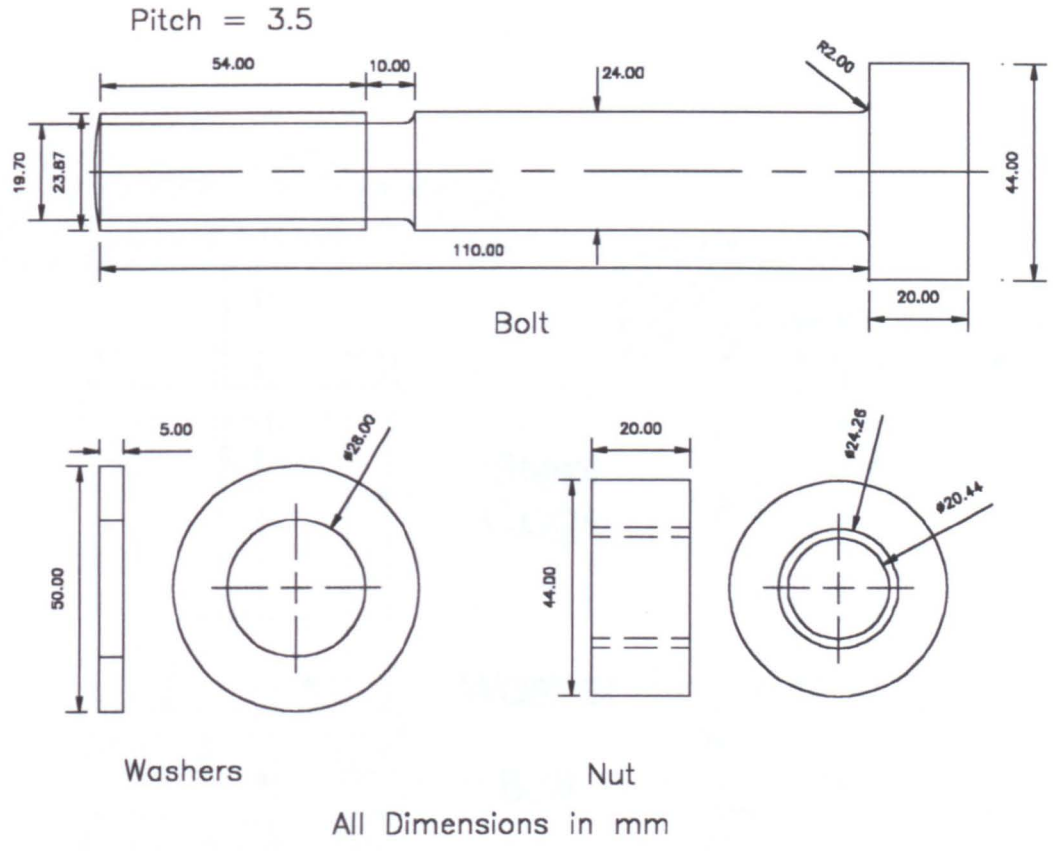

Figure 6.2 Dimensions of epoxy bolts, nuts and washers

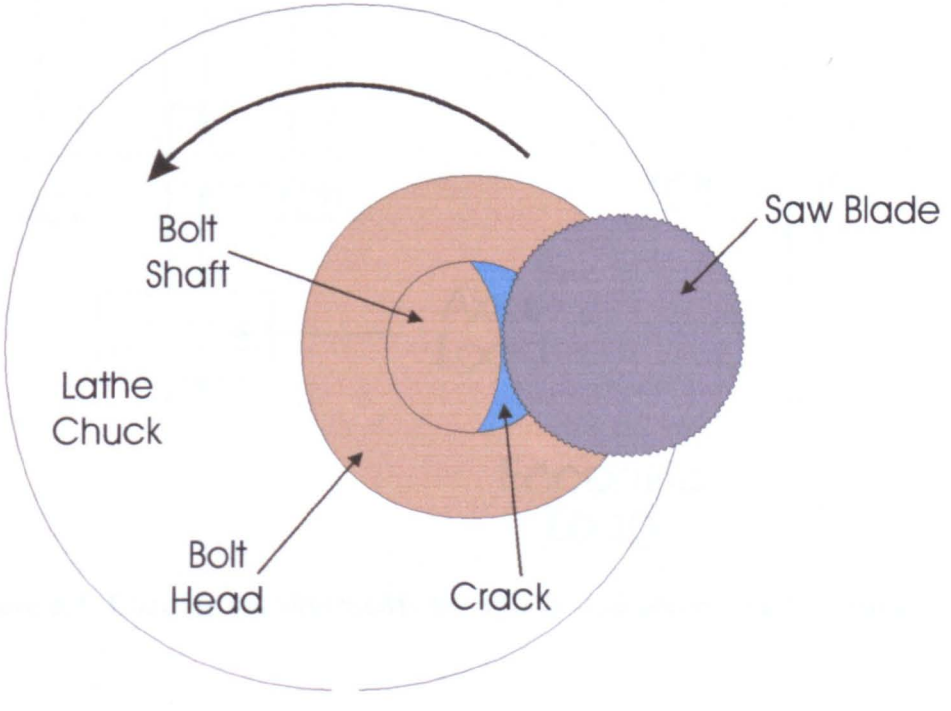

Figure 6.3 Diagram of method for cutting crescent-shaped cracks into the thread roots of bolts

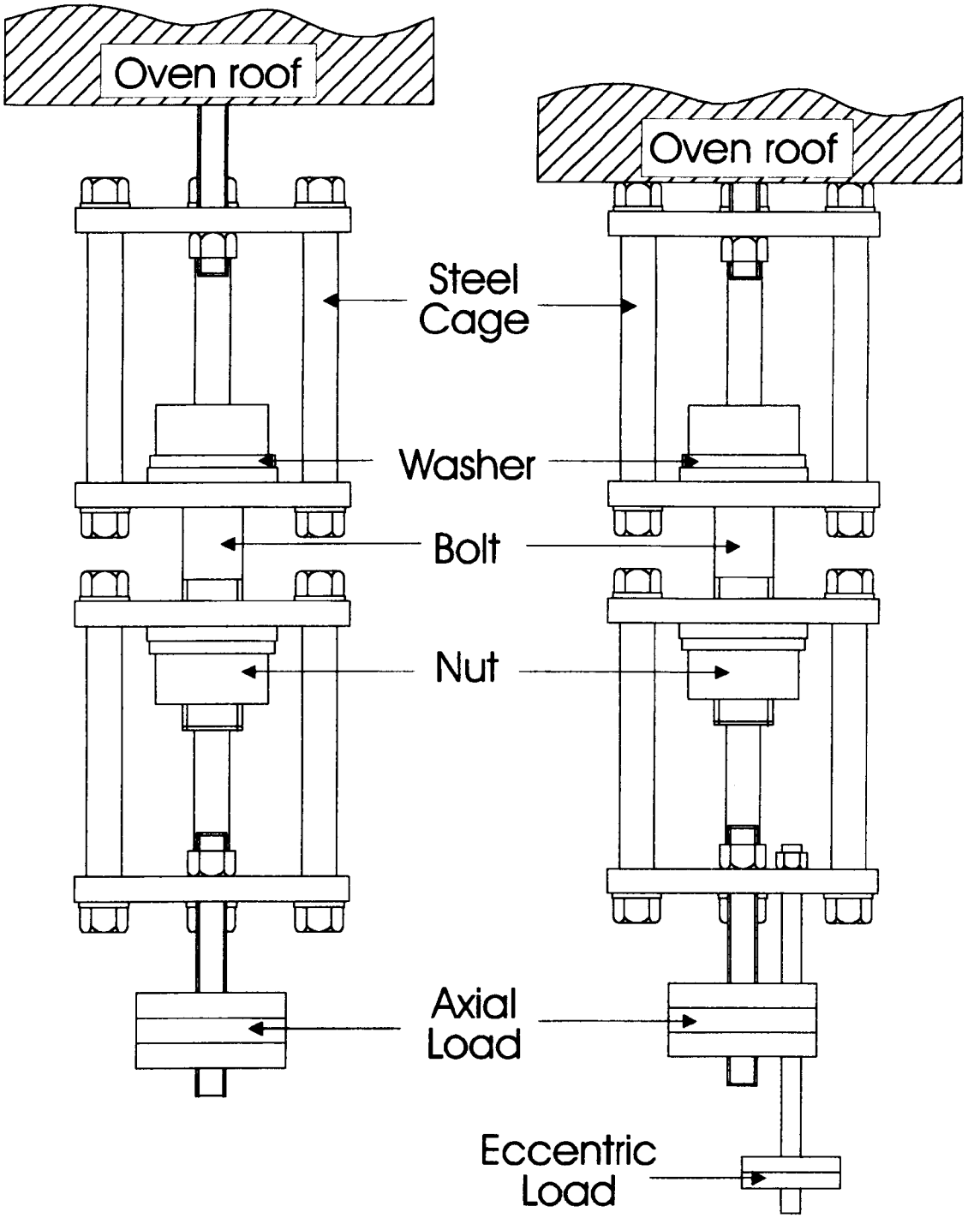

Figure 6.4 Loading arrangements for axially and eccentrically loaded bolts.

Bolt	Crack Length (mm)	Crack shape parameter, c (mm)	Axial Load (N)	Young's Modulus (MPa)
B1	2	2	114	39.8
B2	2	5	114	39.8
B3	2	3	114	45.8
B4	2	1	114	45.8
B5	4	4	97	38.5
B6	4	6	97	38.5
B7	4	3	92	29.4
B8	4	2	87	29.4

Table 6.1 Loads used and Young's Modulus for axially loaded bolts

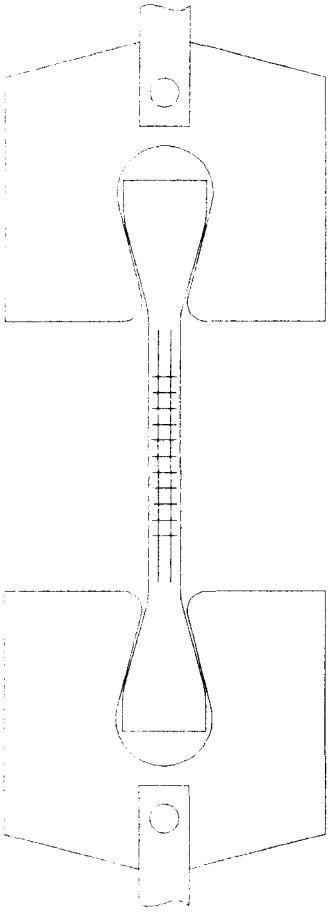

Figure 6.5 Loading arrangement for the tensile specimens

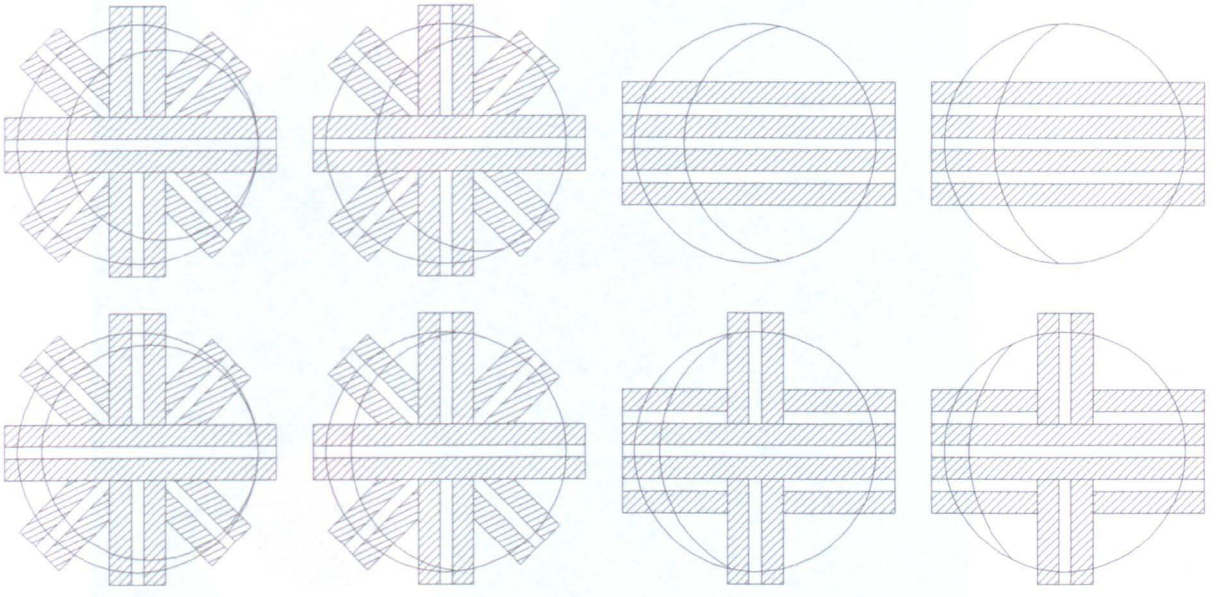

Figure 6.6 Crack slices taken and material lost (hatched)

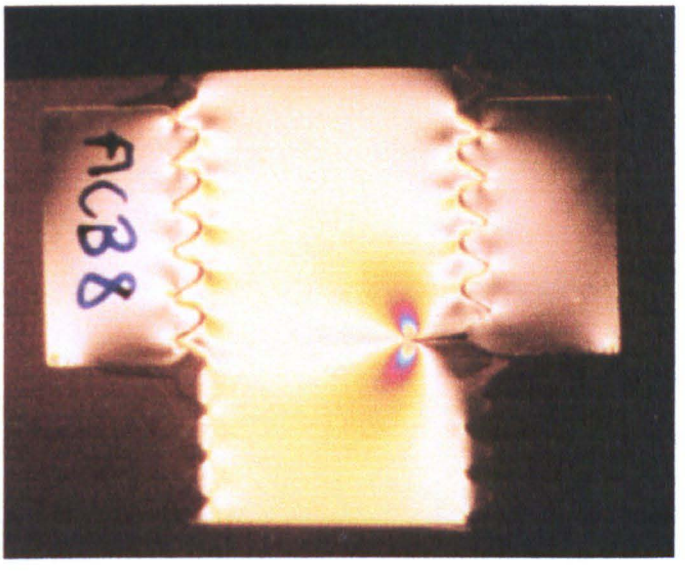

Figure 6.7 Slice taken from an axially loaded bolt viewed in a dark field polariscope

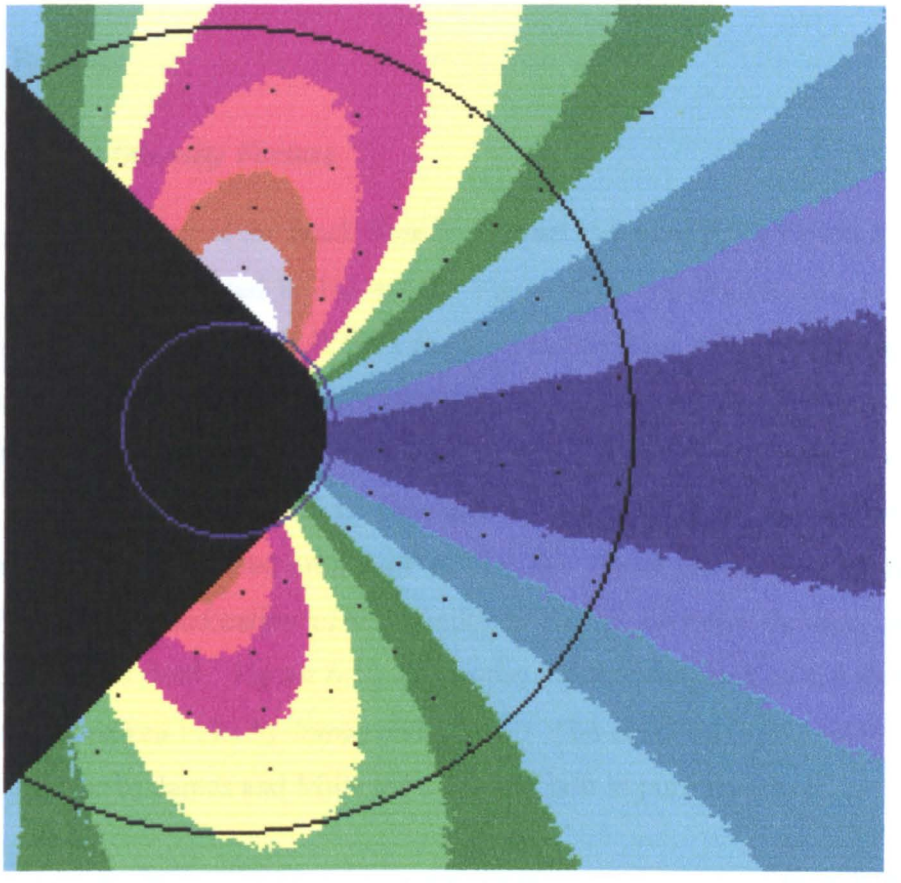

Figure 6.8 Map of wrapped isochromatic fringes with masked area and data points shown

6.2.2 Results

6.2.2.1 Stress Intensity Factors

The SIFs at the centre of the crack front are shown in Figure 6.10, Figure 6.11 and Figure 6.12, and are listed in Table 6.2. Figure 6.10 and Figure 6.11 show the variation in mode I and mode II SIFs at the centre of the crack front as the shape of the crack changes for the two series of tests (nominal crack lengths 2 mm and 4 mm respectively). The 95% confidence limits shown as error bars on the mode I values indicate the quality of fit between the theoretical stress field and the measured stress field, based on a least squares fit. These limits are calculated by the software as an indication of the quality of the fit between the data and the theoretical stress field. Figure 6.12 shows the results compared to the empirical formula for cracked bolts by James and Mills[47]. The equation produced for stress intensity factor by James and Mills for a cracked bolt in pure tension is:

$$\frac{K}{\sigma\sqrt{\pi a}} = Ae^{Bx} + C + Dx + Ex^2 + Fx^3 + Gx^4 \qquad \textbf{Equation 6-2}$$

Where:

A = 2.043	E = 3.0469
B = -31.332	F = -19.504
C = 0.6507	G = 45.674
D = 0.5367	x = a/D

Table 6.3 lists the results for the stress intensity factors around the crack front and the K_I/K_o values are plotted in Figure 6.13 for the 2 mm cracks and Figure 6.14 for the 4 mm cracks. X is the fraction of the crack front length at which the values were taken, as shown in Figure 6.9. Due to the different shapes of the cracks and the different slicing arrangements, values were taken at different values of X for each bolt. SIF values could not be obtained at the ends of the crack fronts, because of the very short crack lengths. This is a plan view, so the crack moves up the helix further into the nut as x increases. In all cases, the highest mode I SIF is located at the centre of the crack front, x = 0.5. The mode II results are plotted in Figure 6.15 and Figure 6.16 for the 2 mm and 4 mm crack

lengths respectively. It can be seen that in mode II, the SIFs generally increase towards the ends of the cracks.

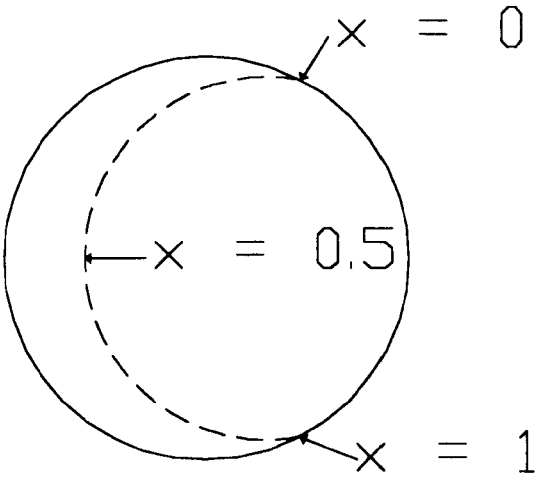

Figure 6.9 Measurement of x, distance along crack front.

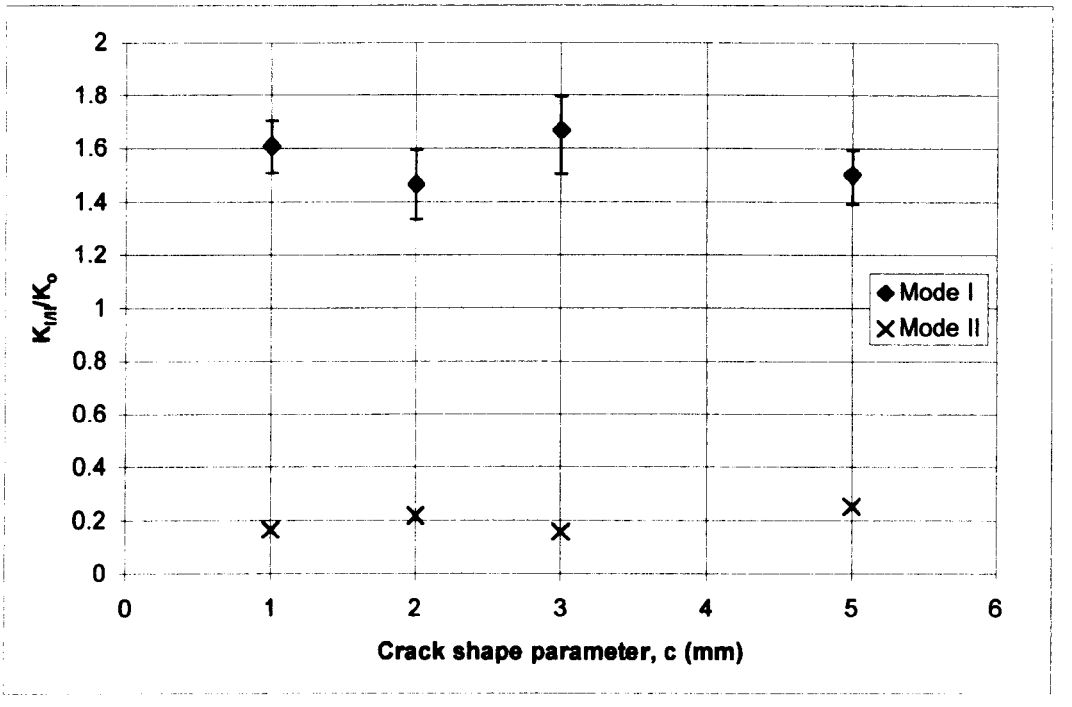

Figure 6.10 SIF at the centre of the crack front against crack shape for 2 mm crack

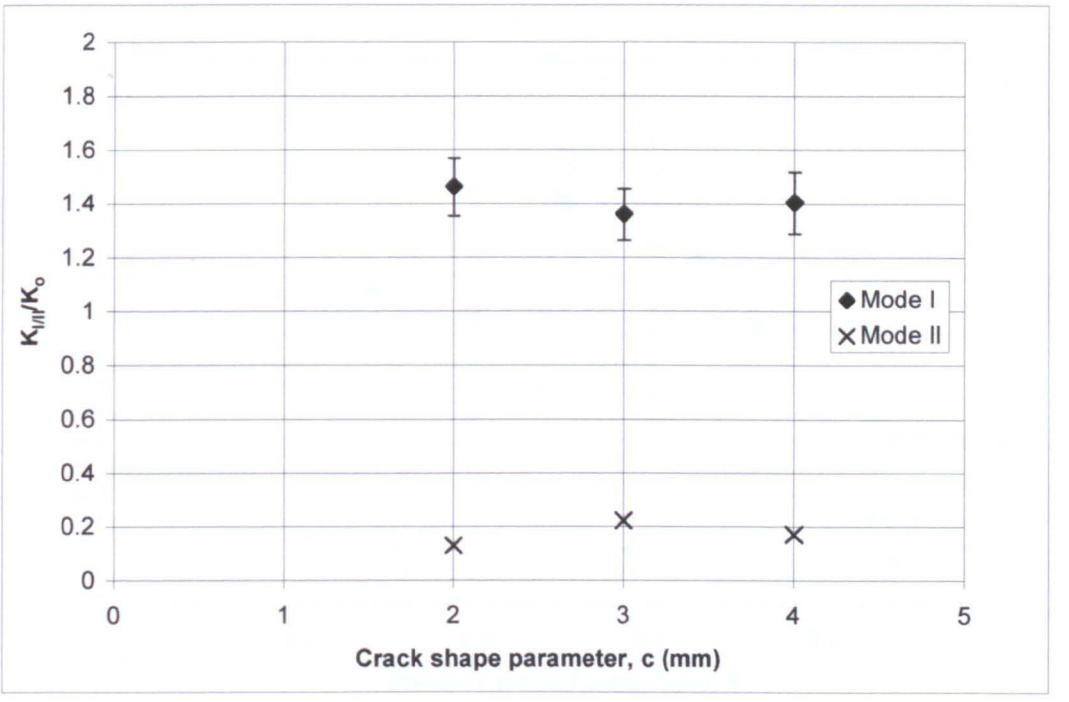

Figure 6.11 SIF at the centre of the crack front against crack shape for 4 mm crack

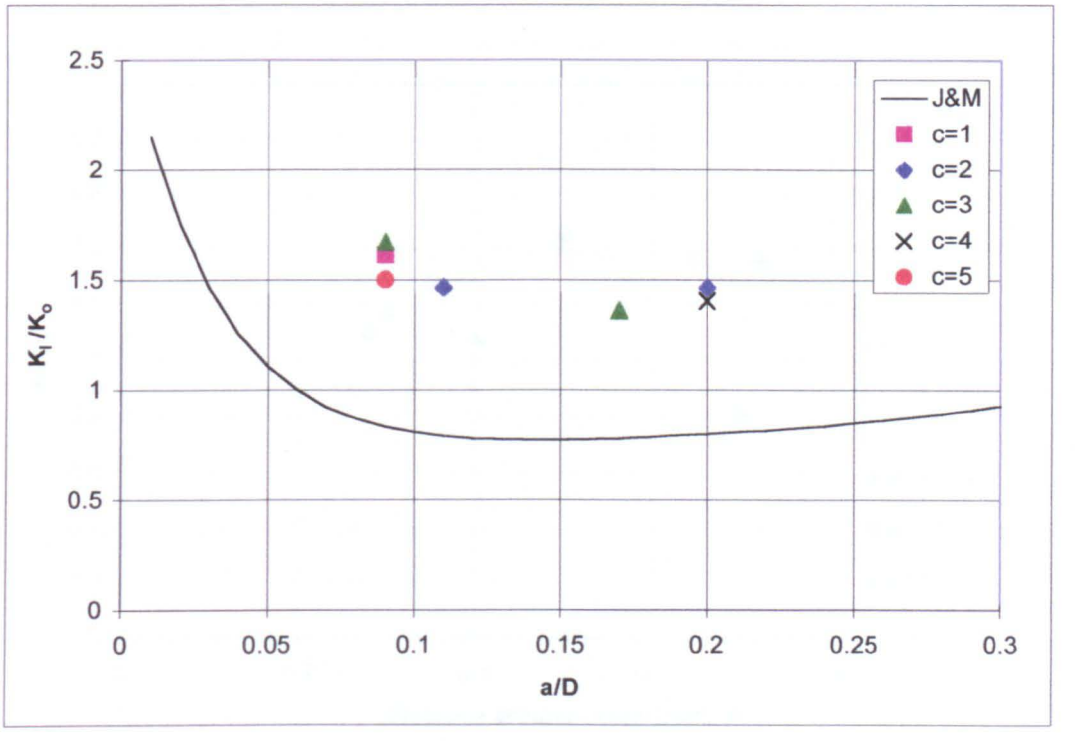

Figure 6.12 SIF at the centre of the crack front from photoelastic analysis compared to empirical equation (James & Mills[47])

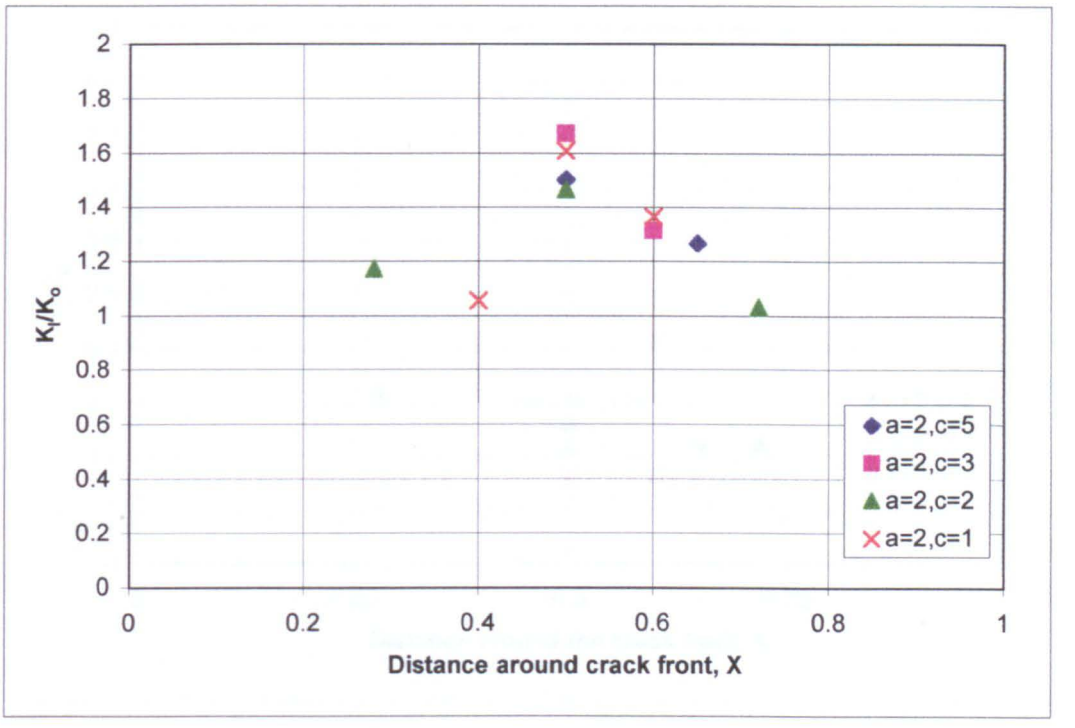

Figure 6.13 Variation of mode I SIFs around the crack front for 2 mm crack length

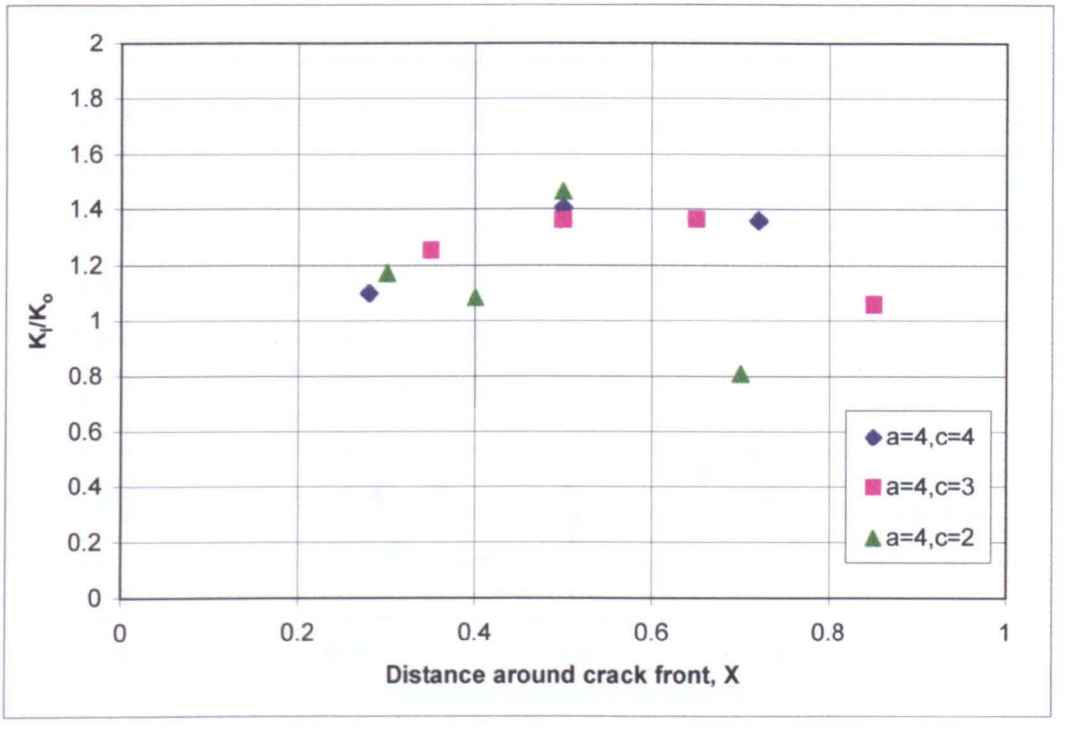

Figure 6.14 Variation of mode I SIFs around the crack front for 4 mm crack length

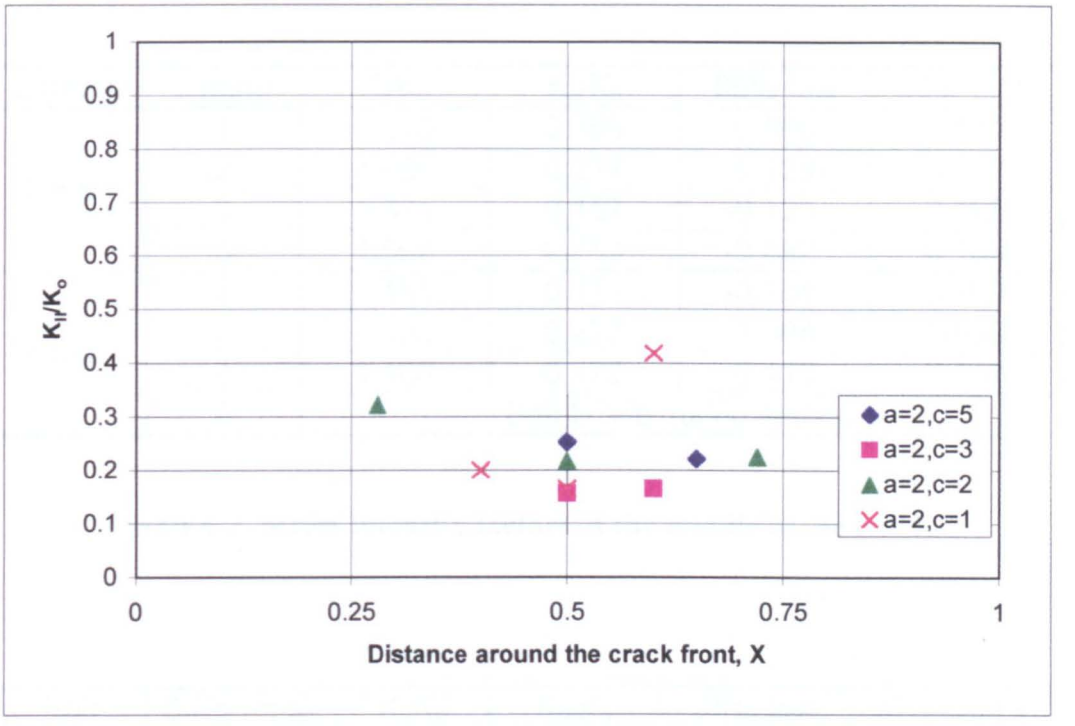

Figure 6.15 Variation of mode II SIFs around the crack front for 2 mm cracks

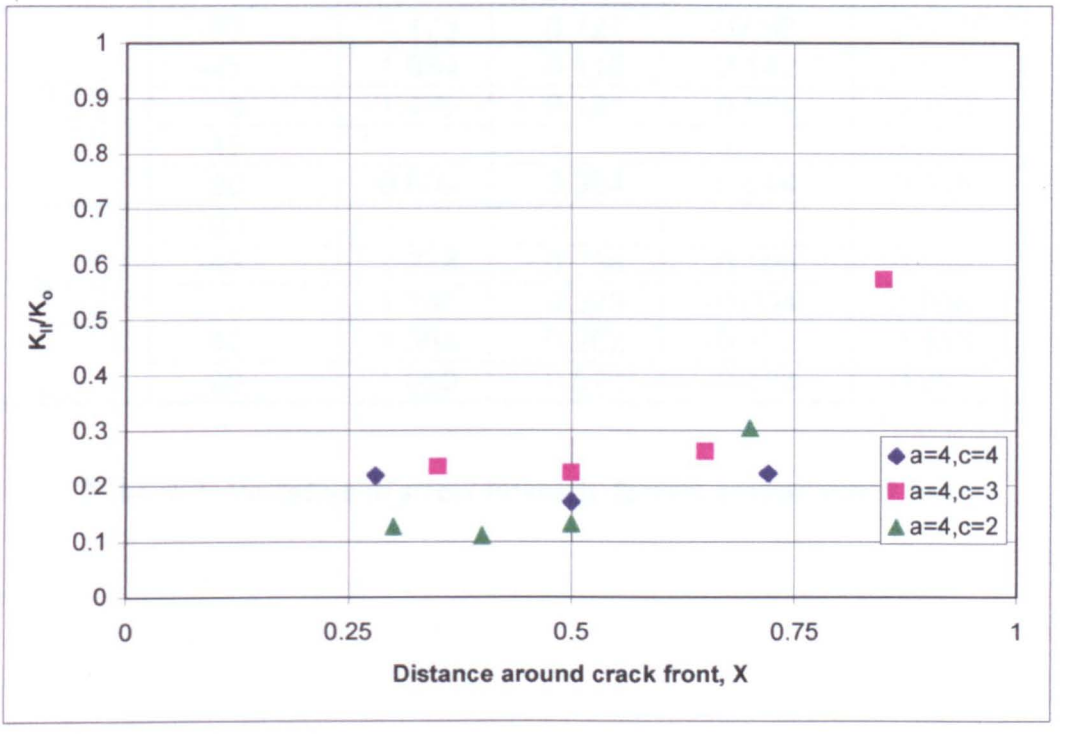

Figure 6.16 Variation of mode II SIFs around the crack front for 4 mm cracks

a (mm)	c (mm)	K_I/K_o	K_{II}/K_o	95% low	95% high
2 mm	1	1.610	0.166	-0.096	0.101
	2	1.466	0.217	-0.129	0.133
	3	1.671	0.157	-0.125	0.168
	5	1.502	0.253	-0.092	0.108
4 mm	2	1.465	0.131	-0.104	0.109
	3	1.363	0.223	-0.094	0.098
	4	1.406	0.172	-0.113	0.117
	6	Bolt broke during testing			

Table 6.2 Stress intensity factors at the middle of the crack.

Bolt	Slice angle	K_I/K_o	K_{II}/K_o	95% low	95% high
a = 2 c = 1	-45	1.055	0.200	-0.081	0.086
	0	1.610	0.166	-0.096	0.101
	45	1.365	0.419	-0.087	0.167
a = 2 c = 2	-45	1.174	0.322	-0.125	0.175
	0	1.466	0.217	-0.129	0.133
	45	1.032	0.225	-0.126	0.143
a = 4 c = 2	-90	1.173	0.127	-0.062	0.073
	-45	1.084	0.110	-0.142	0.153
	0	1.465	0.131	-0.104	0.109
	45	-	-	-	-
	90	0.809	0.304	-0.044	0.048
a = 4 c = 3	-90	-	-	-	-
	-45	1.254	0.234	-0.105	0.109
	0	1.363	0.223	-0.094	0.098
	45	1.364	0.262	-0.122	0.133
	90	1.059	0.573	-0.156	0.207

Table 6.3 Variation of stress intensity factors around crack front

6.2.2.2 Stress Distribution

The stress distributions obtained for all the crack shapes investigated are shown in Figure 6.17. The stresses are plotted in terms of the stress concentration factor, which is calculated thus:

$$SCF = \frac{(\sigma_1 - \sigma_2)}{L / A_s}$$

where:

σ_1, σ_2 = principal stresses

L = applied load

A_s = stress area of bolt

With the maximum SCF always occurring on the surface, σ_2 will be zero, so the difference in the principal stresses will equal the maximum principal stress. The SCF values are not simply a factor of the geometry of the thread roots, but also of the load distribution between the threads.

The crack is positioned half a thread pitch (1.75 mm) from the loaded face of the nut in each case, therefore there is no reading at this position. The crack becomes less crescent-shaped as c increases, as the diagrams in the top right hand corner of each chart show. The results from photoelastic analysis of uncracked bolts is shown in Figure 6.18 for comparison. These sets of results contain twice as many data points, 4 per thread, as the distributions for the cracked bolts. Also, they contain results for half a thread pitch from the loaded face, which is missing due to the position of the crack in the cracked bolts.

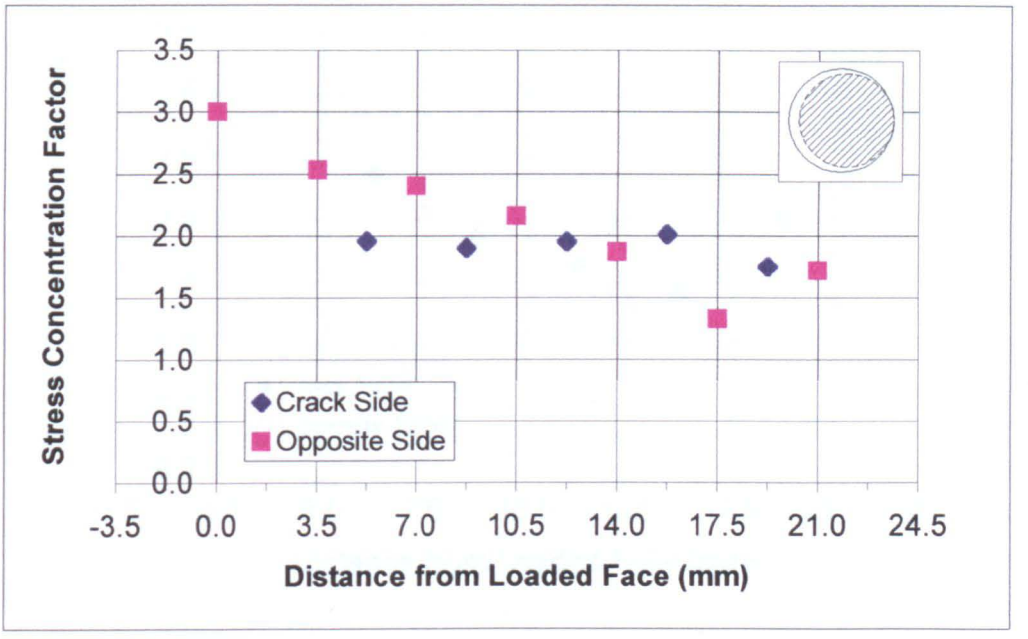

a = 2 mm, c = 1 mm

(a)

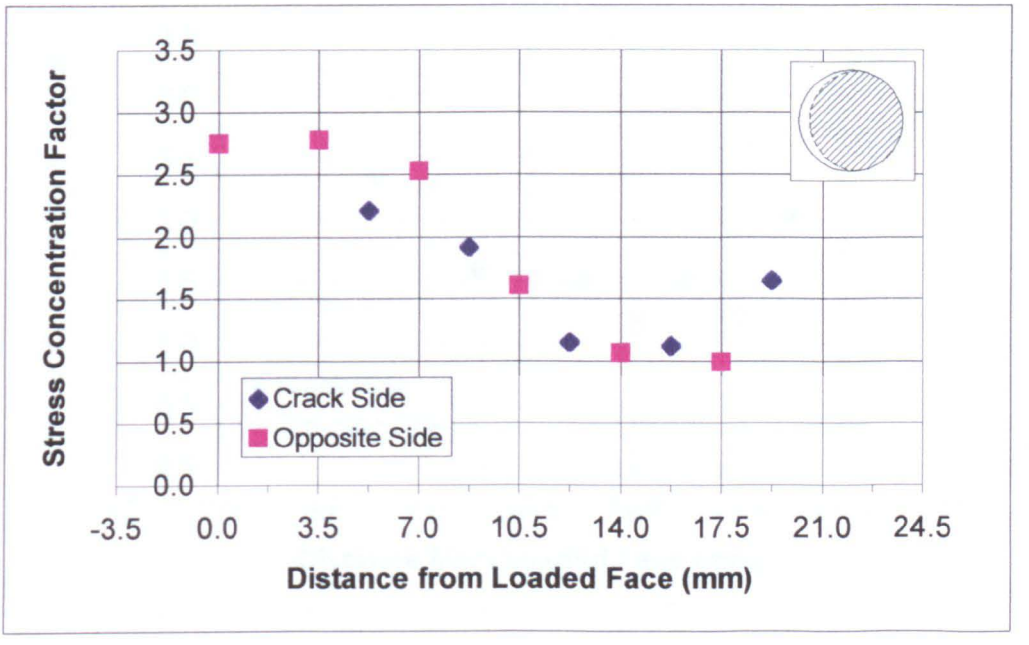

a = 2 mm, c = 2 mm

(b)

Figure 6.17 Stress distributions for crack bolts under axial loading

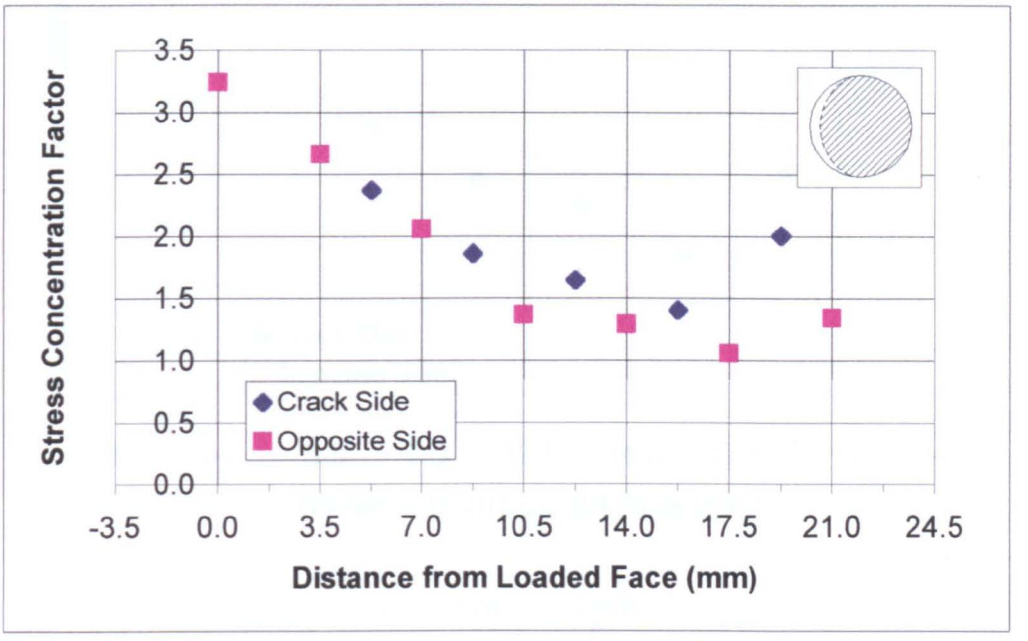

a = 2 mm, c = 3 mm

(c)

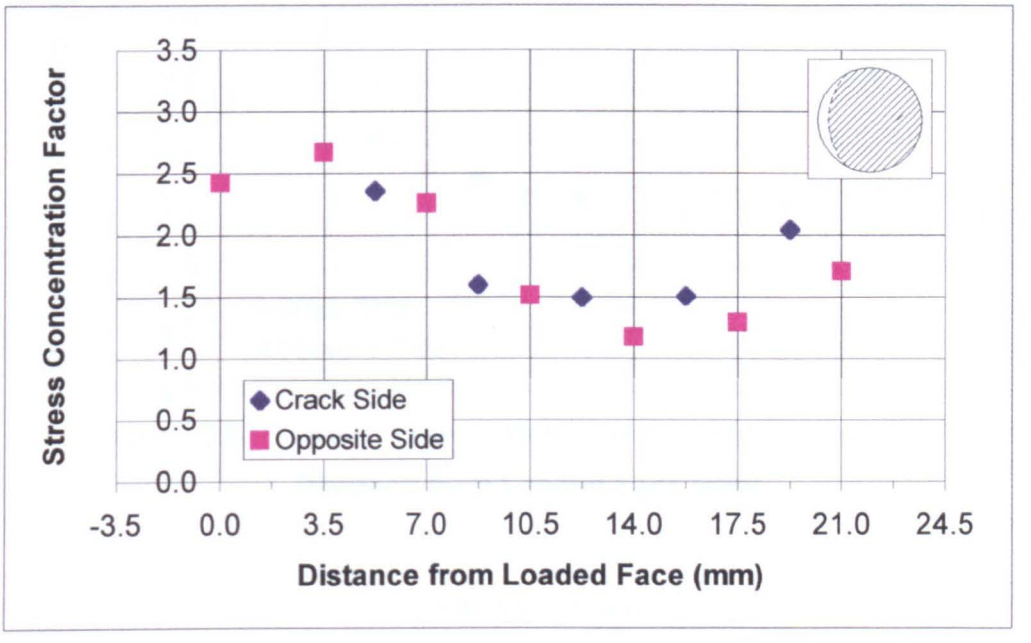

a = 2 mm, c = 5 mm

(d)

Figure 6.17 Stress distributions for crack bolts under axial loading

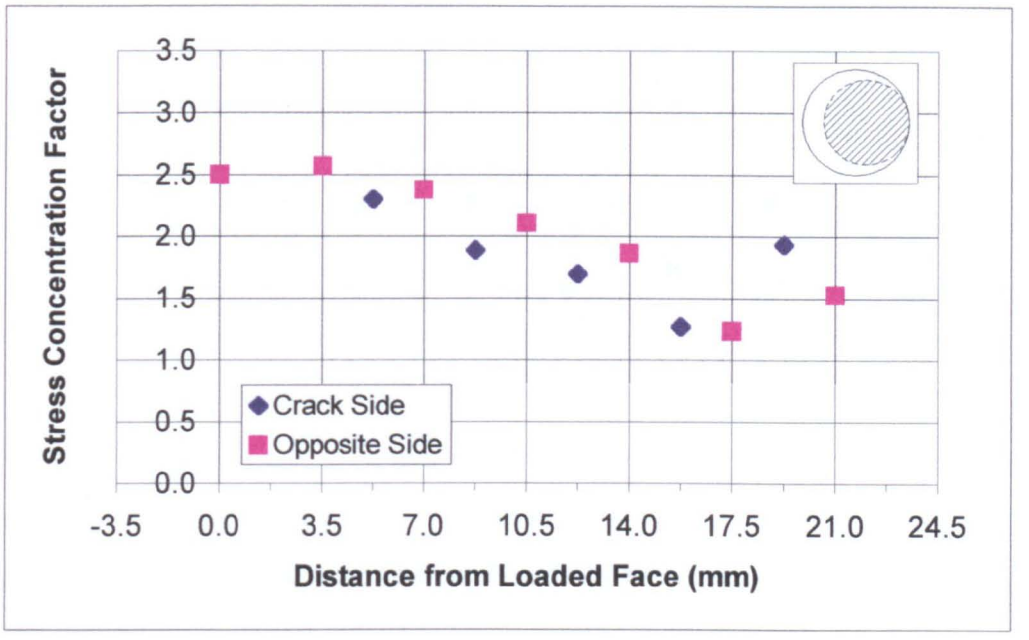

a = 4 mm, c = 2 mm

(e)

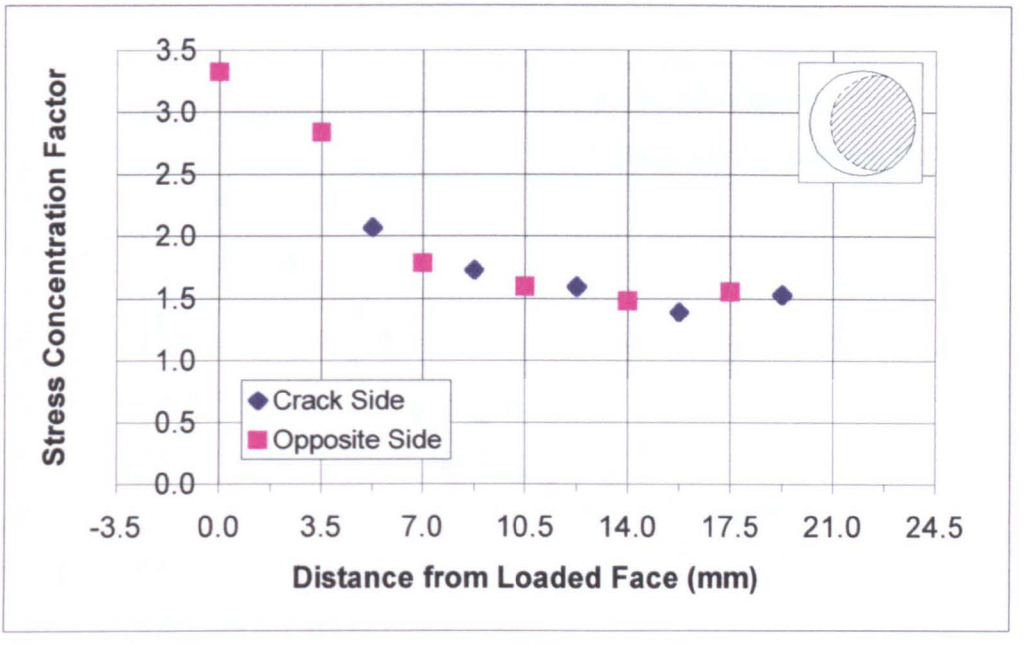

a = 4 mm, c = 3 mm

(f)

Figure 6.17 Stress distributions for crack bolts under axial loading

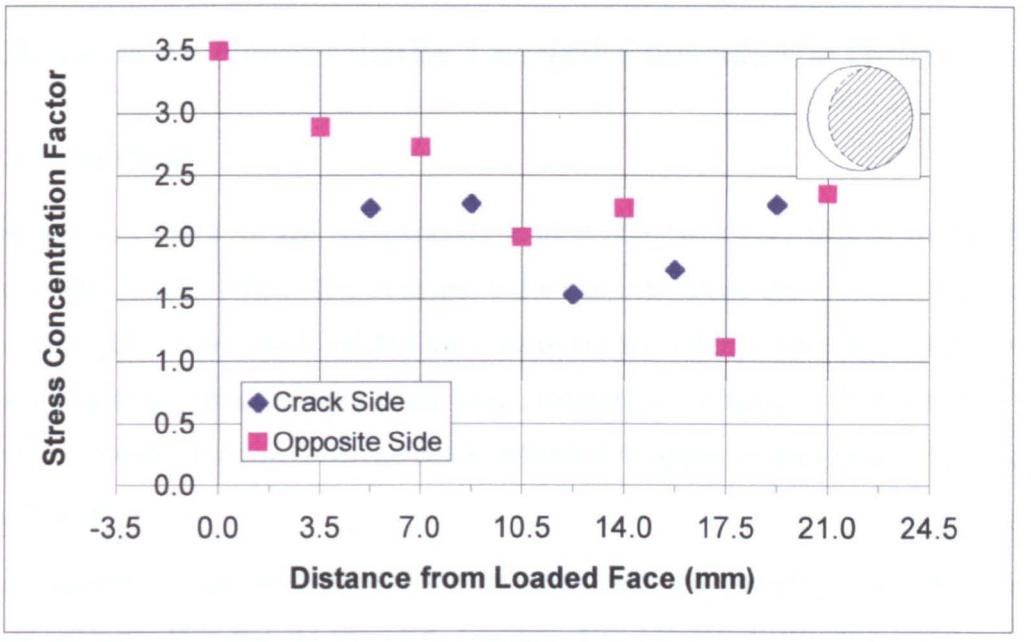

a = 4 mm, c = 4 mm

(g)

Figure 6.17 Stress distributions for crack bolts under axial loading

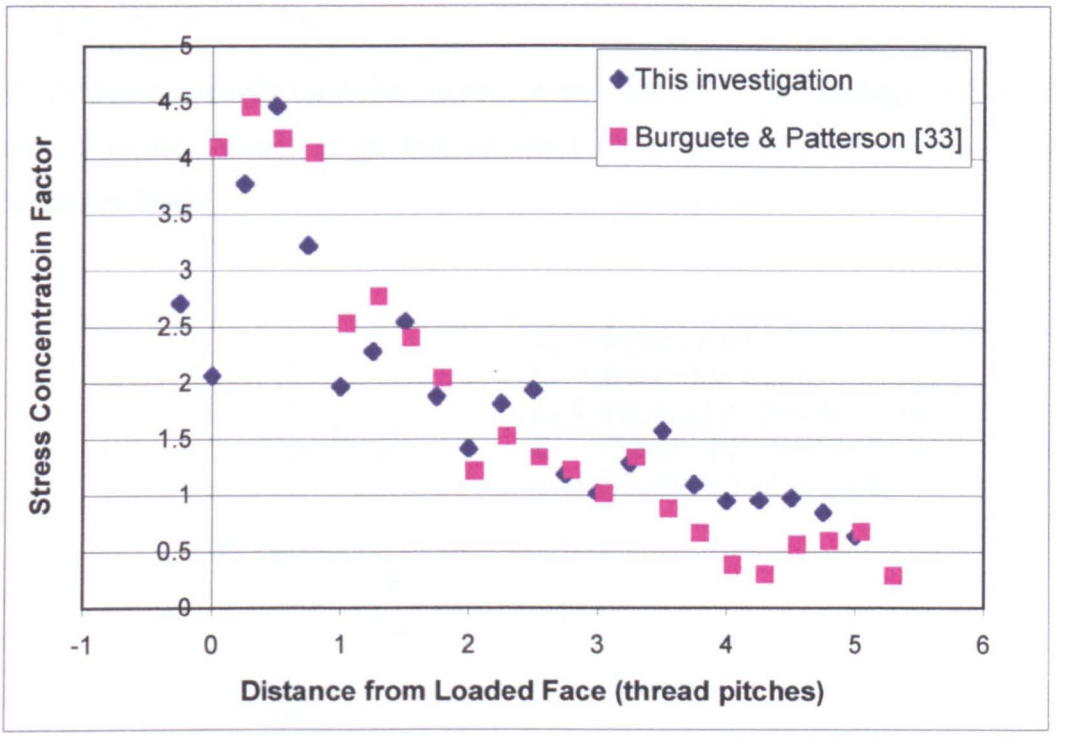

Figure 6.18 Stress distributions for uncracked bolts

6.3 Tests on Eccentrically Loaded Photoelastic Bolts

6.3.1 Method

The test procedure for the eccentrically loaded bolts was very similar to that for the axially loaded bolts. The nuts and bolts were the same dimensions, the same loading cycles were used and the same analysis procedures were followed. One crack shape was used for each of the crack lengths; a = 2 mm, c = 2 mm and a = 4 mm, c = 4 mm. In each case, the crack extended to approximately half way round the bolt helix.

The eccentric loads were applied by hanging additional weights from the lower cage, 20 mm off centre, as shown in Figure 6.4 and Figure 6.19. The eccentricity has been stated in terms of the eccentricity of a single load, L_E, equivalent to the axial and eccentric applied loads. The bending moment caused by the eccentric load is equal to $L_B \times E$. This moment could also be applied by a single load, L_E, at an eccentricity of e. To maintain the same axial load, the single load, L_E, must be equivalent to $L_A + L_B$.

All the loads used for the bolts are shown in Table 6.4. The bending loads were applied so that the side of the bolt on which the crack was situated experienced the higher loads.

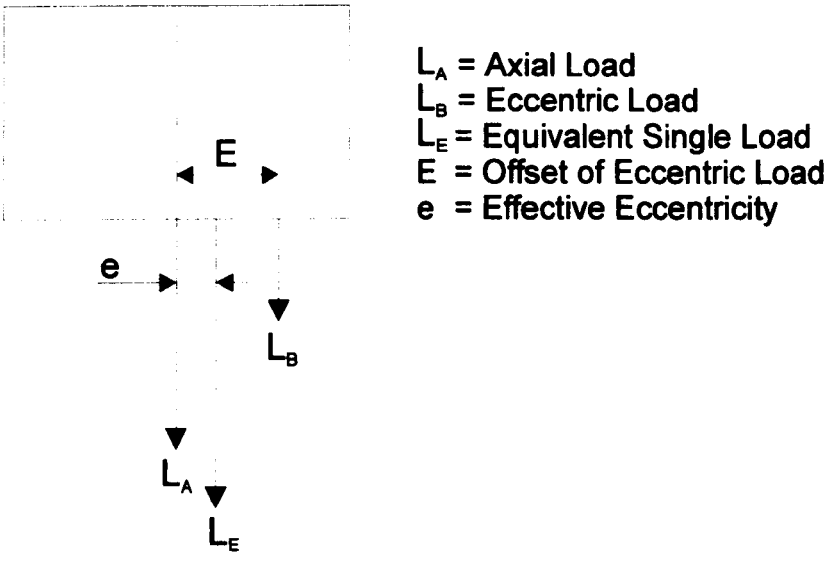

Figure 6.19 Calculation of eccentricity, e

The axial and bending stress caused by the loading can be calculated as follows:

$$\sigma_{axial} = \frac{(L_A + L_B)}{A_s} \qquad \textbf{Equation 6-3}$$

and

$$\sigma_{bending} = \frac{My}{I} = \frac{32L_B e}{\pi d^3} \qquad \textbf{Equation 6-4}$$

Using these equations, it can be found that for bolt E9 the axial and bending stresses are 0.177 MPa and 0.277 MPa respectively. This gives a maximum stress of 0.454 MPa, which is about 156% higher than if the loading had been purely axial. This is neglecting the crack and assuming that axis of the bolt and the axis of the bending load remain in their original positions.

Bolt	Crack Length (mm)	e/D	Axial Load (N)	Eccentric Load (N)	Young's Modulus (MPa)	Comments
E2	2	0.168	78.5	19.9	32.5	
E3	2	0.249	69.9	29.8	31.8	
E4	2	0.084	90.2	10.2	31.8	
E5	4	0.085	89.4	10.1		Broke
E6	4	0.168	78.7	19.9		Crack grew
E7	4	0.082	71.6	7.9	35.4	
E8	4	0.166	64.2	16.0		Broke
E9	4	0.169	47.5	12.1	33.8	
E10	4	0.042	57.1	3.1	36.8	
E11	2	0.040	76.5	3.9	36.8	
E12	4	0.250	41.6	17.9		Crack grew

Table 6.4 Loads used and Young's Modulus for eccentrically loaded bolts

6.3.2 Results

6.3.2.1 Stress Intensity Factors

The variations in stress intensity factors with eccentricity are shown in Figure 6.20 and Figure 6.21 with error bars representing the 95% confidence limits. All the results are also shown in Table 6.5.

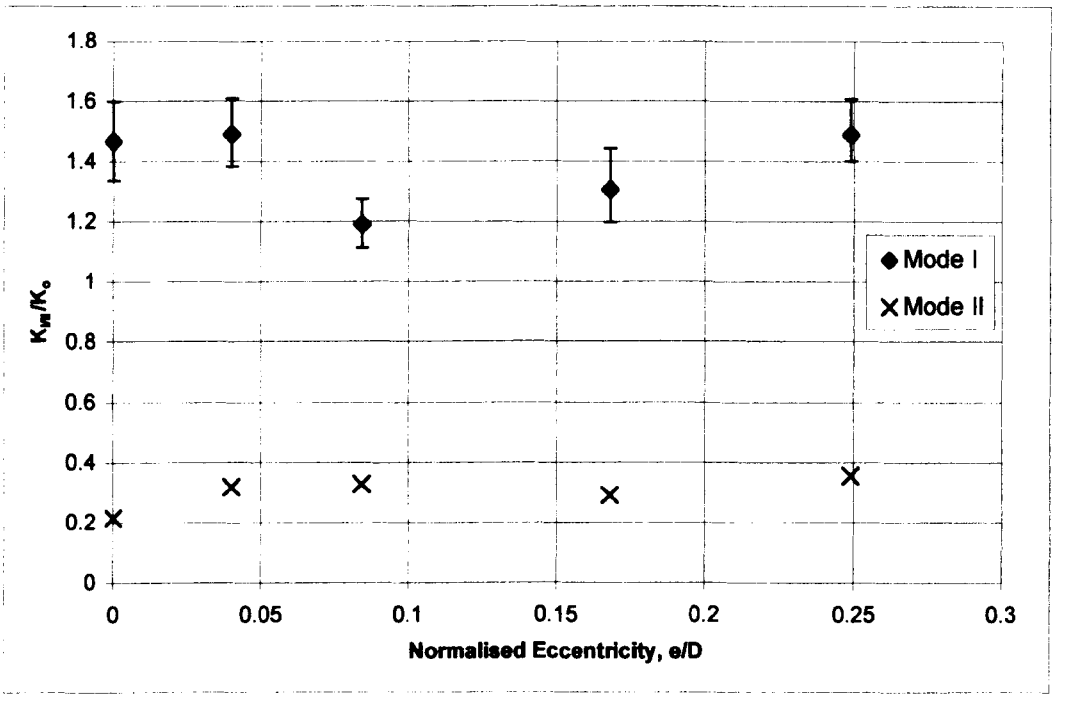

Figure 6.20 SIF at the centre of the crack front against eccentricity for 2 mm cracks

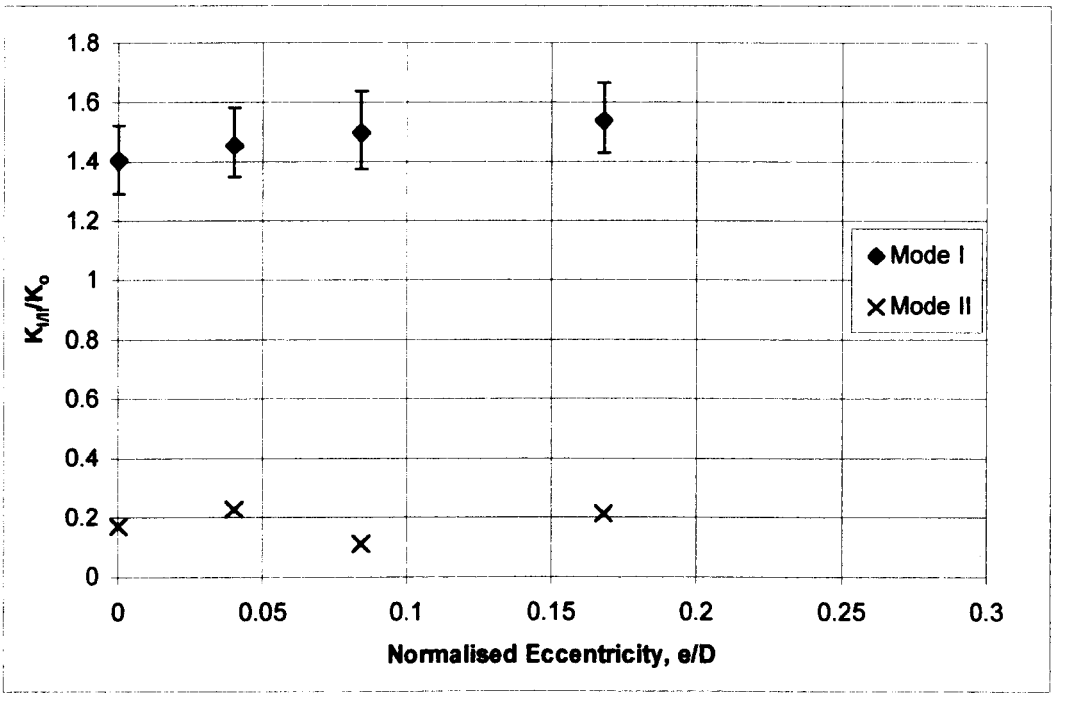

Figure 6.21 SIF at the centre of the crack front against eccentricity for 4 mm cracks

a (mm)	e/D	K_I/K_o	K_{II}/K_o	95% low	95% high
2 mm	0	1.466	0.217	0.129	0.133
	0.04	1.489	0.32	0.107	0.118
	0.084	1.191	0.329	0.077	0.085
	0.168	1.306	0.293	0.109	0.137
	0.249	1.488	0.357	0.086	0.118
4 mm	0	1.406	0.172	0.113	0.117
	0.04	1.456	0.228	0.105	0.129
	0.084	1.499	0.112	0.123	0.138
	0.168	1.54	0.214	0.111	0.126

Table 6.5 Results for eccentrically loaded bolts

6.3.2.2 Stress Distributions

The stress distributions obtained for the 2 mm and 4 mm crack series are shown in Figure 6.22. The crack is positioned half a thread pitch (1.75 mm) from the loaded face in each case, therefore there is no reading at this position. The bending is applied so that the side of the bolt with the crack in experiences the greatest load.

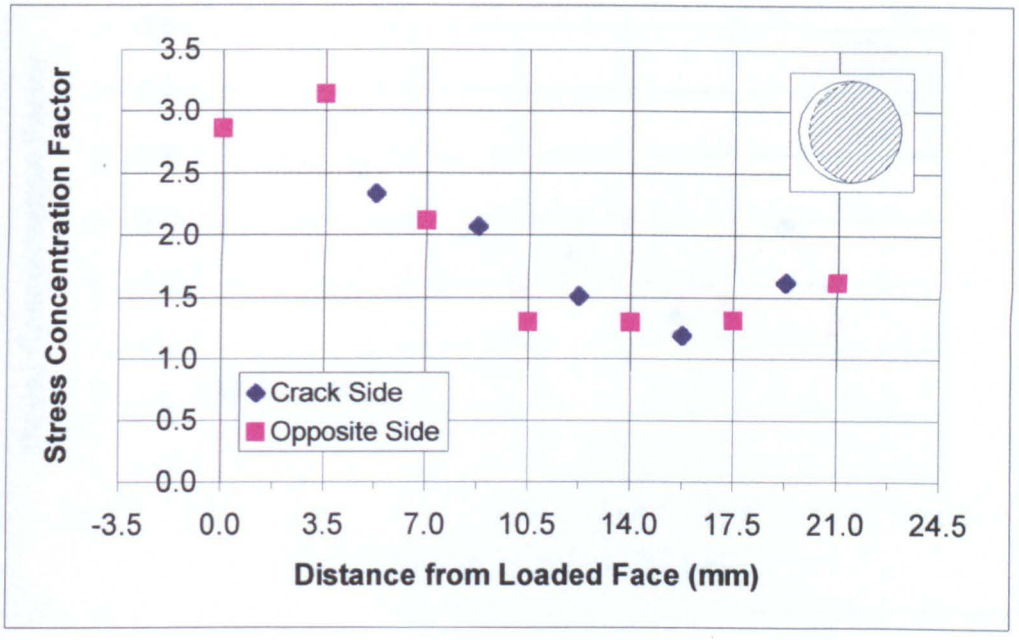

(a) e/D = 0.04

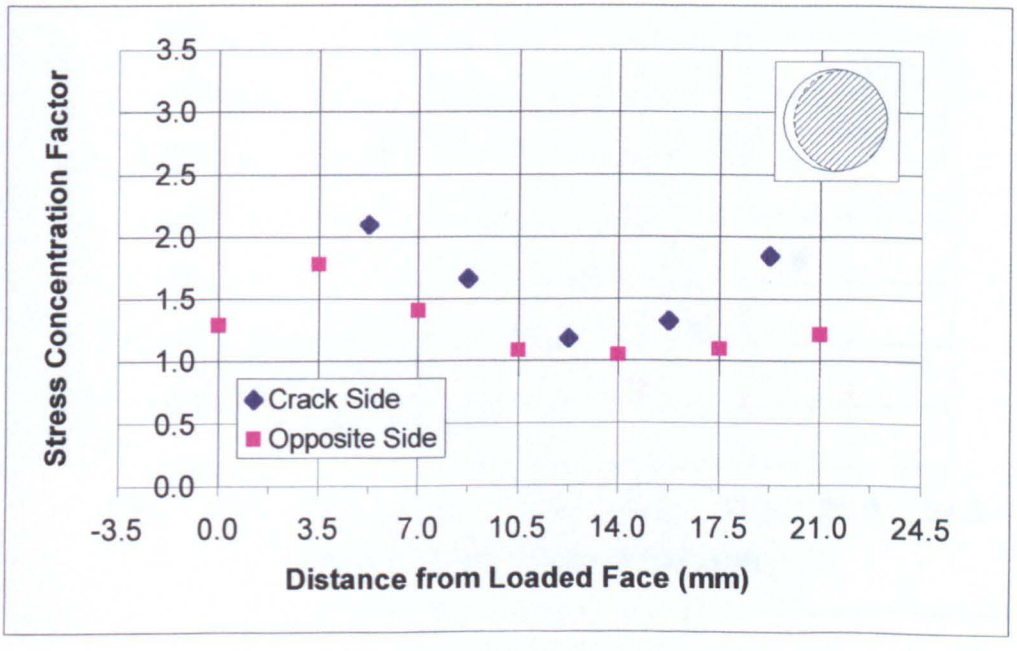

(b) e/D = 0.08

Figure 6.22 Stress distributions for eccentrically loaded, cracked bolts

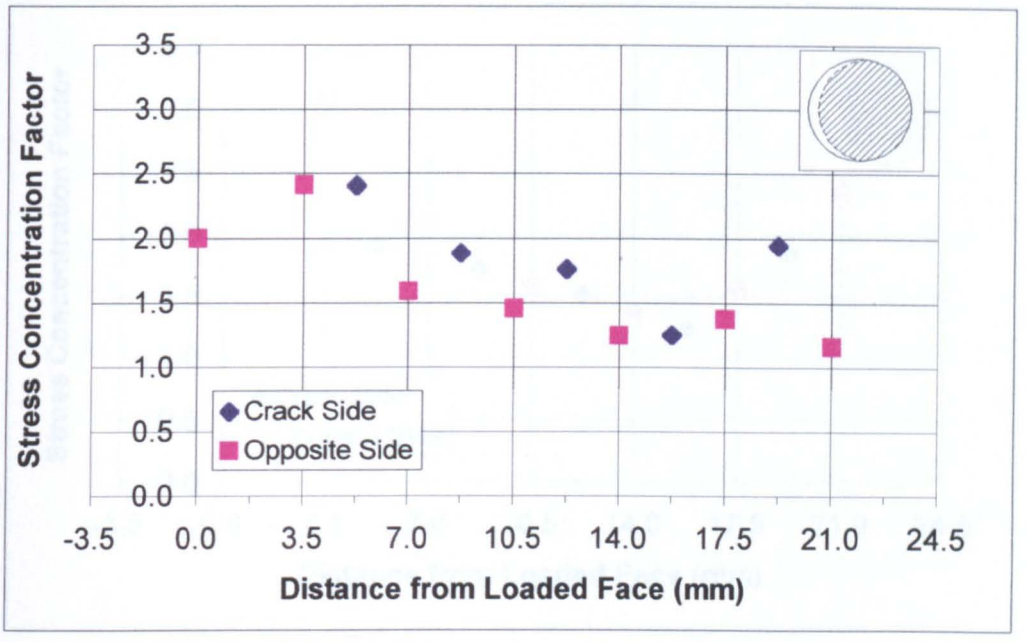

(c) e/D = 0.17

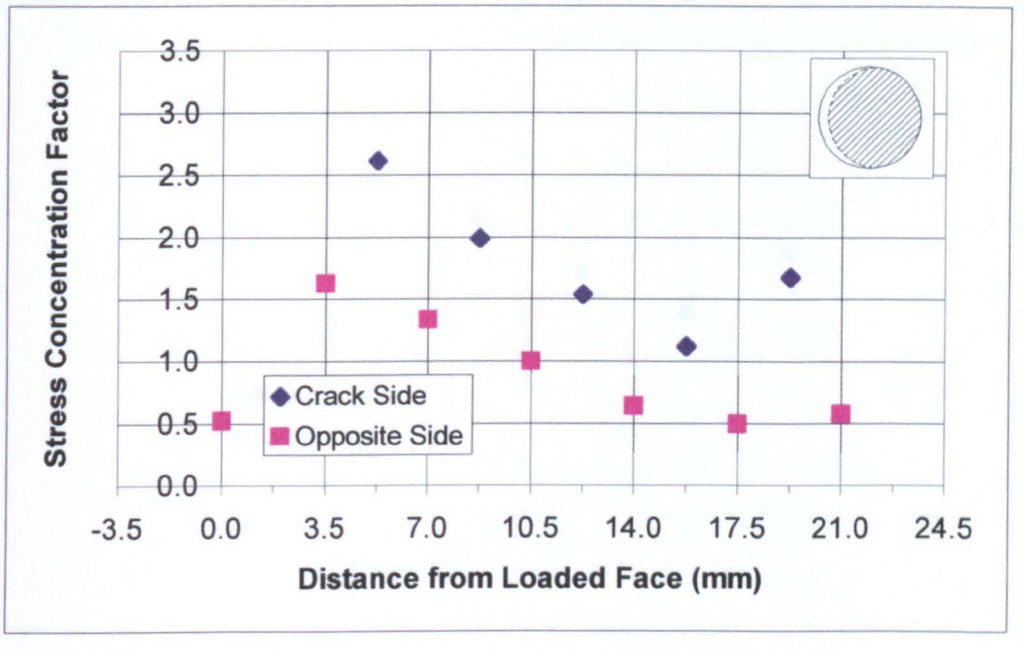

(d) e/D = 0.25

Figure 6.22 Stress distributions for eccentrically loaded, cracked bolts

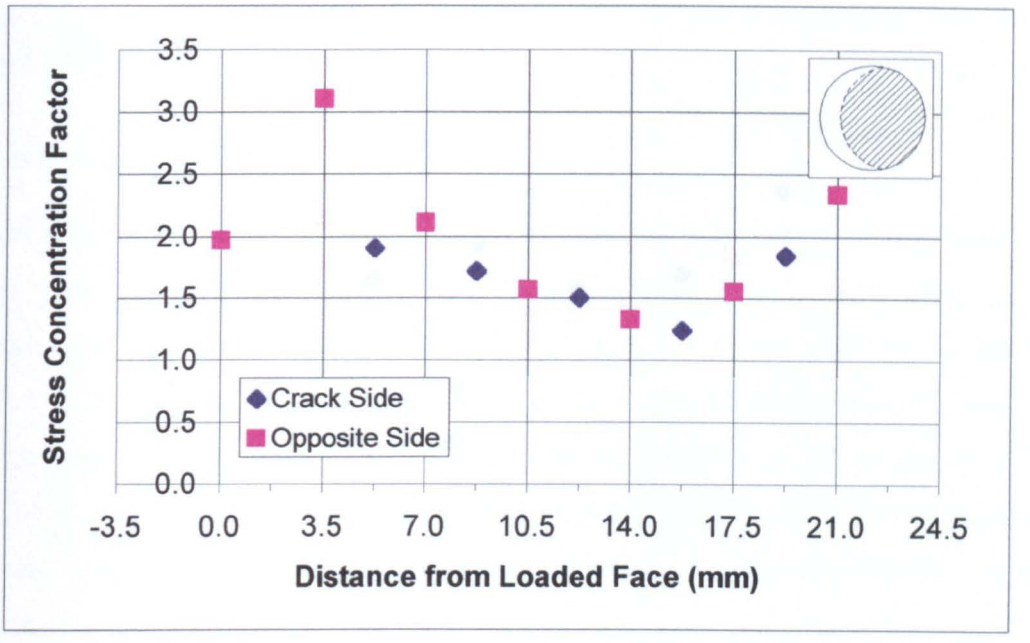

(e) e/D = 0.04

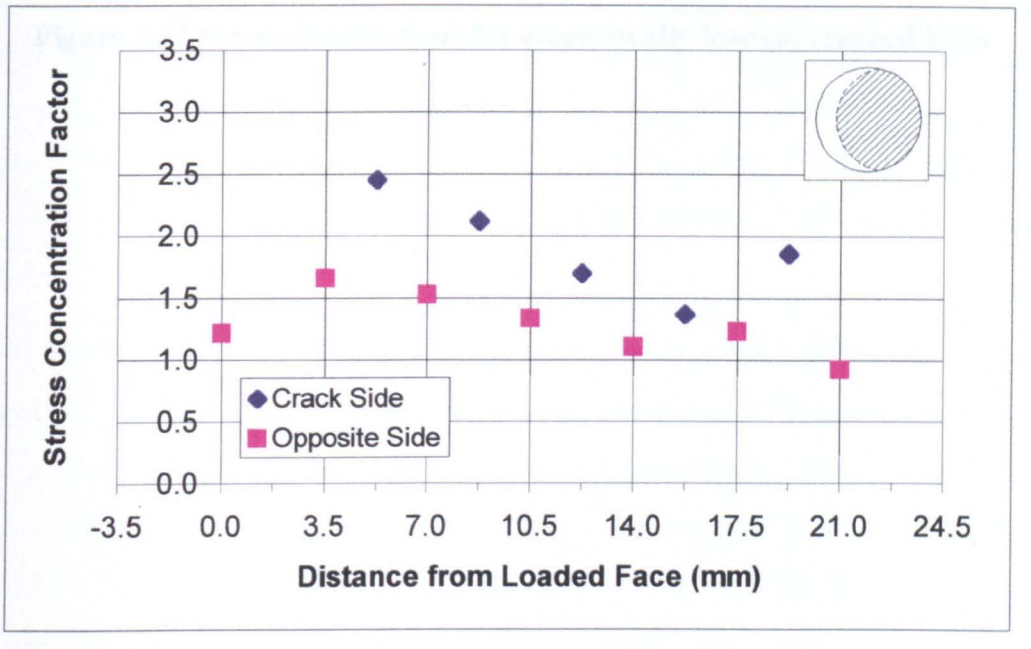

(f) e/D = 0.08

Figure 6.22 Stress distributions for eccentrically loaded, cracked bolts

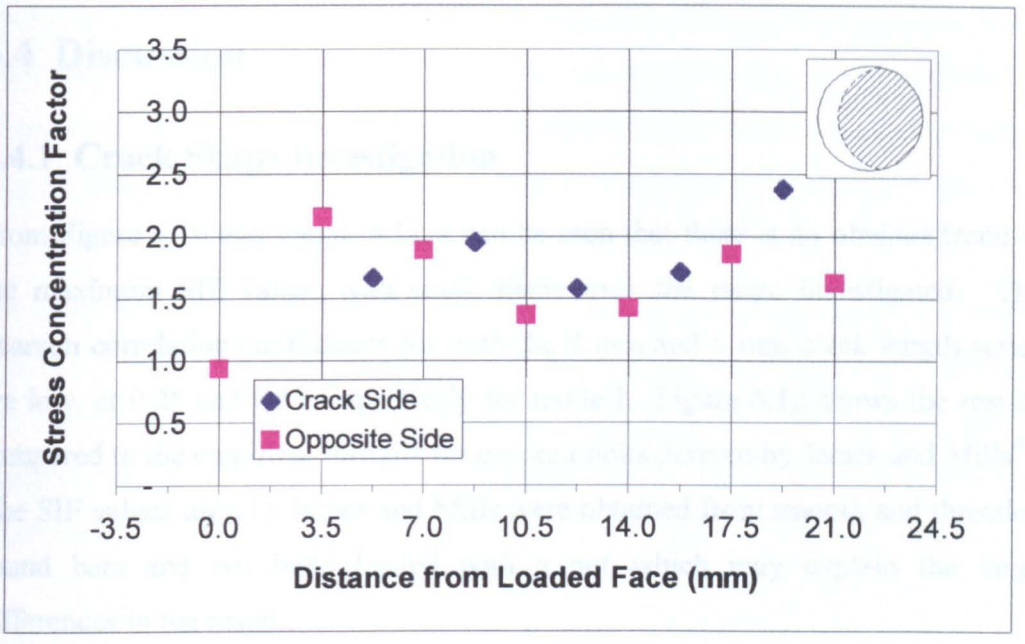

(g) e/D = 0.17

Figure 6.22 Stress distributions for eccentrically loaded, cracked bolts

6.4 Discussion

6.4.1 Crack Shape Investigation

From Figure 6.10 and Figure 6.11 it can be seen that there is no obvious trend in the maximum SIF values with crack shape over the range investigated. The Pearson correlation coefficients for both the 2 mm and 4 mm crack length series are low, at 0.25 and 0.58 respectively for mode I. Figure 6.12 shows the results compared to the empirical formula for cracked bolts derived by James and Mills[47]. The SIF values used by James and Mills were obtained from smooth and threaded round bars and not bolts loaded with a nut which may explain the large differences in the results.

The variations in K_I/K_o values around the crack front are shown in Figure 6.13. James and Mills reported that the SIFs were higher at the surface (x = 0) than at the deepest penetration (middle of crack, x = 0.5) for semi-circular cracks. From Figure 6.13 it can be seen that the converse is true for crescent shaped cracks with the highest SIFs occurring in the middle of the crack front, where x = 0.5, in all cases. This indicates that the crack will grow faster in the middle of the crack front than near the ends of the crack front, therefore, the crack will straighten as it grows.

The values obtained are normalised K values and are therefore not stress intensity values in themselves. If $K = Y\sigma\sqrt{\pi a}$ then the normalised values are in fact the geometric calibration function, Y. The actual stress intensity factors at the crack tip are then a function of the SIF values found, the nominal stress and the crack length. Therefore, even if the SIFs found were the same around the whole length of the crack front, the crack would still grow quickest in the middle of the crack, where the crack is longest and therefore the K values are highest.

If the effective K values were used ($K_{eff} = \sqrt{K_I^2 + K_{II}^2}$) a similar distribution is obtained and the crack should still grow more quickly in the middle of the crack front.

Figure 6.15 shows the variation in K_{II}/K_o values around the crack front. In contrast to the K_I/K_o values, the K_{II}/K_o values increase towards the surface. Both

the mode I and mode II values are slightly higher for the second half of the crack front ($x > 0.5$) than the first half. Due to the thread helix, as x increases the distance of the crack from the loaded face of the nut increases and the nut thread becomes fully formed. The lower K values in the first half of the crack front are probably due to the nut thread not being fully formed and therefore less stiff.

The plots of the stress distributions in Figure 6.17 show that there is little trend. For the 2 mm crack length series, the stress distribution increases near the unloaded end of the nut, the straighter the crack front is. This may be due to straighter cracks causing more load shedding to the end of the nut because of increased bending.

6.4.2 Eccentrically Loaded Bolts

Eccentric loading is seen to increase the stress intensity factors at the crack tips in the bolts with 4 mm cracks. These values for K_I/K_o and K_{II}/K_o were calculated using a value of K_o that did not include bending stress. The bending stress was ignored in the calculation of K_o for two reasons: (i) the bending stress at the crack tip would be difficult to calculate, (ii) relating the SIFs in terms of a stress that would be known would be more useful.

The mode I SIF for an eccentricity, $e/D = 0.168$, for the 4 mm long crack was 10% higher then for the equivalent axially loaded bolt. The maximum stress in the bolt, however, was calculated to be 156% higher than if the load had been axial. Therefore, if the maximum stress had been used to normalise the SIFs instead of the axial load, the SIFs would be lower with higher eccentricity, as shown in Table 6.6. There appears to be an obvious trend to the values when normalised using the maximum stress, with the SIF values reducing with eccentricity. The maximum stress was not measured, only calculated, so there may be some error due to the loads aligning with the axis of the bolt as the bolt bends. Also, the effect of the crack on the bending stress was not taken into account. If the diameter of the remaining ligament was used instead of the bolt diameter in Equations 6-3 and 6-4, different values would be obtained. However, this would result in an even more marked decrease in SIF values.

a (mm)	e/D	K_I/K_o
2 mm	0	1.466
	0.04	1.086
	0.084	0.670
	0.168	0.511
	0.249	0.450
4 mm	0	1.406
	0.04	1.048
	0.084	0.852
	0.168	0.600

Table 6.6 Mode I SIFs when normalised by maximum stress

The values are shown in Figure 6.20 and Figure 6.21. The Pearson correlation coefficient for the 4 mm crack series is 0.97, indicating that there is close correlation between the data and a linear best fit line. The coefficient for the 2 mm crack series is only 0.03, indicating almost no correlation. This may be due to the fact that when the crack tip is further from the thread root it is not influenced by the stress field caused by the threads.

As the eccentricity increases, the difference in the stress concentration factor between the high and low stress sides increases, as expected. Again, the bending is not taken into account and the stresses are normalised with the axial stress only, therefore it is expected that the stresses on the tension side of the bolt would be higher. This is clearly shown in Figure 6.22 (a) - (d) for the 2 mm cracks. Also, the maximum stress concentration factor gets lower as the eccentricity increases, as shown in Figure 6.22 (e) - (g).

6.5 Conclusions

The shape of the crack front does not have a significant effect on the stress intensity factor at the middle of the crack front for the range of crack shapes investigated. It does, however, have an effect on the stress intensity factor variation around the crack front. While it has been reported that the SIFs are highest at the end of the crack front for straight cracks, it has been found that the

maximum SIFs are at the centre of the crack front for crescent-shaped cracks and get lower towards the end. The shape of the crack front has little effect on the stress distribution around the helix.

Eccentric loading has been found to increase slightly the SIFs at the centre of the crack front if normalised using the axial load. The increase is not as large as may be expected and this is probably due to the actual bending load applied being less than the calculated bending load, due to the bending load swinging in toward the axis of the bolt as the bolt bends.

Chapter 7

Finite Element Analysis of a Threaded Connector

7.1 Introduction

Performing many series of experimental tests, like those reported in the previous chapters, is time consuming and expensive. Having a numerical model that could predict stresses in threaded connections accurately, and therefore help to predict fatigue life, would be a great help to the designer. Once such a model was created, any number of loading conditions could be applied and their effects evaluated quickly and easily.

To date, a finite element model that represents the true three-dimensional nature of the connection with a fine enough mesh to obtain stress concentration factors has not been performed. Zhao[4,5] modelled the three-dimensional geometry of the threaded connection, but the coarseness of the mesh limits the accuracy and usefulness of the model. The meshing used by Fukuoka[37,40] in his 2D model varies throughout the model, with a finer mesh in the first thread root than in the rest of the model. If the only information required is the value of the peak stress,

which occurs in the first thread root from the loaded face of the nut, then this is a sensible way to mesh. Only one surface of the thread is actually in contact with the nut thread, assuming that the connection remains in tension, and therefore the mesh could be refined further by having a finer mesh on the contact side of the threads.

The elastic-plastic nature of the material has still not been investigated fully. The high stress concentrations at the thread roots mean that the material is likely to deform plastically and this may alter the load distribution.

The effect of the thread run-out, where the last thread of the nut is not fully formed, has, as yet, been ignored by finite element modellers. It has been found experimentally[33] that the run-out has an effect on the load distribution, with the peak stress occurring half a thread pitch from the loaded face of the nut.

Any new model created should simulate the true three-dimensional nature of the problem, including the helix angle and the thread run-out, with a fine enough mesh to enable accurate stress concentrations to be obtained. Modelling the elastic-plastic material properties would be desirable to ascertain if plasticity has a significant effect on the load distribution.

A series of models have been produced, increasing in complexity. A number of two-dimensional models have been created with slightly different geometries and meshes to determine the salient characteristics. A series of three 3D models has also been created to observe the effect of the thread helix and the nut thread run-out.

The finite element package used for all the analyses was ANSYS version 5.3b. The numbering system used for all the plots of load and stress concentration factor is that shown in Figure 7.1, unless stated otherwise. With two-dimensional, axisymmetric models, only half the model is built and the finite element package assumes the profile exists around 360°.

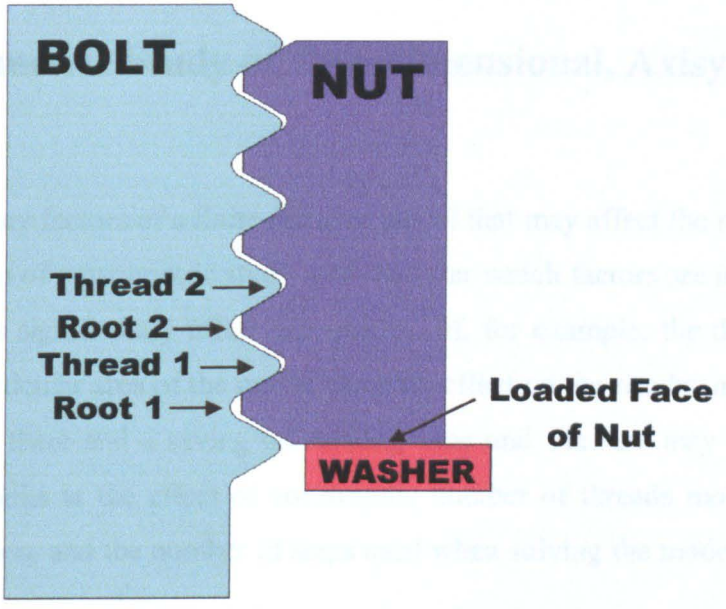

Figure 7.1 Diagram showing naming and numbering system for finite element models

7.2 Parametric Study of Two-dimensional, Axisymmetric Model

There are many factors of a finite element model that may affect the results a great deal. The aim of a parametric study is to discover which factors are important and which do not significantly affect the results. If, for example, the density of the mesh in a particular area of the model has little effect on the results, a coarse mesh may be used there and a saving on running time and file size may be achieved. This study looks at the effect of constraints, number of threads modelled, mesh density, friction, and the number of steps used when solving the model.

All the two-dimensional models created used axisymmetric plane four-node elements to model the nut, bolt and washer. The contact surfaces between the nut and washer and the nut and bolt were modelled using point-to-surface contact elements. Contact elements are created by defining contact and target surfaces as shown in Figure 7.2. When contact occurs, the target surface exerts a force onto the contact node to prevent penetration. To ensure that contact is represented properly it is often advisable to define both surfaces as both contact and target surfaces and this procedure has been followed for all two-dimensional models. Unless specified otherwise, ANSYS creates contact elements between every node specified as a contact node and every surface specified as a target. This can result in a very large number of nodes and is unnecessary when the nature of the contact is predictable. Limiting the number of contact nodes that a target surface makes contact elements with to those that lie within a certain radius can significantly reduce the number of elements. Figure 7.3 shows a close-up view of the contact between the nut and the bolt with red arcs showing the radii in which contact elements were created. Only the nodes on the surface were selected, so contact elements were not created between interior nodes. The size of the radius was chosen so that contact elements were created between nodes and elements that were likely to come into contact.

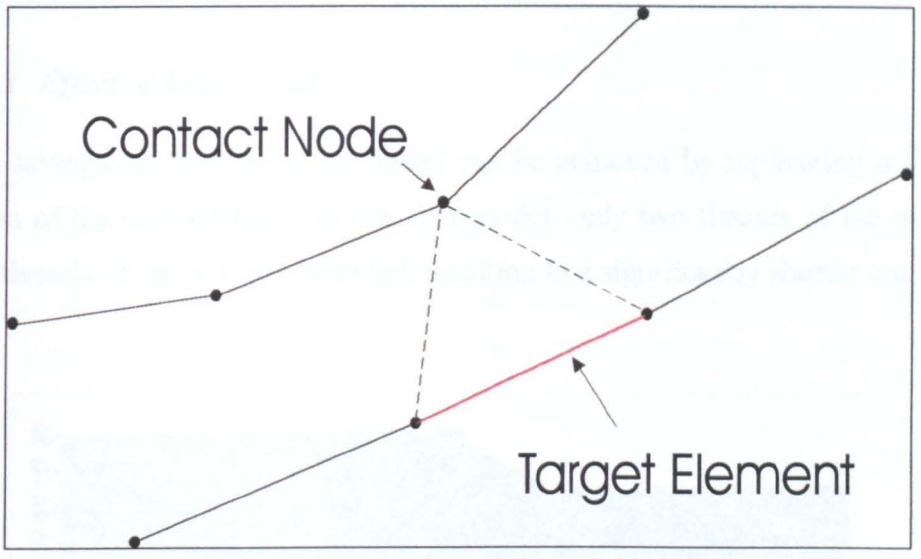

Figure 7.2 Point-to-surface contact elements

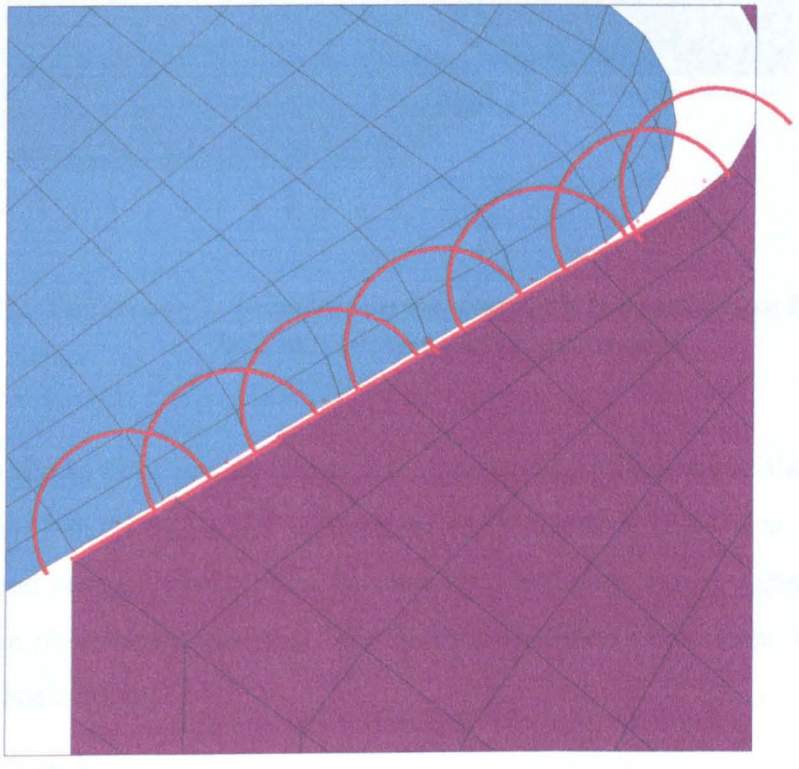

Figure 7.3 Close-up of thread contact surfaces showing red arcs within which contact elements are created

7.2.1 Extent of Model of Joint System

7.2.1.1 Effect of Bolt Length

Great savings on the size of the model can be achieved by replicating a limited portion of the nut and bolt. In this first model, only two threads of the nut and three threads of the bolt are modelled, resulting in a significantly shorter nut.

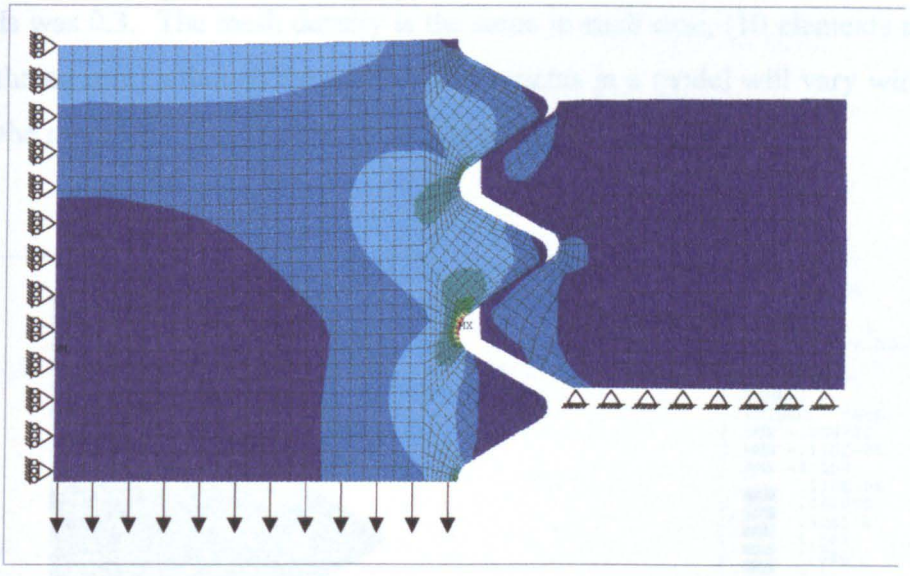

Figure 7.4 Difference in principal stress, constraints and loading for three bolt thread, two nut thread model

Figure 7.4 shows the stress in terms of the normalised difference in the principal stresses $(\sigma_1 - \sigma_2)/(L/A_s)$. The difference in principal stresses was chosen to illustrate and compare the models because this facilitates easy comparison with results from photoelastic analysis. The SCFs are defined in the same way as for the photoelastic study:

$$SCF = \frac{(\sigma_1 - \sigma_2)}{L/A_s}$$

where:

σ_1, σ_2 = principal stresses

L = applied load

A_s = stress area of bolt

The model is two-dimensional, axisymmetric with the bottom edge (loaded face) of the nut constrained in the axial and radial directions and the bolt constrained down its centre line in the radial direction. The load is applied by displacing the nodes on the lower edge of the bolt downward by a uniform distance. The displacement applied was determined by trial and error, to obtain loads comparable with those used for the photoelastic analysis.

The material properties used for these analyses are representative of those for epoxy resin, i.e. Young's modulus of 30 MPa. The Poisson's ratio used for all the models was 0.3. The mesh density is the same in each case, (10 elements around each thread root) although the number of elements in a model will vary with how large the model is. The constraints are the same in each case.

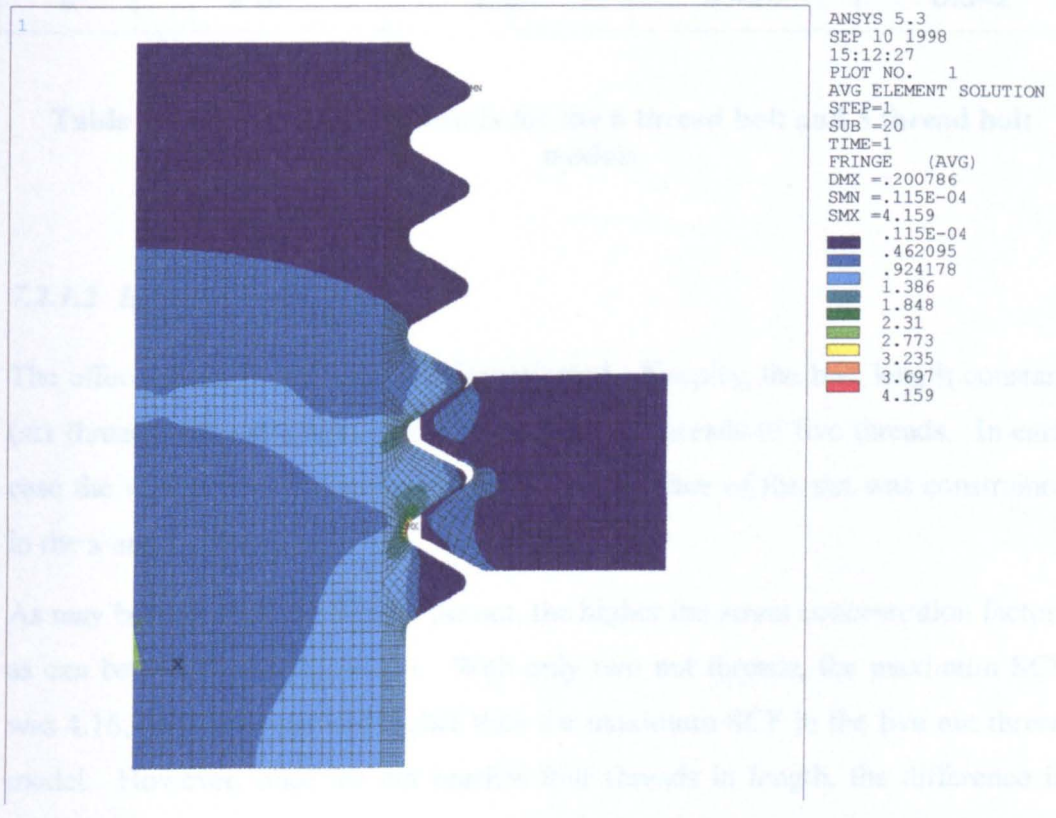

Figure 7.5 Difference in principal stress for six bolt thread, two nut thread model

The effect of increasing the length of the bolt affects the stress distribution as shown in Figure 7.5 and Table 7.1. The load taken by each thread is calculated by summing the reaction load on each node for a given thread. The loads are

normalised against the applied load, giving the fraction of the total load taken by that thread. With little material above the last loaded thread, the thread is free to bend more, thus shifting more of the load to the first loaded thread while increasing the stress concentration at the root of the second thread. Therefore, the simplification of reducing the area of bolt modelled results in an overestimation of the stress concentration at both of the thread roots. This shows that for a two thread nut, it is better not to position the nut at the end of the bolt.

	SCF		Normalised Load / Thread	
Thread	6 Thread Bolt	3 Thread Bolt	6 Thread Bolt	3 Thread Bolt
1	4.16	4.97	0.580	0.658
2	2.30	2.90	0.420	0.342

Table 7.1 Stress and load results for the 6 thread bolt and 3 thread bolt models

7.2.1.2 Effect of Nut Length

The effect of nut length was also investigated. Keeping the bolt length constant (six threads) the nut length was varied from two threads to five threads. In each case the washer was not included and the loaded face of the nut was constrained in the x and y directions.

As may be expected, the shorter the nut, the higher the stress concentration factors as can be seen from Figure 7.6. With only two nut threads, the maximum SCF was 4.16, almost 20 percent higher than the maximum SCF in the five nut thread model. However, once the nut reaches four threads in length, the difference in maximum SCF is less then 2 percent. In all cases it is the first thread, where the maximum SCF occurs, that sees the greatest effect from changing the length of the nut. There is just 0.3 percent difference between the SCFs in the fourth thread root for the four and five thread models.

A similar pattern appears in the normalised load plots, shown in Figure 7.7, although the differences are slightly greater.

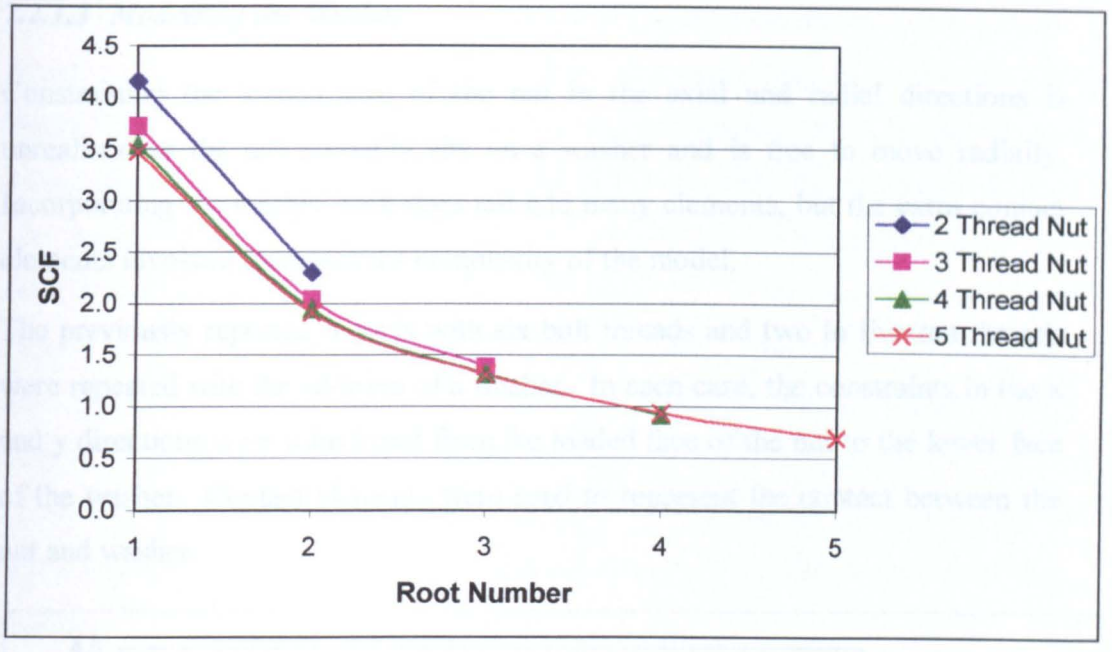

Figure 7.6 Variation of stress concentration factor with length of nut

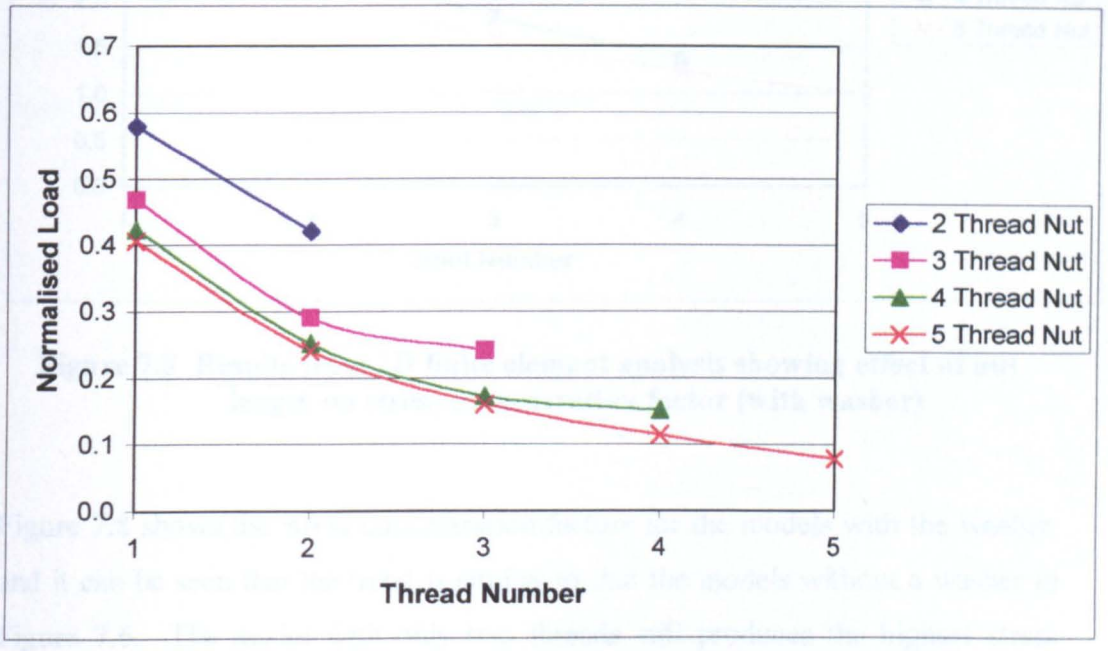

Figure 7.7 Variation of load distribution with length of nut

7.2.1.3 Modelling the Washer

Constraining the loaded face of the nut in the axial and radial directions is unrealistic as the nut normally sits on a washer and is free to move radially. Incorporating the washer itself does not add many elements, but the extra contact elements involved increases the complexity of the model.

The previously reported models with six bolt threads and two to five nut threads were repeated with the addition of a washer. In each case, the constraints in the x and y directions were transferred from the loaded face of the nut to the lower face of the washer. Contact elements were used to represent the contact between the nut and washer.

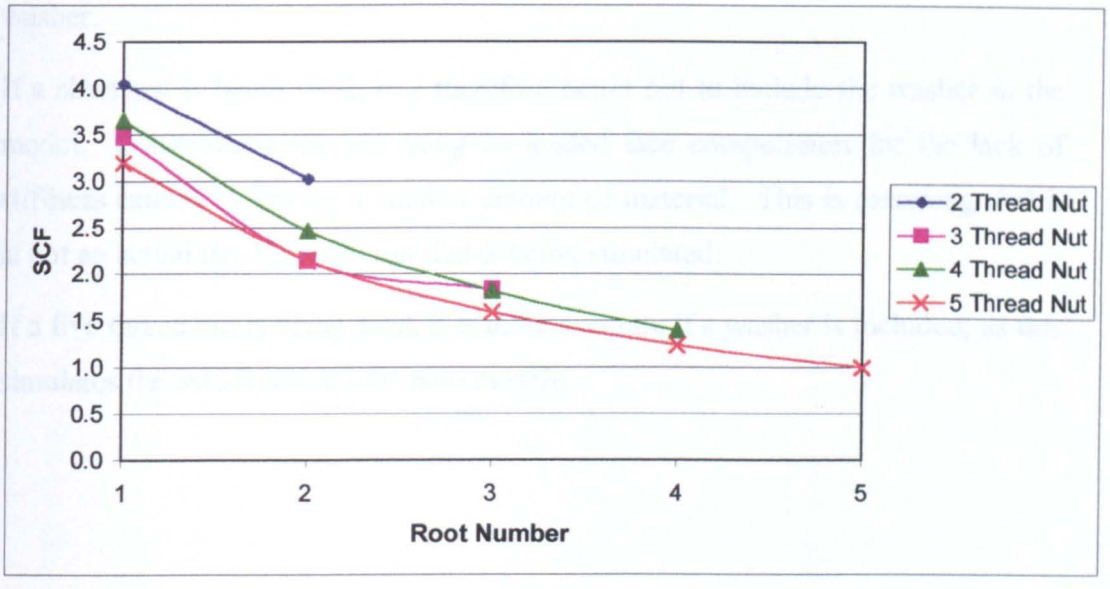

Figure 7.8 Results from 2D finite element analysis showing effect of nut length on stress concentration factor (with washer)

Figure 7.8 shows the stress concentration factors for the models with the washer, and it can be seen that the trend is similar to that the models without a washer in Figure 7.6. The model with only two threads still produces the highest stress concentration factors in the bolt and the lowest stress concentration factors are still found in the bolt loaded by the five thread nut. However, there are some significant differences. Generally, the SCFs are lower in the first thread root when the washer is included, but higher in the other thread roots. This effect is most marked when the nut is short, as shown in Figure 7.9.

The effect of including the washer is even more marked on the load distribution. Again, the effect is greater with the shorter, two thread nut, as can be seen in Figure 7.10. The highest load moves from the first loaded thread to the second loaded thread when the washer is included, which explains the more even SCFs. The reason for the shifting of the load up the nut can be ascertained from the deformed shape plots (Figure 7.11 and Figure 7.12). The two-thread nut can clearly be seen to lift off the washer. This pivoting of the nut allows the first thread to move downwards, taking far less load, while pushing the second thread radially in towards the bolt, increasing the load taken on this thread. The five-thread nut, which is far stiffer in the axial direction and will not dish. The plot of deformed shape (Figure 7.12) shows that the five-thread nut does not lift off the washer.

If a short nut is being used, it is therefore better not to include the washer in the model. Constraining the nut along its loaded face compensates for the lack of stiffness caused by having a smaller amount of material. This is assuming that it is not an actual two threaded nut that is being simulated.

If a five thread nut is being used, it is more accurate if a washer is included, as this simulates the actual conditions more closely.

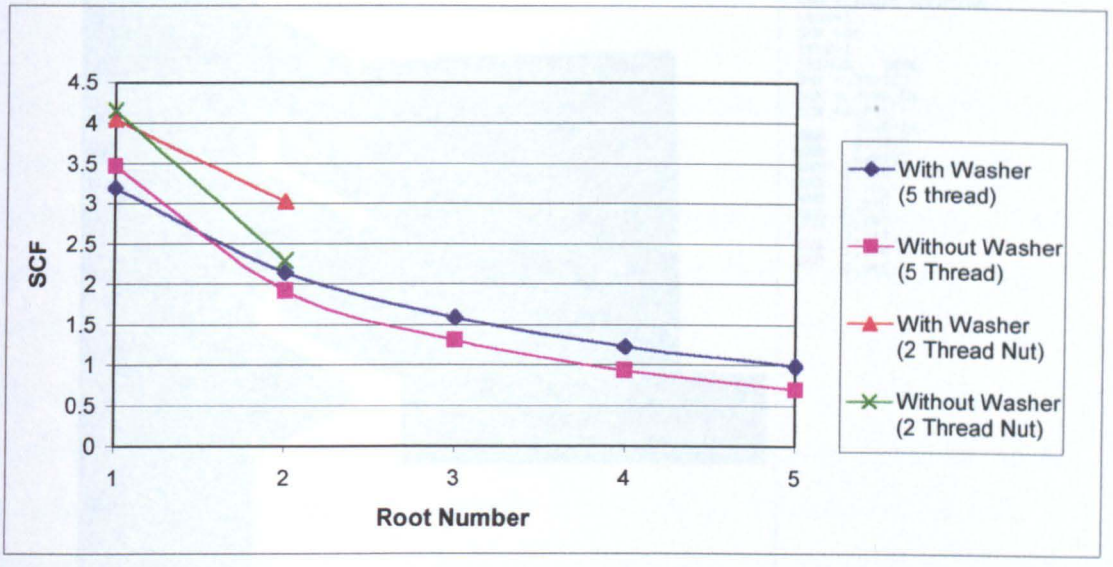

Figure 7.9 Results from 2D finite element analysis showing effect of modelling washer on stress concentration factor for 2 nut thread and 5 nut thread models

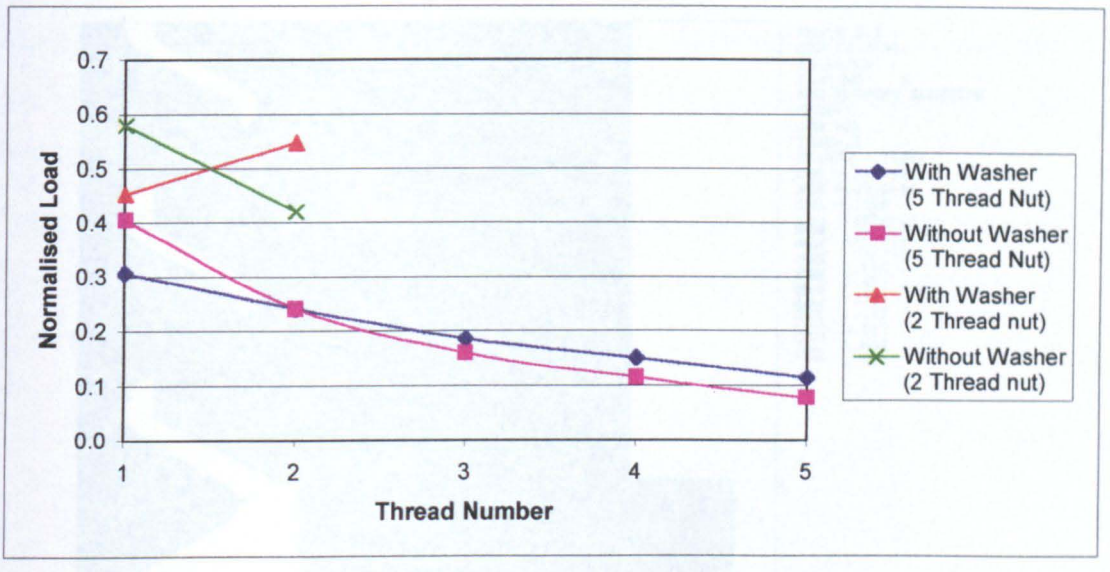

Figure 7.10 Results from 2D finite element analysis showing effect of modelling washer on load distribution for 2 nut thread and 5 nut thread models

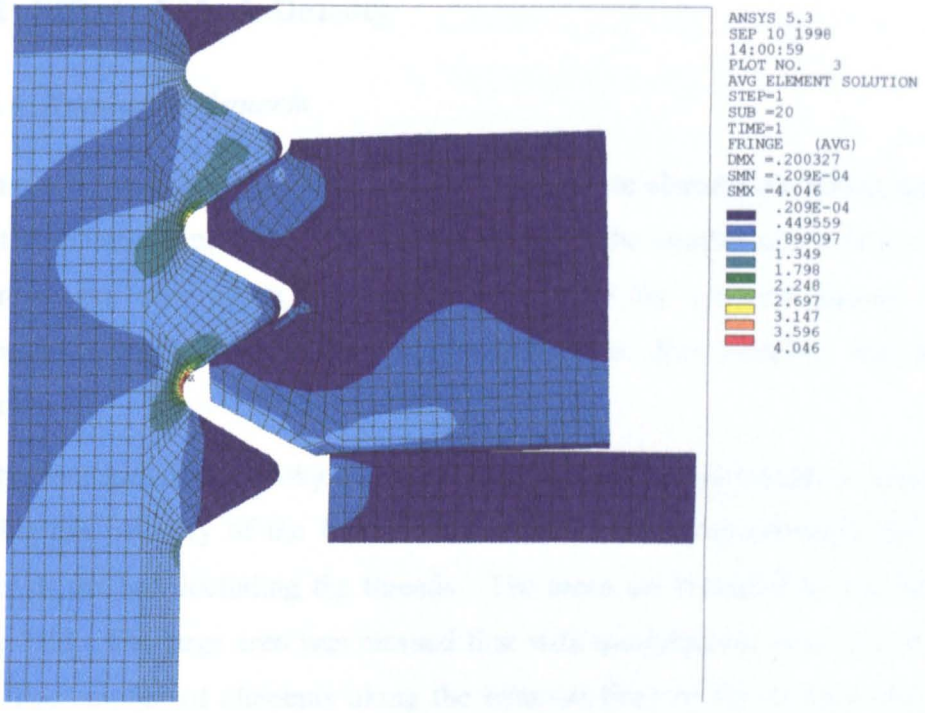

Figure 7.11 Principal stress difference and deformed shape for two thread nut model with washer

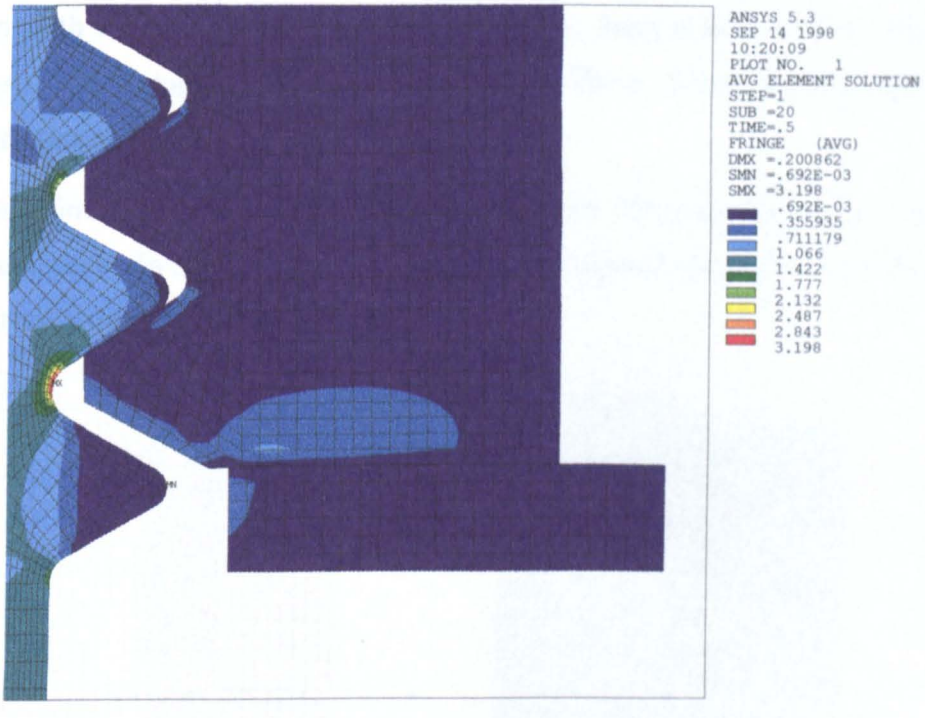

Figure 7.12 Principal stress difference and deformed shape for five thread nut model with washer

7.2.2 Effect of Mesh Density

7.2.2.1 Number of elements

The mesh is one of the most important factors in finite element modelling and it is essential to use an appropriate mesh. It is not only the number of elements that is important, but also where the finest mesh is and the element shapes. Two techniques were used to mesh the threaded areas; free meshing and forced meshing.

For the free meshing technique, the bolt was split into two areas; a large area covering the majority of the bolt and a second smaller area covering the outer quarter of the bolt including the threads. The areas are bounded by red lines in Figure 7.13. The large area was meshed first with quadrilateral elements of fixed size. The number of elements along the external lines of the threads was then specified (for both the thread roots and flanks) and then the second area was meshed with a mixture of quadrilateral and triangular elements. The resulting meshes can be seen in Figure 7.13. Only the coarsest and finest meshes are shown with 1194 and 6335 elements respectively. Intermediate meshes were also analysed containing 2526 and 3443 elements. These figures include both solid and contact elements.

When refining the mesh using this technique, the element distribution was not kept constant. In some of the models the mesh around the first thread root was finer than around those of the other roots.

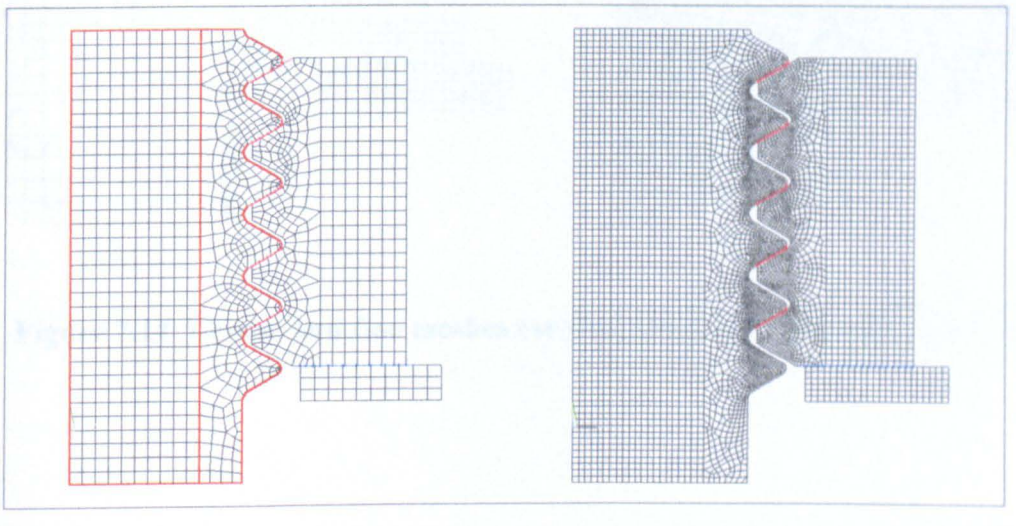

Figure 7.13 Coarse and fine meshes created using free meshing technique

The second meshing method, forced meshing, resulted in a far more even mesh. The bolt was split into more areas for this technique. As before, the main large area was meshed with quadrilateral elements of a set size, although this area was slightly larger than for the free meshes. The main difference was in the threaded region that was now split into many smaller areas, effectively root areas and thread areas, as shown in Figure 7.14. The number of elements along each side of each area was defined and the areas were meshed exclusively with quadrilateral elements. The resulting mesh is far more even and the transition between the fine mesh in the threaded area and the coarser mesh in the main area is more gradual and orderly. Models were created with four mesh densities, with 1777, 4515, 6337 and 12997 elements. The 1777 element and 6337 element models are shown in Figure 7.14. The model containing 6337 elements was found to be the optimum in terms of model size and accuracy and is shown enlarged in Figure 7.15.

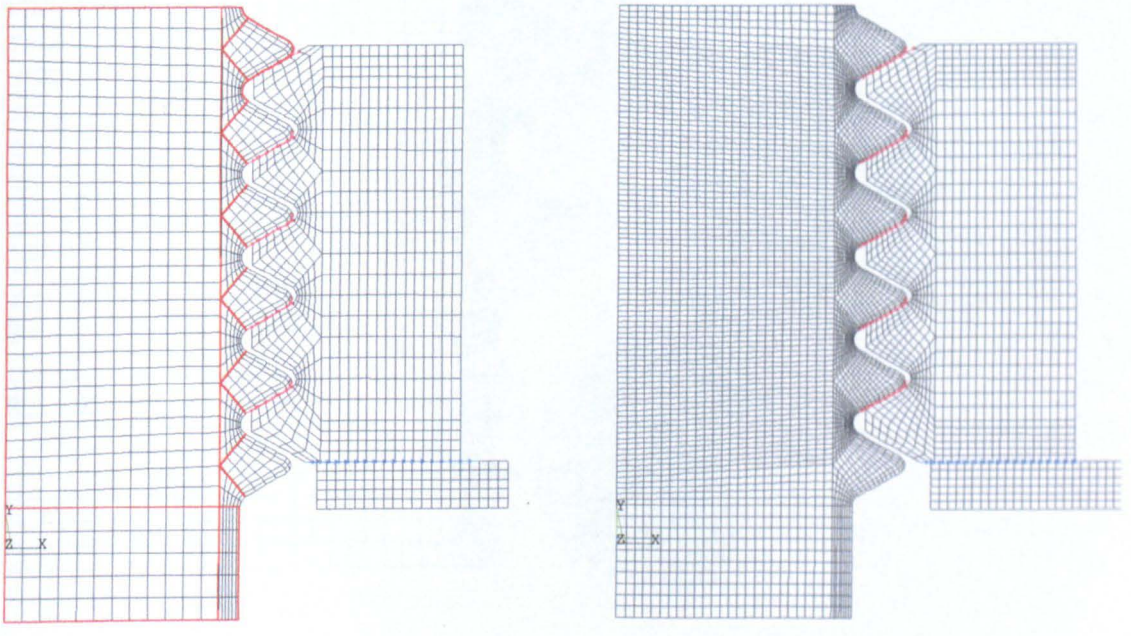

Figure 7.14 Coarse and fine meshes created using forced meshing technique

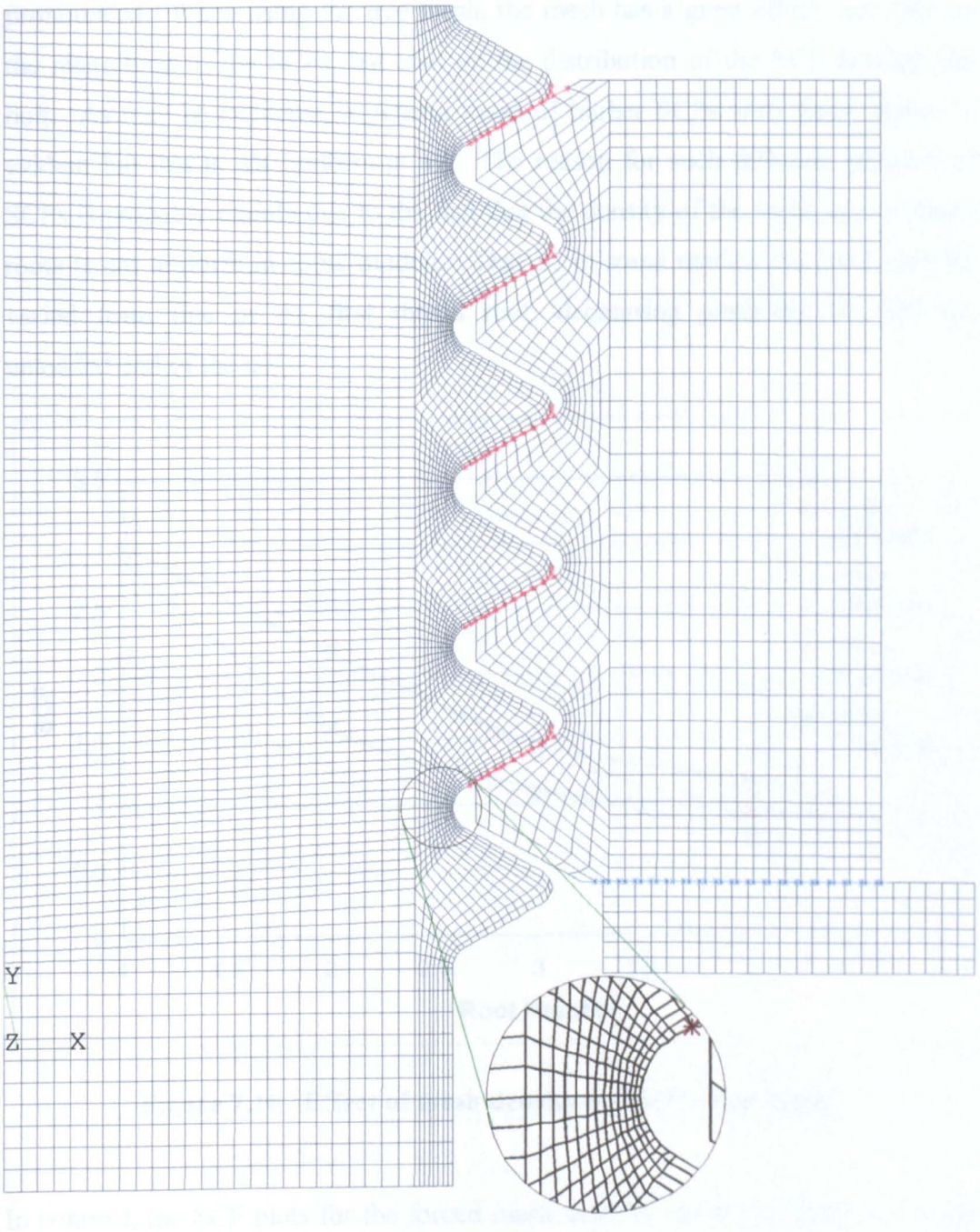

Figure 7.15 Finite element model containing 6337 elements with mesh in thread root enlarged.

The SCF results from the free and forced mesh models are shown in Figure 7.16 and Figure 7.17 respectively. The difference between the two plots is pronounced. When using the free mesh, the mesh has a great effect, not only on the magnitude of the SCFs, but also on the distribution of the SCF through the bolt. As may be expected, a general trend of higher SCFs with finer meshes is evident but this is not uniform at all. The reason for such different patterns of SCFs is probably mainly due to the fact that the density of the mesh in the thread roots is not uniform in some models. That is, in some models the mesh density varied from fine in the first thread root, decreasing gradually towards the unloaded end of the nut.

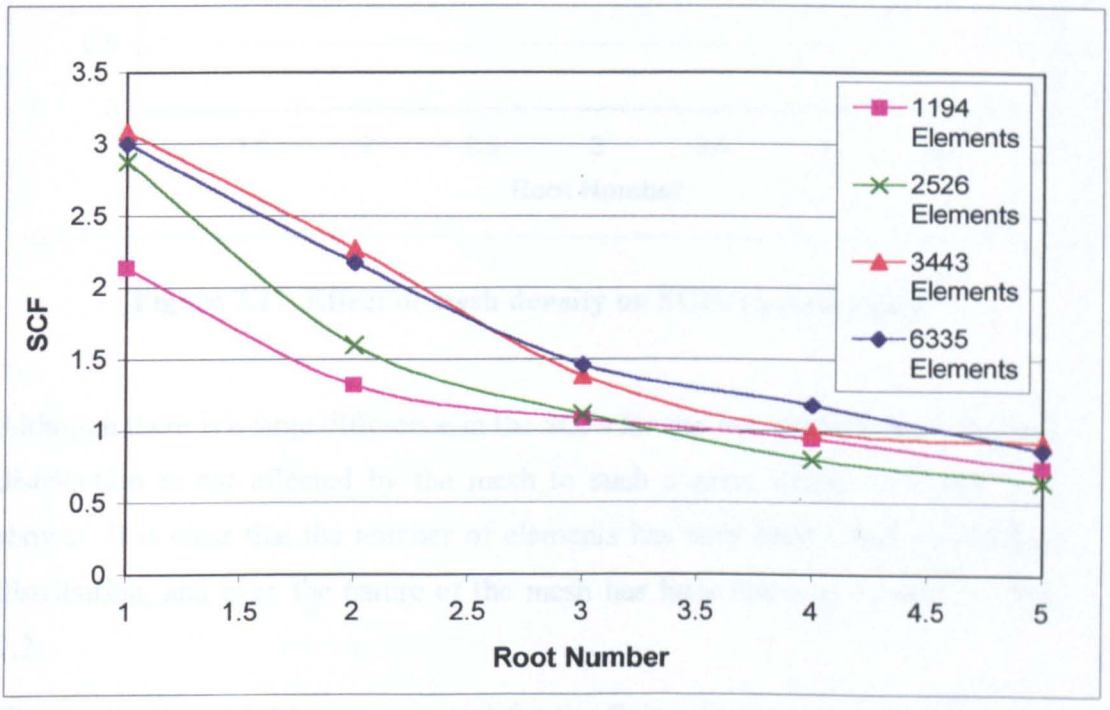

Figure 7.16 Effect of mesh density on SCFs (free mesh)

In contrast, the SCF plots for the forced mesh models, shown in Figure 7.17, are very similar. The shape of the curves is almost identical, with the only real difference being a general increase in SCFs as the mesh density increases. The difference in SCF values between the 1777 element model and the 4515 model is about 15%, whereas the difference between the 6337 element model and the 12997 model is less than 1%. This is an indication that the model has converged.

Therefore, it is better to the model containing 6337 elements as any further increase result in a longer running time with an increase in accuracy of results.

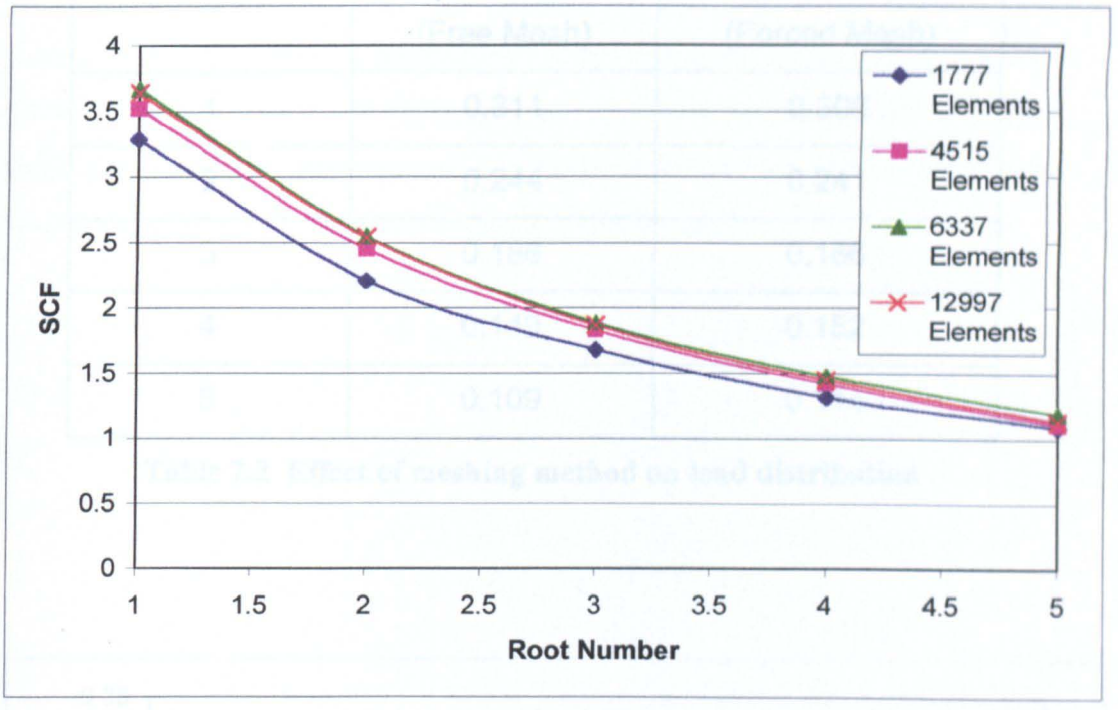

Figure 7.17 Effect of mesh density on SCFs (forced mesh)

Although there is a large difference in the SCFs for the free mesh models, the load distribution is not affected by the mesh to such a great extent as Figure 7.18 shows. It is clear that the number of elements has very little effect on the load distribution, and even the nature of the mesh has little effect as shown in Table 7.2.

The implications of this are important for the finite element analyst. If the load distribution is not affected by the number of elements used in the analysis, a large portion of the component can be modelled with a coarse mesh. Once the load distribution has been found, a smaller submodel can be created with a much finer mesh in the important region.

Thread Number	Normalised Load (Free Mesh)	Normalised Load (Forced Mesh)
1	0.311	0.306
2	0.244	0.241
3	0.186	0.186
4	0.149	0.152
5	0.109	0.114

Table 7.2 Effect of meshing method on load distribution

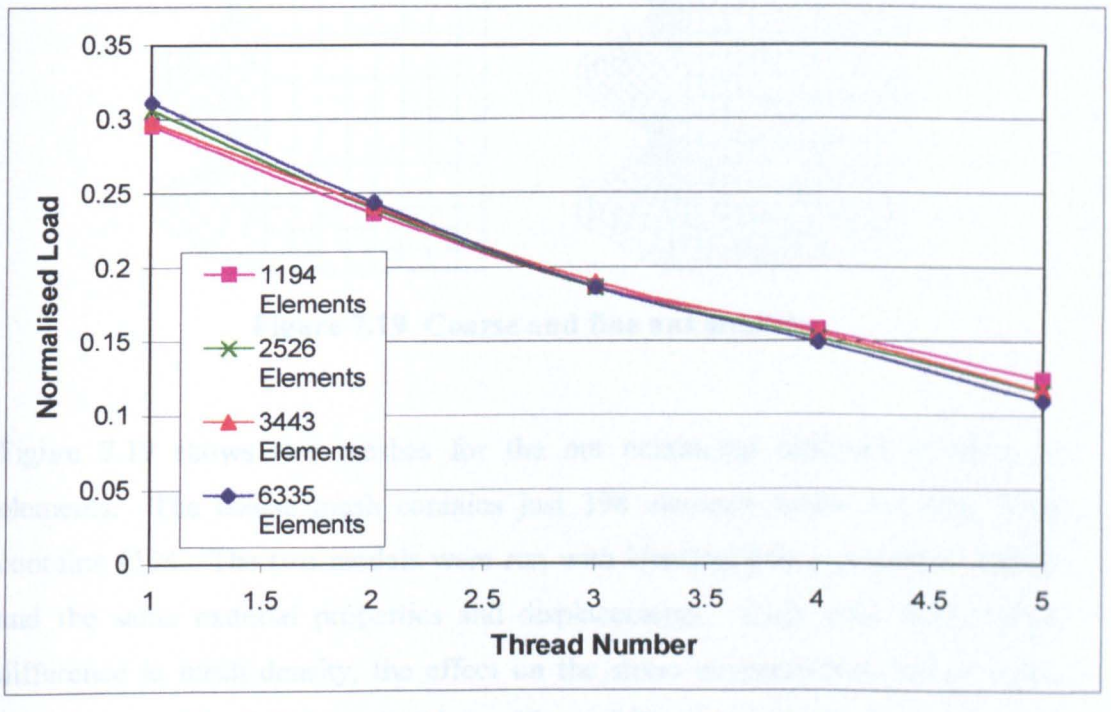

Figure 7.18 Effect of mesh density on load distribution (free mesh)

7.2.2.2 Mesh Density in the Nut

If the general number of elements a model contains affects the stresses in the thread roots but does not significantly affect the load on each thread then it follows that the number of elements used to model the nut is less important. Generally, we are not interested in the stresses in the nut and it is included in the model simply to provide realistic loads on the bolt threads.

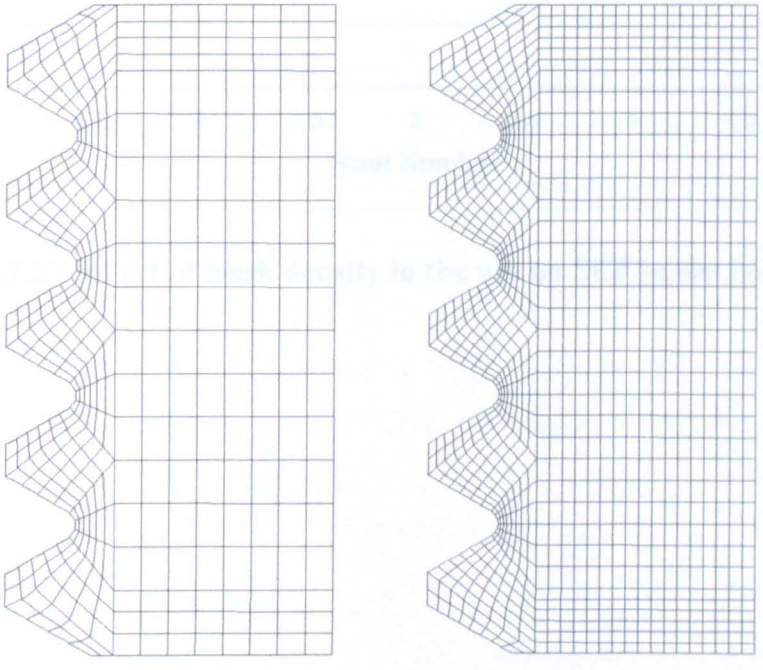

Figure 7.19 Coarse and fine nut meshes.

Figure 7.19 shows two meshes for the nut containing different numbers of elements. The coarse mesh contains just 398 elements while the finer mesh contains 1124. The two models were run with identical bolt and washer meshes and the same material properties and displacements. Even with such a large difference in mesh density, the effect on the stress concentration factors in the thread roots of the bolt is negligible, as Figure 7.20 shows clearly. Using a coarse mesh for the nut allows a finer mesh to be used in the bolt, where it has a greater effect on results.

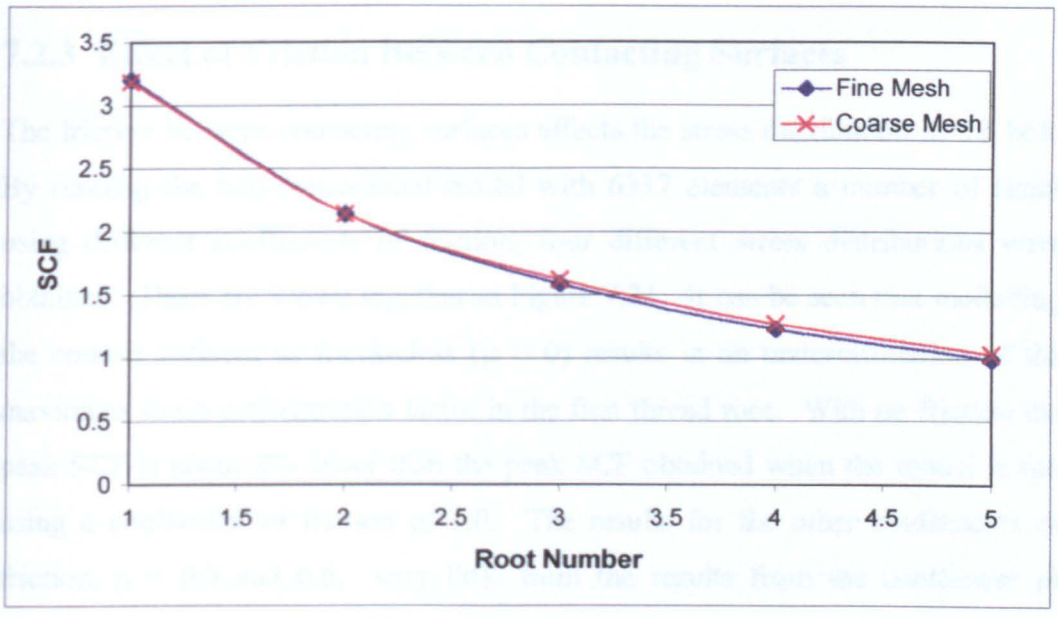

Figure 7.20 Effect of mesh density in the nut on SCF in the bolt roots

7.2.3 Effect of Friction Between Contacting Surfaces

The friction between contacting surfaces affects the stress distribution in the bolt. By running the two-dimensional model with 6337 elements a number of times using different coefficients of friction, four different stress distributions were obtained. These are shown together in Figure 7.21. It can be seen that modelling the contact surfaces as frictionless ($\mu = 0$) results in an underestimation of the maximum stress concentration factor in the first thread root. With no friction the peak SCF is about 8% lower than the peak SCF obtained when the model is run using a coefficient of friction of 1.0. The results for the other coefficients of friction, $\mu = 0.3$ and 0.6, vary little from the results from the coefficient of friction, $\mu = 1.0$.

The results agree with the results of Dragoni[35], who also found that the stress distribution was flatter when the contact surfaces were modelled as frictionless. However, he found that the distribution did not change for coefficients of friction above $\mu = 0.6$, when sticking occurred.

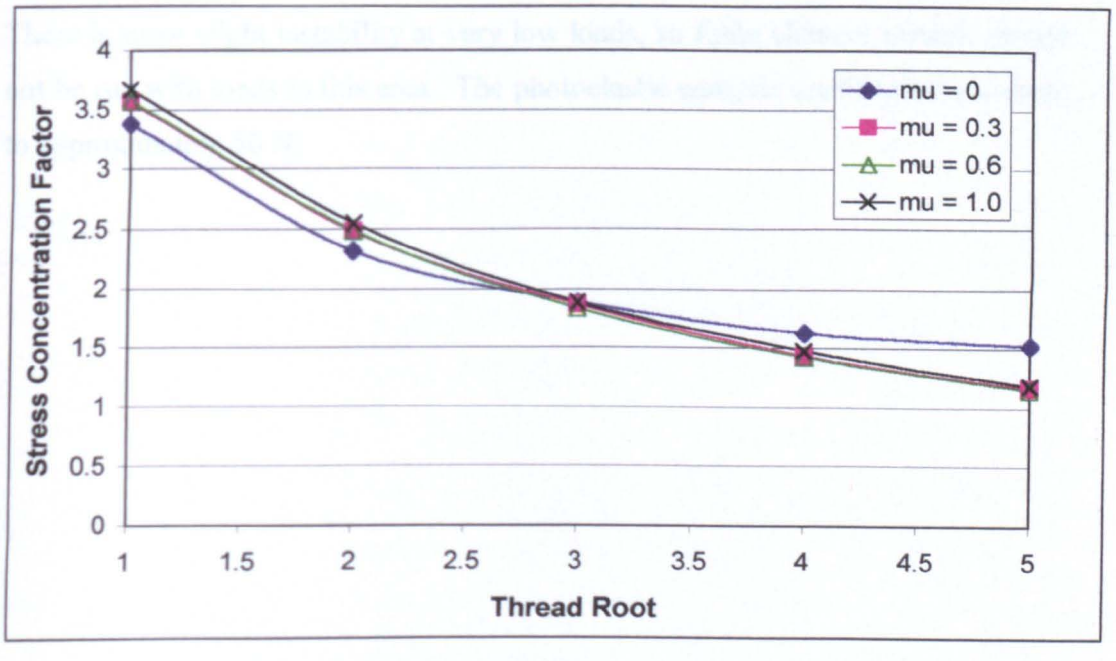

Figure 7.21 Results from 2D finite element analysis showing the effect of coefficient of friction on stress concentration factor

7.2.4 Effect of Applied Load on Load Distribution and Stress Concentration Factors

One of the considerations when performing any stress analysis involving a model rather than an actual component is loading the model in a way that truly represents the loading experienced by the component. Not only are the direction and point of loading important but also the magnitude of the loading. When performing photoelastic analysis the epoxy resin has such a low Young's modulus that using a load that would give comparable strains may not result in high enough fringe orders for easy analysis.

With finite element analysis, applying different load magnitudes is an almost trivial task once the basic model has been created. In one run of the model, a number of sets of results can be obtained, showing how the stresses vary as the load increases.

Figure 7.22 and Figure 7.23 show how the values for the stress concentration factors at each thread root and normalised load per thread vary with applied load respectively. It can be seen that the results are stable over a wide range of applied loads with only a slight decrease in the values for the first thread at high loads. There is some slight instability at very low loads, so finite element models should not be run with loads in this area. The photoelastic analysis used loads equivalent to approximately 50 N.

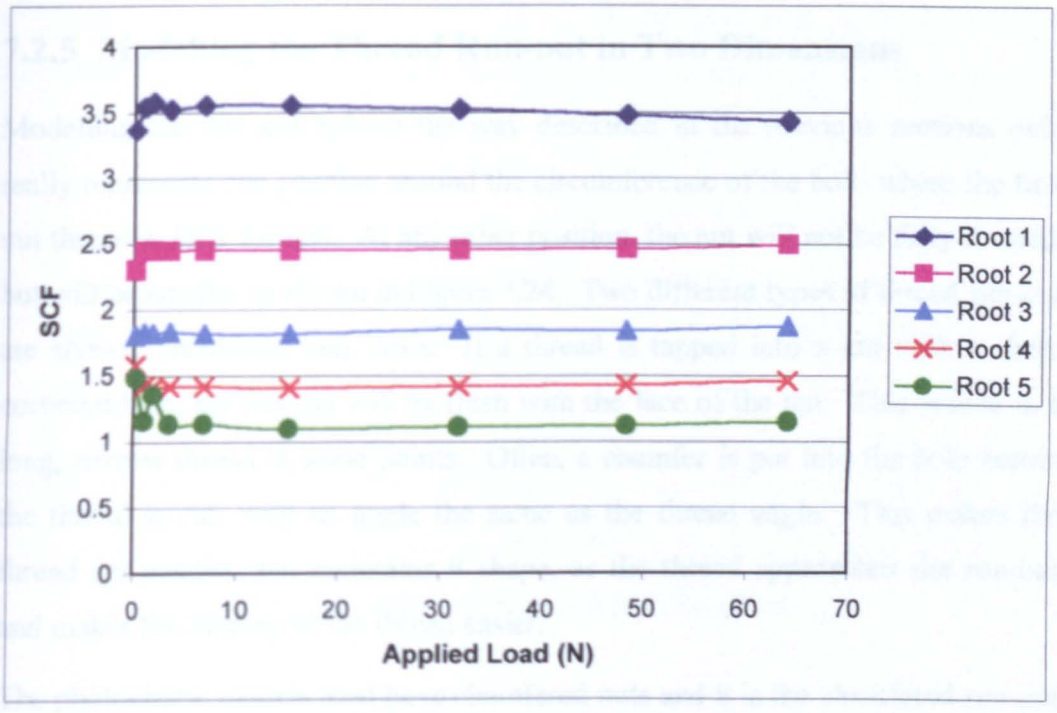

Figure 7.22 Effect of applied load on stress concentration factors in each thread root

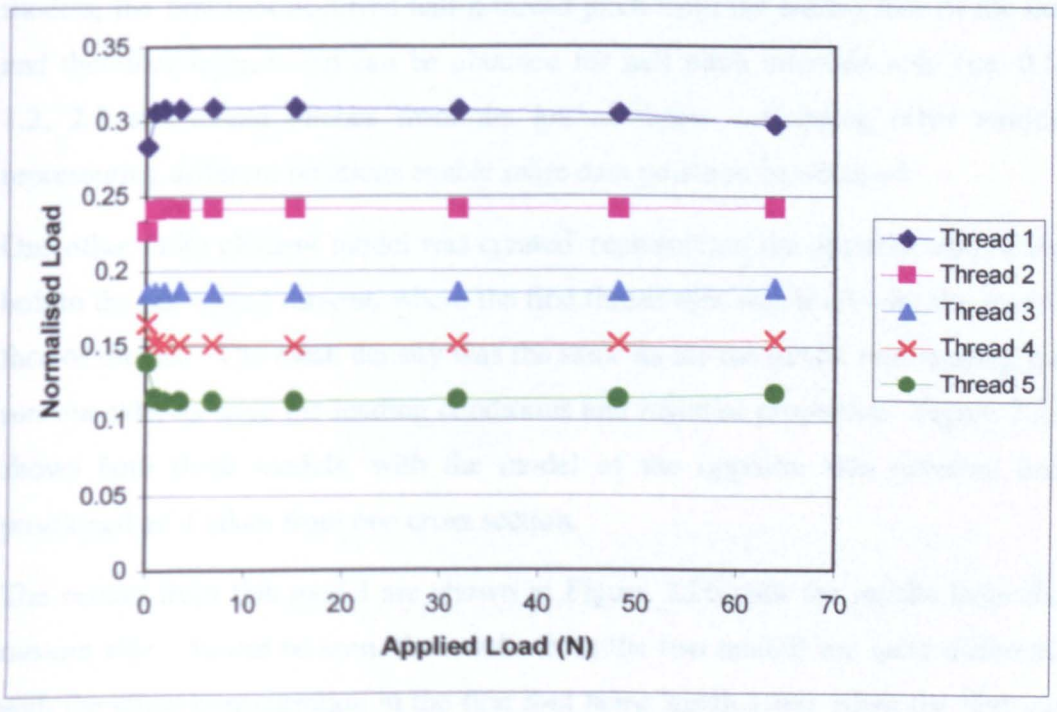

Figure 7.23 Effect of applied load on normalised load on each thread

7.2.5 Modelling the Thread Run-out in Two Dimensions

Modelling the nut and bolt in the way described in the previous sections only really represents one position around the circumference of the bolt, where the first nut thread is fully formed. At any other position, the nut will not be fully formed, but will be smaller as shown in Figure 7.24. Two different types of thread run-out are shown; chamfered and flush. If a thread is tapped into a nut with a sharp cornered hole, the run-out will be flush with the face of the nut. This results in a long, narrow thread at some points. Often, a chamfer is put into the hole before the thread is cut, with an angle the same as the thread angle. This makes the thread get smaller, but maintains it shape, as the thread approaches the run-out and makes the tapping of the thread easier.

The photoelastic models used have chamfered nuts and it is the chamfered run-out that was used for the finite element analysis. If only one model is created, only a certain number of data points can be obtained for the stress concentrations at the thread roots, as the thread roots only occur at certain points. In the previous models, the first root occurred half a thread pitch from the loaded face of the nut and therefore information can be obtained for half pitch intervals only (i.e. 0.5, 1.2, 2.5 etc. thread pitches from the loaded face). Creating other models representing different positions enable more data points to be obtained.

One other finite element model was created, representing the opposite side of the bolt to the nut thread run-out, where the first thread root was level with the loaded face of the nut. The mesh density was the same as for the model representing the run-out side, as were the loading conditions and material properties. Figure 7.25 shows both these models, with the model of the opposite side reversed and positioned as if taken from one cross section.

The results from this model are shown in Figure 7.26 with the results from the run-out side. As can be seen, the results from the two models are quite different, with the stress concentration in the first root being much lower when the first nut thread is smaller. With the first thread taking less load, all the other threads take more load and the stress concentrations in the other thread roots are higher than in the model of the run-out side of the bolt. However, when the stress concentration factors are plotted against the distance from the loaded face of the nut, as shown

in Figure 7.27, the result is a smooth curve, with the peak SCF occurring at half a thread pitch from the loaded face of the nut. This shows that the run-out of the nut thread does have a significant effect on the stresses in the bolt.

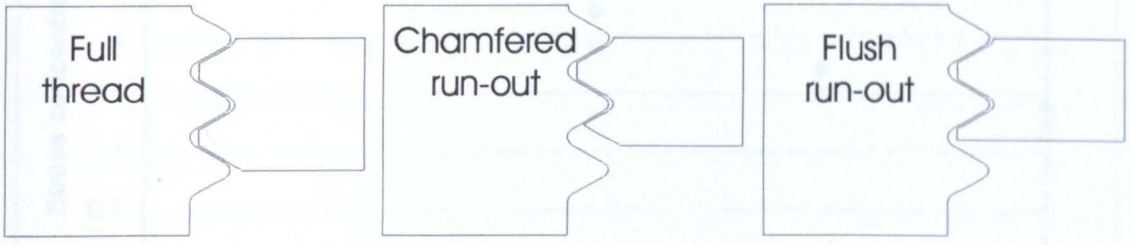

Figure 7.24 Different types of nut thread run-out

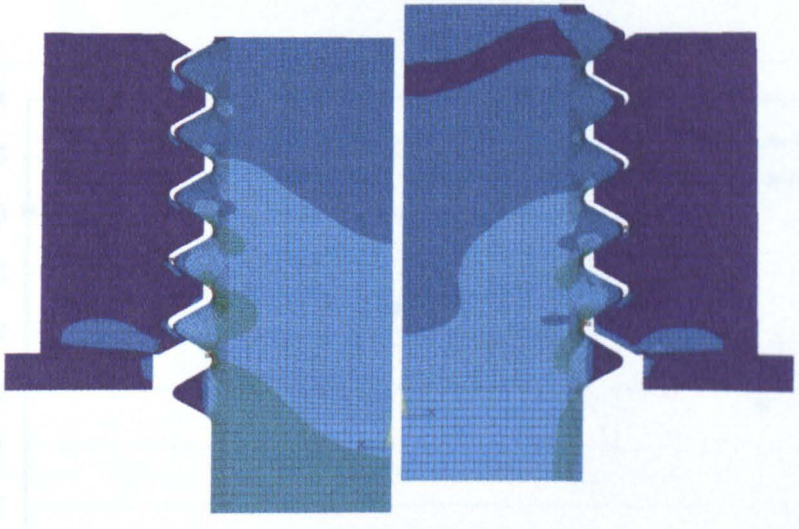

Figure 7.25 Two-dimensional models representing the run-out side of the bolt (right) and opposite side (left). Different colour contours are used in each model so the contours do not match.

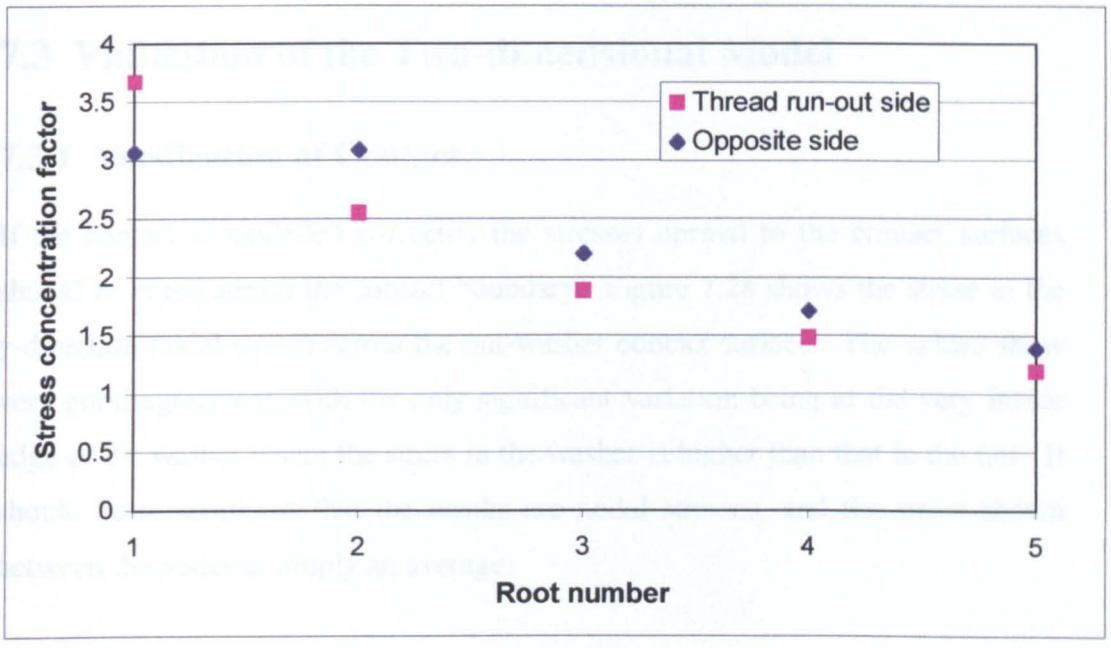

Figure 7.26 Comparison of the results of the models representing the run-out and opposite side positions, based on root number

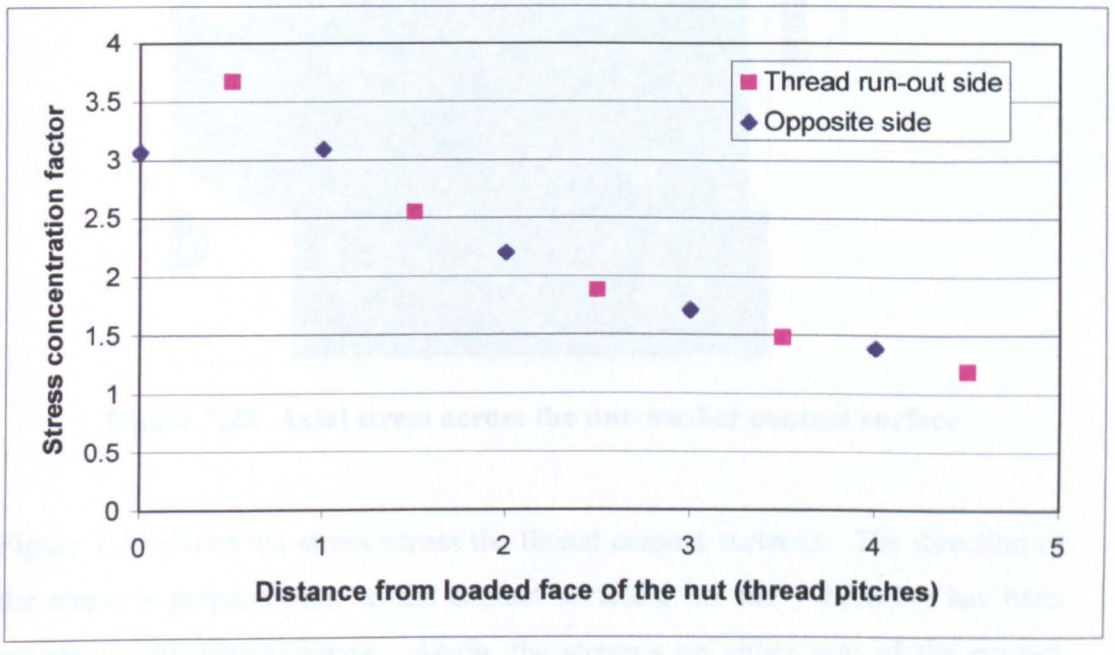

Figure 7.27 Comparison of the results of the models representing the run-out and opposite side positions, based on distance from the loaded face of the nut

7.3 Validation of the Two-dimensional Model

7.3.1 Verification of Contact

If the contact is modelled correctly, the stresses normal to the contact surfaces should be equal across the contact boundary. Figure 7.28 shows the stress in the y-direction (axial stress) across the nut-washer contact surface. The values show very good agreement, with the only significant variation being at the very inside edge of the washer where the stress in the washer is higher than that in the nut. It should be remembered that the results are nodal stresses, and the stress shown between the nodes is simply an average.

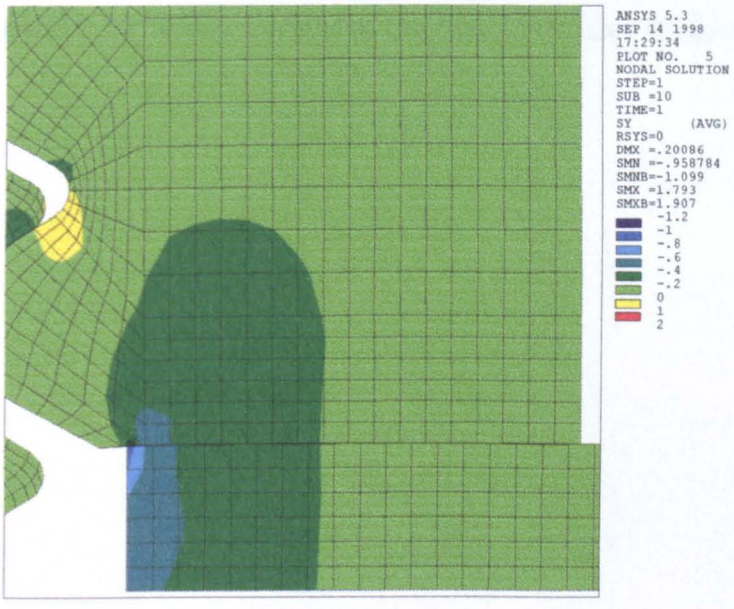

Figure 7.28 Axial stress across the nut-washer contact surface

Figure 7.29 shows the stress across the thread contact surfaces. The direction of the stress is perpendicular to the contact surfaces, i.e. the y-direction has been rotated by 30° anticlockwise. Again, the stresses on either side of the contact surface show very good agreement. Therefore, modelling the contact is shown to be effective and accurate.

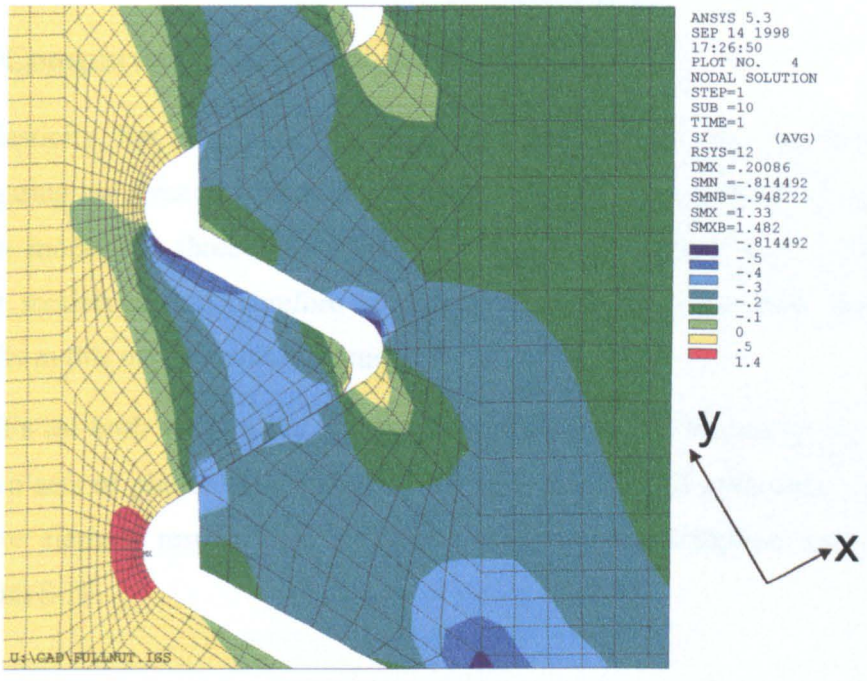

Figure 7.29 Stress normal to the thread contact surfaces

7.3.2 Comparison with Photoelastic Analysis

Photoelasticity has, for some time, been considered as the benchmark for investigating the stresses in threaded connections. It is a well establish technique that can model the three-dimensional nature of the problem well. The finite element models should therefore be validated by comparison with appropriate results from this experimental technique.

The SCFs for both sides of the bolt are plotted in Figure 7.30, along with results from two sets of photoelastic analysis. There is fairly good agreement, although the finite element results have a flatter shape to the distribution and a lower maximum SCF.

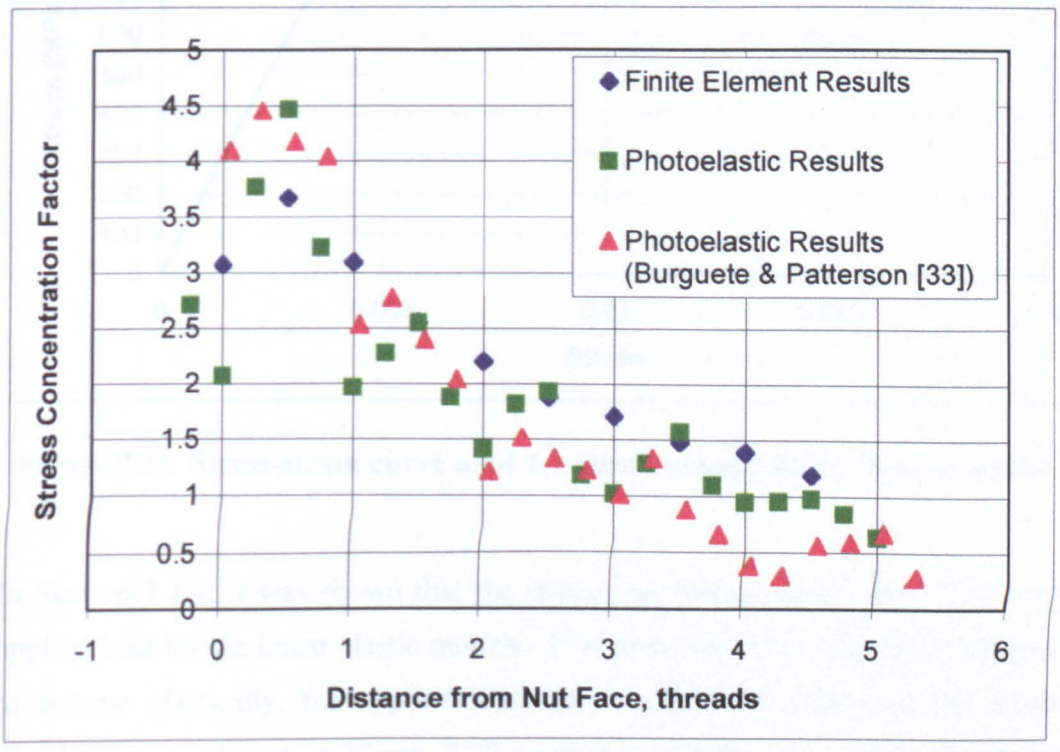

Figure 7.30 Comparison of stress concentration factor results from finite element method and photoelastic analysis

7.4 Plasticity

While modelling the nut and bolt using linear elastic material properties provides a very useful comparison with the results from photoelastic analysis, the majority of nuts and bolts used are made of materials that exhibit plasticity. The material properties for the 6337 element two-dimensional model were changed so that the stresses followed the stress-strain curve shown in Figure 7.31. This is approximately equivalent to a grade 8.8 bolt.

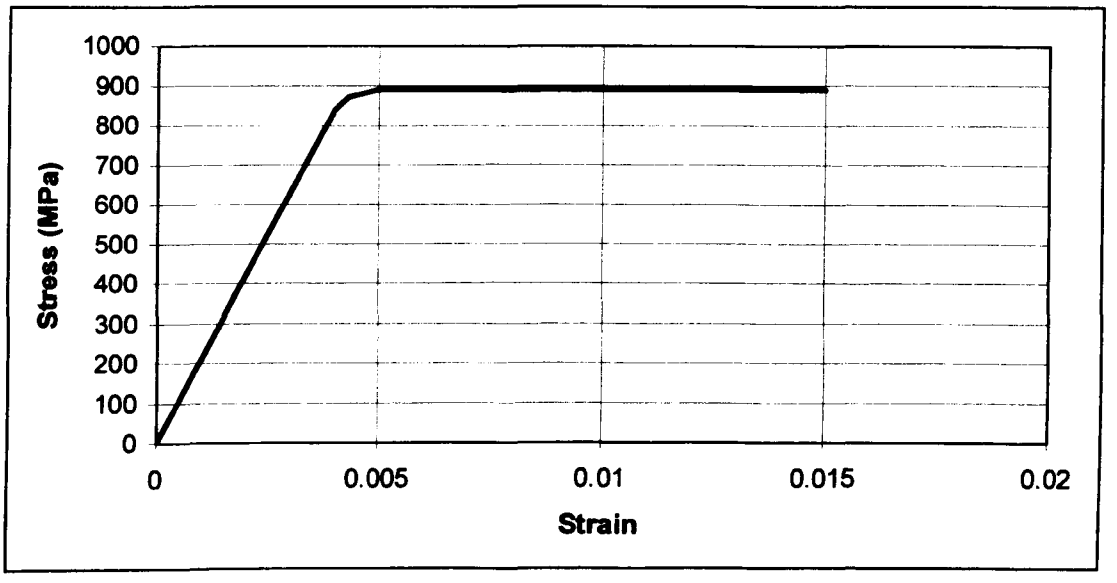

Figure 7.31 Stress-strain curve used for elastic-plastic finite element model

In Section 7.2.4, it was shown that the stress distribution varied very little with applied load for the linear elastic models. However, when the material is allowed to behave plastically, the applied load has a substantial effect on the stress distribution, as shown in Figure 7.32. As more of the bolt yields, the stress distribution becomes flatter, with the stress being more evenly distributed. As the load reaches 25 kN, the load has redistributed so that the stress in the second thread root is almost as high as that in the first root. The stress-strain curve used is perhaps slightly extreme in that the material would yield only very slightly before becoming perfectly plastic, and therefore the effect of plasticity may be slightly exaggerated. However, it is still a useful illustration of the effect of

plastic deformation on the stress distribution. The sharp peak would disappear with more of the thread experiencing the highest stress concentrations.

The development of the plastic zones are shown in Figure 7.33. It shows the stress in terms of equivalent stress for 25kN, 41 kN and 57 kN. The colour contours are set so that areas that are in the plastic zone are coloured red. At 25kN and 41 kN, plasticity is limited to small areas in the thread roots and the magnified views show. This agrees with the plot of stress concentration factors in Figure 7.32 where just the first thread root is affected at 25 kN, but all thread roots are affected at 41 kN. At 57kN, the plasticity is far more extensive and no magnification of the thread roots is needed to see the plastic zones.

The reason for the results for the run-out side being lower at low loads, resulting in an oscillating distribution near the free end of the nut, is not clear. The results are from two different models, and perhaps slight differences in the applied load are the cause. However, it should be noted that this is definitely not due to bending, as the two models were axisymmetric and therefore had no mechanism for bending.

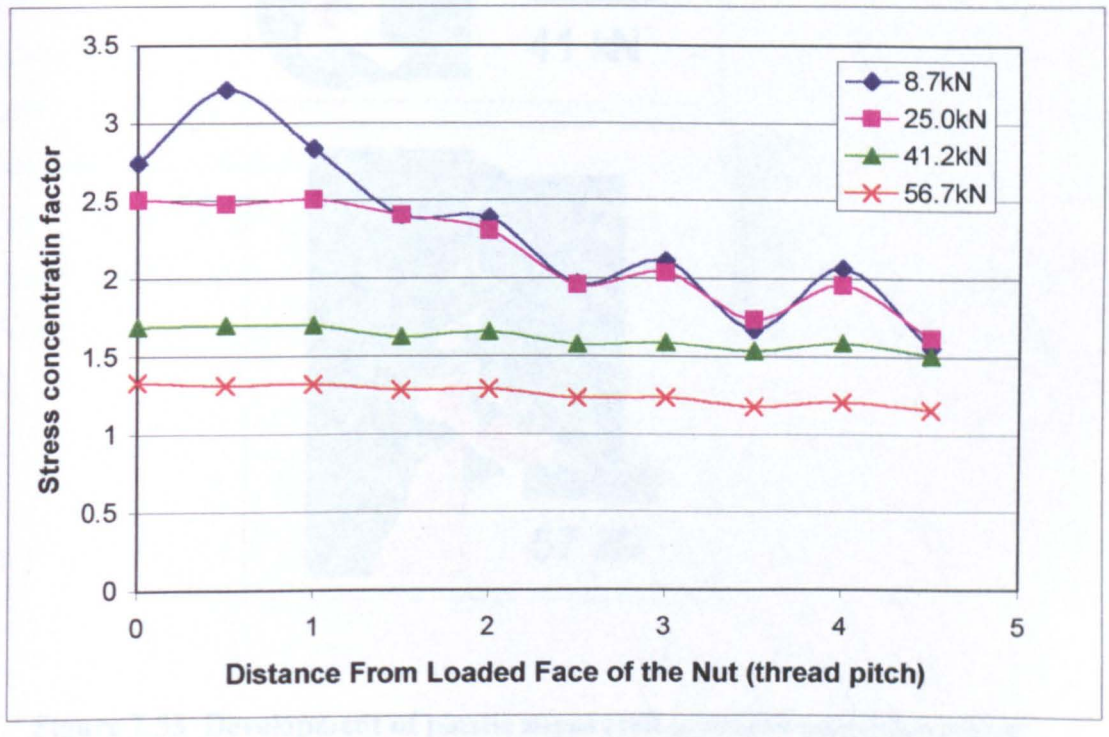

Figure 7.32 Effect of applied load on the stress concentration factors in a bolt with elastic-plastic material properties

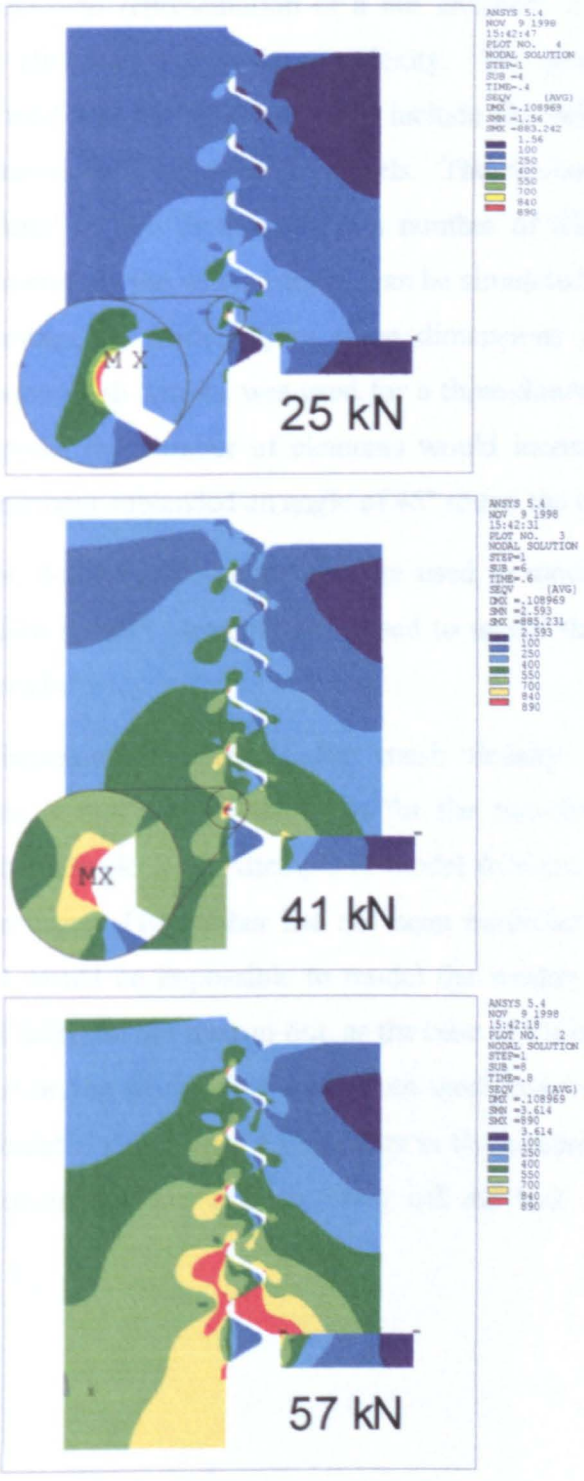

Figure 7.33 Development of plastic zones (red areas) as load is increased from 25 kN (~30% UTS) to 57 kN (~75% UTS)

7.5 Three-dimensional Model

As for a two-dimensional representation of a nut and bolt, a three-dimensional representation can also vary greatly in complexity. The main advantage of a three-dimensional model is the fact that it can include the helix angle, which is ignored in two-dimensional axisymmetric models. The run-out of the nut thread can only be simulated in two dimensions if a number of different models are created, in three dimensions the whole run-out can be simulated in a single model. The main disadvantage of modelling in three dimensions is the number of elements. If the same mesh density was used for a three-dimensional model as a two-dimensional model the number of elements would increase by a factor of eight even if each element subtended an angle of 45° round the circumference.

In all three models, 8-node brick elements were used to model the nut and the bolt. Point-to-surface contact elements were used to model the contact between the bolt and nut threads.

Because of the increased complexity, the mesh density of all the three-dimensional models is much lower than that for the two-dimensional models. Also, friction has been neglected. Attempts to model friction resulted in models that would not converge. The washer has not been modelled in any of the 3D models. In fact, it would be impossible to model the washer in the model that included the thread helix but not the run-out, as the base of the nut was not flat. In all cases, the nodes on the loaded face of the nut were constrained in the axial, radial and circumferential directions. Constraints in the circumferential direction were needed to prevent the nut from winding off the bolt in the absence of friction.

7.5.1 Three-dimensional Axisymmetric Model

There should be very little difference between a two-dimensional, axisymmetric model and a three-dimensional model that is axisymmetric. Any object that is symmetrical about its axis can be modelled using three-dimensional elements, although this results in a large model. Using two-dimensional, axisymmetric elements significantly reduces the size of the model and should result in a similar degree of accuracy.

Constructing a model of an axisymmetric object in 3D would, therefore, appear to be a waste of time, but such a model was created as a first step to modelling the full 3D geometry of a threaded connector. The results from this model enable the effect of replicating the thread helix and the nut thread run-out to be evaluated.

Both a 2D and a 3D model were created using equivalent mesh, shown in Figure 7.34. The 3D model was far larger, though, with over 9000 elements compared to just 293 elements for the 2D models. This resulted in running times going up from a few seconds for the 2D model to about an hour of CPU time for the 3D model. The results are compared in Figure 7.35. As expected, despite the large difference in model sizes, the results are very similar.

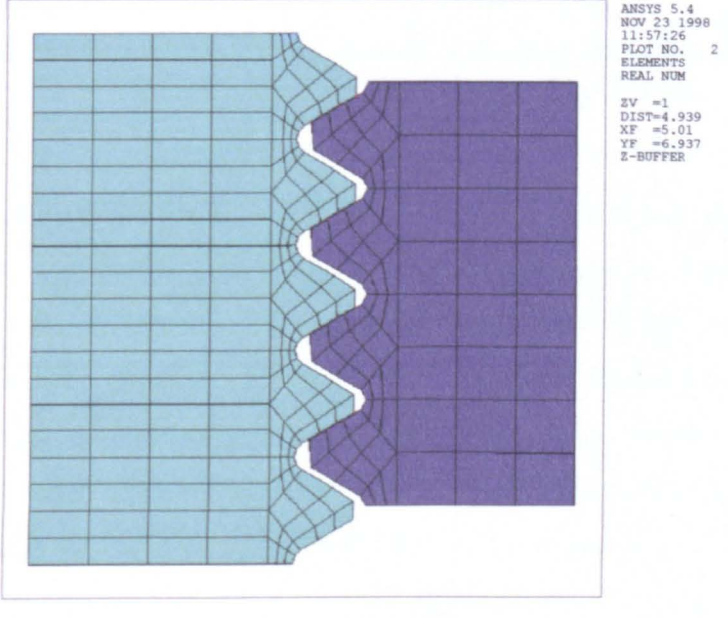

Figure 7.34 Mesh of the 2D model on which the meshes for the 3D models were based

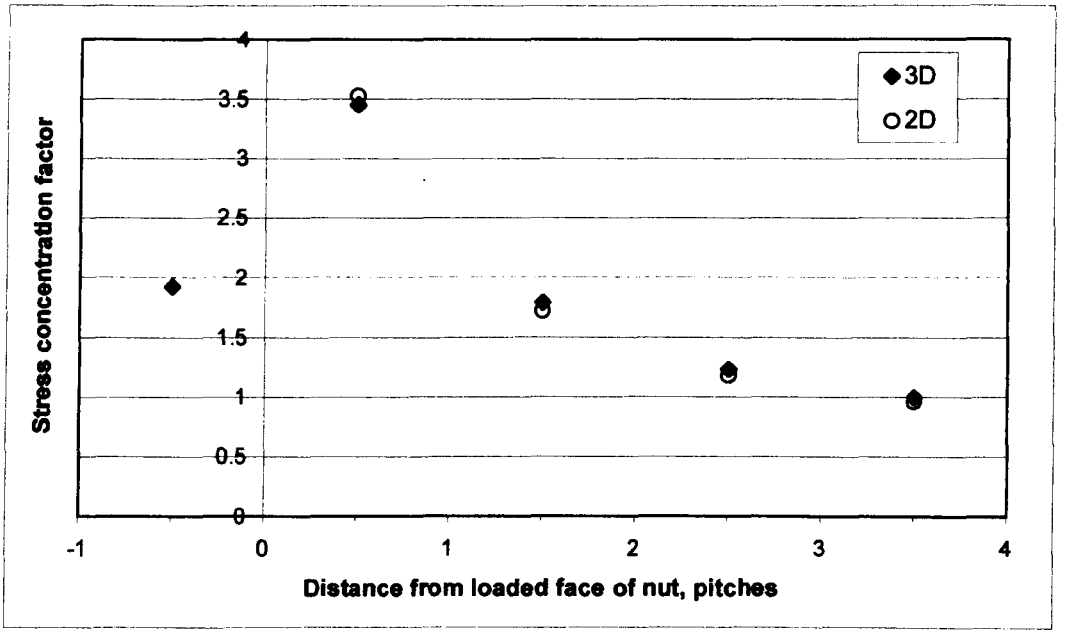

Figure 7.35 Stress concentration factors in the bolt thread roots for the 2D and 3D axisymmetric models

7.5.2 Modelling the Thread Helix

Replicating the helix angle of the threads is relatively straight forward. The basic geometry and mesh are the same as for the axisymmetric model, but each thread moves up to join the thread above after a complete turn to form a continuous thread. In this model, the run-out was not modelled, so the base of the nut and bolt were helical and not flat.

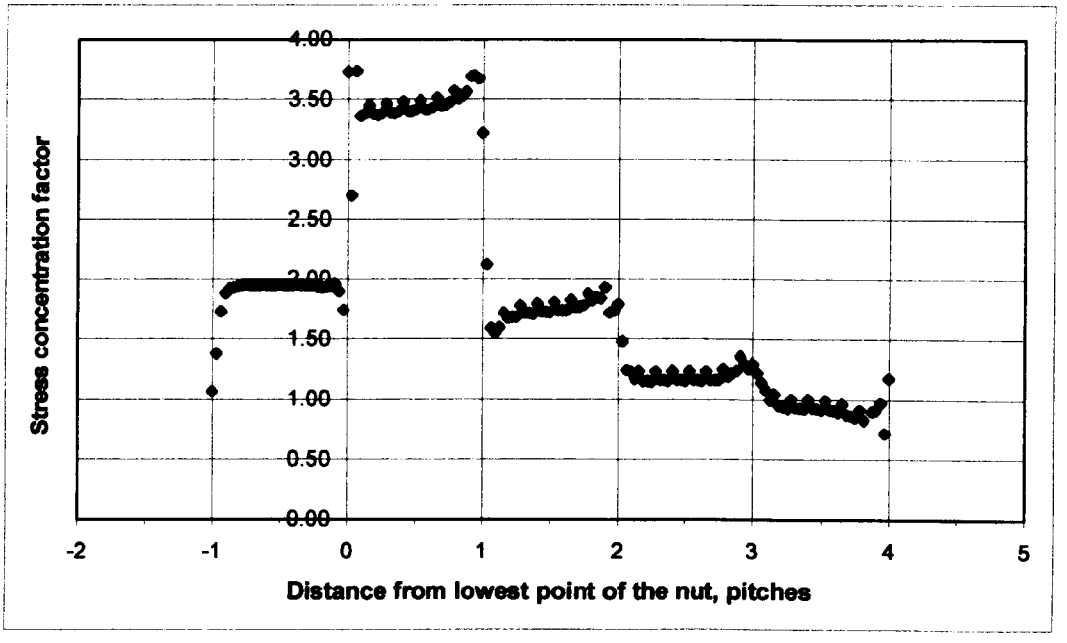

Figure 7.36 Stress concentration factors in the bolt thread roots for the three-dimensional model with thread helix

The stress concentration factor results are shown in Figure 7.36. One advantage of modelling the helix is that the data is continuous, therefore stress concentrations can be found for any point up the height of bolt, not limited to thread roots at discrete points. However, considering the data in Figure 7.36, this may not be so advantageous as the plot shows little resemblance to the photoelastic result in Figure 7.30. The stress concentration factor depends mainly on how many threads are in contact below the thread of interest. The stress drops sharply when the thread is no longer the first to be in contact with the nut.

7.5.3 Modelling the Nut Thread Run-out in Three Dimensions

The geometry of the thread run-out is illustrated below in Figure 7.37. As discussed in Section 7.2.5, there are two main styles of thread run-out; chamfered and flat-faced. The chamfered run-out is more common and was used in the photoelastic and fatigue studies reported in previous chapters, and therefore has been chosen for this analysis. Modelling the run-out is far more involved than modelling the thread helix. The geometry requires careful attention and varies constantly around the helix, and the meshing is complicated by the fact that number of elements has to be reduced in the run-out thread to ensure proper mating of elements. The meshing system of the whole nut was changed to make this slightly easier.

Only the run-out at the loaded face of the nut has been modelled. The free end of the nut finishes suddenly, in the same manner as for the previous model. This was done to reduce the number of the elements and save time in building the model. The free end run-out is less important than the loaded face run-out for two reasons; firstly, the stresses are highest at the loaded face and it is this end in which we are most interested and secondly, the bolt threads do not make contact with the run-out at the free end. As soon as the thread reduces in width, a gap forms between the nut and bolt threads. The model contains 12291 elements, which is considerable more then the 590 elements used by Zhao[4] in her 3D model.

The stress concentration results for this analysis, shown in Figure 7.38, correlate more closely with the result from photoelastic analysis than the results from the model that ignored the run-out. The obvious step in stress concentrations seen in the results for the model without the run-out is gone leaving a fairly smooth curve. Figure 7.41 and Figure 7.42 show that axial stress in the bolt for the models without the run-out and with the run-out respectively. It can be seen that the red area of highest stress stops suddenly in the model that does not model the nut thread run-out. However, when the nut thread run-out is modelled, the high stress concentrations decrease more gradually around the helix.

Comparing the results from the three 3D models, Figure 7.39 shows that there is close agreement at the thread root half a thread pitch from the loaded face. Comparison with the fine mesh 2D model shows that the lower mesh density

results in much lower stress concentration factors. Replicating the thread run-out results in a slightly higher stress concentration factor, but the results from the axisymmetric model and the 3D helical model without the run-out show negligible difference. If the SCFs at any other point are required, there is a large difference between the models. The axisymmetric model simply can not provide that data as the thread roots just occur at set distances from the loaded face. The difference between the stress concentration factor results for the other side of the bolt for the models that include the helix thread are shown in Figure 7.40. The actual difference between these two sets of results depends on precisely the point being considered and whether it is before or after the large step, but it is clear that there is a very large difference.

In conclusion, it is very important to model the run-out of the nut thread if the thread helix is to be replicated. Otherwise, although the stresses at certain points may be similar, the overall shape of the stress distribution curve is very different.

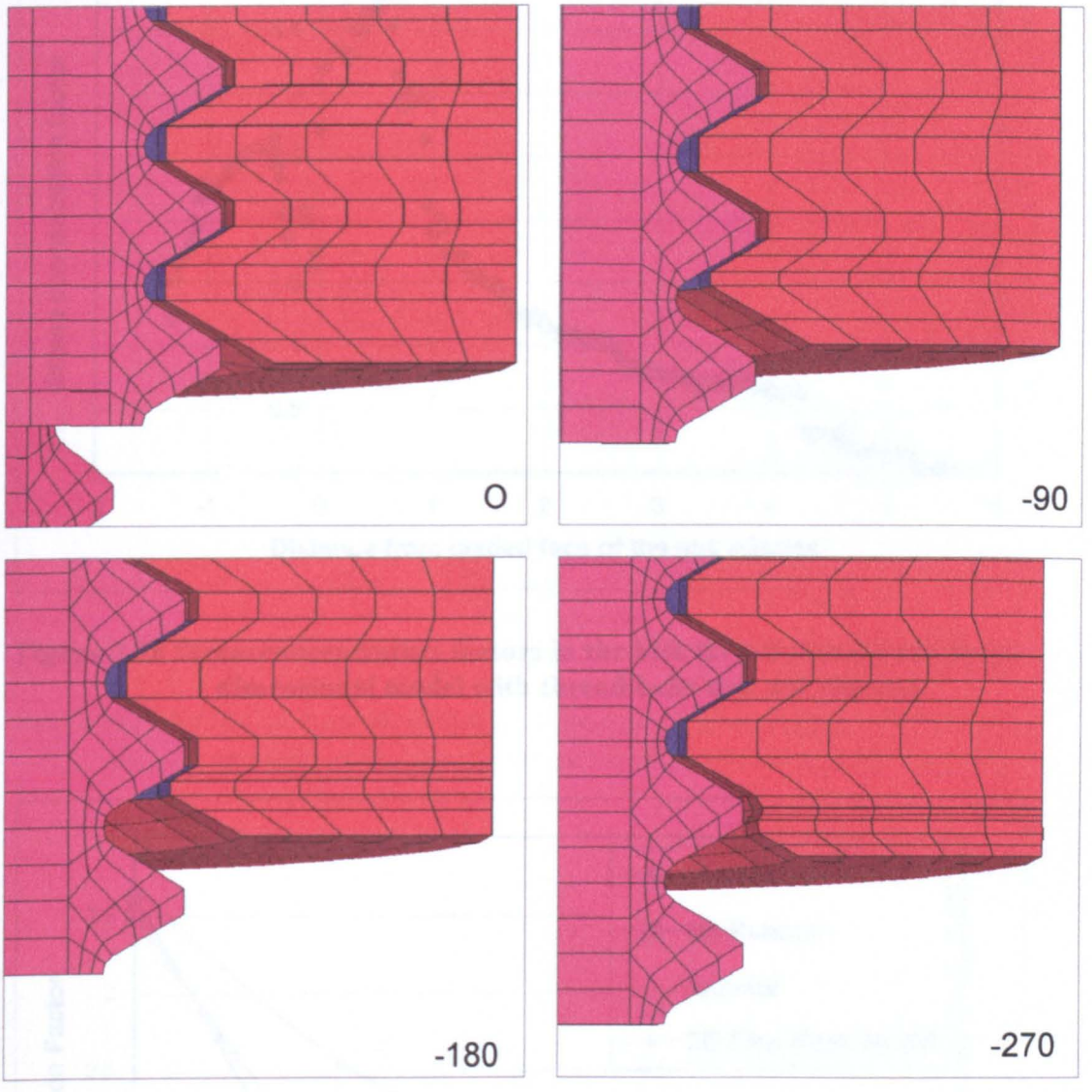

Figure 7.37 Geometry profile of the nut thread run-out

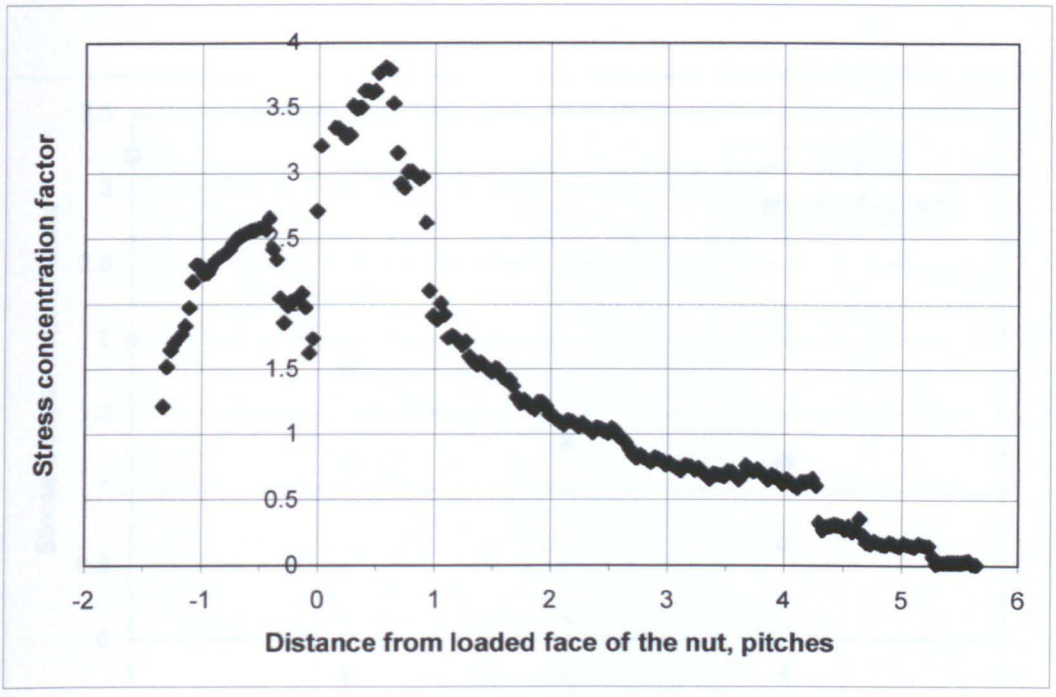

Figure 7.38 Stress concentration factors in the bolt thread root for the three-dimensional model with thread helix and nut run-out

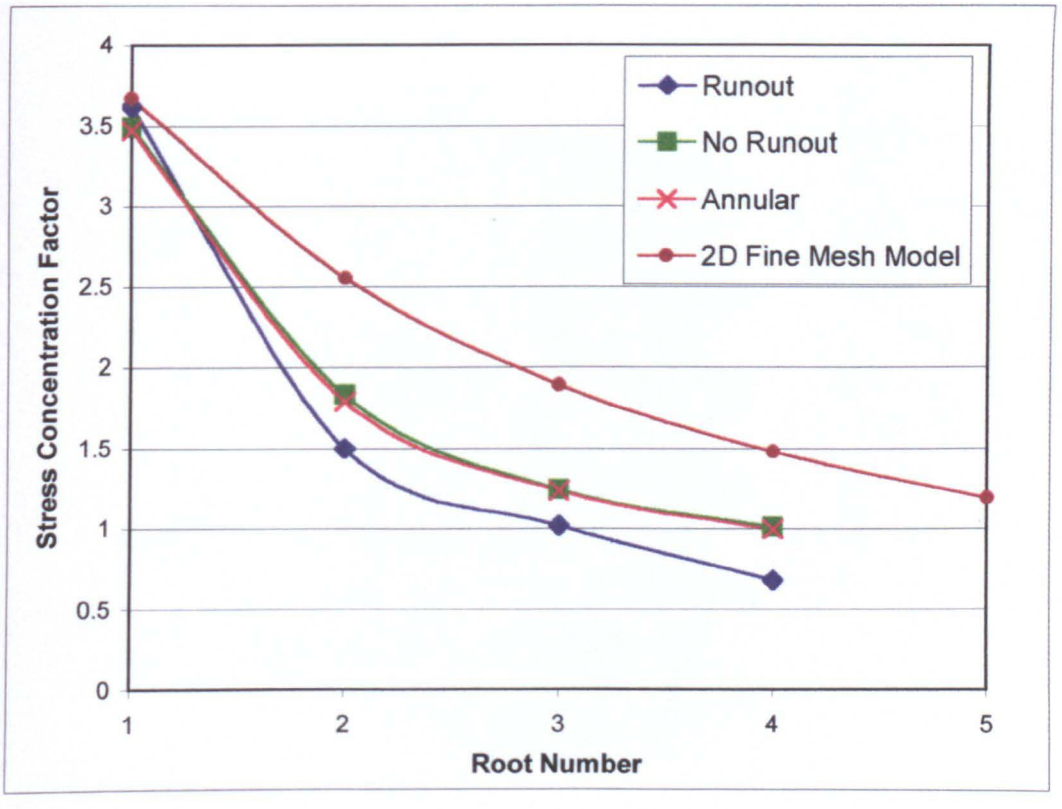

Figure 7.39 Comparison of stress concentration factor results at the run-out side of the thread for three three-dimensional models and the final two-dimensional model (6337 elements, modelling washer)

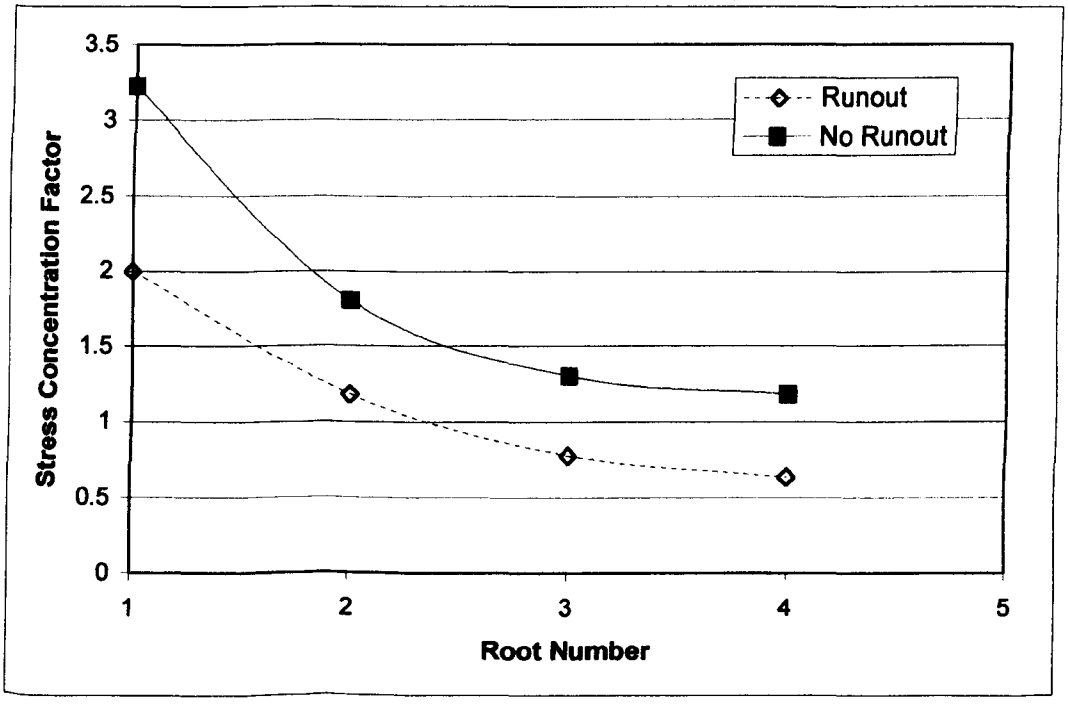

Figure 7.40 Comparison of stress concentration factor results at 180° from the run-out side of the thread for three-dimensional models with helix

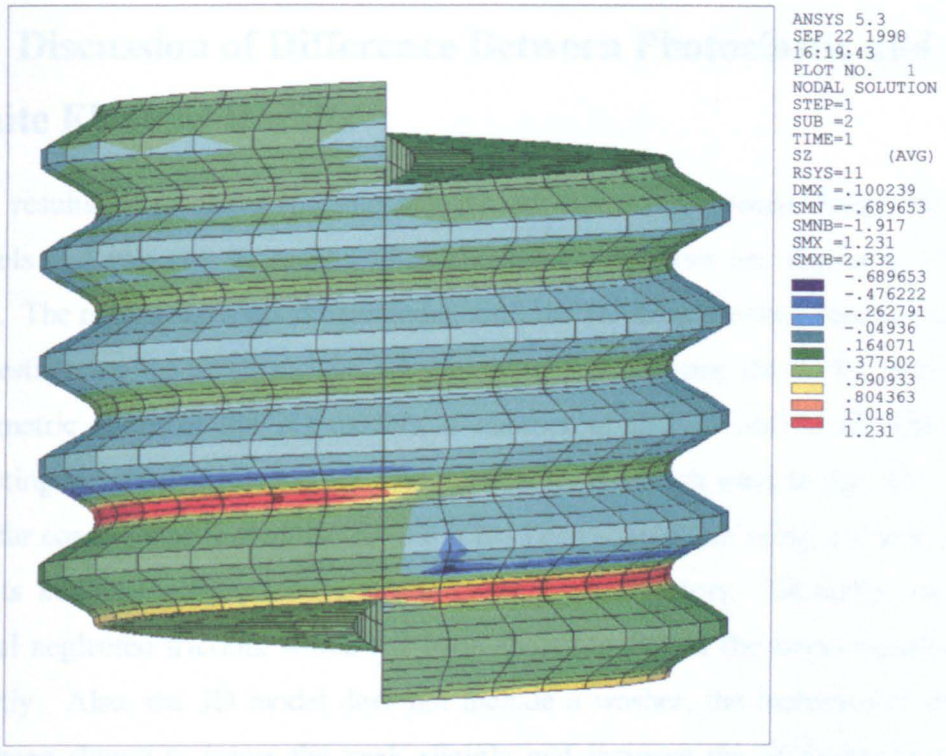

Figure 7.41 Axial stress in bolt when loaded with a nut without the run-out being modelled

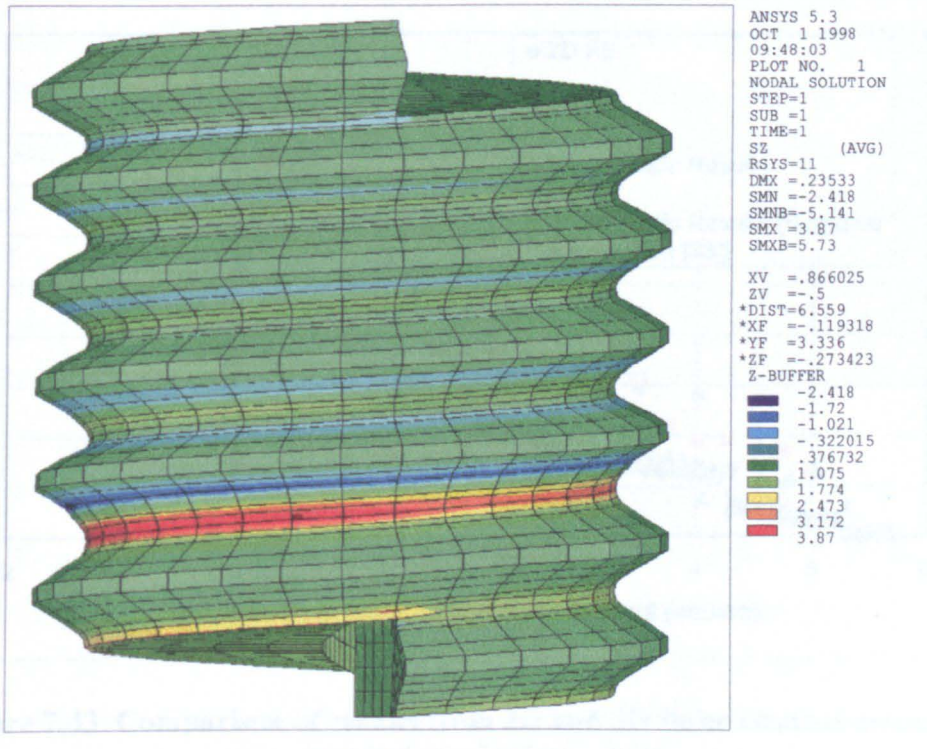

Figure 7.42 Axial stress in bolt when loaded with a nut with the run-out

7.6 Discussion of Difference Between Photoelastic and Finite Element Results

The results from the two-dimensional and three-dimensional finite element models and two sets of results from photoelastic analysis are shown in Figure 7.43. The results show good agreement, with the 2D finite element results slightly overestimating the SCFs and the 3D slightly underestimating the SCFs. From the parametric study of the 2D models, a number of factors can be identified as affecting the result from the 3D model. Firstly, the mesh used in the 3D model was far coarser than that of the 2D and it has been shown that using a coarse mesh results in lower values for the stress concentration factors. Secondly, the 3D model neglected friction, which has been shown to flatten the stress distribution slightly. Also, the 3D model does not include a washer, the inclusion of which has been shown to lower the peak slightly and increase the SCFs in the other roots.

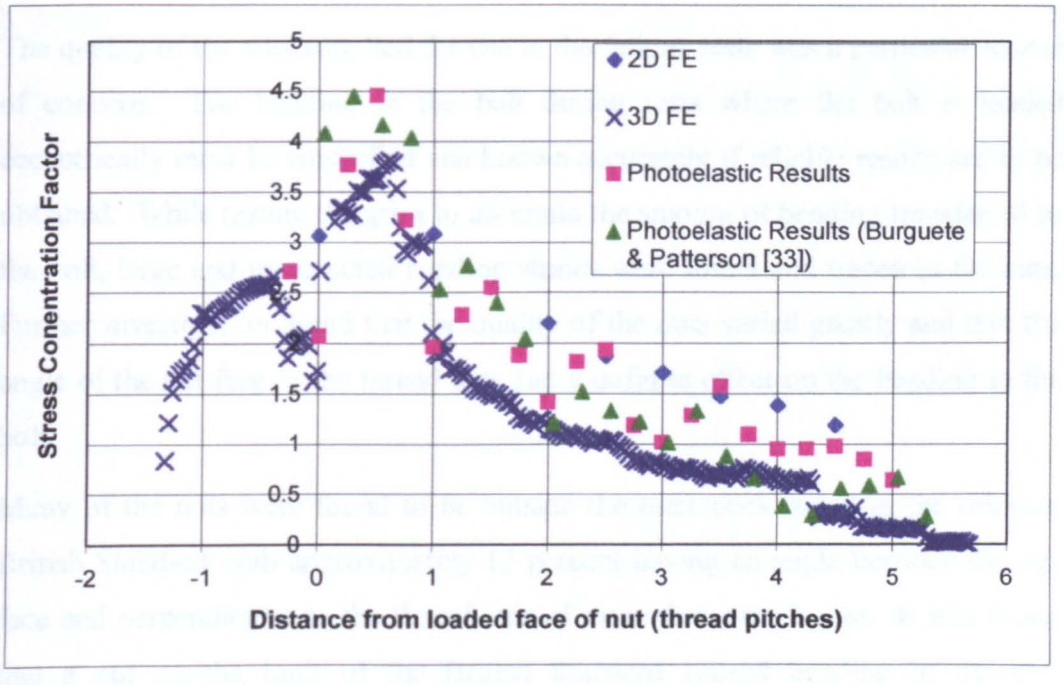

Figure 7.43 Comparison of results from 2D and 3D finite element models and photoelastic analysis

Chapter 8

Discussion

8.1 Eccentric Fatigue Tests

The quality of the nuts supplied for use in the fatigue tests was a particular matter of concern. The bending in the bolt during tests where the bolt is loaded eccentrically must be controlled and known accurately if reliable results are to be obtained. While testing the grips to ascertain the amount of bending transferred to the bolt, large and unexpected bending strains were found and traced to the nuts. Further investigation found that the quality of the nuts varied greatly and that the angle of the nut face to the thread axis had a definite effect on the bending in the bolt.

Many of the nuts were found to be outside the tolerances stated in the relevant British Standard with approximately 15 percent having an angle between the nut face and perpendicular to the thread axis of more than one degree. It was found that a nut on the limit of the British Standard caused bending in the bolt equivalent to an eccentricity of approximately, e/D = 0.08. This small level of eccentricity is unlikely to significantly reduce the fatigue life of the bolt.

The fatigue tests with eccentric loading showed that bolts loaded with an eccentric cyclic load have a lower fatigue strength at 2×10^5 cycles than those loaded with an axial load. The maximum permissible load applied to bolts to obtain a fatigue life of 2×10^5 cycles is approximately 8% lower when the load is applied with an eccentricity, e/D = 0.33. However, this reduction in fatigue strength can be accounted for if the local stress amplitude is considered. The actual stress amplitude will vary spatially in the bolt especially when it is eccentrically loaded. The results from the strain gauges show that the stress amplitudes on different sides of the bolt vary when eccentrically loaded. If the local stress amplitude is used to calculate the fatigue strength it is found that the local stress amplitude to cause failure at 2×10^5 cycles varies very little with eccentricity. From photoelastic analysis performed by Burguete and Patterson[33] it was found that the peak in the stress distribution was flatter and wider for eccentrically loaded bolts. It was suggested by Burguete and Patterson that this would increase the likelihood of crack initiation as a larger section of thread was exposed to high load, and therefore reduce the fatigue life. The results from this fatigue investigation suggest that this is not the case, as the reduction in fatigue life can be wholly accounted for by the increase in local stress amplitude.

Therefore, if the amount of eccentricity and the local stress amplitude could be ascertained at the design stage, the effect of eccentricity on fatigue life could be determined.

To determine the local stress amplitude, the stress concentration effects of the thread geometry does not need to be taken into account. It is assumed that the effect of geometry will be similar regardless of whether or not bending is present. Obviously, the fatigue behaviour of axially loaded bolts needs to be known, before any compensation for bending can be taken into account.

The shape of the cracks does not appear to be affected by the level of eccentricity experienced for the range of eccentricities considered here. This means that no useful information about the amount of bending experienced by a bolt can be obtained from the examination of a fracture surface. The level of mean stress has a far greater effect on the crack shape.

8.2 Photoelastic Analysis

Two main investigations were performed using the technique of photoelastic analysis. The first was into the effect of crack shape on the stress intensity factors at the crack tip and the stress concentration factors in the thread roots of bolts. The second was to investigate the effect of eccentric loading on the same stresses.

The investigation into the effect of crack shape concentrated on crescent-shaped cracks. This shape has been found by the author and other investigators, such as Pacey *et al*[53] and Fuchs and Stephens[58], to be the shape most likely to occur in cyclically loaded bolts. However, this shape of crack had not been used in any stress intensity factor investigation in bolts. Other investigators had used either a semi-circular or straight fronted crack shape.

The results show that the shape of the crack has little effect on the maximum stress intensity factor at the crack tip. However, the SIFs around the crack front vary with crack shape. In all cases, the highest SIF is in the centre of the crack front, with the SIFs decreasing toward the ends of the crack front. The straighter the crack, the less marked this effect becomes. However, the effect is still present, which indicates that the crack would grow more quickly in the centre of the crack front that at the edges. The crack would, therefore, straighten out as it progressed. This is not seen in the experimental investigation into the shape of fatigue cracks in steel bolts, as previously discussed.

The investigation into the effect of eccentric loading showed that the maximum SIFs increased as eccentricity increased. This effect is not dramatic, with the maximum SIF increasing by less than 10 percent between eccentricities of e/D = 0 and e/D = 0.168. If the SIFs were normalised using the maximum stress, instead of the axial stress, the SIFs were found to decrease markedly with eccentricity. Rather than an increase of 10 percent, a decrease in SIF of over 55 percent is seen over the same range of eccentricity. Although this is probably due in part to the calculated bending stresses being higher then the actual bending stresses, the decrease in SIFs is still far greater than the fatigue results would suggest. From the fatigue results, the local stress amplitude, that is, the maximum stress including the bending component, to cause failure is independent of eccentricity. This would suggest that the SIFs normalised using the maximum stress would not

vary with eccentricity. Clearly, the fatigue and photoelastic results do not correlate. The fact that photoelasticity can not model the plastic deformation or residual stresses in steel bolts is probably a major cause for the discrepancy.

As expected, the stress distribution was affected by the eccentricity. The higher the eccentricity, the greater the difference in stress concentration between the tension side and the compression sides of the bolt.

8.3 Finite Element Analysis

A large number of factors affecting the load and stress distribution in nuts and bolts were investigated using the finite element method. Two-dimensional and three-dimensional models were created that varied greatly in complexity and fidelity to the real life component.

The amount of a nut or bolt represented in a finite element model was found to have a significant effect on both the load distribution and the stress concentration factors in the thread roots. If the amount of bolt represented is small (three pitches in length), loaded with a short, two-pitch nut, then the stress concentration factors are significantly overestimated. With the bolt ending immediately after the last loaded thread, the last thread in the bolt lacks stiffness and deforms more. This increases the stress concentration in the second thread root. Also, as the second thread bends, more load is carried by the first thread which increases the stress concentration in the first thread root.

The length of the nut is also important in a similar way. In general, the shorter the nut, the higher the stress concentration factors. If the washer is modelled, and the nut is not constrained at its loaded face, a short nut bends about the inside edge of the loaded face, forcing the free end in toward the bolt. This has the effect of transferring some of the load from the first thread to the second thread. With a two-thread nut, this happens to such an extent that the second thread takes significantly more load than the first thread, but the stress concentration is still higher in the first thread then in the second. This is due to the fact that all the load taken by the bolt effects the stress in the first thread root, whereas the load taken

by the first thread has no effect on the stress in the second root. If the stiffness is increased, by making the nut longer, the nut no longer bends in this way. Similarly, when the washer is not included in the model, and the loaded face of the nut is constrained, this effect does not occur because the nut is not free to bend to the same extent.

The inclusion of a washer in a model changes the stress distribution to a lesser degree if the nut is longer, as shown in Figure 7.9. Excluding the washer and constraining the nut results in a slight increase in the load taken by the first thread and a subsequent reduction in load taken by the other threads. Therefore the peaked shape of the stress distribution is slightly exaggerated.

The mesh used has a great effect on the stress concentration factors. In general, the finer the mesh and the more elements used, the higher the stress concentration factors up the point of convergence. However, the density of the mesh has little effect on the load distribution. As the stress concentration in the nut is of less interest, this means that a coarse mesh can be used in the nut with a finer mesh concentrated in the areas of interest in the bolt. It also indicates that the technique of sub-modelling may be useful and appropriate to the problem. This technique models as large a portion of the structure as is desired with a coarse mesh and the load results are obtained. Then a small portion that is of particular interest is modelled with a much finer mesh and the load results from the first model are applied. The stress results are then accurately obtained in the area of interest. The author has not attempted to use this technique, but believes it may be a useful tool for further investigations.

The results from the two-dimensional models were compared to photoelastic results and agreed well, therefore validating the model parameters and boundary conditions. The maximum stress concentration factor was approximately 17 percent lower from the finite element analysis than from the photoelastic analysis of Burguete and Patterson[33] and the authors own photoelastic results. The peak stress occurred in a similar place, half a thread from the loaded face of the nut. However, a limited number of data points were created, two per thread, so the exact point of the peak stress could not be found. If more points were required, extra models representing different positions around the bolt would have to be created.

Three-dimensional models were created with three levels of complexity. The first model was axisymmetric and, therefore, did not replicate the thread helix. The nut was four threads long, which was found from the two-dimensional analyses not to vary greatly from a five-thread nut. Despite using a far coarser mesh, the results differed only slightly from the two-dimensional, axisymmetric model of the four thread nut. The three-dimensional model was far larger, taken over a thousand times longer to solve, with no real advantage over the two-dimensional version.

The real advantage of working with a three-dimensional model is the ability to accurately recreate the thread helix. In the second model this was achieved using the same basic mesh as the axisymmetric model. The results from this analysis, shown in Figure 7.36, were surprising. The stress concentration factors varied little with the angular position around the helix but depended greatly on whether it was the first, second or third etc, loaded thread. As soon as another thread took load between the loaded face the thread of interest, the stress dropped suddenly. This effect is not present in the photoelastic results. The stress concentration values at each thread root show good agreement with previous models, but the shape of the curve is very different to what has been found experimentally. It has been recognised for a long time that the first thread root takes a larger proportion of the load due to the difference in thread pitch caused by differential strain in the nut and the bolt. When the thread starts suddenly, the load taken by the bolt thread starts suddenly. The load remains fairly constant around the helix until the thread suddenly becomes the second loaded thread. Here the load drops suddenly to the value for the second loaded thread.

Replicating the run-out of the nut thread as it approaches the loaded face of the nut was the challenge faced in the third of the three-dimensional models. It has been believed for some time that the run-out has a significant effect on the stress distribution in the bolt. The results from this analysis, shown in Figure 7.38, show that this is true. Not only is the maximum stress concentration slightly higher but the whole shape of the distribution is different to the models without the nut thread run-out. The steps in stress concentration from the model without the run-out are not present and the resulting curve bears close resemblance to that obtained from photoelastic analysis. The first thread no longer starts suddenly,

but gradually increases in size and stiffness around the thread helix. Therefore, there is no sudden jump in the load taken by the bolt thread at any point. It appears that if the thread helix is to be modelled, it is essential to also model the run-out of the nut thread.

The results from the three-dimensional models show a larger drop-off in stress concentration factors away from the first thread, therefore underestimating the stress in the less stressed portions of the bolt. A similar effect is seen for the 2D model that does not include the washer. The lack of a washer in the 3D models is therefore the most likely cause for the lower stresses. Including the washer would be likely to provide results that matched those from photoelastic analysis more closely, but then friction would have to be included to stop the nut twisting off the bolt.

The question of what type of finite element model to create depends to a great extent on what information is required. If the stress distribution is required only at certain points then a two-dimensional model is probably adequate. If computer time is at a premium, it would be more efficient to run a number of 2D models representing a number of slices through positions around the helix rather than running one large 3D model. However, if the stress distribution is required to a higher resolution, i.e. using more data points to describe the shape of the distribution, then a 3D model would probably be quicker.

If the aim of the finite element analysis is to analyse a loading condition that is not axisymmetric, or if the bolt contains a non-axisymmetric crack, then 3D models are required. For these models, the thread run-out should be modelled, to provide an accurate stress distribution. It is not only the region around the thread run-out that it affected, but the effect is present all the way through the bolt, albeit less significant toward the free end of the nut.

8.4 Crack Shape

The results from photoelastic analysis show a large peak in the stress concentration factors in the bolt at approximately half a thread pitch from the loaded face of the nut. The results from the three-dimensional finite element model show a very similar peak for the model that includes the nut thread run-out. However, from actual cracked bolts, it can be seen that the crack shape is likely to be crescent shaped, even for very small crack lengths. This implies that the crack starts to grow along a large section of the thread helix at about the same time, either by a process of many small initiation sites around the helix merging, or the crack initially growing around the helix before growing in towards the centre of the bolt. This does not fit with the stress concentration results from the photoelastic and finite element analyses that would suggest a more localised starting point for the crack, where the sharp peak stress occurs.

Once the crack is growing, the beach marking tests show that the shape changes very little as the crack grows. The crack tends to maintain a crescent shape as it grows and it does not straighten out. The stress intensity factors around the crack tip obtained from the photoelastic analysis show that in every case investigated, the highest values were for the middle of the crack front. Moving along the crack front away from the middle, the stress intensity factors decreased. This suggests that the crack would be growing more quickly in the middle of the crack front than near the edges, resulting in the crack straightening out.

Clearly, it seems that photoelasticity and the finite element method have not managed to fully assess the stresses involved. The most likely explanation for the discrepancy is the effect of plasticity. The results from the 2D finite element models that include plastic material behaviour indicate that the peak in the stress distribution would be far less sharp if yielding of the material occurs. This could account for the crescent shaped cracks occurring at higher levels of mean stress. At higher stresses, more yielding would take place and a larger section of the thread would experience high stress resulting in a crack initiating simultaneously around the thread. Also, the effect of residual stresses in the rolled threads has be modelled in the photoelastic or finite element models and this may have an effect

on the crack shape. While modelling residual stresses is beyond the capabilities of photoelasticity, it may be possible using finite element analysis.

The comparison of the finite element results with results from photoelasticity show good agreement. Both assume linear elastic material properties and the stresses in terms of the difference in principal stresses have been compared.

The lack of ability to replicate plastic material behaviour is probably a problem for the photoelastic analysis of threaded connectors. The inability of photoelastic analysis to be used to predict the shape of the cracks that occurred in the steel bolts shows that is can be a problem.

Chapter 9

Conclusions and Recommendations for Future Research

9.1 Conclusions

9.1.1 Infinite Life

- The number of cycles to which fatigue tests on high tensile bolts should be performed has been investigated. Comparing fatigue limits calculated using 2 $\times 10^6$ cycles to represent infinite life to fatigue limits calculated using 5 $\times 10^6$ cycles shows that they differ by typically 9%. It is therefore concluded that using 5 $\times 10^6$ cycles produces more accurate results, but cheaper tests can be performed using 2 $\times 10^6$ cycles that would produce adequate results if a suitable allowance, such as reducing the fatigue limit by 2 standard deviations, was made.

9.1.2 Crack Shape

- It was found that the shape of cracks growing through grade 8.8, M12 steel bolts under cyclic loading does not change greatly as the crack grows. The cracks tend to have a more crescent shape at higher mean loads than low mean loads.
- Eccentricity of loading was found not to affect the shape of cracks significantly.

9.1.3 Fatigue

- Eccentric loading does affect the fatigue life of threaded connectors. An eccentricity of e/D = 0.33 reduces the fatigue life of a bolt by almost 40%. The fatigue strength at 2×10^5 cycles is reduced by approximately 15% for the same eccentricity.
- The effect of eccentricity can be predicted by considering the local stress amplitude. The fatigue strength in terms of local stress amplitude remains constant regardless of eccentricity.
- The quality of nuts supplied was variable, with about 15% falling outside the British Standard. While it was found that poor quality nuts did induce bending into the bolt, it is thought that the effect of a nut of the quality tested on the fatigue life of bolts would be negligible.

9.1.4 Photoelastic Analysis

- The shape of the crack does not have any discernible effect on the maximum stress intensity factor at the centre of the crack front for the range of crack shapes investigated.
- For all the crack shapes investigated, it was found that the maximum stress intensity factor occurred at the centre of the crack front. This suggests that the crack would grow most quickly at this point and therefore straighten out. This finding is not supported by crack shapes in cyclically loaded steel bolts.

- Crack shape does affect the distribution of stress intensity factors around the crack front. The more crescent-shaped a crack is, the more quickly the stress intensity factor decreases away from the centre of the crack.
- Eccentric loading increases the stress intensity factors at the centre of the crack front slightly, is SIFs are normalised using axial stress. If maximum stresses are used for normalisation, the SIFs reduce with eccentricity.

9.1.5 Finite Element Analysis

- There are a number of factors that were found to affect the stress distribution in the 2D models:

  ⇒ A short nut greatly increases the stress concentrations in bolt thread roots.

  ⇒ If a short nut is not fully constrained on its loaded face, it is likely to bend inwards toward the bolt at the free end, resulting in much higher stresses in the thread roots near the free end of the nut.

  ⇒ Using a short nut very close to the end of the bolt increases the stress concentrations as the last loaded thread of the bolt is less stiff and transfers more load to the other threads.

  ⇒ Not including a washer in the model and constraining the loaded face of the nut results in a higher peak stress in the first thread root and lower stresses in the bolt near the free end of the nut.

  ⇒ Neglecting friction results in a slightly flatter shape for the stress distribution, reducing the peak stress at the first thread root and slightly increasing the stresses in the bolt near the free end of the nut.

  ⇒ The applied load has little effect on the stress distribution provided no plasticity is included.

- Plasticity has a dramatic effect on the stress distribution, flattening the peak in the stress distribution. This effect increases with load as the plastic zones increase in size.

- The run-out of the nut thread has a large effect on the stress distribution throughout the whole length of the bolt. If the run-out is not modelled, sharp steps in the stress distribution are present. Therefore, if a 3D model of a threaded connector is created that includes the thread helix, it is very important to model the nut thread run-out.
- Any model, whether photoelastic or finite element, that does not simulate the plastic behaviour of the material will result in a stress distribution that is different to that occurring in steel bolts under normal to high loads. The discrepancy in the crack shape predicted from the photoelastic analysis compared to the crack shape occurring in cyclically loaded steel bolts indicates that the photoelastic model is inadequate in some way. The results from the 2D finite element model that includes plastic behaviour suggest that it is the inability of the photoelastic technique to model the yielding of the material that is the cause of this difference.

9.2 Industrial Implications and Recommendations to Designers

Eccentric loading has been shown to have a significant effect on the fatigue life of bolts. This must be taken into account if components designed are to operate safely. The effect of eccentricity can be calculated if the local stress amplitude can be determined.

The shape of cracks does not significantly change with eccentricity for the ranges of eccentricity used. Unfortunately, this means that the level of eccentricity experience by the bolt can not be determined by inspecting the fracture surface.

A two-dimensional finite element model can provide accurate information on the stresses in a bolt. It is important to use a fine mesh in the area of interest, and to model the washer and friction. If a non-axisymmetric loading condition, or non-axisymmetric crack is to included, or if data for the whole thread helix if needed, a three-dimensional model must be created. To provide accurate results, a three-dimensional model must replicate the nut thread run-out.

9.3 Recommendations for Future Research

- Investigating the effect of poor quality nuts by performing fatigue tests using nuts that are on or beyond the limit of the British Standard.
- A more thorough investigation into the parameters affecting the shape of cracks, including the effects of residual stresses. This would provide valuable information about the cause of failure from inspecting fracture surfaces.
- Adapting the 3D model that included the nut thread run-out to include plasticity and a washer to obtain more accurate stress distributions.
- Using this model to analysis the effect of eccentricity and cracks.

References

[1] BS 7608:1993 "Code of practice for fatigue design and assessment of steel structures"

[2] *JIS B1081, Axial load fatigue testing for threaded fasteners.* 1986

[3] **Burguete, R.L.** and **Patterson, E.A.**, The effect of mean stress on the fatigue limit of high tensile bolts, *Proc. Instn. Mech. Engrs.*, **209**: 257-262. 1995

[4] **Zhoa, H.**, Analysis of the load distribution in a bolt-nut connector, *Computers & Structures*, **53**(6): 1465-1472. 1994

[5] **Zhoa, H.**, A numerical method for load distribution in threaded connections, *Trans. ASME J. Mechanical Design*, **118**: 274-279. 1996

[6] **Kenny, B.** and **Patterson, E.A.**, The Distribution of Load and Stress in the Threads of Fasteners: A Review, *J. Mech. Behaviour of Mat.* **2**, 87-105 (1989).

[7] **Stromeyer, C.E.**, Stress Distribution in bolts and nuts, *Inst. Naval Arch. Trans.*, **60** 112-122 and plates XIII and XV, (1918).

[8] **Den Hartog, J.P.**, The mechanics of plate rotors for turbo-generators, *Trans. ASME*, Paper no. APM 51-1. **51** 1-10 (1929).

[9] **Solakian, A.G.**, Why threaded parts fail?, *Product Engineering*, **4** 261-262 (1933).

[10] **Sopwith, D.G.**, The distribution of load in screw threads, *Inst. Mech. Engrs., App. Mech. Proc.*, **159**: 373-383. 1948

[11] **Stoeckly, E.E.** and **Macke, H.J.**, Effect of taper on screw thread load distribution, *ASME, Trans.*, **74**(1): 103-112. 1952

[12] **Zhukovskii, N.E.**, Load distribution in the threads of a screw and nut, *Bull. Politekhnicheskogo obshchestva*, **1**. 1902

[13] **Kolenchuk, K.I.**, Load distribution in the threads of bolt-nut pair, *Collection of articles, 'Bolted connexions', Mashgiz.* 1949

[14] **Moore, H.F.**, and **Heywood, P.E.**, The strength of screw threads under repeated tension, University of Illinois, Engineering Experimental Station, Bulletin No. 264. 1934

[15] **Thurston, R.C.A.**, The fatigue strength of threaded connections, *Trans. ASME*, Paper no. 51-SA-11, **73**(11): 1085-1092. 1951

[16] **Goodier, J.H.**, Distribution of load on threads of screws, *Trans. ASME*, **62**: A10-A16. 1940

[17] **Hetényi, M.**, The distribution of stress in threaded connections, *Expt. Stress Anal.*, **1**(1): 147-156. 1943

[18] **Hetényi, M.**, A photoelastic study of bolt and nut fastenings, *J. Appl. Trans. ASME,* **65**: A93-A100. 1943

[19] **Seika, M., Sasaki, S.** and **Hosono, K.**, Measurement of stress concentrations in threaded connections, *Bull. JSME,* **17**(111): 1151-1156. 1974

[20] **Motosh, N.**, Load distribution on threads of titanium tension nuts and steel bolts, *J. Eng. Ind. Trans. ASME,* **97**(B): 162-166. 1975

[21] **Doniselli, C.** and **Mondina, A.**, Influence of shape of nut on stresses in threaded connections, 6th Canadian Eng. App. Mechs., Vancouver, B.C., Ed. V.J. Modi. Cancam, Vancouver. 1977

[22] **Brown, A.F.C.** and **Hickson, V.M.**, A photoelastic study of stress in screw threads, *Proc. I.Mech.Eng.,* **IB**: 605-612. 1952

[23] **Maruyama, K.**, Stress analysis of a nut-bolt joint by the finite element method and the copper-electroplating method (1st report), *Bull. JSME.* **16**(94), 671-678. 1973

[24] **Maruyama, K.**, Stress analysis of a nut-bolt joint by the finite element method and the copper-electroplating method, *Bull. JSME.* **17**(106), 442-450. 1974

[25] **Bretl, J.L.** and **Cook, R.D.**, Modelling the load transfer in threaded connections by the finite element method, *Int. J. Numer. Methods Eng.,* **14**(9): 1359-1377. 1979

[26] **Grosse, I.R.** and **Mitchell, L.D.**, Non-linear axial stiffness characteristics of axisymmetric bolted joints, *ASME J. Mech. Transm. Autom. Des.,* **112**(3): 442-449. 1990

[27] **Fessler, H.** and **Jobson, P.K.**, Stresses in the bottoming stud assembly with chamfers at the ends of the threads, *J. Strain Anal.,* **18**(1): 15-22. 1983

[28] **Fessler, H.** and **Wang Jiong-Hua**, Stresses analysis of some unsymmetric screwed connections, *J. Strain Anal.,* **19**(2): 111-119. 1984

[29] **Tanaka, M., Miyazama, H., Asaba, E.** and **Hongo, K.**, Application of the finite element method to bolt-nut joints - Fundamental studies on analysis of bolt-nut joints using the finite element method, *Bull. JSME,* **24**(192): 1064-1071. 1981

[30] **Kenny, B.** and **Patterson, E.A.**, Load and stress distributions in screw threads, *Experimental Mechanics,* (25): 208-213. 1985

[31] **Dragoni, E.**, Effect of nut compliance on screw thread distribution, *Journal of Strain Analysis,* **25**(3): 147-150. 1990

[32] **Dragoni, E.**, Effect of nut geometry on screw thread stress distribution: photoelastic results, *Journal of Strain Analysis,* **27**(1): 1-6. 1992

[33] **Burguete, R.L.** and **Patterson, E.A.**, The effect of bending on the normalized stress at roots of threaded connectors, *J. Offshore Mechs. & Arctic Eng.,* **116**:163-166. 1994

[34] **Burguete, R.L.** and **Patterson, E.A.**, The effect of eccentric loading on the stress distribution in thread roots, *Fatigue Fract. Engng Struct.*, **18**(11): 1333-1341. 1995

[35] **Dragoni, E.**, Effect of thread pitch and frictional coefficient on the stress concentration in metric nut-bolt connections, *OMAE - Volume III-B, Materials Engineering. ASME 1992*: 255-262

[36] **Patterson, E.A.** and **Kenny, B.**, The optimisation of the design of nuts with partly tapered threads, *Journal of Strain Analysis*, **21**: 77-84. 1986

[37] **Fukuoka, T., Yamasaki, N., Kitagawa, H.** and **Hamada, M.**, Ratio of flank loads of screw threads in hollow-bolt, *Bull. JSME*, **29**: 265-272. 1986

[38] **Joanovics, L.** and **Varadi, K.**, Non linear finite element analysis of the contact, strain and stress states of a bolt-nut-washer-compressed sheet joint system, *Periodica Polytechnica Ser. Mech. Eng.*, **39**(2): 151-162. 1995

[39] **Bahai, H., Esat, I.** and **Lawrence, J.**, A hybrid modelling approach to 3D stress analysis of threaded connections, *ASME Engineering Systems Design & Analysis, Vol 1*, **PD-Vol 47-1**: 235-241. 1992

[40] **Fukuoka, T.**, Evaluation of the method for lowering stress concentration at the thread root of bolted joints with modifications of nut shape, *Trans. ASME J. Pressure Vessel Tech.*, **119**: 1-9. 1997

[41] **Bush, A.J.**, Experimentally determined stress intensity factors for single-edge-crack round bars loaded in bending, *Exp. Mech.*, **16**: 251-257. 1976

[42] **Blackburn, W.S.**, Calculation of stress intensity factors for straight cracks in grooved and ungrooved shafts, *Engng. Fracture Mech.*, **8**: 731-736. 1976

[43] **Daoud, O.E.K.** and **Cartwright, D.J.**, Strain energy release rates for a straight-fronted edge crack in a circular bar subject to bending, *Engng. Fract. Mechanics*, **19**: 701-707. 1984

[44] **Forman, R.G.** and **Shivakumar, V.**, Growth behaviour of surface cracks in the circumferential plane of solid and hollow cylinders, *Fracture Mechanics: Seventeenth Volume, ASTM STP* **905**: 59-74. 1986

[45] **Nord, K.J.** and **Chung, T.J.**, Fracture and surface flaws in smooth and threaded round bars, *Int. J. Fracture*, **30**: 47-55. 1986

[46] **Mackay, T.L.** and **Alperin, B.J.**, Stress intensity factors for fatigue cracking in high-strength bolts, *Engng. Fract. Mechanics*, **21**(2): 391-397. 1985

[47] **James, L.A.** and **Mills, W.J.**, Review and synthesis of stress intensity factor solutions applicable to cracks in bolts, *Engng. Fract. Mechanics*, **30**: 641-654. 1988

[48] **Cipolla, R.C.**, Stress intensity factor approximation for semi-elliptical cracks at the thread root of fasteners, *Improved Technology for Critical Bolting Applications*, MPC-Vol **26**: 49-58. ASME 1986

[49] **Lefort, P.**, Stress intensity factors for a circumferential crack emanating from a notch in a round tensile bar, *Engng. Fract. Mechanics*, **10**: 897-904. 1978

[50] **Athanassiadis, A., Boissenot, J.M., Brevet, D., Francois, D.** and **Raharinaivo, A.**, Linear elastic fracture mechanics computations of cracked cylindrical tensioned bodies, *Int. J. Fracture*, **17**(6): 553-566. 1981

[51] **Caspers, M.** and **Mattheck, C.**, Weighted average stress intensity factors of circular-fronted cracks in cylindrical bars, *Fatigue Fract. Engng. Mater. Struct.*, **9**(5): 329-341. 1987

[52] **Caspers, M., Mattheck, C.** and **Munz, D.**, Fatigue crack propagation in cylindrical bars, *Z. Werstofftech.*, **17**: 327-333. 1986

[53] **Pacey, M.N., Burguete, R.L.** and **Patterson, E.A.**, A study of the stress distribution in threads of bolts with cracks, *OMAE - Volume III, Materials Engineering. ASME 1995*: 255-262

[54] **Toribio, J.**, Stress intensity factor solutions for a cracked bolt loaded by a nut, *Int. J. Fracture*, **53**: 367-385. 1992

[55] **Toribio, J., Sanchez-Galvez, V., Astiz, M.A.** and **Campos, J.M.**, Stress intensity factor solutions for a cracked bolt under tension, bending and residual stress loading, *Engng. Fracture Mech.*, **39**: 359-371. 1991.

[56] **Brennen, F.P.** and **Dover, W.D.**, Stress intensity factors for threaded connections, *Engng. Fracture Mech.*, **50**(4): 545-567. 1995

[57] **Bahai, H., Glinka, G.** and **Esat, I.**, Numerical and experimental evaluation of SIF for threaded connectors, *Engineering Fracture Mechanics*, **54**(6):835-845. 1996

[58] **Fuchs, H.O.** and **Stephens, R.I.**, *Metal Fatigue in Engineering.* Wiley, New York, 1980.

[59] **Hagiwara, M., Iwata, H., Fujino, Y.** and **Yoshimoto, I.**, Prediction of the fatigue fracture of a bolt by ultrasonic flaw detection, *JSME Int. J.*, **30**(259): 141-145. 1987

[60] **Mueller, R.A.**, Valve redesign blocks broken-bolt damage, *Oil and Gas J.*, **89**: 49-50. 1991

[61] **Arnold, S.M.**, Effects of screw threads on fatigue, *Mech. Engng.*, **65**: 497-505. 1943

[62] **Glinka, G., Dover, W.D.** and **Topp, D.A.** Fatigue assessment of tethers, *Proc. IMechE*, paper no. C135/86: 187-198. 1986

[63] *BS 3518 Part 1; 1993 Guide to General Principles.* 1993

[64] *BS 3518 Part 3; 1963 Direct Stress Fatigue Tests.* 1963

[65] *BS 3518 Part 5; 1966 Guide to the Application of Statistics.* 1966

[66] **Ohashi, N., Hagiwara, M.** and **Yoshimoto, I.**, On the standardization of the fatigue testing method for threaded fasteners, *JSME Int. J. Ser III,* **33**(4): 614-619. 1990

[67] *ISO 3800/1. Threaded fasteners - Axial load fatigue testing - Part 1: Test methods.* 1977

[68] *JSME Standard S 002, Standard methods of statistical fatigue testing.* 1981

[69] *JIS B1081, Axial load fatigue testing for threaded fasteners.* 1986

[70] **Shigley, J.E.** and **Mischke, C.R.**, *Mechanical Engineering Design,* 5th edition, (McGraw-Hill, New York) 1989.

[71] **Cook, N.H.**, *Mechanics and Materials for Design,* (McGraw-Hill, New York) 1985

[72] **Patterson, E.A.**, A comparative study of methods for estimating bolt fatigue limits, *Fatigue Fract. Engng. Mater. Struct.*, **13**(1): 59-81. 1990

[73] **Gunn, K.** Effect of yielding on the fatigue properties of test pieces containing stress concentrations, *Aeronaut. Q.*, 1955, **6**: 277-294

[74] **Hagiwara, M.** and **Yoshimoto, I.** The relation between load and strength in bolted joints subject to fatigue loading, *Bull. JSME,* **29**(257): 3917-3922. 1986

[75] **Hagiwara, M.** and **Yoshimoto, I.** Fatigue design of bolted joints taking into account reliability concepts, *Exp. Mechs.*, **27**(4): 398-403. 1987

[76] **Nakagome, M., Yasuda, K.** and **Mizuno, M.** Fatigue strength of bolted connections under conditions of eccentric clamping and eccentric loading, *Bull. JSPE,* **21**(4): 275-280. 1987

[77] **Rötscher, F.** *Die Maschinenelemente,* (Springer-Verlag, Berlin) 1927.

[78] **Bosch, M ten** *Berechnung der Maschinenelemente,* 3rd Edition, (Spinger, Berlin) 1951

[79] **Stuck, K.** *Untersuchungen zur Ermittlung der verspannten Teile einer Schrau-benverbindung,* Dissertation, Aachen THE. 1986.

[80] **Samonov, C.** Stiffness constants in bolted connections—Their determination and influence on resulting working loads, *Mech. and Chem. Eng. Trans., Inst. Eng. Austrailia,* MC2(2): 35-42. 1966

[81] **Motosh, N.** Determination of joint stiffness in bolted connections, *ASME J. Engg. Ind.,* **93B**(3): 858-861. 1976

[82] **Fritsche, G.** *Grundlagen einer genaureren Berechnung statisch und dynamisch beanspruchter Schraubenverbindungen,* Dissertation, Berlin TU. 1962

[83] **Stuck, K.** *Untersuchungen über die Federeigenschaften der verspannten Teile von Schraubenverbindungen,* Dissertation, Aachen TH. 1968

[84] **Fernlund, I.** A method to calculate the pressure between bolted riveted plates, *Trans. Chalmers Univ. of Technology,* Gothenburg, Sweden, no. 245. 1961.

[85] **Boenick, U.** *Untersuchungen an Schraubenverbindungen,* Dissertation, Berlin TU. 1966

[86] **Hagiwara, M.** Non-linear behaviour of bolted joints due to separation at the contact plane, *Bull. Japan Soc. Prec. Engg.,* **19**(4): 273-278. 1985

[87] **Grosse I.R.** and **Mitchell, L.D.** Nonlinear axial stiffness characteristics of axisymmetric bolted joints, *ASME J. Mech. Transm. Autom. Des.* **112**(3): 442-449. 1990

[88] **Beitz, W.** and **Neuendorf, K.** Load deflection analysis in eccentrically loaded connections, *VDI-Berichte,* **220**: 69-78. 1974

[89] **Junker, G.H.** and **Wallace, P.W.** Moderne Steuerungsmethoden für das Motorische Anziehen von Schraubenverbindungen, *VDI-Berichte,* **220**: 87-98. 1974

[90] Systematische Berechnung von hochbeanspruchten Schraubenverdindungen. Richtlinie VDI 2230, October 1977. Berlin, Köln, Frankfurt, Beuth Vertieb GmbH.

[91] **Thomala, W.** Elastische Nachgiebigkeit verspannten Teile einer Schraubenver-bindung, Dissertation, Aachen THE. 1982

[92] **Junker, G.H.** and **Wallace, P.W.** The bolted joint: Economy of design through improved analysis and assembly methods, *Proc. IMechE.,* **198B**(14): 255-266. 1984

[93] **Boys, J.T.** and **Wallace, P.W.** Design and performance of an automated control system for fastener tightening, *Proc. IMechE.,* **191**(33): 371-380. 1977

[94] **Nakagome, M., Suzuki, I., Yasuda, K.** and **Mizuno, M.** On the compliance and load factor of bolted connections subjected to eccentric loading, *JSME Int. J. Ser I,* **32**(1): 61-66. 1989

[95] **Burguete, R.L.** Methods to calculate joint stiffness: A review and classification of joint types, *OMAE - Vol III-B, Materials Engg..* 1992

[96] **Burguete, R.L.** and **Patterson, E.A.** Photoelastic stress freezing of bolts in bending using real parameters, *Conference on Modern Practice in Stress Vibration Analysis,* Ed. J.L. Wearing, Sheffield Academic Press, pp 403-413. 1993

[97] **Kenny, K.,** The casting of a low exotherm epoxy resin, *J. Scientific Instruments,* **42**:719-720. 1965

[98] **Patterson, E. A.** and **Kenny, K.** Stress analysis of some nut-bolt connections with modifications to the nut thread form, *J. Strain Analysis.* **20**(1):35-40. 1985.

[99] **Wang, Z.,** and **Patterson, E. A.,** Use of phase-stepping with demodulation and fuzzy sets for birefringence measurement, *Optics and Lasers in Engineering,* **22**:91-104, 1995

[100] **Nurse, A.**, and **Patterson, E. A.**, Determination of predominantly mode II stress intensity factors from isochromatic data, *Fatigue and Fracture of Engineering Materials & Structures*, **16:** 1339-1354, 1993

[101] **Sanford, R.J.** and **Dally, J.W.** A general method for determining mixed mode stress intensity factors from isochromatic fringe patters, *Engng. Fract. Mech.*, **11**: 621-633. 1978

[102] **Muskhelishvili, N.I.**, *Some Basic Problems of the Mathematical Theory of Elasticity*, 3rd Edition, Noordhoff, Groningen. 1963